The Dissertation Committee for Di Song Certifies that this is the approved version of the following dissertation:

Effect of Liquid Viscosity on Liquid Film Mass Transfer for Packings

Committee:

Gary T. Rochelle, Supervisor

A. Frank Seibert, Co-Supervisor

R. Bruce Eldridge

Benny D. Freeman

Venkat Ganesan

Effect of Liquid Viscosity on Liquid Film Mass Transfer for Packings

by

Di Song

Dissertation

Presented to the Faculty of the Graduate School of

The University of Texas at Austin

in Partial Fulfillment

of the Requirements

for the Degree of

Doctor of Philosophy

The University of Texas at Austin

December 2017

Dedication

To my family.

Acknowledgements

I would like to first thank my advisor, Dr. Gary Rochelle. His passion towards life and research has deeply enlightened me. He is a mentor as well as a friend, always resourceful, humorous, patient, and encouraging. I feel blessed to be his student, for both my graduate study and for life. I also want to thank my co-advisor, Dr. Frank Seibert, who has provided day-to-day advice on my research. His expertise and meticulosity in the separations technology gave me a role model for a good engineer and researcher. I want to additionally thank Dr. Eric Chen, who has been so patient and supportive when teaching me those hands-on experiences in pilot plant design and operation.

My friends Qi Zhou, Yi Ren, Kai Luo, and Guofeng Li have supported me always, whether in the US or cross the ocean back in China. In the five years of graduate study, I've met great colleagues and friends in the Rochelle group: Peter Frailie, Brent Sherman, Darshan Sachde, Nathan Fine, Omkar Namjoshi, Yu-Jeng Lin, Yue Zhang, Ye Yuan, Paul Nielsen, Matt Beaudry, Steven Fulk, Kent Fischer, Yang Du, Matt Walters. I especially value the experience of working closely with and learn from Lynn Li in the wetted-wall column experiments and Chao Wang in the packed column experiments. The staff of the Separations Research Program (SRP) Steve Briggs, Robert Montgomery, Micah Perry, and Henry Bautista have provided consistent help with my experiments with the pilot column. I'm grateful to Jerret Spinhirne for his support on the gas chromatograph trouble shooting, to Maeve Cooney, who has been a huge support in my writing as well as all other administrative stuff.

This project would not have been possible without the support of the SRP, Process Science and Technology Center consortium (PSTC), and the Texas Carbon Management Program.

Most of all, I want to thank my parents and grandparents for their unconditional love. I'm proud to be their son and grandson, and I will try my best to be a good chemical engineer as they all are.

Effect of Liquid Viscosity on Liquid Film Mass Transfer for Packings

Di Song, Ph.D.

The University of Texas at Austin, 2017

Supervisors: Gary T. Rochelle and A. Frank Seibert

The effect of liquid viscosity (μ_L) on liquid film mass transfer for packings was investigated in a pilot-scale column with 0.43 m (16.8 in) ID and 3 m (10 ft) maximum packing. Mass transfer area (a_e) of three structured packings, one random packing, and one hybrid packings was measured by chemical absorption of CO_2 into dilute (~ 0.1 mol/L) NaOH. Liquid film mass transfer coefficient (k_L) of eight structured packings, one random packing, and one hybrid packing was measured by air stripping toluene from water. Liquid viscosity was varied 0.8-70 mPa·s by adding 0-89 wt % glycerol to water in one a_e and nine k_L experiments. In the experiments, the liquid load was varied 6-75 $m^3/m^2 \cdot hr$ (2.5-30 gpm/ft^2), and the gas rates were 0.6, 1, and 1.5 m/s (180, 300, and 450 ACFM).

The models of $a_{e,packing}$ and k_L were developed based on data for 39 packings from this work and the SRP air-water column database:

$$\frac{a_e}{a_P} = 1.16 \cdot \eta \cdot \left[\left(\frac{\rho_L}{\sigma}\right) \cdot g^{1/2} \cdot u_L \cdot a_P^{-3/2}\right]^{0.138}$$

$$k_L = 0.12 \cdot u_L^{0.565} \cdot \left(\frac{\mu_L}{\rho_L}\right)^{-0.4} \cdot D_L^{0.5} \cdot g^{1/6} \cdot a_P^{-0.065} \cdot \left(\frac{Z}{1.8}\right)^{-0.54}$$

The model of the gas film mass transfer coefficient, k_G, was developed based on data for 20 packings in the SRP air-water database:

$$k_G = 0.28 \cdot u_G^{0.62} \cdot \left(\frac{\mu_G}{\rho_G}\right)^{-0.12} \cdot D_G^{0.5} \cdot a_P^{0.38} \cdot (\sin 2\alpha)^{0.65}$$

The secondary (wall and end) effect of a_e was corrected in the area model. A taller packing bed consistently gave smaller k_L due to maldistribution. Liquid viscosity does not have a significant effect on a_e. The k_L depends on μ_L to the -0.75 power, in which the -0.4 is the direct influence on the liquid turbulence, and -0.35 is the indirect effect via diffusivity of the mass transfer species. The effect of μ_L on k_L is the same for different packing geometry and types.

To prepare for the pilot-scale area experiment with glycerol, reaction kinetic model of CO_2 and hydroxide in aqueous glycerol was developed based on the wetted-wall column (WWC) experiments.

Table of Contents

List of Tables

List of Figures

Chapter 1: Introduction

The cause and impact of CO_2-induced global warming is included in this chapter. Methods to reduce CO_2 emitted from major point sources such as coal-fired power plant and cement plant are introduced. Packing internals used in the industrial separation process including post-combustion CO_2 capture with aqueous amines are summarized. After a brief review of previous work, the motivation and the scope of this work are explained.

1.1 Global Warming and CO_2 Capture

The global temperature has been increasing rapidly over the past century (Figure 1.1). This is caused by the increase of energy consumption and the subsequent increase of green-house gas (GHG) emissions. Figure 1.2 shows the global emission of CO_2, which is the major component of GHG. Despite the recent shift of power generation from coal to natural gas in the USA, the coal-fired power plants still produce more than 28% of total carbon emissions, and about three quarters of the power plant emissions (Figure 1.3).

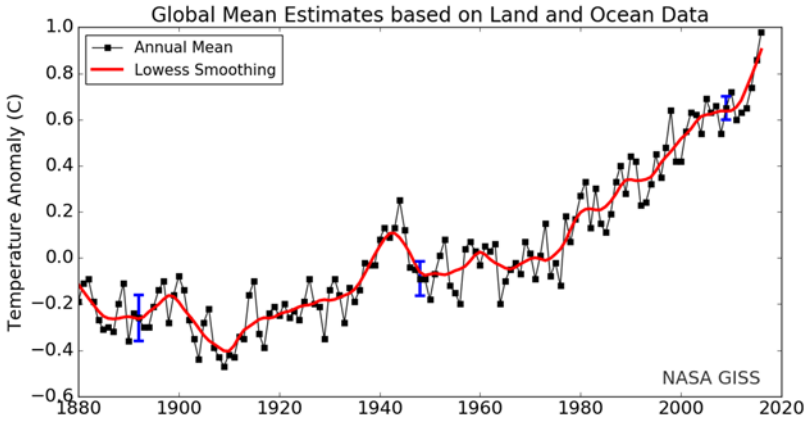

Figure 1.1: Global mean temperature change from Hansen (2010)

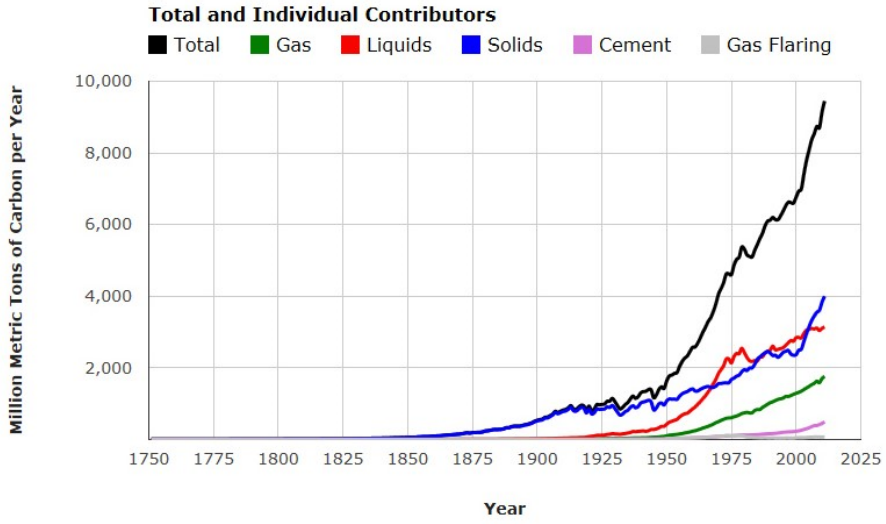

Figure 1.2: Global carbon emission increase from Boden (2017)

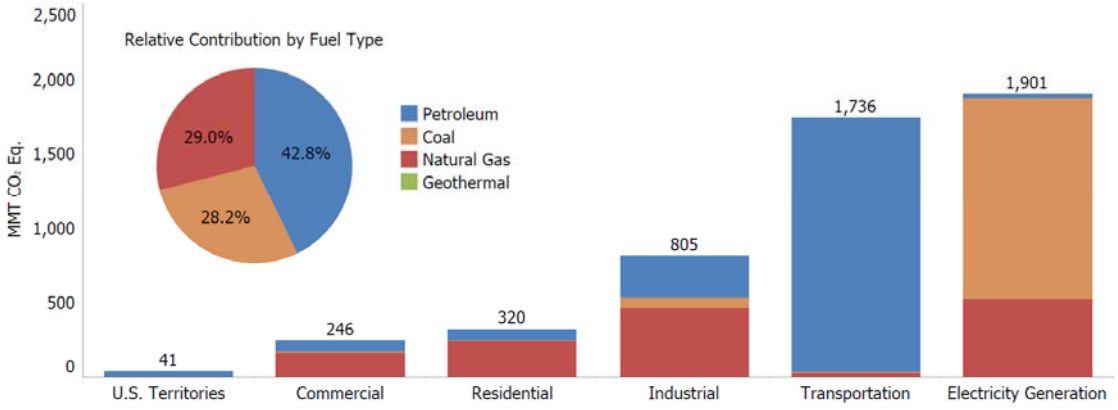

Figure 1.3: 2015 CO_2 emissions from fossil fuel combustion by sector and fuel type in the USA from EPA (2017)

Global warming can cause severe problems in the long run, such as sea level rise, shifting precipitation and climate pattern, more frequent severe weather, and species extinction (IPCC, 2014). Therefore, it is necessary to reduce or control carbon emissions especially from large point source such as coal-fired power plants.

Carbon capture and sequestration (CCS) is a way to reduce carbon emission from power plants. There are three types of capture technology: pre-combustion capture, post-combustion capture, and oxy-fuel combustion (Figure 1.4). Among them, post-combustion is the best understood, most economically feasible, and least invasive method to the existing power plants.

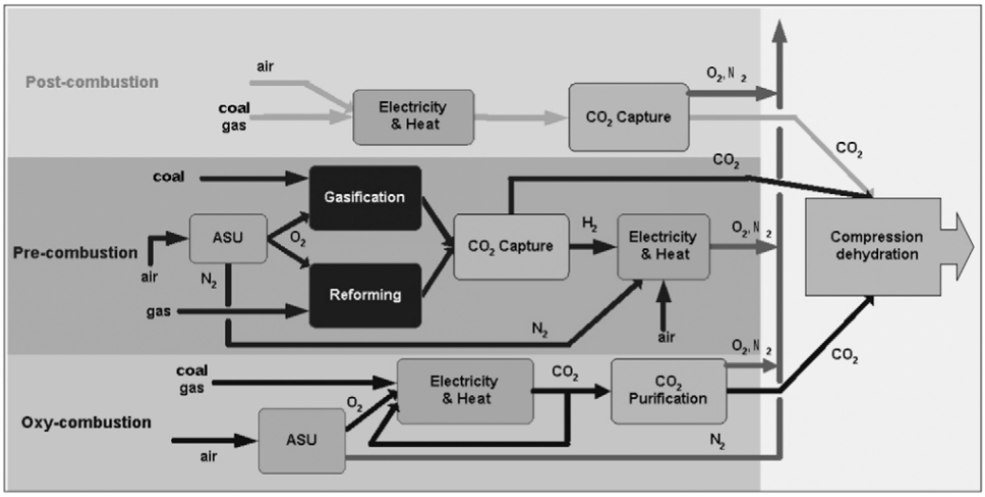

Figure 1.4: Three types of carbon capture approach from Kanniche (2010)

A process diagram of post-combustion carbon capture with concentrated amine such as monoethanolamine (MEA) and piperazine (PZ) is sketched in Figure 1.5. The flue gas from power plants is sent into the absorber where CO_2 is absorbed into the lean amine to give rich amine, which is then sent to the stripper where the loaded CO_2 is stripped out by the high temperature provided by the steam in the reboiler. The high-concentration CO_2 from the stripper is compressed and sequestered.

In the two most important unit operations of the capture process, the absorber and the stripper, packing is most commonly used as column internals because of its greater capacity and mass transfer efficiency compared to trays. Since the viscosity of typical

amine solutions is significantly greater than water (at 40 °C, $\mu_{PZ@0.4\alpha}$ = 11.4 mPa·s, μ_{water} = 0.65 mPa·s), it is important to understand how the liquid viscosity affects mass transfer in the packings for more efficient column design (Rochelle et al., 2015a).

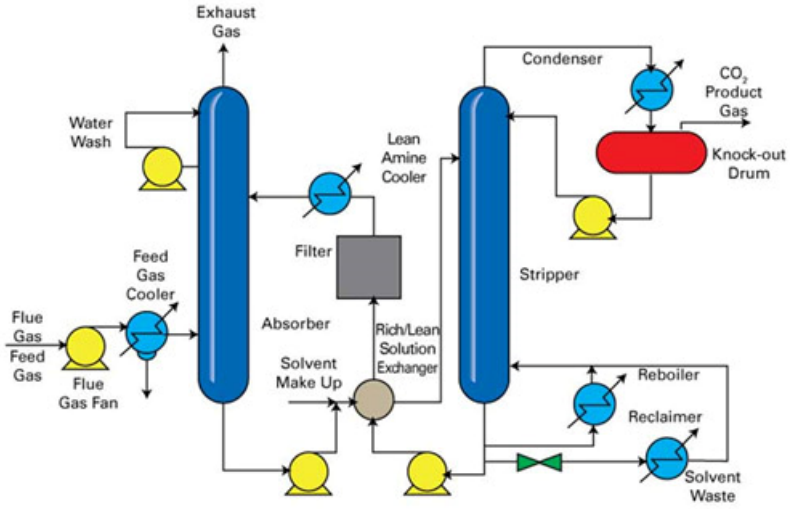

Figure 1.5: Process diagram of post-combustion carbon capture with amine solution from Rochelle (2009)

1.2 PACKINGS

Packings are not only used in the post-combustion carbon capture process, but are widely used in various industrial separations processes including distillation and extraction. The fluids in the column flow either counter-currently or co-currently through the void spaces on the packing surface, which improves both the wetting for greater contact area and the turbulence for greater separation efficiency.

Traditionally there are two types of packings: random and structured (Figure 1.6). The former comes with specific geometric shape in small pieces and are dumped into the column randomly. The later are manufactured in ordered shapes with multiple

corrugation sheets to fit the size of the column. The performance of the two types of packings are summarized in Table 1.1. Other types of packings include gauze packing and grid packings, which are not as frequently used.

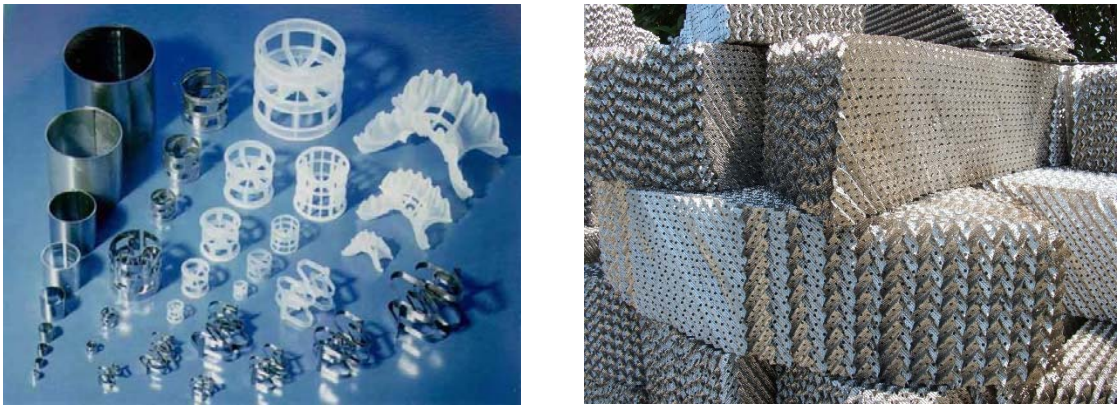

Figure 1.6: Random (left) and structured (right) packings
(left picture from www.raschig.com, right picture credit to Luigi Chiesa)

Table 1.1: General performance of random and structured packings

Packing	Random		Structured
	Traditional	4th generation*	
Relative cost	Low	Moderate	High
Pressure drop	Moderate	Low	Very low
Efficiency	Moderate	High	Very high
Vapor capacity	Moderate	High	High

* Packings such as VSP Fleximax®, and Raschig Super Rings®

A relatively new kind of packing is hybrid packing such as Raschig Super-Pak® (Figure 1.7). It is a combination of random and structured packings with randomly shaped small units fixed uniformly to form open corrugation channels in a whole piece like structured packings. Hybrid packing has the advantages of both structured packings such

as low pressure drop, and random packings such as greater resistance to liquid maldistribution.

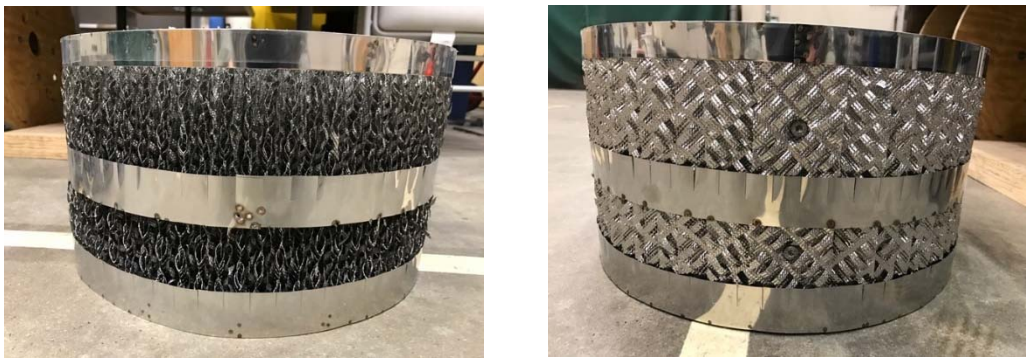

Figure 1.7: Front and side views of Raschig Super-Pak® 250Y

Figure 1.8 shows the basic geometry and dimensions of the triangular corrugation channel in structured packings. There are two important parameters: specific area (a_P) and corrugation angle (α). The a_P is the metal surface area per unit volume of the packing, which is closely related to the corrugation channel dimension (b, s, and h). The α is the inclination angle of the channels to the ground.

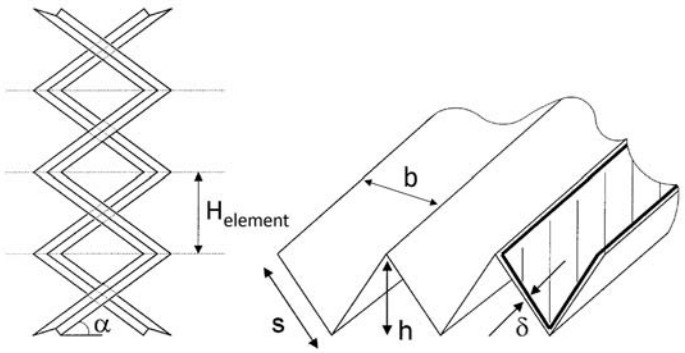

Figure 1.8: Basic geometry and dimension of triangular corrugation channel of structured packing (slightly modified from Olujic, 1999)

Since random packings do not have the ordered geometry of structured packings, the corrugation angle is not applicable to random packings. The a_P of random packings is determined by the size of the packing pieces.

Other properties of packings include surface modification (embossing, perforation, etc.), number and type of wiper bands, material (metal, ceramic, plastic, etc.), and packing element height ($H_{element}$).

1.3 MASS TRANSFER PARAMETERS FOR PACKINGS

For gas-liquid mass transfer in packings, there are two important parameters: effective mass transfer area (a_e) and mass transfer coefficient in the two films (k_G and k_L). The former is the area contributable to effective mass transfer of the packing. It is different from a_P considering the wetting condition and ineffectively wetted region such as channeling or dead zones. The a_e is strongly affected by operating conditions and packing/column geometry. The ratio of a_e to a_P, fractional packing area (Φ), is usually below unity. However, it can be greater than unity at relatively high liquid loads or for coarse packings. Fluid properties may also affect a_e.

The gas or liquid film mass transfer coefficients are parameters used to describe the rate of mass transfer at the interface films. Like the a_e, the k_G and k_L are also affected by the operating conditions, packing geometry, and fluid property. Either film could be dominant in the mass transfer process based on the system property.

Both a_e, k_G, and k_L are important for column design. For post-combustion amine carbon capture specifically, the a_e and reactive liquid film mass transfer coefficient (k_g') are important for the absorber, while the a_e and physical liquid film mass transfer coefficient (k_L^0) are important for the stripper.

1.4 PREVIOUS WORK

Many area and mass transfer coefficient models have been proposed in the literature. Tsai (2010) did a thorough review on the area models and developed his own model based on data in the air-water column database of the Separations Research Program (SRP) at the University of Texas at Austin. His model solved the problem that many previous correlations share: having to use packing-specific parameters which may cause discontinuity for apparently related packings. He also investigated the effect of surface tension (σ) and liquid viscosity (μ_L) on a_e, for which previous correlations have conflicting predictions. Since the Tsai model was developed, a significant amount of new area data has been generated with greater variance in packing geometry and liquid properties. Therefore, it is necessary to revisit the model with the expanded database and update/modify the model if needed.

Among many researchers such as Onda (1968b) and Billet and Schultes (1993, 1999) whose correlations have been widely used, Wang (2015) has comprehensively studied the decoupled mass transfer coefficients of packings. In his work, water systems were used in the experiments without liquid property variance. The mixing point theory central to the Wang model needs to be further validated against the SRP database since detailed analysis was missing in his dissertation.

For most applications, the overall volumetric mass transfer coefficient ($K_{OG} \cdot a_e$ or $K_{OL} \cdot a_e$) is sufficient for the design purpose, and that is the form many correlations (such as Rocha, 1996) are based on. By reporting the lumped mass transfer coefficient, the k_G/k_L and a_e are either not separated or separated based on simplified assumptions on either parameter with the other forced to fit. Doing this will result in contradictory conclusions about the effect of each experimental variable on the individual mass transfer parameter and thus limit the reliability of the overall model especially when extrapolated beyond the

operating conditions or physical property range of the work. Moreover, it can be problematic to use k_G/k_L and a_e from different sources where inconsistency in the experimental setup, chemical system, or analysis assumption always exist.

One way to decouple k_G/k_L from a_e is to fix the mass transfer area by proper design of the gas-liquid contact media such as the bench scale wetted-wall column and the pilot-column in the study of Shulman et al. (1955) with naphthalene packings. The other way is to choose the physical or reactive test system with a different controlling mechanism in mass transfer, as is proposed by Hoffman (2007) and Rejl (2009). Several researchers (such as Linek and co-workers) have reported individual mass transfer parameters using the latter method.

Most of the large number of mass transfer correlations for packings are focused only on water-like systems ($\rho_L \sim 1000$ kg/m^3, $\sigma \sim 72$ mN/m, $\mu_L \sim 1$ mPa·s). Extrapolating to more viscous systems such as ionic liquids, concentrated amine solutions, or polymer solutions may cause trouble in both design and operation. Only a few (such as Mangers, 1980 and Brunazzi, 1997) examined the viscosity effect on the mass transfer with limitations that will be explained in detail in the next chapter.

A systematic study of the effect of μ_L on the liquid film mass transfer (both the a_e and the k_L) is needed.

1.5 Research Objectives and Scope

The primary objective of this work is to update/develop comprehensive models of a_e and k_L by experiments with both water and aqueous solution with viscosity enhancer (1~100 mPa·s orders of magnitude) in a pilot-scale column with packings of various type

and geometry to predict the effect of liquid viscosity, operating condition, and packing geometry on the liquid film mass transfer. Detailed scope of this work includes:

- Determine suitable liquid viscosity enhancer taking into account safety, material compatibility, and liquid property.
- Investigate the effect of the viscosity enhancer on the reaction kinetics of CO_2/ $NaOH/H_2O$ with wetted-wall column experiments. Develop kinetic model for the viscous system if necessary.
- Check the conclusion of Tsai (2010) that viscosity does not affect a_e by pilot-scale a_e experiments with the viscous reactive system based on the wetted-wall column kinetic model. Update or modify the area model with expanded database.
- Investigate the effect of liquid viscosity, operating condition, and packing geometry on the liquid film mass transfer coefficient by air/toluene/H_2O/viscosity enhancer in pilot-scale column. Update or modify the k_L model of Wang (2015), or develop new model if necessary with expanded database.
- Develop fundamental understanding of how the liquid viscosity affects k_L in packings with various type and geometry.

Chapter 2: Literature Review[1]

This chapter introduces the fundamental models of physical and reactive mass transfer between two fluids. Theoretical and empirical models of a_e and k_L for packings in the literature are introduced with emphasis on those with elevated liquid viscosity.

2.1 Fundamental Mass Transfer Models

2.1.1 Fundamentals of Multi-Phase Mass Transfer

Mass transfer is the movement of component from one location to another. It can happen in one phase or multiple phases. Figure 2.1 illustrates the concentration profile of species A absorbed from gas to liquid, which is fundamental to the mass transfer processes studied in this work.

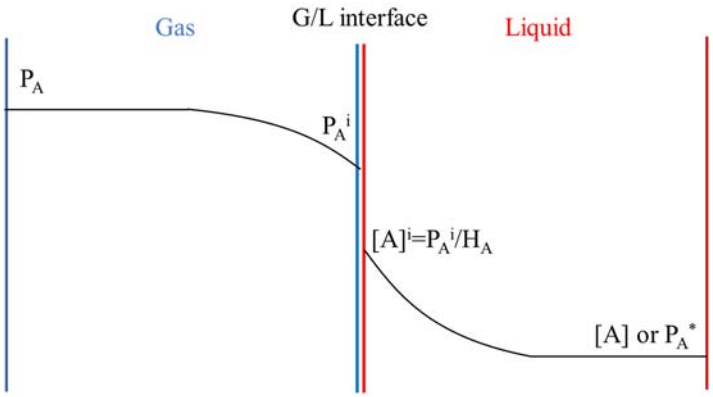

Figure 2.1: Concentration profile of A absorbed from gas to liquid

By mass balance, the overall flux of A (N_A) through the two phases is equal to the flux in each single phase:

[1] D. Song, A.F. Seibert, G.T. Rochelle. "Effect of liquid viscosity on the liquid phase mass transfer coefficient of packing." Energy Proc. (2014) 63:1268-86.

$$N_A = K_G \cdot (P_A - P_A^*) = k_G \cdot \left(P_A - P_A^i\right) = k_L^0 \cdot \left([A]^i - [A]\right) \quad (2.1)$$

Per Equation 2.1, the mass transfer process can be depicted in a way similar to heat transfer by using a term of driving force and resistance:

$$Rate = \frac{Driving\ force}{Resistance} \quad (2.2)$$

The resistance is the reciprocal of mass transfer coefficient *K* or *k*, and the driving force is the difference of concentration. Equilibrium is assumed at the gas-liquid interface. To unify the driving force across phases, a distribution factor (Henry constant, H_A) is used:

$$k_L^0 \cdot \left([A]^i - [A]\right) = \frac{k_L}{H_A} \cdot \left(P_A^i - P_A^*\right) \quad (2.3)$$

Combining Equation 2.1 and 2.3 gives:

$$\frac{1}{K_G} = \frac{1}{k_G} + \frac{H_A}{k_L^0} \quad (2.4)$$

The mass transfer resistance is expressed as a series with the overall resistance ($1/K_G$) being the sum of the gas film ($1/k_G$) and liquid film resistance ($H_A/k_L{}^0$). The overall mass transfer can be controlled by either one or both phases, and proper choice of the system is an effective tool to characterize the mass transfer process (Hoffmann et al., 2007; Rejl et al., 2009).

2.1.2 Physical Mass Transfer

Film theory (Lewis & Whitman, 1924) is the most fundamental theory depicting mass transfer between two phases (Figure 2.2). Each phase is divided into two regions: the bulk fluid where rapid mixing occurs with uniform concentration, and the stagnant thin film close to the interface where molecular diffusion occurs with a linear concentration profile. The mass transfer coefficient predicted by the Film theory (Equation 2.5) can be

obtained by solving the differential equation (Equation 2.6) with proper boundary conditions:

$$k_L^0 = D_{A,L}/\delta_L \tag{2.5}$$

$$D_{A,L}\frac{d^2[A]}{dx^2} = 0 \tag{2.6}$$

Per the equation, the mass transfer coefficient is proportional to the diffusivity of the mass transfer species, while most experimental data show that k is proportional to the square root of D (Geankoplis, 2003). The film thickness is not readily available and the discontinuity of concentration between the film and the bulk fluid is not realistic physically. Due to the limitations above, the Film theory is not widely applied. However, it serves as an illustration for the multi-phase mass transfer process and as a foundation for other models closer to reality.

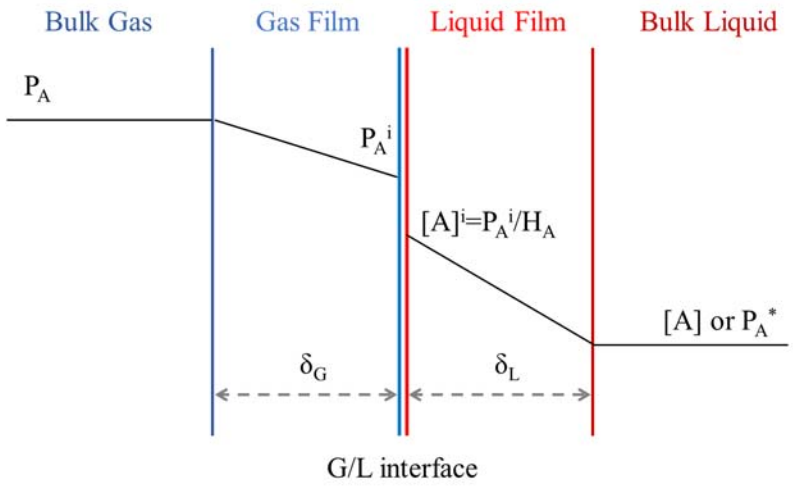

Figure 2.2: Concentration profile of A absorbed from gas to liquid predicted by the Film theory

The Penetration theory (Higbie, 1935) replaced the concept of stagnant film in the Film theory with dynamic film where molecules continuously commute between the film and the bulk fluid. Each molecule transferred to the film is exposed to mass transfer in a constant time, *t*. Equation 2.7 is the differential equation of mass transfer. The liquid film mass transfer coefficient predicted by the Penetration theory (Equation 2.8) depends on the diffusivity to the square root, which is more realistic than the Film theory.

$$D_{A,L}\frac{\partial^2[A]}{\partial x^2} = \frac{\partial[A]}{\partial t} \tag{2.7}$$

$$k_L^0 = 2\sqrt{\frac{D_{A,L}}{\pi t}} \tag{2.8}$$

Surface Renewal theory (Danckwerts, 1951) is a modification of the Penetration theory with distributed exposure time ($\bar{t}$) replacing constant exposure time for the commuting molecules. The liquid film mass transfer coefficient is predicted in terms of fraction of liquid surface renewed per time ($s = 1/\bar{t}$) in Equation 2.9. The form is similar to that of the Penetration theory with square root dependence on the diffusivity.

$$k_L^0 = \sqrt{D_{A,L} \cdot s} \tag{2.9}$$

2.1.3 Mass Transfer with Chemical Reaction

Mass transfer with chemical reaction is the process where the moving species from the gas can react with one or more components in the liquid. The rate of reactive mass transfer is enhanced compared to physical diffusion, and the degree of enhancement is described by the enhancement factor, *E*. Rewriting Equation 2.3 gives:

$$N_A = \frac{E \cdot k_L^0}{H_A} \cdot \left(P_A^i - P_A^*\right) \tag{2.10}$$

The term in front of the driving force is defined as k_g', which is the reactive liquid film mass transfer coefficient expressed in gas units:

$$k_g' = \frac{E \cdot k_L^0}{H_A} \tag{2.11}$$

Thus, Equation 2.4 can be rearranged for reactive systems:

$$\frac{1}{K_G} = \frac{1}{k_G} + \frac{1}{k_g'} \tag{2.12}$$

The enhancement factor, E, depends on the kinetics of the reactive system. The absorption of CO_2 into dilute NaOH is discussed in detail here because of its close relevance to the area measurement in this and previous studies (Tsai, 2010; Wang et al., 2012; Zakeri, 2011). The kinetics of the system is extensively studied and well-established (Faurholt, 1924; Kucka et al., 2002; Nijsing et al., 1959; Pinsent et al., 1956; Pohorecki & Moniuk, 1988). A thorough review of k_{OH^-} is given by Haubrock et al. (2005).

$$CO_2 + OH^- \xrightarrow{k_{OH^-}} HCO_3^- \tag{2.13}$$

$$HCO_3^- + OH^- \rightleftharpoons H_2O + CO_3^{2-} \tag{2.14}$$

The forward reaction of 2.14 is a proton transfer process, and thus is several orders of magnitude faster than Reaction 2.13 in a basic environment (Eigen, 1963). As the rate-governing reaction, 2.13 is practically irreversible with its rate constant described as follows:

$$r = k_{OH^-}[CO_2][OH^-] \tag{2.15}$$

Reaction 2.13 can be assumed to be pseudo-first-order when the caustic concentration is relatively unchanged (with relatively low CO_2 and excess [OH^-]), which applies to the pilot column area experiments in this work:

$$r \approx k_1[CO_2] \tag{2.16}$$

Inserting the reaction term into the differential mass transfer Equation 2.7 under the pseudo-first-order assumption gives:

$$D_{CO_2,L}\frac{\partial^2[CO_2]}{\partial x^2} - k_1[CO_2] = \frac{\partial[CO_2]}{\partial t} \tag{2.17}$$

The solution to the equation in the context of Surface Renewal theory is presented in Equation 2.18 (Bishnoi & Rochelle, 2000):

$$N_{CO_2} = k_L^0\sqrt{1 + \frac{k_1 D_{CO_2,L}}{(k_L^0)^2}} \cdot \frac{\left(P_{CO_2}^i - P_{CO_2}^*\right)}{H_{CO_2}} \tag{2.18}$$

The enhancement factor can be obtained by comparing Equations 2.18 and 2.10:

$$E = \sqrt{1 + \frac{k_1 D_{CO_2,L}}{(k_L^0)^2}} \tag{2.19}$$

The second term under the square root of Equation 2.19 is the Hatta number (*Ha*) defined by Kucka (2002) and Haubrock (2005), which represents the ratio of chemical reaction to physical diffusion in a liquid film (Bird et al., 2002):

$$Ha = \frac{\sqrt{k_1 D_{CO_2,L}}}{k_L^0} \tag{2.20}$$

$$E = \sqrt{1 + Ha^2} \tag{2.21}$$

When Ha^2 is significantly greater than 1 (which means chemical reaction is much faster than physical diffusion and the liquid film mass transfer is controlled solely by the reaction rate), the k_g' can be expressed in a simplified form:

$$k_g' = \frac{E \cdot k_L^0}{H_{CO_2}} = \frac{\sqrt{1+Ha^2} \cdot k_L^0}{H_{CO_2}} \approx \frac{Ha \cdot k_L^0}{H_{CO_2}} = \frac{\sqrt{k_1 D_{CO_2,L}}}{H_{CO_2}} = \frac{\sqrt{k_{OH^-}[OH^-] D_{CO_2,L}}}{H_{CO_2}} \quad (2.22)$$

Certain premises are required for Equation 2.22 to be valid for interpreting the measured a_e from the pilot column experiments:

- Mass transfer should be controlled by the liquid film resistance, not the gas film resistance ($1/k_g'$ term in the Equation 2.12 is significantly greater than $1/k_G$). This is achievable with a relatively slow reaction rate (by reducing P_{CO2}^i or $[OH^-]$).
- Reaction instead of physical diffusion should be dominant in the liquid film mass transfer ($Ha^2 \gg 1$). This is achieved with a relatively fast reaction rate (by increasing P_{CO2}^i or $[OH^-]$).
- Caustic depletion at the gas-liquid interface should be negligible to satisfy the pseudo-first-order assumption central to the deduction of Equation 2.18 ($E_\infty/Ha > 5$). Similar to the first premise, this requires a relatively slow reaction rate and excessive caustic reserve. The E_∞ is the enhancement factor for an instantaneous, irreversible reaction (Bishnoi & Rochelle, 2000):

$$E_\infty = 1 + \frac{D_{OH^-,L} \cdot [OH^-] \cdot H_{CO_2}}{D_{CO_2,L} \cdot P_{CO_2}^i} \quad (2.23)$$

It is notable that these premises can be satisfied by adjusting the concentrations of CO_2 and NaOH. Details of the experimental concerns of the reactive system are discussed in Chapter 3.

When glycerol is added to the caustic solution, part of it will change to glyceroxide (Reaction 2.24) in the strong basic environment, consuming an equal amount of hydroxide (Fairbourne et al., 1930; Faurholt, 1927a). The CO_2 reacts with both hydroxide (Reaction 2.13) and glyceroxide (Reaction 2.25) when reaching the liquid surface (Fairbourne et al., 1930; Heston et al., 1943), and the measured k_g' from WWC is a combined effect of the

two reactions. Since the two primary hydroxyl groups on glycerol are more reactive than the single secondary hydroxyl (Fairbourne et al., 1931; Glycerine Producers, 1965), and glycerol is in excess relative to hydroxide, it is assumed that Reaction 2.25 only occurs with the primary glyceroxide. Though there are reports showing that the CO_2 insertion into metal alkoxide is reversible (Kato & Ito, 1985; Offermans et al., 2015), the decomposition of alkyl carbonate is very slow at high pH (> 10) compared to the forward reaction (Faurholt, 1927b, 1927c). This is also demonstrated by the steep pH curve of the post-experiment WWC liquid samples in the total alkalinity titration.

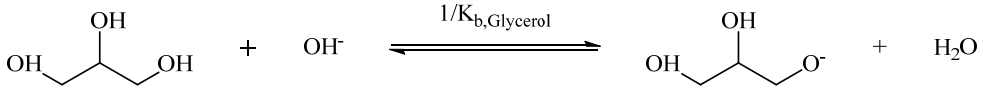

(2.24)

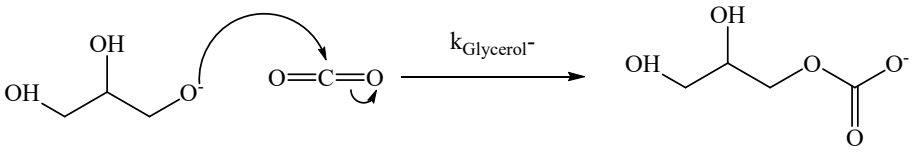

(2.25)

The CO_2 reacts with alkoxide faster than with hydroxide in an aqueous environment. Faurholt (1927b) investigated competing reactions with a limited amount of CO_2 between hydroxide and methoxide. The rates of the reactions were demonstrated by the relative ratio of the end products carbonate and methylcarbonate, which were determined by adding barium chloride. Heston et al. (1943) extended Faurholt's measurement to greater methanol concentrations. Metal was also shown to enhance CO_2 absorption in a metal-organic framework (Stergiannakos et al., 2015) and organic solutions (Darensbourg et al., 1987; Tsuda & Saegusa, 1972). Though few direct data were found in literature of the reaction rate between CO_2 and glyceroxide, Fairbourne (1931; 1930) did prove the formation of glyceroxide in the strong basic environment.

With glycerol, the three premises for Equation 2.22 to be valid vary compare to water. The first two become easier to satisfy because of the decreased k_L^0 caused by μ_L increase, while the last one is more important since alkalinity depletion should be greater in viscous liquid. Detailed correction of surface alkalinity depletion for caustic aqueous glycerol is addressed in section 3.2.4.

2.2 Models of Mass Transfer Area for Packings

There are many models in the literature that predict the mass transfer area of packings. Most of them concentrate on water or low-viscosity liquids that are commonly seen in the distillation process. The previous area models are generally inferred from measured volumetric mass transfer coefficient data (k_La_e or k_Ga_e), and assume either an area model or a film mass transfer coefficient model to be valid. Therefore, the area model and the film mass transfer coefficient model must be used together to obtain a proper value of the volumetric mass transfer coefficient. Therefore, the previously published area models should be used with caution when applying them to a reactive system. This review focused on those models that involved viscous liquids.

2.2.1 Area Model for Water-like Systems

The Onda model (1968b) is a comprehensive area model for water-like systems (ρ_L~1000 kg/m^3, μ_L~1 mPa·s, and σ~72 mN/m) focused on random packings in early years. The model assumes that the area is constrained by the metal surface area of the packings ($a_e < 1$):

$$\frac{a_e}{a_P} = 1 - \exp\left[-1.45\left(\frac{\sigma_c}{\sigma}\right)^{0.75}\left(\frac{\rho_L u_L}{a_P \mu_L}\right)^{0.1}\left(\frac{u_L^2 a_P}{g}\right)^{-0.05}\left(\frac{\rho_L u_L^2}{\sigma a_P}\right)^{0.2}\right] \tag{2.26}$$

Based on the SRP distillation databank and other external distillation data for various structured packings (Flexipac®, Gempak®, Mellapak®, etc), Rocha et al. (1996) developed a model of a_e based on the surface flow study made by Shi and Mersmann (1985):

$$\frac{a_e}{a_P} = 29.12 \cdot F_{SE} \cdot \left(\frac{\rho_L}{\sigma g}\right)^{0.15} \cdot \frac{u_L^{0.4} \nu_L^{0.2} s^{0.359}}{\varepsilon^{0.6} (\sin\alpha)^{0.3} (1 - 0.93\cos\gamma)} \tag{2.27}$$

$$\cos\gamma = 5.211 \times 10^{-16.835\sigma} \quad \text{(when } \sigma > 55 \text{ mN/m)} \tag{2.28a}$$

$$\cos\gamma = 0.9 \quad \text{(when } \sigma < 55 \text{ mN/m)} \tag{2.28b}$$

The F_{SE} is the correction factor that accounts for variations in surface enhancement based on observations in a surface flow study (McGlamery, 1988). Surface wettability was accounted for empirically using the contact angle γ.

Billet and Schultes (1993, 1999) developed semi-theoretical correlations for k_L and k_G based on the penetration theory. The area model was then developed fitting the area data obtained by separating the volumetric mass transfer coefficient with theoretical k_L and k_G:

$$\frac{a_e}{a_P} = 1.5 \cdot (a_P \cdot d_h)^{-0.5} \cdot \left(\frac{u_L d_h \rho_L}{\mu_L}\right)^{-0.2} \left(\frac{u_L^2 \rho_L d_h}{\sigma_L}\right)^{0.75} \left(\frac{u_L^2}{g d_h}\right)^{-0.45} \tag{2.29}$$

$$d_h = \frac{4\varepsilon}{a_P} \tag{2.30}$$

An extensive database was used for the model development with most of the data on random packings, and water-like systems. The Marangoni effect caused by the axial gradient of surface tension was accounted for by incorporating the Marangoni number.

The Delft model (Olujic, 1997; Olujic et al., 1999) was developed based on a computer simulation program that predicts both the hydraulic and mass transfer

performance of packings. The model uses a relatively simple equation to predict the packings area:

$$a_e = a_P \cdot \frac{1-\Omega}{1+\frac{C_1}{u_L^{C_2}}} \tag{2.31}$$

The model corrects for the void area (holes) on the packing surface by using the term **Ω**.

Several researchers (Dragan et al., 2000; Henriques de Brito et al., 1992; Weimer & Schaber, 1997) reported a_e by absorption of ambient (or air-diluted) CO_2 with caustic solutions (NaOH or KOH) in MellaPak® structured packings. Empirical correlations of a_e were developed based on the experimental data as a function of Reynolds number (Equation 2.32 by Henrique de Brito et al. and Equation 2.33 by Dragan et al.).

$$\frac{a_e}{a_P} = 0.465 \cdot Re^{0.3} = 0.465 \left(\frac{\rho_L u_L}{a_P \mu_L}\right)^{0.3} \tag{2.32}$$

$$\frac{a_e}{a_P} = 0.1245 \cdot Re^{0.4} = 0.1245 \left[\frac{6\rho_L u_L (1-\varepsilon)}{a_P \mu_L}\right]^{0.4} \tag{2.33}$$

The area calculated from the equations above is either unreasonably high (Equation 2.32) or too low (Equation 2.33).

2.2.2 Area Model for Liquid of Elevated Viscosity

Brunazzi et al. (1995) measured $K_G a_e$ by absorption of 1,1,1-trichloroethane with Genosorb 300, a viscous (μ_L = 7.7 mPa·s) mixture of polyethylene glycol dimethyl ethers, in a 0.1 m ID packed column with 1.9 m M 250Y as the internal. Correlations of mass transfer coefficients from Bravo et al. (1992) and liquid holdup from Suess and Spiegel (1992) were used to separate the a_e from the $K_G a_e$. The experimental a_e matches the theoretical model derived from liquid holdup h_L and film thickness δ:

$$\frac{a_e}{a_P} = \frac{d_h}{4} \cdot \left(\frac{h_L}{\varepsilon}\right)^{1.5} \cdot \left(\frac{\rho_L g \sin\alpha}{3\mu_L} \cdot \frac{\varepsilon \sin\alpha}{u_L}\right)^{0.5} \tag{2.34}$$

The model shows a negative 0.5 dependence of a_e on μ_L. However, this conclusion regarding the viscosity effect on the area is arguable for several reasons.

The size of the column is relatively small (0.1 m), which affects the representativeness of the experimental results due to the potentially greater wall flow in the small column. Moreover, viscosity was not varied to directly obtain its effect on mass transfer. The resistance of mass transfer in both phases is significant for the studied system (1,1,1-trichloroethane with Genosorb 300), which adds complexity and uncertainty to the analysis. The effective area, a_e, should be used with the k_L or k_G from the same source, since k_L and k_G are usually determined from a k_La and k_Ga measurement. Correlations of k_G, k_L, and h_L from different sources were used in this study, which may be problematic.

The Separations Research Program (SRP) has routinely performed packing characterization including measurement of a_e by absorption of ambient CO_2 into dilute NaOH. The experiments were conducted in the same column as used in this work, which is a 0.43-m ID column with 3 m maximum packing bed. Part of the data was reported in the theses of Wilson (2004), Tsai (2010), and Wang (2015). In some of the experiments of Tsai, 1–2 wt % polyethylene glycol (PEG) was added to the liquid to increase the μ_L to 5 and 12 mPa·s. Wetted-wall column (WWC) experiments were performed before the pilot test to confirm that the polymer would not affect the reaction kinetics in an measurable way. The a_e was not affected by μ_L variance up to 12 mPa·s under the preloading experimental condition. The correlation is shown in Equation 2.35 in a slightly modified form.

$$\frac{a_e}{a_P} = 1.34\left[\left(\frac{\rho_L}{\sigma}\right) g^{\frac{1}{3}} \left(\frac{u_L}{a_P}\right)^{\frac{4}{3}}\right]^{0.116} \tag{2.35}$$

2.2.3 Conclusions

There are many correlations to predict the a_e of packings. Most of them report the volumetric mass transfer coefficient, which is acceptable since it is usually the k_La or k_Ga that is of interest for column design. However, knowledge of the individual mass transfer property (a_e and k_L/k_G) will help with the fundamental understanding of the mass transfer process in the column as well as with the design of certain processes that require only individual mass transfer property (for example, only a_e is required for the absorber design in the post-combustion CO_2 amine capture process because of the established reaction kinetics). Separating k_L/k_G from a_e using simplified assumptions or data/correlation from other sources may confound the effect of experimental variable on each individual mass transfer property.

Earlier models mostly focus on random packings, while later ones start to emphasize structured packings. Despite the large number of a_e correlations, very few directly varied μ_L in the research, which makes their prediction of the viscosity effect suspect. Tsai (2010) showed that μ_L does not affect a_e from 1–12 mPa·s. On the basis of that, further study on the effect of μ_L on a_e is required with greater range of μ_L and probably with small-molecule viscosity enhancer for representativeness of the post-combustion amine capture process.

2.3 Models of Liquid Film Mass Transfer Coefficient for Packings

Similar to a_e, there are many correlations to predict k_L (k_La) for packings in the literature. Most of them studied only water-like system. This review does not try to cover all the correlations but focuses on those that involved viscous liquids.

In packed columns, μ_L affects k_L in two ways: directly through affecting the turbulence in the liquid phase, and indirectly via its influence on the diffusivity, D, of the mass transfer species. The direct influence should apply for all Newtonian liquids, while the indirect influence is system dependent. The total influence of μ_L on k_L is the sum of the two effects.

To illustrate the two effects, assume a k_L correlation of the simplified form of Equation 2.36, and D is a function of μ_L in the form of Equation 2.37. Combining the two equations gives Equation 2.38, in which ($\alpha+\beta\gamma$) refers to the total influence of μ_L on k_L, while α and $\beta\gamma$ refer to the direct and indirect influence, respectively. The ($\alpha+\beta\gamma$) can be determined from experimental data by varying μ_L. To obtain individual values for α and $\beta\gamma$, a reliable relationship between D and μ_L is required.

$$k_L = C_1 \mu^{\alpha} D^{\beta} \tag{2.36}$$

$$D = C_2 \mu^{\gamma} \tag{2.37}$$

$$k_L(k_L a) = C_1 C_2^{\beta\gamma} \mu^{\alpha+\beta\gamma} = C_3 \mu^{\alpha+\beta\gamma} \tag{2.38}$$

A comprehensive overview of liquid film mass transfer properties for packings can be found in the literature (Au-yeung & Ponter, 1983; Wang et al., 2005). Au-yeung and Ponter (1983) made a detailed review of k_L (k_La) models for packed columns before the 1980s. They pointed out that the lack of data for high viscosity liquids impedes a

thorough understanding of k_L. Wang et al. (2005) discussed k_L, k_G, and a_e correlations for both random and structured packings in literature, but did not focus on the effect of μ_L.

2.3.1 k_L Model for Water-like Systems

As early as 1940, Sherwood and Holloway measured k_La in a 0.5 m diameter column by air stripping of carbon dioxide, oxygen, and hydrogen from water. Liquid viscosity was slightly varied by changing the temperature 5–40 °C. The direct influence of μ_L on k_La (i.e. α) was found to change with packing from -0.04 to -0.28.

Van Krevelen and Hoftijzer (1947) include the effect of chemical reaction in their k_L correlation for different random packings. Data from a technical plant with 0.069 m ID together with other literature data were used to develop the correlation. k_L and a were separated by simply assuming that a_e is equal to a_p. The α was found to vary with Ha with an approximate value of -1/3.

Shulman and co-workers (1952; 1955), in a column with 0.25 m ID, measured k_G by vaporization of naphthalene packings with known surface area. The k_G correlation was used in conjunction with k_Ga data from Fellinger (1941) to obtain a_e, which was then used to separate k_L from k_La data of several investigators (Deed et al., 1947; Sherwood & Holloway, 1940; Vivian & Whitney, 1947; Whitney & Vivian, 1949). Their attempt to separate k_L and k_G from a_e by experimentally measuring a_e is an important contribution to the understanding of mass transfer in packed columns. However, as has been discussed previously, it might be problematic to mix mass transfer data from different sources where inconsistency in the experimental setup, chemical system, or analysis method/assumptions, always exist.

Davidson et al. (1959) proposed a theoretical k_La model based on the penetration theory for random packing with the assumption of laminar flow and complete liquid mixing. The packing surface was assumed to consist of a number of inclined surfaces with random angle and length. The model was later adopted and modified by several authors (Bridgwater & Scott, 1974; Echarte et al., 1984; Ponter & Au-Yeung, 1982). The α was -1/6 in this model and models derived from this one.

After comparing k_La data from multiple sources (Koch et al., 1949; Molstad et al., 1942; Rixon, 1948; Sherwood & Holloway, 1940), Norman (1961) concluded that the influence of types/families of random packings on k_La is remarkably small and a universal k_La correlation can be used for random packings. Direct dependence of k_La on μ_L was -0.25 in the correlation.

Onda and co-workers (1959; 1968a; 1967; 1968b) developed widely-accepted models of a_e and k_L for random packings by correlating extensive literature data and their own experimental data for gas absorption into water and organic solutions. The column ID was 6 cm in the experiment. Liquid viscosity did not vary significantly in any of the data sources for the correlation, which gives an α value of -0.83.

Linek et al. (1984) measured k_La for random packings by desorption of oxygen from water into pure nitrogen in a column with 0.29 m ID. Effective mass transfer area was determined by absorption of carbon dioxide into sodium hydroxide solutions. The overall mass transfer coefficient for this system with fast chemical reaction was known in a theoretical form (Sharma & Danckwerts, 1970), which was confirmed by experiments with the same system at packing surface with known interfacial area. This approach to measure a_e with a fast reaction system with known mass transfer rates enlightened future study of mass transfer in pilot-scale experiments to separate a_e from empirical data of k_La

and $k_G a$. The k_L data showed good agreement with the correlation of Onda et al (1968b). The α was -0.69 for this model.

Billet and Schultes (1992, 1993) developed a semi-theoretical k_L correlation based on the penetration theory. The model was correlated by examining an extensive data set involving different packings and systems. However, the range of μ_L was small (0.3-1.66 mPa·s), and the correlation requires knowledge of a packing-specific shape constant, which is not readily available for all packings. The model was updated (Billet & Schultes, 1999) by further enlarging the data base. The α was -1/6. This model may provide good prediction of mass transfer properties if shape constants of packing are known and when μ_L is close to that of water, but its reliability for viscous liquids is doubtful. The correlations take the form of Equations 2.39–41:

$$k_L = C_L \cdot 12^{1/6} \cdot \bar{u}_L{}^{1/2} \cdot \left(\frac{D_L}{d_h}\right)^{1/2} \tag{2.39}$$

$$d_h = \frac{4\varepsilon}{a_P} \tag{2.40}$$

$$\bar{u}_L = \frac{u_L}{h_L} = \frac{u_L}{\left(\frac{12}{g}\frac{\mu_L}{\rho_L} u_L a_P^2\right)^{1/3}} \tag{2.41}$$

Bravo et al. (1992) from SRP, systematically examined mass transfer for structured packings. The model of k_L was derived theoretically based on the penetration theory. The calculated HETP showed good agreement with the extensive literature data of distillation. The model was modified to included effects of characteristic packing dimension, effective fluid velocity, and contact time by other researchers (Rocha et al., 1996). The model is shown in Equations 2.42–44.

$$k_L = 2\left(\frac{D_L \cdot C_E \cdot U_{Le}}{\pi \cdot S}\right)^{0.5} \tag{2.42}$$

$$U_{Le} = \frac{U_{Ls}}{\varepsilon h_L \sin\alpha} \tag{2.43}$$

$$\cos\gamma = 5.211 \times 10^{-16.835\sigma} \ (\sigma > 0.055\ N/m) \tag{2.44}$$

The Delft model (Olujic, 1997; Olujic et al., 1999) was developed based primarily on distillation data. The model takes a form similar to that of Rocha (1996). Instead of using the corrugation side, *s*, as the characteristic length of packings, the hydraulic diameter (d_{hG}) was used:

$$k_L = 2\left(\frac{D_L \cdot U_{Le}}{0.9 \cdot \pi \cdot d_{hG}}\right)^{0.5} \tag{2.45}$$

$$\delta = \left(\frac{3 \cdot \mu_L \cdot u_{Ls}}{\rho_L \cdot g \cdot a_P \cdot \sin\alpha}\right)^{1/3} \tag{2.46}$$

$$d_{hG} = \frac{\frac{(bh-2\delta s)^2}{bh}}{\left[\left(\frac{bh-2\delta s}{2h}\right)^2 + \left(\frac{bh-2\delta s}{b}\right)^2\right]^{0.5} + \frac{bh-2\delta s}{2h}} \tag{2.47}$$

Valenz et al. (2011) measured k_La of an aqueous system with a_e obtained from absorption of carbon dioxide into sodium hydroxide solution. Strikingly large differences were found between k_La and a_e measured in the work and those predicted by three well-established correlations for structured packings (Billet & Schultes, 1999; Olujic et al., 1999; Rocha et al., 1996). The model takes a very simple form with only superficial liquid velocity included (Equation 2.48). Packing-specific parameters was assigned to different packings.

$$k_L a_e = a_1 \cdot u_L^{\alpha} \tag{2.48}$$

Recent packing characterization tests of SRP before this current study were performed by Wang and co-workers (2015; 2016). The same experimental setup was used in the study as in this work. The k_La of various structured and random packings were

measured in a 0.43-m ID column with 1.8 m packing bed by air stripping of toluene from water. The k_L was separated by using experimental a_e for each packing measured by caustic scrubbing of CO_2. A dimensionless number mixing point density, *Mi*, was used to represent the effect of packing geometry on mass transfer. Only water was used in the experiments.

2.3.2 k_L Model for Liquid of Elevated Viscosity

Norman and Sammak (1963a, 1963b) measured k_L in a 2.5-cm ID column by absorption of sulphur dioxide into water and carbon dioxide in different aqueous and organic solutions. They were the first to vary μ_L over a relatively large range (0.4–20 mPa·s). k_L and a were separated by a preliminary experiment observing the wetted percentage of packing surface as a function of liquid flow rate. Though the packing examined (vertical disc packing) is not commonly used, their endeavor to examine the specific influence of μ_L on k_L was a step toward a fundamental understanding of the mass transfer process. The α was -0.44 in this correlation.

Mohunta et al. (1969) measured k_L by desorption of carbon dioxide from water in a 0.1-m ID column installed with Raschig rings of various sizes. A few experimental runs were performed with increased μ_L using aqueous glycerol. The k_La with increased μ_L fitted well with a generalized correlation developed based on the bulk of the literature data. The correlation predicts that α is equal to -1.03. This appears to be the first attempt to vary μ_L by using aqueous glycerol, but the variance of μ_L is relatively small (0.73–1.48 mPa·s).

Mangers and Ponter (1980) were the first to systematically investigate the effect of μ_L on k_La. Absorption rates of carbon dioxide into pure water and aqueous glycerol were

measured in a 10-cm ID glass column with 1-cm glass Raschig rings. The range of μ_L (0.9-26 mPa·s) was significantly larger than previous investigators. They found a sharp transition point in the relation between k_La and L/μ_L. The transition was believed to result from whether the packing surface was fully wetted. The k_La correlations at both sides of the transition point were provided. The values of α were different before/after the transition point, but both were close to -0.6. Ponter and Au-yeung (1982) modified the model by introducing a mixing factor with more experimental data.

Echarte et al. (1984) examined the desorption of carbon dioxide from water and aqueous glycerol for k_L in a 0.4-m ID column with 0.058-m ceramic Raschig rings. The a_e was obtained in the same column by water cooling. The use of a_e data obtained from water for k_L of the much more viscous system assumes that a_e is not a function of μ_L, which needs further research. Compared to the experiment of Mangers and Ponter (1980), the range of μ_L (0.9–6.1 mPa·s) is smaller but the column size is larger. The correlation is a modification of the theoretical model of Davidson et al. with α equals to -0.46.

Delaloye et al. (1991) studied the effect of μ_L on k_La for 0.025-m glass Raschig rings by stripping oxygen from aqueous solutions with different viscosity enhancers including sodium alginate, glycerol, and polyethylene glycol (PEG). The range of μ_L was 0.8-9.6 mPa·s and the column ID was 0.3 m. The authors pointed out that, despite the large number of k_L correlations in literature, few of them gave reliable prediction on α, which was illustrated by the fact that even correlations that agreed for water-like viscosities diverged by an order of magnitude for μ_L of only 10 mPa·s. For sodium alginate and glycerol, α was found to be -0.52, which was in good agreement with the result of Echarte et al. For PEG, α was found to be -0.26. The authors attributed the discrepancy to the inaccuracy of D model for PEG and the fact that actual physical properties of the PEG sample might be different from those indicated by the manufacturer.

In the study of Brunazzi and co-workers (1997), the k_La was measured by absorption of chlorinated compounds into solvents with elevated μ_L (mixture of polyethylene glycol dimethylethers with μ_L of 4 and 7.7 mPa·s). The packing height was varied from 0.42–1.89 m. The k_L was separated from k_La_e by using the area correlation developed in a previous study with the same column and system (Brunazzi et al., 1995). Packing-specific parameters were assigned to different packings (metal/plastic M 250Y, and Sulzer BX plastic gauze packing). The k_L correlation suggests a positive value of α (0.7) for M 250Y, which is unreasonable since the increased viscosity is supposed to impede liquid film mass transfer. The positive α probably results from confounding the effects of μ_L on a_e and k_L, considering the negative dependence on μ_L of a_e predicted in the area model which uses external correlations for liquid holdup and mass transfer coefficient.

2.3.3 Conclusions

Despite the large number of k_L (k_La) models in literature, few of them provide reliable prediction on how μ_L will affect k_L because of two major problems:

- The total effect of μ_L on k_L ($\alpha + \beta\gamma$) was not correlated from actual variance of μ_L in the experiment.
- The direct (α) and indirect ($\alpha + \beta\gamma$) effects were not correctly separated.

To illustrate the first problem, assume k_L correlation takes the form of Equation 2.49a, which is equivalent to Equation 2.49b when dimensionless groups are expanded. In Equation 2.49b, the total influence of μ_L on k_L is (b-a), which is determined by exponents on Re (a), and Sc (b). Typically a is correlated by varying the liquid flowrate, and b is directly assigned the value of 0.5 in order to satisfy the 0.5 dependence on D_L dictated by penetration theory (Higbie, 1935). As a result, the μ_L term only appears in Equation 2.49a

as a part of dimensionless groups without being empirically varied. The α obtained this way is obviously not reliable.

$$Sh = Sh_0 \left(\frac{Re}{Re_0}\right)^a \left(\frac{Sc}{Sc_0}\right)^b \tag{2.49a}$$

$$k_L = k_L^0 \left(\frac{d}{d_0}\right)^{a-1} \left(\frac{\rho}{\rho_0}\right)^{a-b} \left(\frac{u}{u_0}\right)^a \left(\frac{D}{D_0}\right)^{1-b} \left(\frac{\mu}{\mu_0}\right)^{b-a} \tag{2.49b}$$

The second problem arises from the accuracy of the D_L model. This is important because what is measured experimentally is the overall effect of μ_L, thus the inaccuracy of $\beta\gamma$ will lead to a corresponding inaccuracy of α. Though the 0.5 dependence (β) has been confirmed by Vivian and King (1964) via desorption of different gases from water in a packed column, an accurate/detailed D-μ relationship is still lacking in most of the models, which makes the value of γ suspect, especially for viscous liquid where the D_L can be orders of magnitude smaller than that in water. Therefore, a good understanding of the D-μ_L relationship is crucial to correctly separate the indirect and direct influence of μ_L on k_L.

Figure 2.3 summarizes the predicted value of α in the k_L (k_La) correlations in the literature (Table 2.1). The drastic disagreement on α (-1.03 to 0.7) implies the unreliability of the existing models. For the few correlations in which μ_L was varied over a relatively large range (solid points in the figure), either the column size is too small to be representative of an industrial-scale situation considering the wall/end effect, or only random packings were investigated.

A systematic investigation of the effect of μ_L on k_L in columns with random and structured packings is necessary. The ideal research should include a comprehensive packing database, relatively large-scale column, individually determined a_e at elevated μ_L, and a relatively simple form of the correlation without incorporating packing-specific parameters.

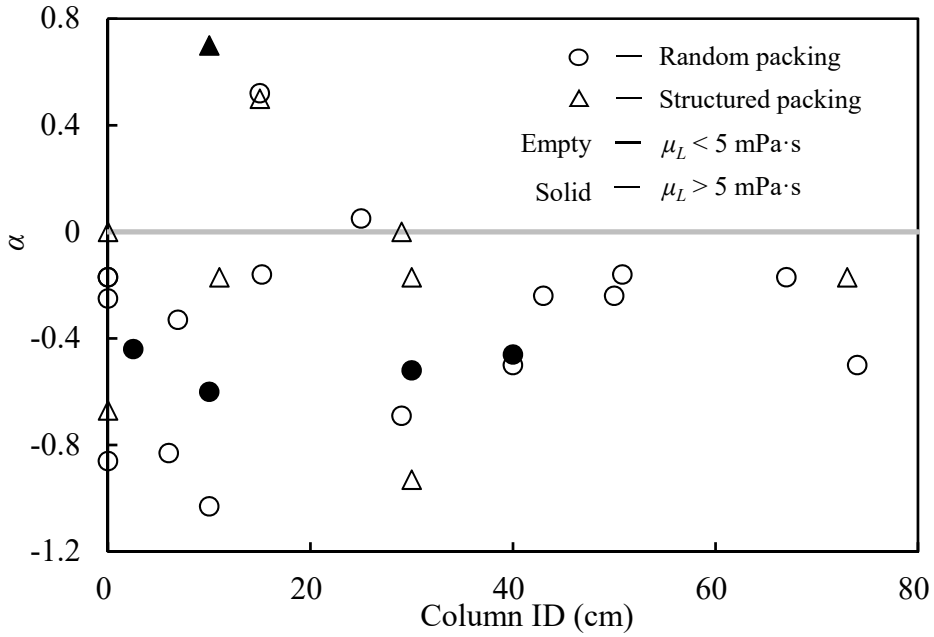

Figure 2.3: Predictions of α for k_L ($k_L a_e$) correlations in literature

Table 2.1: Detailed information of k_L (k_La_e) correlations in literature in Figure 2.3

Year	Author	k_L or k_La	α	β	ID (cm)	Packing	$\Delta\mu_L$ > 5 cP?	system
1940	Sherwood & Holloway	k_La	-0.16	0.5	50.8	random	No	$CO_2/O_2/H_2 + H_2O$ + Air
1942	Molstad et al.	k_La	-0.24	0.5	50	random	No	$O_2 + H_2O$ + Air
1947	Van Krevelen and Hoftijzer	k_L	-0.33	0.67	6.9	random	No	$CO_2 + H_2O$ + Air; O_2 + susp. Purssian white + Air; CO_2 + carbonate soln.; CO_2 + NaOH soln.
1947	Deed et al.	k_La	-0.16	0.5	15.2	random	No	$CO_2/O_2 + H_2O$ + Air
1954	Knoedler and Bonilla	k_La	0.52	0.47	15	random	No	$O_2 + H_2O$ + Air
1955	Shulman et al.	k_L	0.05	0.5	25	random	No	$CO_2/O_2/H_2 + H_2O$ + Air
1959	Davidson et al.	k_La	-0.17	0.5	N/A	random	N/A	N/A
1960	Cornell et al.	k_La	-0.50	0.5	5-76	random	No	$CO_2/O_2/H_2 + H_2O$ + Air
1961	Norman	k_La	-0.25	0.5	0	random	No	$CO_2/O_2/H_2 + H_2O$ + Air
1963	Norman & Sammak	k_L	-0.44	0.5	2.5	random	Yes	$SO_2 + H_2O$; CO_2 + aqueous/organic solutions
1968	Onda et al.	k_L	-0.83	0.5	6	random	No	$CO_2/H_2 + H_2O$; $CO_2/O_2/H_2$ +
1969	Mohunta & Laddha	k_L	-1.03	0.5	10	random	No	CO_2 + (H_2O+glcerol) + Air
1974	Bridgwater & Scott	k_La	-0.17	0.5	N/A	random	N/A	N/A
1980	Mangers & Ponter	k_La	-0.60	0.5	10	random	Yes	$CO_2 + H_2O$ + glycerol
1982	Bolles & Fair	k_La	-0.50	0.5	25-122	random	No	Multiple

Table 2.1 (Cont'd): Detailed information of k_L (k_La_e) correlations in literature in Figure 2.3

Year	Author	k_L or k_La	α	β	I.D. (mm)	Packing	$\Delta\mu_L$ > 5 cP?	System
1982	Ponter & Au-yeung	k_La	-0.86	0.5	0	random	No	CO_2 + H_2O + glycerol
1984	Linek et al.	k_La	-0.69	0.5	29	random	No	O_2+H_2O+N_2
1984	Echarte et al.	k_L	-0.46	0.5	40	random	Yes	CO_2 + (H_2O+glycerol) + Air
1991	Delaloye et al.	k_La	-0.52	0.5	30	random	Yes	O_2 + (H_2O+sodium alginate/glycerol/polyethylene glycol) + Air
1999	Billet & Schultes	k_L	-0.17	0.5	6-140	random & structured	No	Multiple
2011	Maćkowiak	k_L	-0.17	0.5	15-120	random	No	CO_2 + H_2O + Air
1985	Bravo et al.	k_L	-0.17	0.5	7-15	random & structured	No	Multiple distillation systems
1993	Weiland et al.	k_L	0.50	0.5	15	structured	No	CO_2 + NaOH/(Na_2CO_3+$NaHCO_3$) solution + Air
1994	Hanley et al.	k_L	0.00	0.5	N/A	random & structured	N/A	N/A
1997	Brunazzi and Paglianti	k_L	0.70	~0.2	10	structured	Yes	CO_2 + H_2O + Air; chlorinated compounds + mixture of polyethylene glycol dimethylethers
1999	Maćkowiak	k_L	-0.93	0.5	30	structured	No	CO_2 + H_2O + Air
2004	Murrieta et al.	k_L	-0.17	0.5	30	structured	No	CO_2 + H_2O + Air
2011	Valenz et al.	k_La	N/A	N/A	29	structured	No	O_2 + H_2O + Air
2012	Hanley & Chen	k_L	-0.67	0.67	0	random & structured	No	Multiple

2.4 STUDIES ON GAS FILM MASS TRANSFER COEFFICIENT FOR PACKINGS

Although k_G is not the primary focus of this work, a modified k_G model was developed by the author with an expanded database. Therefore, a brief review of k_G correlations in the literature is made here for a comprehensive view of the methods of packing characterization.

Mehta and Sharma (1966) measured k_Ga by absorption and vaporization with a gas-film controlled process in a 5.2-cm ID bubble column. Fourteen-fold gas diffusivity was achieved by matching various solutes (sulfur dioxide, chlorine, Freon-22, and Freon-114) and carrier gases (including ammonia, sulphur dioxide, and chlorine). The results confirm the square root dependence on D_G of k_Ga in the bubble column, which is believed to be applicable to packed columns as well.

Onda and co-workers (1968b) developed a k_G correlation based on k_Ga data from various external sources for random packings together with their own a_e model. The model is shown in Equation 2.50. The prefactor is changed to 2.00 for Raschig rings and Berl saddles smaller than 15 mm. The model was confirmed by data from water vaporization experiments.

$$\frac{k_G}{a_P D_G} = 5.23 \cdot \left(\frac{u_G \rho_G}{a_P \mu_G}\right)^{0.7} \cdot \left(\frac{\mu_G}{\rho_G D_G}\right)^{\frac{1}{3}} \cdot (a_P d_P)^{-2} \tag{2.50}$$

Moucha et al. (2005) measured k_Ga in a 0.29-m ID column packed with 0.5 m bed of random packings (IMTP 25, 40, and 50). The system used was chemical absorption of air-diluted SO_2 into 1 N NaOH. The k_Ga_e was regressed in a simplified form as the exponential function of superficial gas velocity.

In the Delft model (1999), k_G is described as the average of the laminar and turbulent regime contributions as a function of *Re*, *Sc*, and hydraulic diameters. Billet and Schultes (1993, 1999) developed their k_G model similar to k_L. The model is a semi-

theoretical one based on the penetration theory. The model is shown in Equation 2.51. The hydraulic diameter, d_h, is the same with Equation 2.40. A packing-specific parameter, C_G, is required in the model.

$$k_G = C_G \frac{1}{(\varepsilon - h_L)^{1/2}} \left(\frac{a_P}{d_h}\right)^{1/2} D_G \left(\frac{u_G \rho_G}{a_P \mu_G}\right)^{3/4} \left(\frac{\mu_G}{\rho_G D_G}\right)^{1/3} \quad (2.51)$$

Chapter 3: Experimental Methods[2]

The experimental equipment, protocol, concerns, and chemical system are summarized in this chapter. The overall research approach is shown in Table 3.1. The effect of the viscosity enhancer on the reaction kinetics of CO_2/NaOH/H_2O was first examined in a bench-scale wetted-wall column (WWC). If the viscosity enhancer has a significant effect on k_g', kinetic model would be developed. The a_e was then measured in the pilot-scale packed column using the same reactive system to investigate the effect of μ_L on area. If μ_L did not affect a_e significasntly, the a_e for water would be used to separate k_L from k_La, which was measured by air stripping of toluene from water and viscosity enhancer.

Table 3.1: Overall research plan

Stage	1	2	3
Target data	k_g'	a_e	k_L
Objective	Provide kinetic data for stage 2	Confirm the effect of μ_L on a_e	Provide raw data for k_L correlation
System	CO_2/NaOH/H_2O + viscosity enhancer	CO_2/NaOH/H_2O + viscosity enhancer	Air/Toluene/H_2O + viscosity enhancer
Equipment	WWC	Pilot PVC column	Pilot PVC column
Packing	N/A	Structured, random, and hybrid packings	
Range of μ_L	0.9–70 mPa·s	0.9–70 mPa·s	0.9–70 mPa·s

[2] D. Song, A.F. Seibert, G.T. Rochelle, "Effect of liquid viscosity on mass transfer area and liquid film mass transfer coefficient for GT-OPTIMPAK 250Y." Energy Proc. (in press)

3.1 LIQUID VISCOSITY ENHANCER

3.1.1 Candidates of Viscosity Enhancer

Candidates for liquid viscosity enhancer include glycerol as a small molecule like amine and polymers such as polyethylene glycol (PEG) and polyvinyl alcohol (PVA). Glycerol was used by several previous researchers in separations research (Delaloye et al., 1991; Echarte et al., 1984; Mangers & Ponter, 1980; Mohunta et al., 1969), and PEG (POLYOX^{TM} WSR N750) was used by Tsai (2010) in some of his experiments. Comparison of glycerol and PEG is summarized in Table 3.2.

Glycerol was chosen as the liquid viscosity enhancer because it dissolves readily in water, is relatively cheap and safe, and provides Newtonian behavior (Dontula et al., 1999). The last property guarantees that the μ_L measured offline by the viscometer is identical with the actual μ_L of the liquid film on the packing surface, and that the fluid exhibits the same μ_L in the WWC and pilot column experiments regardless of the shear rate. Glycerol does not change the controlling mechanism for mass transfer. For air stripping of toluene, though the addition of glycerol deceases the infinite dilution activity coefficient of toluene, it is still well above 100 at the highest proposed glycerol concentration (Figure 3.1). Moreover, the elevated μ_L will also ensure the tripping process is liquid film controlled. For the reactive system, CO_2/NaOH/H_2O/glycerol, the effect of physical liquid film mass transfer (i.e. surface depletion of alkalinity) has been corrected in the kinetic model and is believed not to be an issue for the packed column experiments considering the relatively low CO_2 concentration and flux.

Another advantage of glycerol is its complete solubility and easy dissolution in water. Special techniques are needed for PEG to avoid agglomeration, which makes dissolution much longer than expected. Preliminary dissolution experiments for PEG

showed that once the μ_L is above 10–15 mPa·s, the dissolution rate became unacceptably low.

Table 3.2: Comparison of viscosity enhancer candidates

Chemical	Glycerol	PEG (POLYOX™ WSR N750)
M (g/mol)	92.09	Approx. 300,000[1]
Approx. wt % to reach 100 mPa·s at 25 °C	88[2]	3.3[3]
Solubility in water	Complete	Greater than 5 wt %[4]
Dissolution in water	Easy	Special technique needed[4]
Rheological behavior	Newtonian	Pseudoplastic[5]
Bacteria growth	No (Rochelle et al., 2014)	No[6]
Influence on D	Significant	Limited
Compatibility with present testing systems[7]	Yes	Yes

[1] Data from Dow (http://www.dow.com/products)
[2] Data from Dow (http://msdssearch.dow.com)
[3] Extrapolated from raw data of Dow (http://dowwolff.custhelp.com)
[4] Data and information from Dow (http://msdssearch.dow.com)
[5] Data from Dow (http://dowwolff.custhelp.com)

One disadvantage of glycerol is that, as a small molecule, it will influence both μ_L and D significantly. Therefore, knowledge of $D_{Toluene}$ in the aqueous glycerol is needed to separate the direct and indirect influence of μ_L on k_L. For polymers like PEG, diffusivity will not change significantly when μ_L increases since the long polymer chain

will only affect bulk viscosity not local viscosity (Lohse et al., 1981). Because polymers are chemically inert and do not affect the diffusivity of CO_2, the addition of PEG will not affect the k_g' for CO_2/NaOH/H_2O (Tsai, 2010). However, for glycerol, its nature as a weak acid as well as its effect on D_{CO2} make a kinetic study necessary prior to pilot-scale experiments.

Another disadvantage of glycerol is that it is likely to induce bacteria growth as a carbohydrate. However, sterilization experiments were performed to show that no significant bacteria growth was observed at room temperature for the proposed concentrations of glycerol.

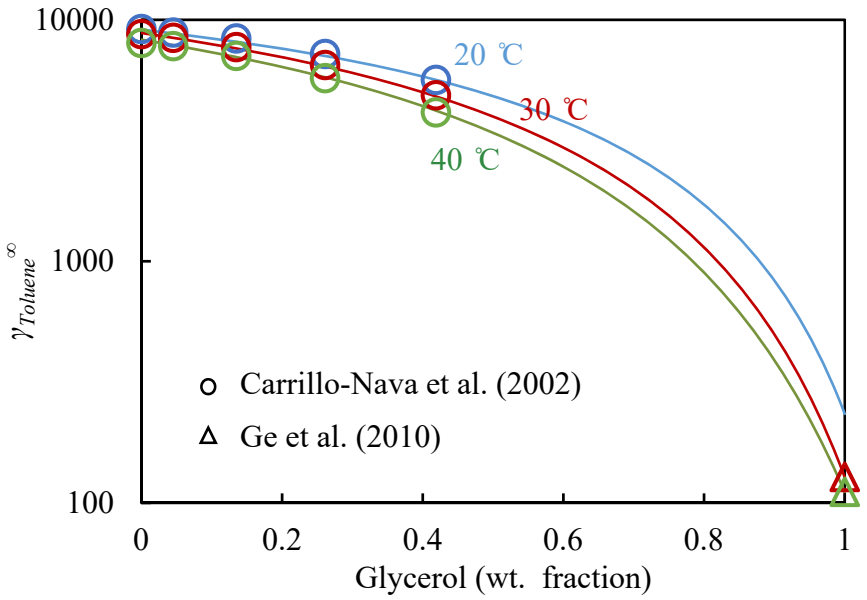

Figure 3.1: Infinite-dilution activity coefficient of toluene in aqueous glycerol (lines are calculated value based on model in section 3.1.2)

3.1.2 Physical Properties of Aqueous Glycerol

Knowledge of the physical properties of glycerol and its aqueous solution is important for data analysis of both the kinetic and mass transfer experiments. Models of density (ρ_L), viscosity (μ_L), surface tension (σ), diffusivity of CO_2 and toluene (D), Henry's constant of CO_2 (H_{CO2}), and infinite dilution activity coefficients of toluene (γ) of aqueous glycerol are summarized in this section. The models are either regressed from literature data or modified based on correlations available in the literature.

3.1.2.1 Density and Viscosity

The model developed by Cheng (2008) was used to calculate the density (Equations 3.1–3.3) and viscosity (Equations 3.4–3.9) of aqueous glycerol. The temperature in the equations is °C. The calculated values match well with the measured values of liquid samples from WWC experiments (Figure 3.2). As can be seen in the figure, μ_L increases exponentially with increasing glycerol. Ions with approximately 0.1 N concentration will increase μ_L by 5–10 %. Ions up to 0.7 N have relatively small influence on density (Takamura et al., 2012).

$$\rho_{aq} = \rho_g w_g + \rho_w (1 - w_g) \tag{3.1}$$

$$\rho_g = 1277 - 0.654T \tag{3.2}$$

$$\rho_w = 1000 \left[1 - \left(\frac{T-4}{622}\right)^{1.7}\right] \tag{3.3}$$

$$\mu_{aq} = \mu_w^{\alpha}\, \mu_g^{(1-\alpha)} \tag{3.4}$$

$$\mu_w = 1.79\, exp\left(\frac{(-1230-T)T}{36100+360T}\right) \tag{3.5}$$

$$\mu_g = 12100\, exp\left(\frac{(-1233+T)T}{9900+70T}\right) \tag{3.6}$$

$$\alpha = 1 - w_g + \frac{abw_g(1-w_g)}{aw_g+b(1-w_g)} \tag{3.7}$$

$$a = 0.705 - 0.0017T \tag{3.8}$$

$$b = (4.9 + 0.036T) \cdot a^{2.5} \tag{3.9}$$

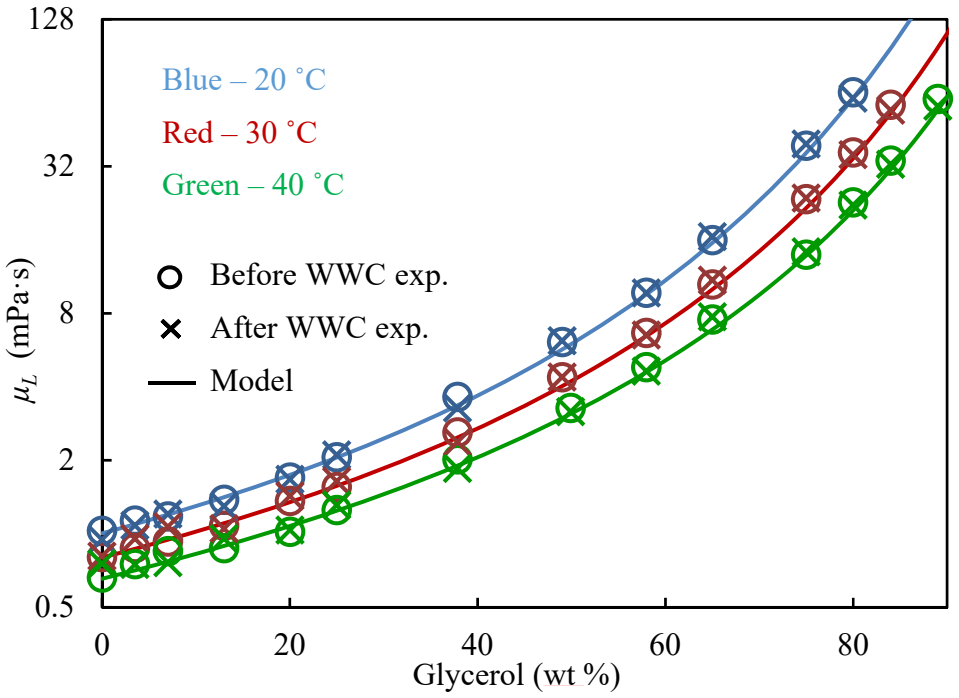

Figure 3.2: Measured and calculated μ_L of aqueous glycerol

3.1.2.2 Surface Tension

An empirical model of surface tension for aqueous glycerol was developed based on the experimental data of Takamura et al (2012). The model is shown in Equations 3.10–3.12. Temperature in the model is °C. Experimental and calculated σ is compared in Figure 3.3. Though σ decreases with increasing glycerol, the σ for the aqueous solution is still close to that of water.

$$\sigma_{aq} = \sigma_w + aw_g \tag{3.10}$$

$$\sigma_w = 71.7 - 0.0145(T - 30) \tag{3.11}$$

$$a = 0.058T - 8.6 \tag{3.12}$$

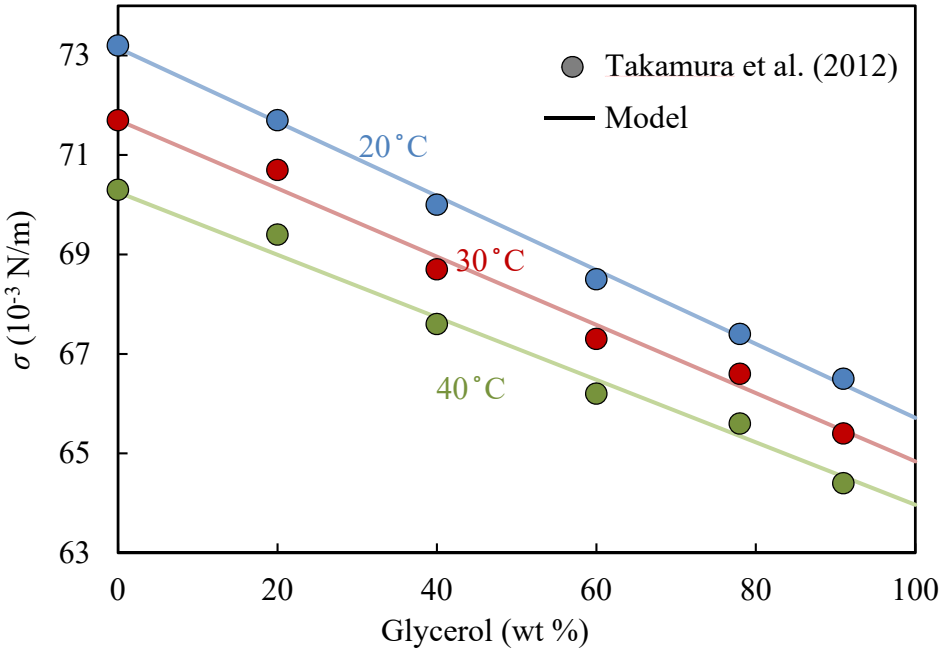

Figure 3.3: Measured and calculated σ of aqueous glycerol

3.1.2.3 Henry's constant of CO_2

The H_{CO2} model of aqueous glycerol (Equations 3.13, 3.14, and Table 3.3) was developed based primarily on the experimental data from Buzek and Jaroszynski (1973) together with data from other sources (Laddha et al., 1981; Rischbieter et al., 1996; Vazquez Una et al., 1994). The unit for HCO2 in the model is atm·L/mol. The H_{CO2} of pure water and pure glycerol used for model development was calculated from models of Pohorecki and Moniuk (1988), and Ostonen et al. (2014), respectively. Compared to

glycerol, the effect of ions on H_{CO2} is relatively small (< 10 %) according to Pohorecki and Moniuk (1988), and thus not included.

As is shown in Figure 3.4, H_{CO2} increases with increasing glycerol. The model fits the experimental data fairly good except for pure glycerol. Since the proposed glycerol range was 0–89 wt % in this work, the discrepancy of the model for pure glycerol should not affect its reliability significantly.

$$\log\frac{H_{CO_2,aq}}{H_{CO_2,w}} = (Aw_g + B\ln(w_g+1) + C ln^2(w_g+1)) \times \left(\frac{D}{T(°C)} + E + FT(°C) + G\ln T(°C)\right) \quad (3.13)$$

$$\log H_{CO_2,w} = -7.8857 \times 10^{-5}T(K)^2 + 5.9044 \times 10^{-2}T(K) - 9.1229 \quad (3.14)$$

Table 3.3: Parameters in H_{CO2} model of aqueous glycerol

Parameter	A	B	C	D	E	F	G
Value	3.28	-3.43	-2.26	14.6	-7.09	-0.00416	1.51

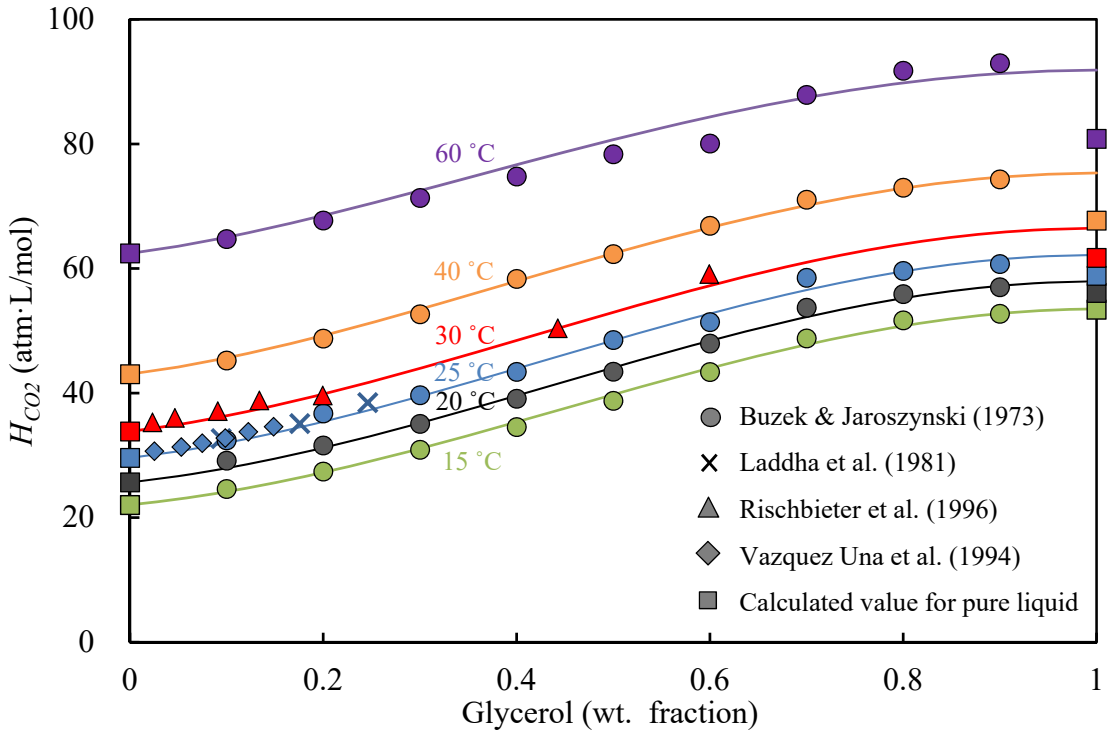

Figure 3.4: Experimental and calculated H_{CO2} over aqueous glycerol

3.1.2.4 Diffusion coefficient

Mutual diffusivity of glycerol and water, and diffusivity of CO_2 and toluene in aqueous glycerol are important to interpret the kinetic and mass transfer data obtained in experiments. Popular models such as the one proposed by Wilke and Chang (1955) are based mainly on liquid with relatively low viscosity and significantly underestimates diffusivity when the solvent viscosity is high (Hayduk & Cheng, 1971). Limited data on diffusion in viscous liquids (especially aqueous glycerol) is found in the literature. Most investigated the diffusion of ions rather than molecules such as toluene. Models of diffusivity in aqueous glycerol are developed based on available literature data.

The correlation of mutual diffusion coefficient of water and glycerol, $D_{g\text{-}w}$, is developed based on various literature sources (D'Errico et al., 2004; Garner & Marchant, 1961; Grossmann & Winkelmann, 2005; Nishijima & Oster, 1960; Riede & Schlunder, 1991; Rutten, 1992; Ternström et al., 1996). The mutual diffusivity was used to calculated the depletion of surface alkalinity in the analysis of WWC data (section 3.2.4.2). The model (Equation 3.15) is compared with experimental data in Figure 3.5. In the model, the units of temperature, viscosity, and diffusivity are °C, mPa·s, and m^2/s, respectively.

$$D_{g-w} = 3.4 \times 10^{-10} \cdot T^{0.313} \cdot \mu^{-0.556} \tag{3.15}$$

The diffusivity of CO_2 in water is calculated by Equations 3.16 using the model of Pohorecki & Moniuk (1988). A -0.7 dependence on μ_L is added to calculate the diffusivity of CO_2 in aqueous glycerol (Equation 3.17). The dependence is obtained by least-square fitting of experimental data in the literature for not only CO_2 but also other solutes (including O_2, N_2O, Sucrose, Urea, C_2H_4, and NaCl) in aqueous glycerol (Brignole & Echarte, 1981; Calderbank, 1959; Hoshino et al., 1972; Jordan et al., 1956; Jordan & Bauer, 1959; Kreulen et al., 1993; Laddha et al., 1981; Nogami & Kato, 1962; Onda, 1961; Thomas & Adams, 1965). Figure 3.6 shows the -0.7 μ_L dependence of diffusivity in aqueous glycerol in general, and Figure 3.7 shows the diffusivity of CO_2 in aqueous glycerol, specifically.

$$\log_{10} D_{CO_2,H_2O} = -8.1764 + \frac{712.5}{T} - \frac{2.591\times10^5}{T^2} \tag{3.16}$$

$$D_{CO_2,Gly} = D_{CO_2,H_2O} \times \left(\frac{\mu_{H_2O}}{\mu_{Gly}}\right)^{0.7} \tag{3.17}$$

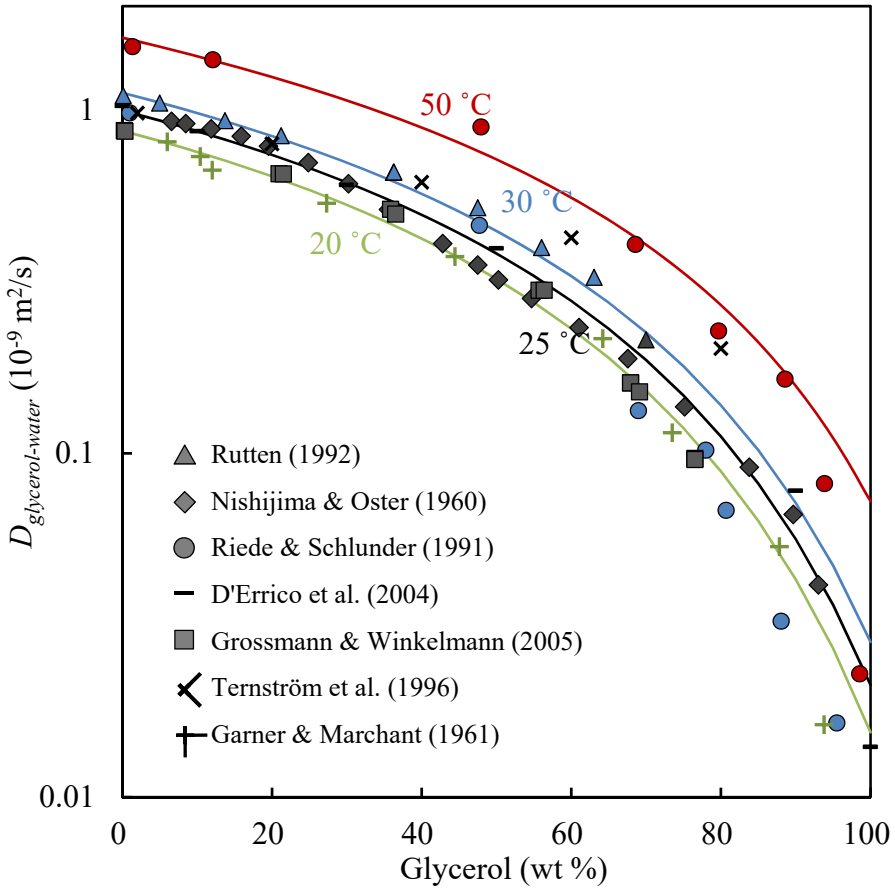

Figure 3.5: Experimental and calculated mutual diffusivity of glycerol and water

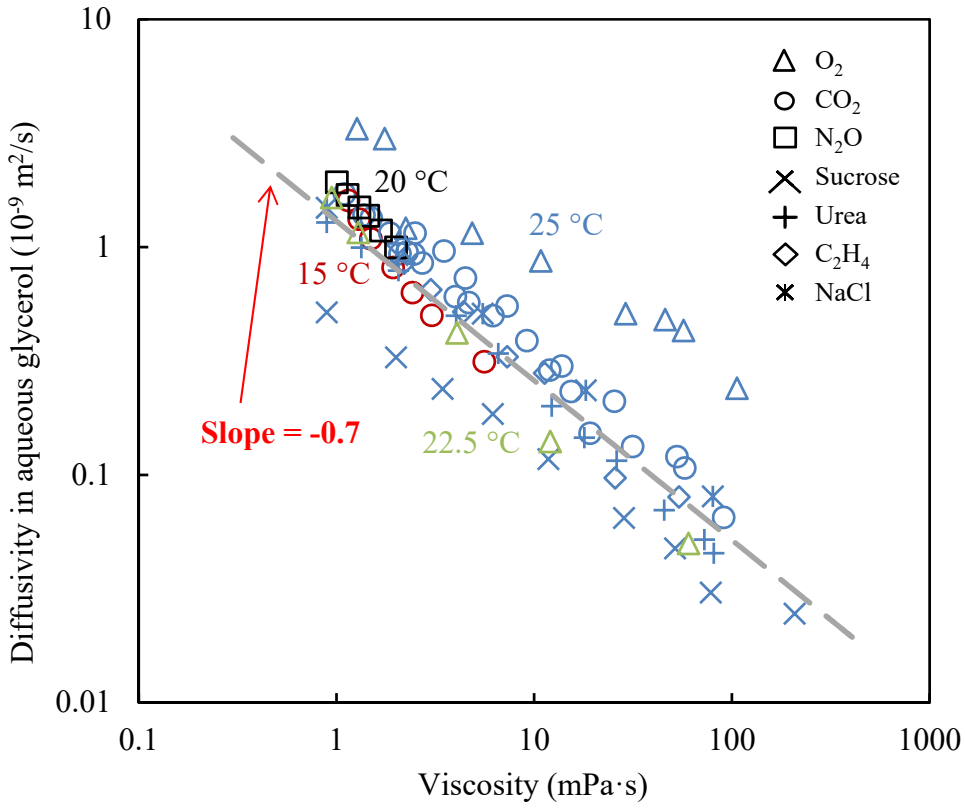

Figure 3.6: The D-μ_L relationship in aqueous glycerol in general
Literature data from (Brignole & Echarte, 1981; Calderbank, 1959; Hoshino et al., 1972; Jordan et al., 1956; Jordan & Bauer, 1959; Kreulen et al., 1993; Laddha et al., 1981; Nogami & Kato, 1962; Onda, 1961; Thomas & Adams, 1965)

It is notable that available experimental data of D_{CO2} in aqueous glycerol are rather limited with full-range data at only one temperature (25 °C). However, the model is believed to be reliable considering the uniform -0.7 μ_L dependence of diffusivity in aqueous glycerol observed with various solutes at various temperatures in Figure 3.6. The model is used in interpreting the kinetic data from the WWC experiments and provided reasonable results which is shown in Chapter 4. The effect of NaOH ions on D_{CO2} is negligible compared to the calculated effect of glycerol (Onda et al., 1960; Versteeg & Van Swaalj, 1988).

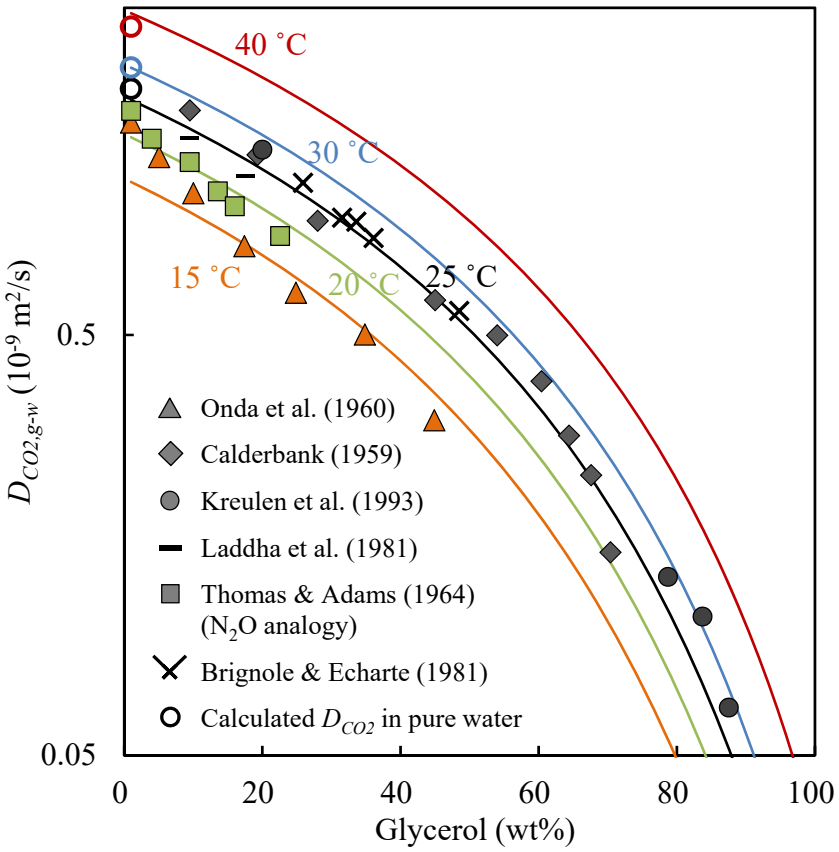

Figure 3.7: Experimental and calculated diffusivity of CO_2 in aqueous glycerol

The diffusivity of toluene in aqueous glycerol is calculated by Equation 3.18. No literature data is found for this specific system, so the model assumes that diffusivity ratio of CO_2 and toluene is the same in aqueous glycerol as in pure water. The assumption is similar to that of N_2O analogy of amine solutions (Versteeg & Van Swaalj, 1988), however, without support of experimental data. It is recommended that the model be checked with experimental data, but it is not in the scope of this work. Relating the diffusivity of a gaseous molecule with a liquid one is reasonable because once in solution, these all form true liquid state solutions (Hayduk & Cheng, 1971).

$$D_{tol,Gly} = D_{CO_2,gly} \times \left(\frac{D_{tol,H_2O\ 25℃}}{D_{CO_2,H_2O\ 25℃}}\right) \tag{3.18}$$

3.1.2.5 Activity Coefficient

Parameters of NRTL (Equations 3.19–3.22) and UNIQUAC (Equations 3.23–3.27) models for water and glycerol are correlated based on literature data of activity coefficient (Zaoui-Djelloul-Daouadji et al., 2014). The parameters are summarized in Table 3.4. Figure 3.8 compares the predicted and experimental values.

$$\ln \gamma_i = x_j^2 \left[\tau_{ji}\left(\frac{G_{ji}}{x_i + x_j G_{ji}}\right)^2 + \frac{\tau_{ij} G_{ij}}{\left(x_j + x_i G_{ij}\right)^2}\right] \tag{3.19}$$

$$\ln G_{ij} = -\alpha_{ij}\tau_{ij} \tag{3.20}$$

$$\alpha_{ij} = \alpha_{ji} \tag{3.21}$$

$$\tau_{ij} = A_{ij} + \frac{B_{ij}}{T} \tag{3.22}$$

$$\ln \gamma_i = \ln \frac{\Phi_i}{x_i} + \left(\frac{Z}{2}\right) q_i \ln \frac{\theta_i}{\Phi_i} + \Phi_j \left(l_i - \frac{r_i}{r_j} l_j\right) - q_i \ln\left(\theta_i + \theta_j \tau_{ji}\right) + \theta_j q_i \left(\frac{\tau_{ji}}{\theta_i + \theta_j \tau_{ji}} - \frac{\tau_{ij}}{\theta_j + \theta_i \tau_{ij}}\right) \tag{3.23}$$

$$\Phi_i = \frac{r_i x_i}{r_i x_i + r_j x_j} \tag{3.24}$$

$$\theta_i = \frac{q_i x_i}{q_i x_i + q_j x_j} \tag{3.25}$$

$$\ln \tau_{ij} = A_{ij} + \frac{B_{ij}}{T} \tag{3.26}$$

$$l_i = \left(\frac{Z}{2}\right)(r_i - q_i) - (r_i - 1) \tag{3.27}$$

Table 3.4: NRTL and UNIQUAC[a] parameters for aqueous glycerol

Model[b]	A_{12}	A_{21}	B_{12}	B_{21}	α_{12}	Z	σ^{2} [c]	AAD[d]
NRTL	0.0933	-0.8763	752.1	-193.3	0.4757	-	0.00103	2.93%
UNIQUAC	-0.0101	1.9212	537.9	-284.4	-	10	0.7181	1.39%

[a] Van der Waals parameters were obtained from Aspen Plus®: $q_1 = 1.4$, $q_2 = 3.06$, $r_1 = 0.92$, $r_2 = 3.385$; [b] subscript 1 = water, 2 = glycerol; [c] $\sigma^2 = \sum(\gamma_{calc} - \gamma_{expt})^2/(\text{no. of data points} - \text{no. of parameters})$; [d] $AAD = (100\%/(\text{no. of data points}))\sum(|\gamma_{calc} - \gamma_{expt}|/\gamma_{expt})$

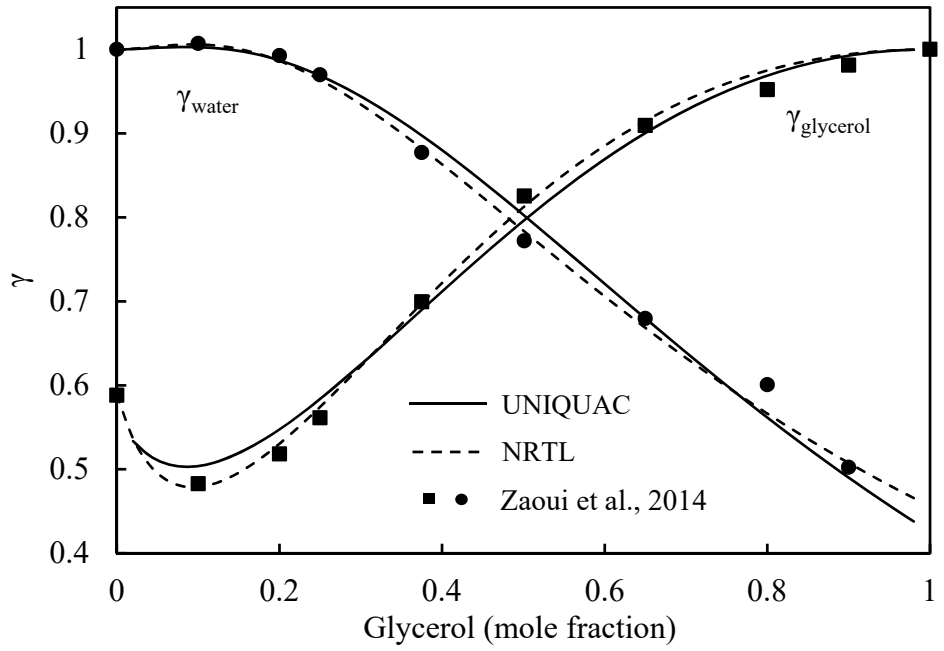

Figure 3.8: Activity coefficient of water and glycerol at 20 °C

The infinite dilution activity coefficient of toluene in aqueous glycerol is calculated by Equations 3.28–3.30. Parameters in the equations are shown in Table 3.5. The model is modified based on the one developed by Carrillo-Nava et al. (2002). Per Figure

3.1, though the addition of glycerol deceases the infinite dilution activity coefficient of toluene, it is still well above 100 at the highest proposed glycerol concentration.

$$\ln \gamma^{\infty}_{Tol,\,aq} = \ln \gamma^{\infty}_{Tol,\,H_2O} + (a + b/\tau + c \ln \tau) x_{Gly} + (d + e/\tau + f \ln \tau) x^2_{Gly} \quad (3.28)$$

$$\ln \gamma^{\infty}_{Tol,\,H_2O} = A + B/\tau + C \ln \tau \quad (3.29)$$

$$\tau = T(K)/298.15 \quad (3.30)$$

Table 3.5: Parameters in the model of $\gamma^{\infty}_{Tol,\,aq}$

Parameter	A	B	C	a	b	c	d	e	f
Value	39.9	-30.8	-31.8	-373.7	369.2	337.1	-82.0	82.4	97.6

3.1.3 Experimental Concerns of Aqueous Glycerol

3.1.3.1 Material Compatibility

A compatibility check of aqueous glycerol with the materials of the experimental equipment (such as 304 stainless tube in the WWC, Viton of O-ring in the pump, and polyvinylchloride as the pilot column body) is summarized in Table 3.6. Detailed information can be found at various online resources (http://www.fmctechnologies.com, http://spectrumlabs.com, http://www.vp-scientific.com, http://sevierlab.vet.cornell.edu, etc). Aqueous glycerol shows good compatibility with all the materials of the experimental equipment.

Table 3.6: Material compatibility of glycerol

Chemical	Compatibility*
Carbon steel	B
304 SS	A
316 SS	A
Viton	A
PTFE	A
Carbon	A
Aluminum	A
Bronze	A
Polyethylene	A
Polypropylene	A
Polyvinylchloride	A
Nylon	A
Glass Fiber	A
LDPE	A
HDPE	A
Polycarbonate	A
Teflon	A

* A – Excellent, B – Good, C – Poor, D – Not Recommended

3.1.3.2 Sterilization

As a potential source of nutrient, glycerol solution may induce bacteria growth, which will change the chemical component and thus property of the solution. Indoor and outdoor experiments were performed to test the necessity of using biocide in aqueous glycerol. The 0.02 w/v % of NaN_3 was chosen as biocide based on previous successful experiences (Holtzhauer, 2006; Yamamoto et al., 2007; Zirnsak et al., 1999).

In the indoor experiments, aqueous glycerol with different concentrations were prepared with or without biocide. Solutions were kept in open beakers at room environment (22 °C and 1 atm) for 45 days. Appearance of solutions were checked daily for any visible microbe growth. Total weight, density, viscosity, surface tension, and pH of the solutions were measured weekly. Information about solution preparation is summarized in Table 3.7. Water vaporization (or condensation for 90 wt % sample) caused the total sample weight decrease and glycerol concentration increase (Figure 3.9). The higher the glycerol concentration, the slower the solution lost its weight. This results

from the hydrophilic nature of glycerol which enables it to keep water from evaporating. No bacteria growth was observed for all samples. No significant property change was observed other than those caused by water vaporization/condensation, which is confirmed by Figure 3.10 where both the density and viscosity of sterilization samples match the model value well. No significantly difference was observed between blank solutions and those with biocide. The indoor experiments suggested that biocide is not necessary for aqueous glycerol at the proposed range of concentrations. The glycerol concentration was calculated based on the total sample weight and on the assumption that glycerol has minimal vaporization.

Table 3.7: Solution preparation for indoor sterilization experiment

Solution	Volume (mL)	Glycerol (wt %)	0.02 w/v% NaN3	0.1 N NaOH
1 Blank				
1 NaN_3	800	10	√	
1 NaOH				√
2 Blank				
2 NaN_3	800	25	√	
2 NaOH				√
3 Blank				
3 NaN_3	800	50	√	
3 NaOH				√
4 Blank				
4 NaN_3	800	75	√	
4 NaOH				√
5 Blank				
5 NaN_3	800	90	√	
5 NaOH				√

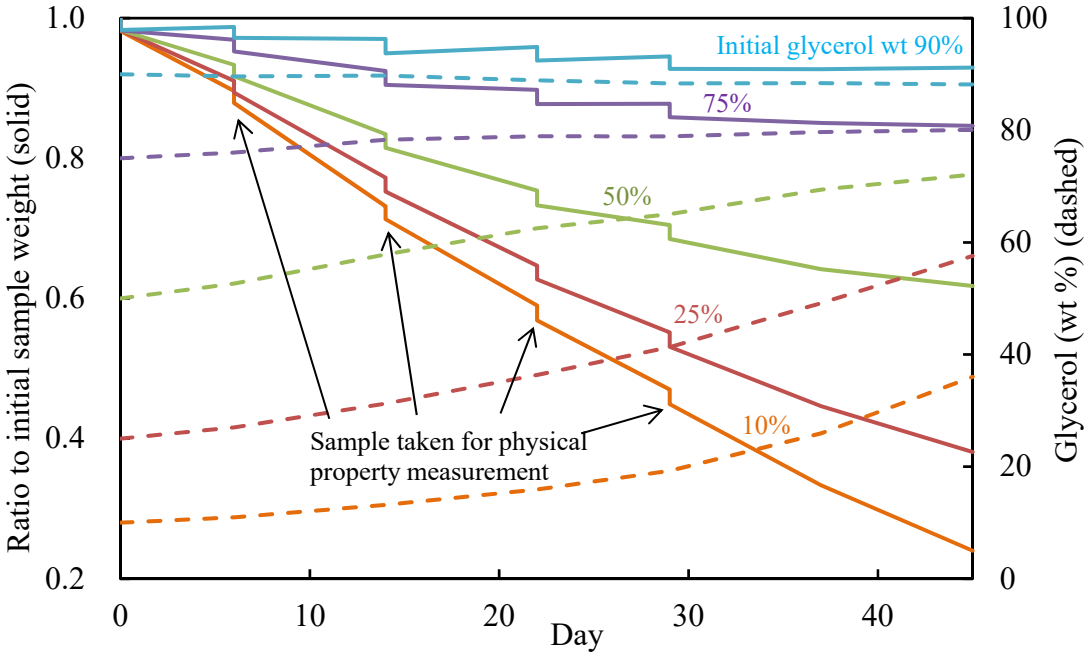

Figure 3.9: Weight and glycerol concentration of sterilization samples

(lines of blank samples, samples with 0.1 N NaOH, and with biocide are the same)

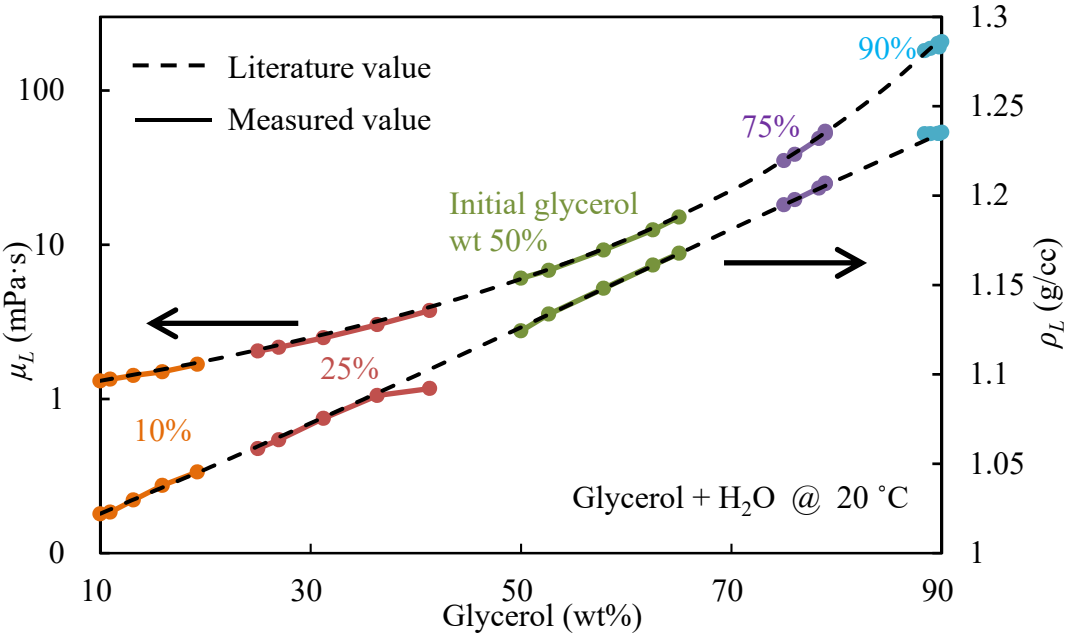

Figure 3.10: Measured and model value for μ_L and ρ_L of sterilization samples

The pH of sterilization samples was measured as a function of time and glycerol concentration. From Figure 3.11, the samples with NaOH lost their alkalinity rapidly (e.g., from 13 to 10 within 14 days). Therefore, a_e measurement in the pilot column should be completed in a relatively short time. The pH of the liquid should be checked frequently even though alkalinity may decline more slowly for pilot-scale experiment because of the higher volume-surface area ratio of the liquid reservoir.

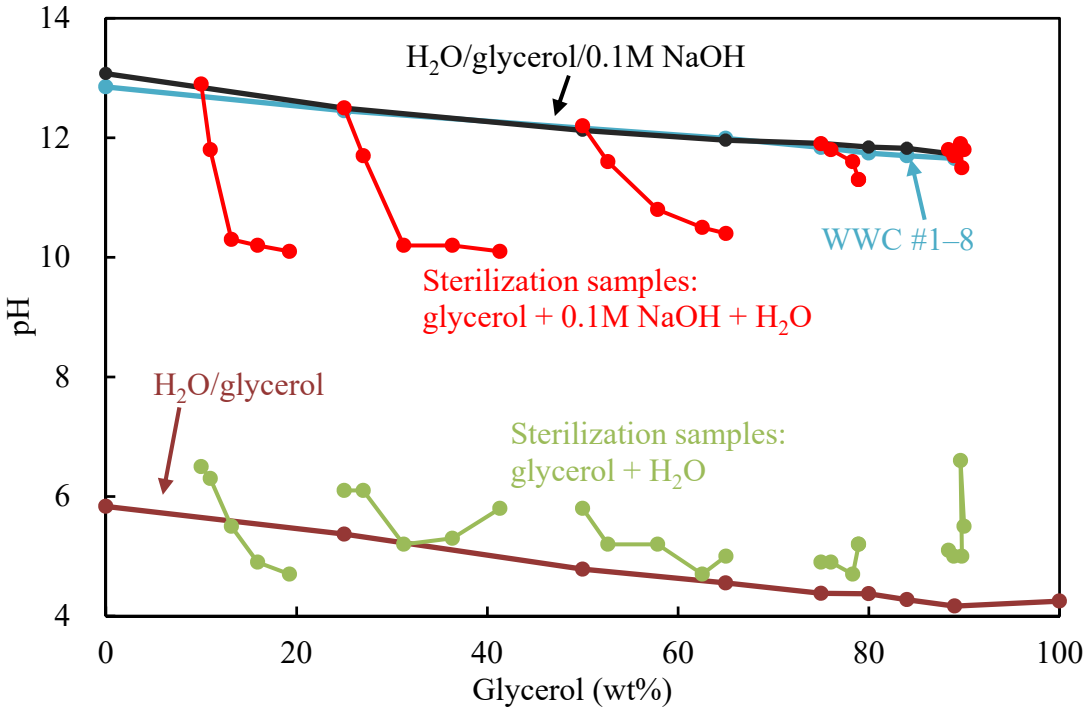

Figure 3.11: pH of aqueous glycerol samples in WWC and sterilization experiments

To ensure biocide is not necessary for aqueous glycerol at the proposed range of concentrations, outdoor sterilization experiments with probably the worst-case scenario were performed. Like the indoor experiments, blank samples and sample with caustic and biocide (0.02 w/v % of NaN_3) were kept in open beakers left at outside of the air-water

column (AWC) with roofs to prevent rain water. After one month exposure to extreme condition (above 30 °C with frequent rainfall), only slight mold growth was observed in the blank sample with the lowest glycerol concentration (30 wt %). All other samples with greater concentration were still clear. Based on the results of both the indoor and outdoor sterilization experiments, it is confirmed that the use of biocide is not necessary for aqueous glycerol at the proposed range of concentrations. The possible reason for the immunity of aqueous glycerol is that the elevated μ_L inhibit normal mass transfer related life activities of bacteria, and this explain why mold was observed only at the samples with the lowest glycerol concentration (and thus μ_L).

The immunity of aqueous glycerol to bacteria makes it possible to reuse the batch for k_L experiments, where only the mass transfer of volatile toluene (and water) occurs. However, for a_e experiments where chemical reaction is involved, the batch should not be reused considering the bulk caustic depletion and ion accumulation.

3.1.3.3 Miscellaneous Experimental Concerns

Since glycerol barely vaporizes, extra caution should be exercised to prevent spilling especially in the pilot-scale experiments. A bucket of clean water and absorbing pads should be prepared during experiments, so that once a spill happens, it can be cleaned up quickly by dilution and absorption with water and absorbent.

The freezing of liquid can be detrimental to process equipment because of the potential volume change. The freezing point of aqueous glycerol is shown in Figure 3.12 (Lane, 1925). Per the figure, the freezing point at the proposed concentrations (45–89 wt % of glycerol) is below 0 °C. Therefore, the anti-freezing protocol for water can be safely used for aqueous glycerol during experiments.

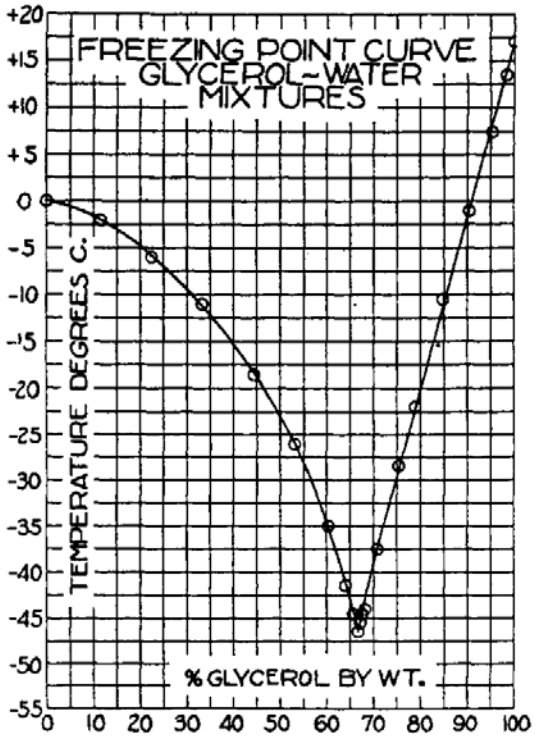

Figure 3.12: Freezing point of aqueous glycerol from Lane (1925)

3.2 WETTED-WALL COLUMN

A bench-scale wetted-wall column (WWC) was used to investigate the reaction kinetics of CO_2/NaOH/H_2O/glycerol. The kinetic model based on the WWC results was then used in the pilot-scale experiments in the packed column to investigate the effect of μ_L on a_e. The apparatus was previously used by Cullinane (2005), Tsai (2010), Chen (2011), and Li (2015). This section includes detailed equipment description, experimental protocol, data analysis, and experimental concerns.

3.2.1 Equipment Description

Figure 3.13 shows the sketch of the WWC. Inside the reaction chamber (2.54 cm OD) is a stainless-steel tube of 1.26 cm OD and a height of 9.1 cm. Liquid is pumped by a Cole-Parmer Micropump at a constant rate of 2–4 cm^3/s from a 1000 cm^3 stainless-steel solvent tank to the top of the tube and then flows down in a smooth film back to the tank. Typical gas flow rate is 3–5 stdL/min (0.12-0.2 m/s) in a concentric flow area of 4.2 cm^2, and the typical liquid flow is 0.35 cm^3/s. The gas and liquid have counter-current contact in the chamber, which simulates the packing surface. Pressure in the reaction chamber is kept at 3.7 atm.

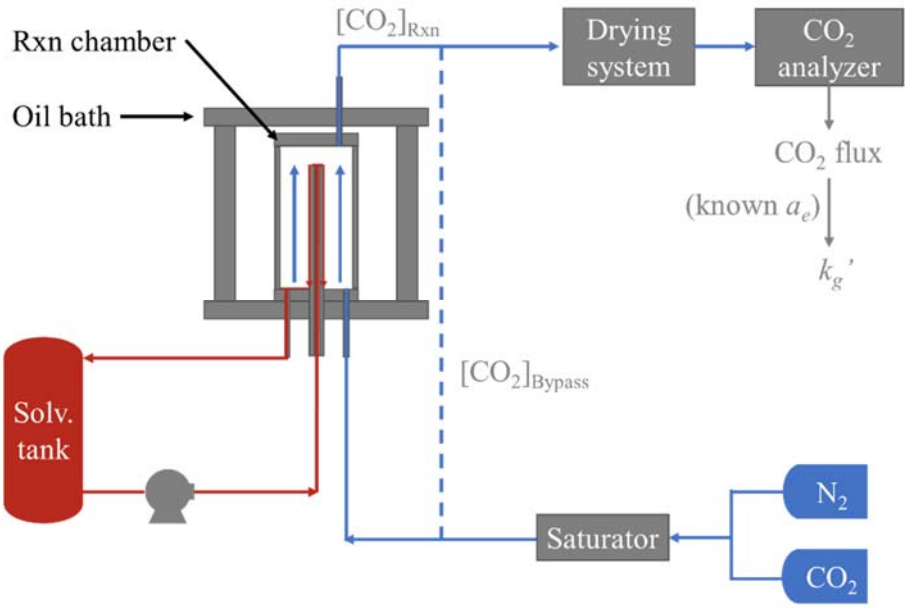

Figure 3.13: Diagram of the wetted wall column

The contact area is 38.52 cm^2 based on the tube geometry. Liquid temperature is controlled by an oil bath before the reaction chamber. Gas temperature is controlled by

water temperature in the pre-saturator and a thick-walled glass cylinder (10.16 cm OD) oil bath outside the reaction chamber. The CO_2 flux is calculated based on the concentration difference between the gas stream passing through the reaction chamber and the bypass stream. The CO_2 partial pressure of the inlet gas is varied from 150 to 1000 Pa to obtain multiple measurements at one temperature. A drying system consisting of an ice-bath flask condenser and a glass tube packed with $CaSO_4$ is installed before the Horiba VIA-510 CO_2 analyzer.

3.2.2 Experimental Protocol

For each experimental run, two litters of solution was prepared gravimetrically from distilled and deionized (DDI) water, 1 N sodium hydroxide solution, and pure glycerol. Different amounts of glycerol (0–89 wt %) was added to achieve μ_L of 0.89–70 mPa·s. The solutions were mixed by magnetic stirrer in capped jug for at least two hours before experiments. The upper limit of μ_L (70 mPa·s) was set due to the mechanical limitations of the Cole-Parmer Micropump.

After thorough mixing, the solution was charged into the solvent tank to circulate in the system till the temperature stabilized. After that, gas mixture of N_2 and 5000 ppm_v CO_2 in N_2 was sent through the bypass line with the CO_2 controlled by two mass flow controllers. When the reading of CO_2 was stabilized, the gas mixture was switched to the reaction chamber. The CO_2 flux was obtained based on the total gas rate and the difference of the CO_2 concentration between the bypass flow and the flow through the reaction chamber. After the CO_2 flux was known and gas mixture switched back to the bypass line, operating condition was changed and the above processes were repeated.

Liquid samples were taken from the batch before the experiment starts, and from an in-line septum near the pump suction after each experiment run. The carbonate concentration, total alkalinity, and μ_L of the sample was measured offline by total inorganic carbon analysis (TIC), acid titration, and viscometer.

The solution preparation and experimental conditions are summarized in Tables 3.8 and 3.9, respectively. Five series of experiments were performed. The first three series (#1–8, #1–10R, and #1–8RR) with 0.1 M NaOH were performed to check the WWC reproducibility and to provide basis of kinetic data for model development. One series (#1–9Triple) with 0.3 M NaOH was performed to provide data with increased caustic concentration and thus to further validate the kinetic model. One series (#1–3Na_2CO_3) with 0.1 M NaOH and 0.025 M Na_2CO_3 was performed to check the effect of accumulated carbonate on the k_g'. Experiments with different liquid flow rate were performed at some conditions (#5 and #4R at 30 °C) to make sure that liquid flow rate has insignificant influence on k_g'. Experiments with presaturator both on and off were performed at some conditions (#4–7 at 40 °C) to investigate the effect of water mass transfer on the results. The total gas flow rate, G, and the partial pressure of CO_2, $P_{CO2,inlet}$, were varied for some runs to obtain a favorable outlet CO_2 reading for the analyzer.

Table 3.8: Solution preparation for WCC experiments

Solution					Glycerol (wt %)	NaOH (mol/L)	Na_2CO_3 (mol/L)	μ_L (mPa·s)		
#1–8	#1–10R	#1–8RR	1– 9Triple	Na_2CO_3				20 °C	30 °C	40 °C
1	1R	-	-	-	0	0.1	0	1.01	0.81	0.66
-	-	-	1Triple	-	0	0.3	0	1.04	0.82	0.70
-	-	8RR	-	-	3.5	0.1	0	1.09	0.87	0.71
-	-	1RR	-	-	7	0.1	0	1.20	0.95	0.77
-	-	-	2Triple	-	10	0.3	0	1.36	1.03	0.83
-	2R	-	-	-	13	0.1	0	1.42	1.11	0.89
-	-	2RR	-	-	20	0.1	0	1.74	1.35	1.08
-	-	-	3Triple	-		0.3	0	1.89	1.42	1.15
2	3R	-	-	-	25	0.1	0	2.13	1.60	1.26
-	-	-	-	$1Na_2CO_3$		0.1	0.025	2.13	1.65	1.29
-	-	-	4Triple	-	35	0.3	0	2.37	2.51	1.96
-	4R	-	-	-	38	0.1	0	3.37	2.48	1.90
-	-	-	5Triple	-	45	0.3	0	5.37	3.86	2.90
3	5R	-	-	-	50	0.1	0	6.04	4.24	3.12
-	-	-	6Triple	-	55	0.3	0	9.29	6.36	4.58
-	-	3RR	-	-	58	0.1	0	9.56	6.45	4.59
4	6R	-	-	-		0.1	0	14.30	9.48	6.60
-	-	-	7Triple	-	65	0.3	0	18.75	12.02	8.29
-	-	-	-	$2Na_2CO_3$		0.1	0.025	16.55	10.81	7.56
-	-	-	8Triple	-	70	0.3	0	28.25	17.56	11.70
5	7R	4RR	-	-	75	0.1	0	35.79	21.30	13.69
6	8R	5RR	-	-		0.1	0	58.62	33.32	20.42
-	-	-	9Triple	-	80	0.3	0	78.24	43.94	26.76
-	-	-	-	$3Na_2CO_3$		0.1	0.025	65.81	38.01	23.70
7	9R	6RR	-	-	84	0.1	0	-	51.82	30.31
8	10R	7RR	-	-	89	0.1	0	-	-	53.30

Table 3.9: WWC experimental condition

Soln. #	T (°C)	L (cc/s)	G (stdL/min)	P (atm)	$P_{CO2,\ Inlet}$ (Pa)				
					1	2	3	4	5
1–4, 6	20, 30, 40	0.3–5.0	5	3.7	150	300	450	600	750
5	20, 30[a], 40	2.2–3.8							
7	30, 40	0.3–0.4			350	450	550	650	750
8	40	0.3							
1–3R	20, 30, 40	4.0–4.8	4	3.7	150	300	450	600	750
4R	20, 30[a] ,40	2.0–3.7			200	400	600	800	1000
5–8R	20, 30, 40	0.5–2.5	3–4						
9R	30, 40	0.4–0.6	3						
10R	40	0.3							
1–3RR, 8RR	20, 30, 40	1.3–4.5	4	3.7	150	300	450	600	750
4–5RR	20, 30, 40[b]	0.3–0.9			200	400	600	800	1000
6RR	30, 40[b]	0.3–0.5			180	360	540	720	900
7RR	40[b]	0.3							
1–3 Triple	20, 30, 40	3.3–4.3	5	3.7	150	300	450	600	750
4–6 Triple		1.4–3.5			75	150	250	350	450
7–9 Triple		0.3–1.5			100	175	250	325	400
1–2 Na_2CO_3	20, 30, 40	0.8–3.6	4	3.7	150	300	450	600	750
3 Na_2CO_3		0.3–0.6			180	360	540	720	900

[a]Runs with varied L at the same condition; [b]Runs with presaturator both on and off.

3.2.3 Data Analysis

Per Equation 2.12, the overall mass transfer resistance in the WWC is composed of resistances in both the liquid and gas phases. The overall volumetric mass transfer coefficient, $K_G a$, is determined experimentally from the WWC by plotting the CO_2 flux against the partial pressure of CO_2 as the driving force.

K_G is the $K_G a$ divided by the surface area of the WWC. The gas side mass transfer coefficient, k_G, is calculated using Equation 3.31 (Pacheco et al., 2000). Since k_G is a strong function of column geometry, it is important to use the k_G correlation developed specifically for this WWC. With the knowledge of K_G and k_G, kg' can be obtained from Equation 2.12.

$$\frac{1}{K_G} = \frac{1}{k_G} + \frac{1}{k_g'} \tag{2.12}$$

$$k_G = 1.075 \left(\frac{u_G \cdot d_{WWC}^2}{h_{WWC} \cdot D_{CO_2,G}} \right)^{0.85} \left(\frac{D_{CO_2,G}}{R \cdot T \cdot d_{WWC}} \right) \tag{3.31}$$

As is discussed in section 2.1.3, the k_g' for $CO_2/NaOH/H_2O$ can be described by Equation 2.22 based on the surface renewal theory and pseudo-first order assumption.

$$k_g' = \frac{\sqrt{k_{OH^-}[\mathrm{OH}^-] D_{CO_2,L}}}{H_{CO_2}} \tag{2.22}$$

As is discussed in part 2.1.3, the CO_2 reacts with both hydroxide and glyceroxide when reaching the gas-liquid surface of caustic aqueous glycerol. For simplification, the overall reaction rate constant, k_{Alk}, is used (Equations 3.32–34). The k_{Alk} is expressed as a basic combination of the two reactions based on the assumption that no interaction occurs between the CO_2, hydroxide, and glyceroxide. This assumption is supported by previous studies that saw no second-order base dependence on the bicarbonate formation reaction from CO_2 (Hikita et al., 1976; Pinsent et al., 1956; Pohorecki & Moniuk, 1988).

$$k_g' = \frac{\sqrt{k_{Alk}[\mathrm{Alk}]D_{CO_2,L}}}{H_{CO_2}} \tag{3.32}$$

$$k_{Alk} = k_{OH^-}\left(\frac{[\mathrm{OH^-}]}{[\mathrm{Alk}]}\right) + k_{Glycerol^-}\left(\frac{[\mathrm{Glycerol^-}]}{[\mathrm{Alk}]}\right) \tag{3.33}$$

$$[\mathrm{Alk}] = [\mathrm{OH^-}] + [\mathrm{Glycerol^-}] \tag{3.34}$$

In Equation 3.33, the total active alkalinity, [Alk], is determined experimentally by acid titration and total inorganic carbon (TIC) analysis. The hydroxide reaction rate constant, k_{OH^-}, is calculated by a correlation (Equation 3.35) modified from Pohorecki and Moniuk (1988). The glyceroxide reaction rate constant, $k_{Glycerol^-}$, is calculated from Equation 3.36. The effect of ionic strength on the rate constant is neglected because of the relatively small change in the ionic concentrations. The equilibrium constant for Reaction 2.24, K_b, is defined in Equation 3.37 and calculated from Equation 3.38. The glyceroxide concentration is determined from Equation 3.40, which is derived from Equations 3.34, 3.37, and 3.39. The hydroxide concentration is determined by Equation 3.34.

$$\ln\left(\frac{k_{OH^-}}{k_{OH^-,298.15K}}\right) = \frac{-E_{OH}}{R}\left(\frac{1}{T} - \frac{1}{298.15}\right) \tag{3.35}$$

$$\ln\left(\frac{k_{Glycerol^-}}{k_{Glycerol^-,298.15K}}\right) = \frac{-E_G}{R}\left(\frac{1}{T} - \frac{1}{298.15}\right) \tag{3.36}$$

$$K_{b,Glycerol} = \frac{K_W}{K_{a,Glycerol}} = \frac{[OH^-][Glycerol]}{[Glycerol^-]} \tag{3.37}$$

$$\ln\left(\frac{K_{b,Glycerol}}{K_{b,Glycerol,298.15K}}\right) = \frac{-H_{KG}}{R}\left(\frac{1}{T} - \frac{1}{298.15}\right) \tag{3.38}$$

$$[Glycerol]_T = [Glycerol^-] + [Glycerol] \tag{3.39}$$

$$[Gly^-]^2 - \{[Gly]_T + K_{b,Glycerol} + [Alk]\}[Gly^-] + [Alk][Gly]_T = 0 \tag{3.40}$$

By rearranging Equation 3.32, the overall rate constant, k_{Alk}, can be determined from the empirical k_g' (Equation 3.41) with physical properties (H_{CO2}, D_{CO2}) calculated by models shown in section 3.1.2.

$$k_{Alk} = \frac{\left(k_g' H_{CO_2}\right)^2}{[Alk] D_{CO_2,L}} \tag{3.41}$$

Parameters in Equations 3.35, 3.36, and 3.38 were determined by fitting the calculated k_{Alk} (Equation 3.33) with empirical k_{Alk} (Equation 3.41) using least-squares regression by MATLAB. The rate and equilibrium constants were all concentration-based.

3.2.4 Safety and Experimental Concerns

3.2.4.1 Liquid Flow Rate

Calibration of the liquid flow rate measured by the floating ball rotameter in the WWC (Equation 3.42) was developed by Cullinane (2005). The correlation corrects for liquid density and worked well for previous researchers who used amine solutions (Chen et al., 2011; Dugas, 2009; Li, 2015). However, the ball float rotameter is not immune to the effect of μ_L, and the correlation significantly over-predicts flow rate for viscous liquid (e.g. over-predicts the flow rate by ten times for 80 wt % aqueous glycerol at 24 °C). A modified correlation (Equation 3.44) was developed with correction for μ_L based on the timed flow experiments into a container with known volume. With corrected liquid flow rate, depletion of surface alkalinity (discussed in detail in the next section) can be calculated with greater accuracy.

$$L = (0.45x - 0.29) \cdot \sqrt{\frac{7.83 - \rho_{L,T_{ref}}}{(7.83 - 0.99)\rho_{L,T_{ref}}}} \cdot \sqrt{\frac{7.83 - \rho_L^2}{7.83 - \rho_{L,T_{ref}}^2}} \tag{3.42}$$

$$T_{ref} = 25\ ^{\circ}\mathrm{C} \tag{3.43}$$

$$L = (10.9x - 14.9) \cdot \sqrt{\frac{7.83-\rho_{L,T_{ref}}}{(7.83-0.99)\rho_{L,T_{ref}}}} \cdot \sqrt{\frac{7.83-\rho_L^2}{7.83-\rho_{L,T_{ref}}^2}} \cdot (-0.02\mu_L^2 + 1.8\mu_L + 6.3)^{-1.4} \tag{3.44}$$

3.2.4.2 Depletion of Surface Alkalinity

Because of the smaller physical liquid-phase mass transfer rate (k_L^0), surface depletion of alkalinity becomes a more serious problem for viscous liquid than for water. In the kinetic models, the depletion ratio for each WWC run was calculated from the total CO_2 flux and the overall k_L^0 weighted by hydroxide and glyceroxide concentrations (Equations 3.45 and 3.46). The k_L^0 is estimated from Equation 3.47, a theoretical model for falling film developed by Pigford (Bird et al., 2002; Pigford, 1942) and later verified to fit the WWC data of CO_2 desorption from water (Pacheco, 1998).

$$N_{Alkalinity} = 2N_{CO_2} = k_L^0 \left([Alk]^b - [Alk]^i\right) \tag{3.45}$$

$$k_L^0 = k_{L,\,OH^-}^0 \left(\frac{[OH^-]}{[Alk]}\right) + k_{L,\,Glycerol^-}^0 \left(\frac{[Glycerol^-]}{[Alk]}\right) \tag{3.46}$$

$$k_{L,A}^0 = \left(\frac{3^{1/3}2^{1/2}}{\pi^{1/2}}\right)\left(\frac{Q^{1/3}h^{1/2}W^{2/3}}{A}\right)\left(\frac{g\rho}{\mu}\right)^{1/6} D_A^{1/2} \tag{3.47}$$

Equation 3.47 is only valid when Equation 3.48 is satisfied, which is true for all the experimental conditions examined. Effective diffusivities of hydroxide and glyceroxide in the multi-component ionic system used for k_L^0 calculation are calculated by Equations 3.51–54 (Taylor & Krishna, 1993). The diffusivity of glyceroxide is approximately equal to the mutual diffusivity of H_2O/glycerol, D_{Gly}, which is shown in part 3.1.2.

$$\frac{D_A h}{u_s \delta^2} < 0.01 \tag{3.48}$$

$$u_s = \frac{\rho_L g \delta^2}{2\mu_L} \tag{3.49}$$

$$\delta = \sqrt[3]{\frac{3\mu Q}{\rho g W}} \tag{3.50}$$

$$D_{i,eff} = D_{in}^0 - \frac{t_i}{z_i} \sum_{j-1}^{n-1} z_j D_{jn}^0 \frac{\nabla c_j}{\nabla c_i} \tag{3.51}$$

$$t_i = \frac{K_i}{K} \tag{3.52}$$

$$K_i = \frac{F^2}{RT} c_i z_i^2 D_{in}^0 \tag{3.53}$$

$$K = \sum_{i=1}^{n-1} K_i = \frac{F^2}{RT} \sum_{i=1}^{n-1} c_i z_i^2 D_{in}^0 \tag{3.54}$$

A corrected CO_2 flux is then calculated as if no surface depletion occurs (Equations 3.55–57). The corrected CO_2 flux gives a corrected k_g', based on which a set of corrected parameters in the kinetic model can be obtained. From the corrected kinetic model, corrected concentrations of hydroxide and glyceroxide for each WWC run were calculated, and this gives a new ratio of surface depletion. Based on this new depletion ratio, the whole correction process can be calculated in a loop until it converges.

$$N_{CO_2,Corr} = \frac{1+x}{1+\sqrt{1-depletion\%\cdot x}} \cdot N_{CO_2} \tag{3.55}$$

$$x = \left(k_G / k_g'\right)_{Before\ correction} \tag{3.56}$$

$$Depletion(\%) = \frac{[Alk]^b - [Alk]^i}{[Alk]^b} \times 100\% \tag{3.57}$$

The k_{Alk} and k_g' data used to develop the kinetic model are values after the correction of alkalinity surface depletion. The use of the kinetic model that assumes no depletion occurs to the pilot column experiments is reasonable considering the relatively low partial pressure of CO_2 (ambient) in the pilot experiments compared to the WWC condition.

3.2.4.3 Approach to Determine k_g' from Experimental Data

Two different approaches can be used to determine k_g' from the experimental data. The k_g' could be calculated using a point-by-point approach. Individual values for K_G and k_G are used to calculate k_g' for each CO_2 partial pressure condition (typically 5 within an experiment at a constant temperature). Alternatively, a single value for K_G could be obtained from the slope of the curve of CO_2 flux against log-mean CO_2 partial pressure difference ($P_{CO2,LM}$). Theoretically, the two approaches should give similar results when the flux-partial pressure curve goes through zero. However, it is expected that the depletion of surface alkalinity will cause an intercept of the curve especially when viscosity is high. Thus the "overall slope" approach is used since it "smooths" the k_g' after the depletion correction and gives an "internally-averaged" k_g'.

3.2.4.4 Other Experimental Concerns

The WWC experiments were designed to provide reliable kinetic data for model development and to address miscellaneous experimental concerns before pilot-scale runs. The internal and external reproducibility was checked by three parallel runs (#1–8, #1–10R, and #1–8RR). One series (#1–9Triple) with increased caustic concentration (0.3 M NaOH) was performed to provide data with increased caustic concentration and thus to further validate the kinetic model and to provide confidence for the pilot-scale experiments where the caustic concentration cannot be controlled and maintained as precise as in the WWC. One series (#1–3Na_2CO_3) with 0.1 M NaOH and 0.025 M Na_2CO_3 (equivalent to 50% original caustic carbonated) was performed to check the effect of accumulated carbonate on the k_g' and thus provide guidance on how long one batch can last without compromising the accuracy of kinetic calculation in the pilot-scale experiments. Experiments with different liquid flow rate were performed at some conditions (#5 and

#4R at 30 °C) to make sure that liquid flow rate has insignificant influence on k_g'. Experiments with presaturator both on and off were performed at some conditions (#4–7RR at 40 °C) to investigate the effect of water mass transfer on the results. This is important since no pre-saturation is included in the pilot packed column. According to Figure 3.2, mass transfer of water does not change the μ_L of the WWC batch significantly during the experiments.

3.2.4.5 Safety

When switching the gas mixture between the bypass line and WWC reaction chamber, the valve on one line should always be opened before valve on the other line is closed to prevent fast pressure build-up. Pressure gauge should be checked regularly when operating condition is changed. Solution should be prepared inside the fume hood, with window slide down. Personal protective equipment (PPE) including lab coat, safety glasses, and chemical resistant (nitrile) gloves are required to work in the lab.

3.3 PACKED COLUMN

A pilot-scale PVC air-water column (AWC) was used to investigate the mass transfer properties of water and aqueous glycerol with various packings. The effective mass transfer area, a_e, was measured with chemical absorption of ambient CO_2 into aqueous NaOH because of the well-established kinetics (Pohorecki & Moniuk, 1988). The k_L was measured with air stripping of toluene from water because of the high volatility of the organic substance. The k_G was measured with chemical absorption of injected trace SO_2 from air by dilute aqueous NaOH because of the instantaneous nature of the reaction.

The column has been used extensively by the Separations Research Program (SRP) of the University of Texas at Austin (Tsai, 2010; Tsai et al., 2011; Wang et al., 2012; Wang et al., 2016; Wilson, 2004). The SRP air-water column database contains valuable hydraulic and mass transfer data for structured, random, and hybrid packings. Based on the database, models of a_e and k_L/k_G were developed previously by Tsai (2010) and Wang (2016). Tsai showed that a_e was not a function of μ_L over a range of 1 to 10 mPa·s with viscosity varied by the addition of polyethylene glycol (PEG). His conclusion must be confirmed from 1 to 70 mPa·s with glycerol before proceeding to any k_L measurement. In this case, a_e can be assumed to be the same as with water at the same operating condition. Otherwise, a_e will need to be measured individually for each packing with a reactive system.

The Tsai area model was developed seven years ago, and new data with totally different packing geometries have been generated continuously. For the k_L model developed by Wang, though it is relatively new, a large amount of new data with water and aqueous glycerol was generated during the past two years. Therefore, it is necessary to validate or update both models with the expanded database. The model of k_G was developed based on 20 packings in the SRP database. Compared to the Wang model (2016), it is a simplified version applicable to structured, random, and hybrid packings without incorporating the geometry-oriented dimensionless number, mixing-point density (Mi), which is different for different packing types.

3.3.1 Equipment Description

The pilot-scale PVC column is located in the outdoors area within the Separation Research Program (SRP) pilot plant facility at Pickle Research Campus of the University

of Texas at Austin. The column has 0.43-m ID and a maximum packing height of 3 m (Figure 3.14). Liquid countercurrently contacted air supplied by a 30-kW blower with a variable speed drive from a duct (0.2 m outside diameter) below the packing support. Up to 34 m^3/h of liquid was delivered by a centrifugal pump with a variable speed drive from a 1.3-m^3 storage tank. The liquid could either flow to the column top and be distributed by an F40 pressurized fractal distributor (430 drip points/m^2) or flow back to the column sump and storage tank via a bag filter for the pump to operate in a more favorable drive-speed region. The gas and liquid flow rates were monitored by an Annubar flow meter and a micromotion coriolis meter, respectively. Above the distributor was a Trutna collector to knock out any liquid reaching the column exhaust. Typical liquid inventory was 1–1.2 m^3. Typical gas and liquid rates were 0.5–1.5 m/s and 6–73 $m^3/m^2 \cdot h$ respectively. A level transmitter was installed at the column sump to estimate the liquid inventory in the system. Pressure drop through the packing was determined by a pair of differential pressure transmitters. The temperature of the inlet and outlet gas was measured by thermocouple and RTD, and the temperature of the liquid was measured by the Micromotion™ meter. DeltaV software developed by Emerson was used for system control. A more detailed column description with pictures and valve arrangement is included in Appendix A.1.

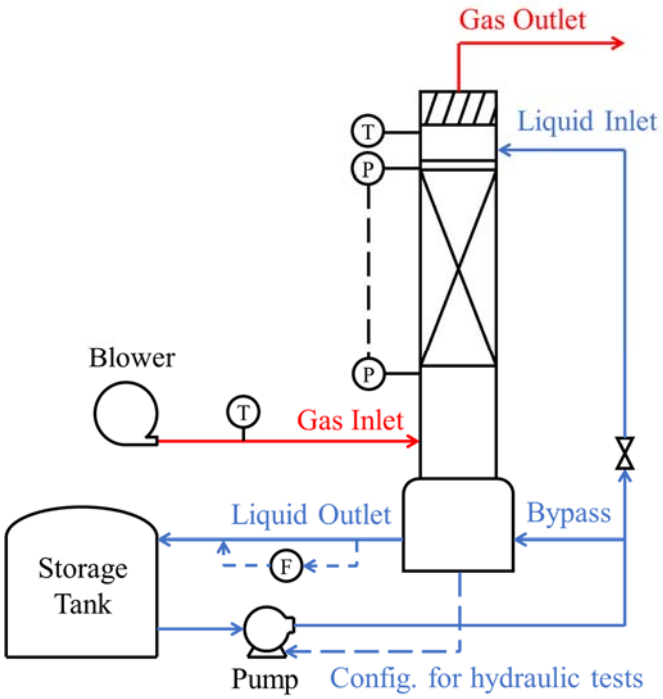

Figure 3.14: Configuration of air-water column (AWC)
(F: filter, P: pressure transmitter, T: thermocouple)

Approximately 3 m of packing was installed for a_e and k_L measurement with aqueous glycerol. A shorter 1.8 m bed was used for k_L measurement with water because of the difficulty of GC analysis for the low outlet toluene concentration caused by high mass transfer efficiency. An even shorter bed (0.5–1 m) was used for k_G measurement because of the extremely high absorption rate of SO_2 with NaOH. Each packing element was installed with a 90° rotation to facilitate liquid distribution. Wiper bands were arranged so that each element fits tight with the column wall.

Samples of inlet liquid were collected at a sample valve between pump discharge and liquid distributor. Samples of outlet liquid were collected from a bayonet collector installed immediately below the packing to minimize end effects. The sample collecting area was designed slightly shorter than the column inner diameter to be able to collect the

radial average of liquid sample. Stainless steel wiper bands were welded onto the bayonet sample collector to prevent taking wall flow into the outlet liquid samples (Figure 3.15a). The sampling protocol minimized additional mass transfer. The minor distributor leak was fixed by applying organic plastic glue (Figure 3.15b). Residue in the distributor that partially blocked the liquid flow paths was cleaned mechanically by pressurizing the distributor with compressed air. The distributor elbows and connections whose treads were partially worn out by Teflon tape residues were replaced.

(a) (b)

Figure 3.15: Modifications on the PVC column: (a) wiper bands welded on the bayonet; (b) new connections of liquid distributor

A carbon steel extension structure was designed, constructed, and installed to the side of the 3rd floor of the existing structure to provide easy and safe access to the top section of the column (Figure 3.16). A flooding line was rerouted to avoid the extension structure. An adjustable stainless steel column support was installed to replace the carbon steel support which was badly corroded (Figure 3.17).

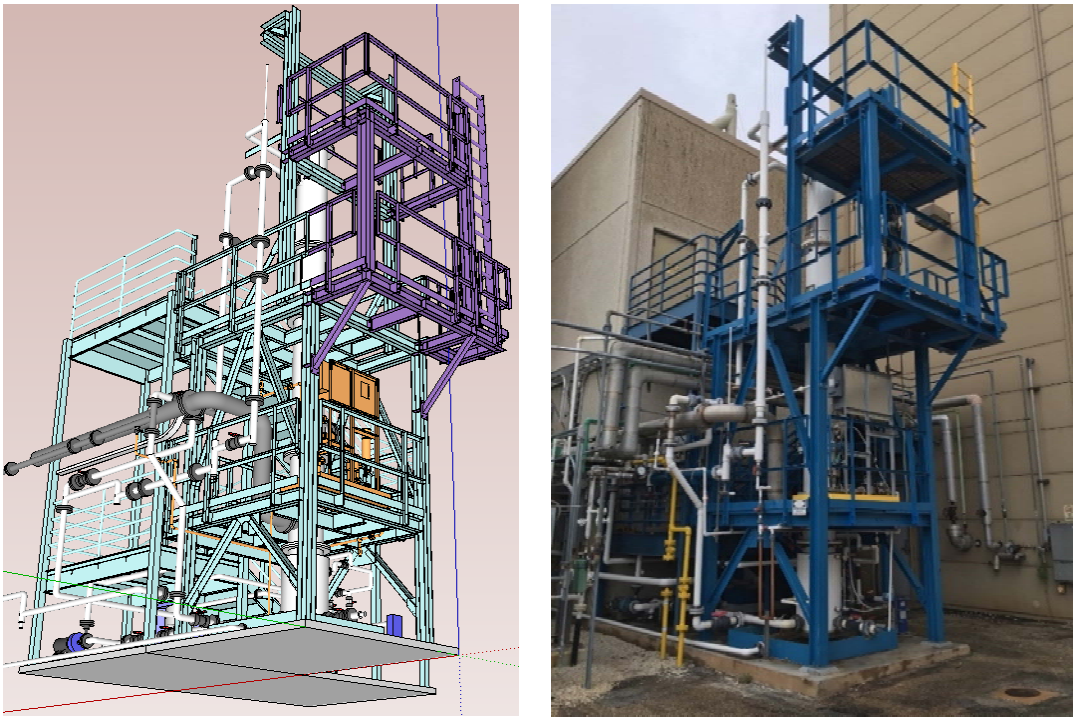

Figure 3.16: 3D drawing and picture of the extension structure (purple part in the 3D drawing) to the PVC column

Figure 3.17: Adjustable stainless steel column support

3.3.2 Packings

Both the packings measured in this work and those measured by previous researchers in the SRP air-water database were used for model development and are summarized in Table 3.10. The database includes packings of various types (structured, random, hybrid, and gauze) and from different families (such as MellaPak and Raschig Super-Pak). For a_e, there are a total of 39 packings: 21 structured packings, four hybrid packings, 12 random packings, one grid packing, and one gauze packings. Aqueous glycerol was tested with one packing (GTO 250Y) for a_e. For k_L and k_G, there are a total of 20 packings: 12 structured packings, three hybrid packings, four random packings, and one grid packings. Aqueous glycerol was tested with seven structured packings, one hybrid packing, and one random packing for k_L. The dimensions of some of the packings in the database are summarized in Table 3.11. Pictures of some of the packings are shown in Appendix A.2.

Table 3.10: List of packings

Type	Family	Packing	Water			aq. Glycerol	
			a_e	k_L	k_G	a_e	k_L
Grid	-	MG 64Y					
Gauze	-	A3 500X					
Structured	Mella-Pak®	M 125Y					
		M 2Y					
		M 2X					
		M 250Y					
		M 250YS					
		M 252Y					
		M 250X					
		M 500Y					
	Montz-Pak Type B1™	B1 250					
		B1 250MN					
		B1 350					
		B1 500P					
	GT(Optim)-Pak®	GTO 250Y					
		GTP 350Y					
		GTP 350Z					
		GTP 500Y					
	Flexipac®	F AQ 20					
		F 1.6YHC					
		F 1Y					
	-	A 350Y					
	-	B 350X					
Hybrid	Raschig Super-Pak®	RSP 200X					
		RSP 250Y					
		RSP 300Y					
	-	HFP 2 (P)					
Random	Raschig Super-Ring®	RSR 1.5					
		RSR 0.7					
		RSR 0.5					
		RSR 0.3					
	Pall Ring	PR 2.0					
		PR 1.0					
		PR 1.0 (P)					
	IMTP®	IMTP 40					
		IMTP 25					
	Cascade Mini-Rings®	CMR 2A					
		CMR 2A (P)					
	-	SB-2P 4050					

Shaded: measured by previous researchers in the SRP database; Diagonal: measured in this work; (P): Plastic

Table 3.11: Dimensions of packings

Type	Name	a_p (m^2/m^3)	α (°)	b (m)	s (m)	h (m)	ε	$H_{element}$ (m)
Grid	MG 64Y	64	45	0.090	0.069	0.053	0.99	0.13
Gauze	A3 500X*	500	60	-	-	-	0.92	?
Structured	M 125Y	125	45	0.051	0.038	0.028	0.99	0.21
	M 2Y*	205	45	0.033	0.022	0.014	0.99	(0.22)
	M 2X*	205	60	0.026	0.019	0.014	0.99	(0.22)
	M 250Y	250	45	0.024	0.016	0.011	0.95	0.21
	M 250YS*	250	45	0.024	0.016	0.011	0.95	0.21
	M 252Y*	250	45	0.024	0.017	0.012	0.95	0.21
	M 250X	250	60	0.024	0.017	0.012	0.95	0.22
	M 500Y	500	45	0.010	0.008	0.007	0.92	(0.22)
	B1 250*	250	45	0.023	0.017	0.012	0.98	(0.20)
	B1 250 MN	250	45	0.022	0.016	0.011	?	0.20
	B1 350*	350	45	0.017	0.012	0.008	?	0.20
	B1 500P*	500	45	?	?	?	0.93	(0.20)
	GTO 250Y	250	45	0.027	0.016	0.010	?	0.22
	GTP 350Y	350	45	0.016	0.013	0.010	0.95	0.21
	GTP 350Z*	350	70	0.016	0.011	0.008	0.95	0.21
	GTP 500Y	500	45	0.010	0.008	0.006	0.95	0.20
	F AQ 20*	213	45	?	?	?	?	?
	F 1.6YHC*	295	45	0.020	0.015	0.011	?	(0.22)
	F 1Y*	413	45	0.013	0.009	0.006	0.91	(0.22)
	A 350Y*	350	45	0.016	0.013	0.010	?	(0.22)
	B 350X*	350	60	0.016	0.011	0.009	?	(0.22)
Hybrid	RSP 200X*	200	60	0.027	0.015	0.005	0.95	0.23
	RSP 250Y	250	45	0.019	0.013	0.008	0.95	0.23
	RSP 300Y*	300	45	?	?	?	?	(0.23)
	HFP 2	100	60	0.041	0.025	0.015	0.95	0.20
Random	RSR 1.5	120	-	-	-	-	0.98	-
	RSR 0.7*	180	-	-	-	-	0.98	-
	RSR 0.5*	250	-	-	-	-	0.97	-
	RSR 0.3*	307	-	-	-	-	0.96	-
	PR 2.0*	115	-	-	-	-	0.98	-
	PR 1.0*	230	-	-	-	-	0.96	-
	PR 1.0 (P)*	210	-	-	-	-	0.96	-
	IMTP 40*	150	-	-	-	-	0.98	-
	IMTP 25*	230	-	-	-	-	0.97	-
	CMR 2A*	144	-	-	-	-	0.97	-
	CMR 2A (P)*	129	-	-	-	-	0.97	-
	SB-2P 4050*	119	-	-	-	-	?	-

* data from SRP database or vendor; () estimated value; otherwise data was measured by author

3.3.3 Experimental Protocol

This section explains the general protocol for the experiments performed at the pilot packed column. The detailed standard operating procedure (SOP) is shown in Appendix B.

3.3.3.1 Experimental Protocol for a_e Experiments

About three meters of packing is installed for a_e experiments. Before experiments start, the inlet and outlet CO_2 analyzers are calibrated with ultra-pure nitrogen and 450 ppm_V CO_2 in nitrogen. Entrained liquid is checked in lines of pressure transmitters. About 0.75 m^3 dilute caustic solution (approximately 0.1 N NaOH) is prepared gravimetrically with tap water and NaOH pellets. The solution is mixed by pump between the column sump and storage tank until the alkalinity concentration stabilizes (confirmed by constant readings from acid titration). A medium-high (37 or 49 $m^3/m^2 \cdot h$) liquid load is used for prewetting the packing for 10–15 minutes. After prewetting, gas is introduced to the column and the measurements start. For each batch of solution, the gas rate is kept constant while the liquid rate is first increased till it reaches the pump limit then decreased. Typical sequence of liquid rate is: 49, 61, 73, 37, 24, 12, and 6 $m^3/m^2 \cdot h$. The operating condition is changed when CO_2 readings from both analyzers are stabilized, which is usually within five minutes. The bulk alkalinity depletion is corrected online by mass balance. After sufficient data is measured for one gas rate, the solution is neutralized by concentration hydrochloric acid to pH 6–9 and then drained to sewer. A new batch is prepared for experiment at another gas rate. Typically, three gas rates (0.6, 1, and 1.5 m/s) are measured for one packing. Areas for relatively high gas rates (2 and 2.5 m/s) at one medium liquid load (24 or 37 $m^3/m^2 \cdot h$) are measured for interpretation of $k_{OG}a_e$ data.

3.3.3.2 Experimental Protocol for k_L Experiments

About 1.8 meters of packing is installed for k_L measurement with water. After that, the packing is increased to three meters to check the effect of packing height. Before experiments, the functionality of the gas chromatography (GC) is checked with blank sample of extract liquid (heptane). About 0.75 m^3 batch is prepared from tap water. Packing is pre-wetted at a medium-high liquid rate (37 or 49 $m^3/m^2 \cdot h$) for 10–15 minutes before measurement. The gas rate is kept constant (usually at 1 m/s) during experiments. When experiment starts, about one liter of toluene is spiked into the batch, and the toluene metering pump is turned on to maintain the bulk toluene concentration at a level favorable to the GC. Toluene concentration will be kept well below saturation to avoid introducing liquid-phase toluene in the flow which will result to a lower k_L. Typical sequence of liquid rate is like that in a_e experiments: 49, 61, 73, 37, 24, 12, and 6 $m^3/m^2 \cdot h$. For each operating condition, 10–15 minutes is allowed for the system to reach steady state before the liquid samples are taken and sent to GC. Different gas rate (0.6 and 1.5 m/s) is used at one medium liquid load (24 or 37 $m^3/m^2 \cdot h$) to check the effect of gas rate on k_L in the pre-loading zone. After satisfactory number of data points are measured, the batch is drained to 55-gallon drums for disposal by the Environmental Health and Safety (EHS) service of the University of Texas at Austin.

3.3.3.3 Experimental Protocol for k_G Experiments

About 0.5–1 m packing is installed for k_G measurement. Before experiments, the SO_2 analyzer is calibrated with zero-air instrument and 90 ppm_V SO_2 in nitrogen. About 0.75 m^3 dilute caustic solution (approximately 0.1 N NaOH) is prepared gravimetrically with tap water and NaOH pellets. The SO_2 is controlled by a rotameter connected to 2% SO_2 cylinders. Both the inlet and outlet sample lines are flushed with concentrated SO_2

(300–400 ppmv) at low gas rate (0.6 m/s) to saturate the water residues until the two readings become stabilized at the same value. For concerns of SO_2 inventory, the gas rates are changed from low to high (typically 0.5, 0.1, 1.5, 2.0, and 2.5 m/s). The SO_2 rotameter is varied accordingly with the gas rate to keep the inlet SO_2 concentration 50–100 ppmv. Liquid load is kept constant (usually 24 or 37 $m^3/m^2 \cdot h$) during experiments. Operating condition is changed when the SO_2 analyzer gives stable reading (typically about 10 minutes). After experiments, the solution is neutralized by concentration hydrochloric acid to pH 6–9 and then drained to sewer.

3.3.3.4 Experimental Protocol for Aqueous Glycerol

Glycerol concentration required to obtain the desired μ_L at the projected experiment temperature (ambient) is calculated based on density and viscosity correlations. When preparing solutions for k_L experiments, tap water is first added to the tank, and then pure glycerol is gradually charged into the tank by an air pump. The batch is then mixed between column sump and storage tank for 4–8 hours. Three 0.75-m^3 batches (3–5, 12–15, and 30–60 mPa·s) are made to reuse in k_L measurements for different packings. In order to compensate for the water loss or gain during each experiment, either pure water or glycerol was added to the batch to keep the solution at its target viscosity before reuse.

To prepare aglycerol batch to measure, concentrated (about 2 mol/L) caustic is first prepared with NaOH pellets in 5-gallon plastic drums and then mixed with the bulk glycerol batch to avoid lengthy dissolving time of the pellets. The solutions are mixed by the pump between column sump and tank for 4–8 hours and the a_e measurements only start when acid titration gives constant readings. The a_e batch is not reused across packings like k_L to prevent excessive carbonate accumulation. However, it is reused for each

packing with decreasing order of μ_L, i.e., the most viscous batch is first prepared and measured, after which the batch is diluted to the next lower μ_L with extra caustic added to compensate for alkalinity lost caused by CO_2 absorption and batch dilution. In consideration of the availability of the column and the price of glycerol, extra k_L measurements are made (apart from measurements made with the reused batches) while measuring a_e. The gas phase CO_2 concentration is measured by the CO_2 analyzer at the same time while liquid samples are taken for toluene concentration. Simultaneous measurement of k_L and a_e with water was performed prior to measurements with aqueous glycerol to ensure that the technique would generate reliable data compared to previous separate measurements of k_L and a_e.

Between experiments with different liquid batches, the column is washed by circulating tap water for 0.5–1 hour to avoid cross contamination. Reused k_L batches are stored in closed-top 55-gallon (~208 L) drums with 4 drums for each batch in a ventilated storage shed between experiments.

The operating conditions for aqueous glycerol are similar to that of water unless either the pump capacity or hydraulic condition make measurements of the most viscous (30 – 60 mPa·s) batch in fine packings (a_P = 350–500 m^2/m^3) infeasible. Liquid samples at both inlet and outlet are collected at each operating condition for offline measurement of physical properties. The average value of physical properties was used for model development. The sampling time is recorded so that the liquid temperature can could be retrieved and used in the offline measurement.

Because of the low mass transfer efficiency of aqueous glycerol, a 30-min gap instead of 10 min is used between operating conditions to reach steady state in k_L experiments. The speed of the toluene metering pump is lowered accordingly for mass balance. There are more entrained gas bubbles in the liquid samples of aqueous glycerol

compared to water. Therefore, in the liquid extraction process to make GC samples, liquid samples are not mixed with heptane until all the visible entrained gas bubbles have moved up to the top of the vials to avoid reabsorption of toluene. However, the waiting time should be controlled to avoid excessive toluene desorption from the liquid samples, which will result in a higher k_L. Since density of aqueous glycerol is significantly different from water, care is taken to calculate the toluene concentration from the mass-based GC results.

Figure 3.18 shows the process flow chart of experiments in the pilot-packed column. Besides experiments of k_L with water and aqueous glycerol, packing characterization tests were performed for some packing. Packing characterization test including measurement of hydraulic properties of pressure drop (ΔP), liquid hold-up (h), and mass transfer properties of k_L, k_G, and a_e with water.

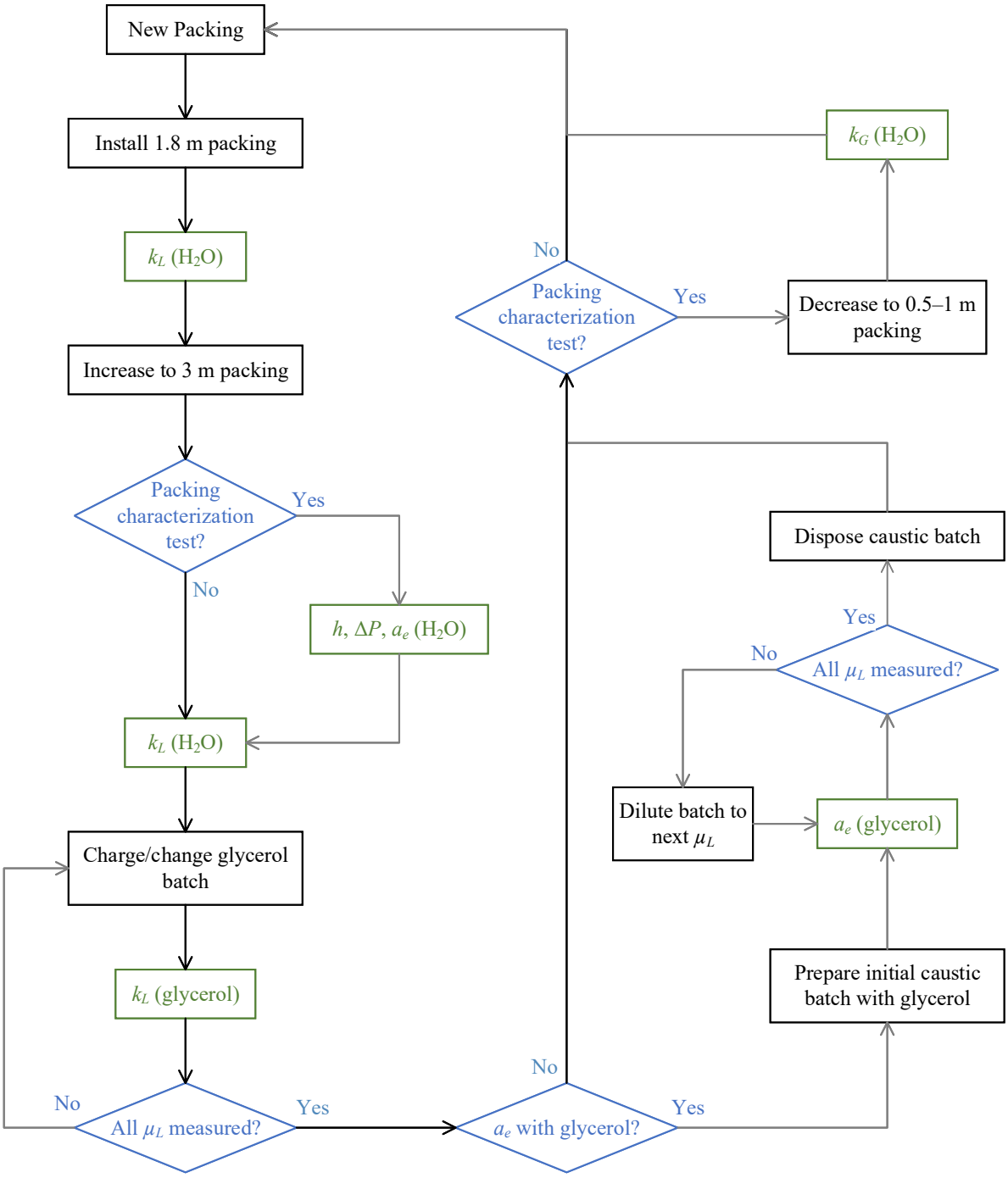

Figure 3.18: Process flow chart of AWC experiments

3.3.4 Data Analysis

3.3.4.1 Effective Mass Transfer Area (a_e)

The overall volumetric mass transfer coefficient, $K_G a_e$, is determined experimentally from the inlet and outlet CO_2 in the gas phase (Equation 3.58). Neglecting the gas side mass transfer resistance gives Equation 3.59. Thus, the a_e can be determined when the reaction kinetics are known (Equation 3.60).

$$K_G a_e = \frac{u_G \ln\left(\frac{y_{CO2,in}}{y_{CO2,out}}\right)}{ZRT} \tag{3.58}$$

$$K_G a_e \approx k_g{}' a_e \tag{3.59}$$

$$a_e = \frac{K_{OG} a_e}{K_{OG}} \approx \frac{K_{OG} a_e}{k_g'} = \frac{u_L}{k_g' Z} \ln\left(\frac{C_{CO_2,\,in}}{C_{CO_2,\,out}}\right) \tag{3.60}$$

As is discussed in section 2.1.3, k_g' has a simplified form based on penetration theory and the pseudo-first order assumption (Equation 2.22). The kinetics of CO_2/NaOH/H_2O is well-established and the reaction rate constant, k_{OH^-}, can be calculated using the model developed by Pohorecki and Moniuk (1988), which is shown in Equations 3.61 and 3.62.

$$k_g' = \frac{\sqrt{k_{OH^-}[OH^-] D_{CO_2,L}}}{H_{CO_2}} \tag{2.22}$$

$$\log_{10}\left(\frac{k_{OH^-}}{k^{\infty}_{OH^-}}\right) = 0.221I - 0.016I^2 \tag{3.61}$$

$$\log_{10} k^{\infty}_{OH^-} = 11.896 - \frac{2382}{T} \tag{3.62}$$

The k_g' of CO_2/NaOH/H_2O/glycerol is expressed by a relationship comparable to that of the water system (Equation 3.32). The rate constant, k_{Alk}, is dependent on the

WWC experimental data, which is shown in detail in Chapter 4 with analyzing method shown in section 3.2.3.

$$k_g' = \frac{\sqrt{k_{Alk}[\mathrm{Alk}]D_{CO_2,L}}}{H_{CO_2}} \tag{3.32}$$

Physical properties (density, viscosity, surface tension, diffusivity, and Henry's constant of CO_2) of water and aqueous glycerol are calculated using models shown in section 3.1.2. Liquid temperature is not controlled in the system, so gas and liquid properties vary with ambient temperature. The temperature used in reaction kinetic and physical property calculation is the average of gas and liquid temperature with the liquid weighted more heavily (Equation 3.63). This practice is found to be more accurate in reconciling the mass transfer area data at ambient temperature extremes (i.e., summer and winter) than simply using the liquid temperature. The "corrected" temperature is on average within 3 °C of the liquid temperature, so the applied correction was not extreme.

$$T_{system} = \left(T_{liquid} + \left(T_{gas,in} + T_{gas,out}\right)/2\right)/2 \tag{3.63}$$

Secondary effects (end and wall effects) on mass transfer area ($a_{secondary}$) are subtracted from the total area measured experimentally (a_e) to give the corrected effective mass transfer area of the packing surface ($a_{e,corr}$):

$$a_e = a_{e,corr} + a_{secondary} \tag{3.64}$$

$$a_{secondary} = a_{top} + a_{wall} + a_{bottom} \tag{3.65}$$

The correction for secondary effects is a worst-case scenario. The wall area includes that in the packing section and in the section between packing bottom and liquid sump (specifically 4.5 m for the column in this work). The column wall is assumed to be fully wetted:

$$a_{wall} = \pi \cdot D_{column} \cdot \left(Z_{packing} + Z_{auxiliary}\right) \tag{3.66}$$

The top area includes area generated by the liquid streams from the distributor to packing top with both stream peripheral and impact area (Equation 3.67). The impact area is the area created when liquid from distributor splashes onto the top packing element, which can be calculated from the model of liquid phase number of transfer units (NTU_L) developed by Yeh (2002) in a spray tower for liquid-solid impact (Equation 3.68), and definition of NTU_L (Equation 3.69).

$$a_{top} = a_{top,imp} + a_{top,str} \tag{3.67}$$

$$NTU_L = 0.026 \cdot u_{L,imp}^{0.7} \cdot u_{L,spary}^{-0.2} \tag{3.68}$$

$$NTU_L = \frac{k_L^0 a_e}{Q} \tag{3.69}$$

Combining Equations 3.68 and 3.69 gives:

$$a_{top,imp} = 0.026 \cdot u_{L,imp}^{0.7} \cdot u_{L,spary}^{-0.2} \cdot \left(\frac{Q}{k_L^0}\right) \tag{3.70}$$

The $k_L{}^0$ is assumed to be constant (1×10^{-4} m/s). The spray velocity, $u_{top,spray}$, is calculated from the volumetric liquid load (Q), dripping-point density of the distributor (430 points/m^2), and the diameter of the dripping points (3 mm):

$$u_{top,spray} = \frac{Q}{\left(\frac{\pi}{4} \cdot {d_{drip\ point}}^2\right) \times \left(\rho_{drip\ point} \cdot \frac{\pi}{4} \cdot {D_{column}}^2\right)} \tag{3.71}$$

The impact velocity, $u_{top,imp}$, is calculated by energy balance of the liquid streams (Equation 3.72). The correction is a worst-case scenario, so the distance between the distributor and packing, $d_{distributor\text{-}packing}$, is assumed to be 12 cm (the actual distance varies with packing but is always between 3–8 cm).

$$\frac{u_{top,imp}^2}{2} = g d_{distibutor-packing} + \frac{u_{top,spray}^2}{2} \quad (3.72)$$

The peripheral area of top streams is calculated by Equation 3.73:

$$a_{top,str} = \pi \cdot d_{drip\ point} \cdot d_{distibutor-packing} \cdot \left(\rho_{drip\ point} \cdot \frac{\pi}{4} \cdot {D_{column}}^2\right) \quad (3.73)$$

Similar to top area, the bottom area includes area generated by the liquid streams falling from the packing bottom to the sump. The impact area is calculated based on the model of liquid phase number of transfer units (NTU_L) developed by Yeh (2002) in a spray tower for liquid-liquid impact:

$$a_{bot,imp} = 0.056 \cdot u_{L,imp}^{0.5} \cdot u_{L,spary}^{-0.5} \cdot \left(\frac{Q}{k_L^0}\right) \quad (3.74)$$

The spray velocity, $u_{bot,spray}$, is calculated from the volumetric liquid load (Q) and liquid hold-up (Equation 3.75). The impact velocity, $u_{bot,imp}$, is calculated by energy balance of the liquid streams with the distance, $d_{packing\text{-}sump}$, assumed to be 1.8 m (Equation 3.76).

$$u_{bot,spary} = \frac{Q}{h \cdot (\frac{\pi}{4} {D_{column}}^2)} \quad (3.75)$$

$$\frac{u_{bot,imp}^2}{2} = g d_{packing-sump} + \frac{u_{top,spray}^2}{2} \quad (3.76)$$

Unlike the ordered pattern of top streams from the distributor, the bottom streams from the packings bottom have highly unstable flow pattern, which depends on both the operating condition and the packing geometry. As a result, the peripheral area of bottom streams is not calculated.

3.3.4.2 Liquid and Gas Film Mass Transfer Coefficient (k_L and k_G)

The overall volumetric mass transfer coefficient, $K_L a_e$, is determined experimentally from the inlet and outlet toluene in the liquid phase measured with gas chromatograph (Equation 3.77). Neglecting gas film mass transfer resistance gives Equation 3.78. Thus, with the knowledge of mass transfer area, k_L can be calculated from Equation 3.79.

$$K_L a_e = \frac{u_L}{Z} \ln\left(\frac{C_{Toluene,in}}{C_{Toluene,out}}\right) \tag{3.77}$$

$$K_L a_e \approx k_L a_e \tag{3.78}$$

$$k_L = \frac{u_L}{Za} \ln\left(\frac{C_{Toluene,in}}{C_{Toluene,out}}\right) \tag{3.79}$$

The overall volumetric mass transfer coefficient, $K_G a_e$, is determined experimentally from the inlet and outlet SO_2 in the gas phase (Equation 3.80). Neglecting liquid film mass transfer resistance gives Equation 3.81. Thus, with the knowledge of mass transfer area, k_G can be calculated from Equation 3.82.

$$K_G a_e = \frac{u_G}{Z} \ln\left(\frac{y_{SO2,in}}{y_{SO2,out}}\right) \tag{3.80}$$

$$K_G a_e \approx k_G a_e \tag{3.81}$$

$$k_G = \frac{u_G}{Za} \ln\left(\frac{y_{SO2,in}}{y_{SO2,out}}\right) \tag{3.82}$$

Density of air is calculated from temperature and pressure based on the ideal gas law. Diffusivity of SO_2 in the air was calculated from the Fuller equation (1966).

3.3.5 Safety and Experimental Concerns

3.3.5.1 Experimental Concerns

Due to its low viscosity, the outlet water sample is believed to be well mixed. With viscous glycerol solutions, biased liquid samples might be collected occasionally due to uneven distribution of the liquid. The biased liquid sampling is reflected by unreasonably low mass transfer efficiency. For these cases, the operating condition is repeated. The inlet liquid sample does not have these problems since it is collected directly from inlet liquid pipes.

During the hydraulic and mass transfer test, care should be exercised to ensure minimal condensation or entrainment of liquid in the pressure transmitter lines especially at high liquid loads or around the flood point. The transmitter tubing should be routinely checked and purged to solve this problem.

Packing height is a compromise between the requirement of longer packing to curb end effect and to provide sufficient mass transfer and the requirement of shorter packing to reduce maldistribution and to prevent excessive mass transfer. Experiments performed with different bed height should be normalized to a common level for fair analysis.

With regard to solution preservation, the shelf life of glycerol in proper storage condition could be at least 12 months at 25 °C, and the highest temperature for storage at ambient condition is 52 °C (P&G Chemicals). Though a preliminary bench-scale sterilization experiment in the lab environment has shown that no biocide is needed for glycerol-rich solutions in open containers in 45 days (section 3.1.3), special care should still be exercised to monitor the appearance and physical properties of the solutions when reused.

Pumping pure glycerol to the storage tank using an air pump is time consuming (6 hours to move 0.75 m^3) because of the exceedingly high μ_L (> 1000 mPa·s at 20 °C). To

facilitate the pumping, a large capacity air pump is used with large diameter tubes and connections when possible. The situation is worsened in cold weather, so drum heating belts are used to heat up the glycerol before and during pumping.

Because of the ambient temperature change during the experiment, together with the heat and mass transfer effect of water vaporization/condensation, it is not practical to keep the μ_L constant. Liquid loss during batch preparation and experiments (such as liquid left in the pipe, dead-leg liquid, etc.) also make accurate μ_L control impractical. However, since the μ_L for each operating condition was measured and correlated individually, the variation in μ_L should not be problematic.

3.3.5.2 Safety

- Hard hats are required for experiments outside the control room.
- Caustic (NaOH) should be neutralized to pH 6–10 before draining to sewer.
- Nitrile gloves are required for any experiment that involves alkaline solutions.
- Gas mask with respirator is required when handling volatile and toxic chemicals (such as SO_2 cylinders).
- Steel reinforced gloves are required when handling sheet metal structured packings.
- Solid/liquid waste should be disposed into proper solid/liquid waste drums with explicit labels.
- Valves should be close/opened gradually to avoid sudden disturbance to the system, especially when it will cause significant pressure change.

- Air pressure test should be applied to any unit before opening the liquid path.
- Walking path should be avoided when installing tubing/piping.
- Over-tightening Swagelok connections will damage threads and result in leakage.
- Teflon tape (5–7 circles depending on the applied material) should always be applied to NPT connections.
- Nomex is required when experiments with hydrocarbon are performed in the pilot plant.
- Leak check, especially at pipe connections, should be performed during the pumping process.

3.4 SUPPORTING METHODS AND EQUIPMENT

In the WWC experiments, CO_2 concentration were measured online by two Horiba infrared carbon dioxide analyzers. In the air-water column (AWC) experiments, CO_2 concentration in both the inlet and outlet gas were measured online by an XStream® CO_2 analyzer (Rosemount). The SO_2 concentration in the gas was measured online by a Thermo Scientific Model 43i SO_2 analyzer. During a_e and k_G experiments, gas was sampled through a gas sampling system (Rosemount) to eliminate water vapor that could be condensed inside the sampling tube and cause extra mass transfer (Figure 3.19). The system uses utility nitrogen to cool down the sampled gas through a curled tubing heat exchanger. Flow of the sampled gas can be controlled by an electrical pump that creates a negative pressure in the sampling line.

Figure 3.19: Gas sampling system

A Titrando titrator (Metrohm, Riverview, FL, USA) with automatic equivalence point detection was used to measure pH and total alkalinity of WWC samples. Concentration was measured by titration with 0.2 N H_2SO_4. Samples of known mass were diluted 10–15 times with DDI water and titrated to a pH of about 2. The pH values were recorded over time as acid was added to the solution. The amount of acid corresponding to the equivalence point was used to determine the concentration of total alkalinity. The bulk alkalinity in AWC samples was measured by acid titration with 0.1 N HCl.

Total inorganic carbon (TIC) analysis was performed to verify the carbonate. Samples of known mass were injected into a tube containing 30 wt % H_3PO_4. By contacting with the strong acid, CO_3^{2-} and its equivalent were released as CO_2, which was carried by a N_2 stream to a Horiba IR-2000 infrared analyzer. Each injection generated a

signal peak, the area of which was recorded for the total inorganic carbon. A series of carbon standards (Na_2CO_3/$NaHCO_3$ aqueous solutions, 1000 ppm) of different amounts was injected to obtain the calibration curve.

Liquid density was measured by a Mettler Toledo DE40 densitometer (Columbus, OH). Approximately 3 mL of sample was injected into an oscillating U-shaped glass tube in the instrument. The oscillating frequency was measured and related to the sample density by calibration of samples with known density (dry air and water). DDI water, acetone, and dry air were used consecutively to purge the instrument. Before acquiring the offline data, densities measured online by the Micromotion® flowmeter were used for preliminary calculation of glycerol concentration. The online and offline measurement gave very close density.

Liquid viscosity was measured offline by a TA Instrument AR-2000ex rheometer and a Physica MCR 300 cone and plate viscometer (Anton Paar GmbH, Graz, Austria) depending on their availability. Temperature was regulated with a Peltier unit and a Julabo F25 water bath unit. 800 μL of sample was deposited on the platform. A uniform liquid layer formed between the platform and the spindle when the latter was lowered to 0.5 mm above the former. The spindle then rotated at different logarithmically ramped angular velocities (100–1600 s^{-1}) and the torque required to rotate it was measured. Viscosity was calculated based on these parameters and the system geometry.

One of the viscometer skids (Figure 3.20) used in the 2015 carbon capture campaign (Rochelle et al., 2015b) was moved to the second floor of the PVC column structure and connected to the liquid inlet line with 1" PVC piping (Figure 3.21). The skid can provide online viscosity, density, and temperature measurement. The skid contains a Grundfos CRN1-3 pump, Micro Motion® 7829 Visconic viscometer, Rosemount 8711 flowmeter, and a SMVector VSD. The pump speed can be controlled by a PID

controller in the control box. The flow-through chamber for the viscometer was fabricated by Micro Motion and is believed to improve the accuracy of measurement.

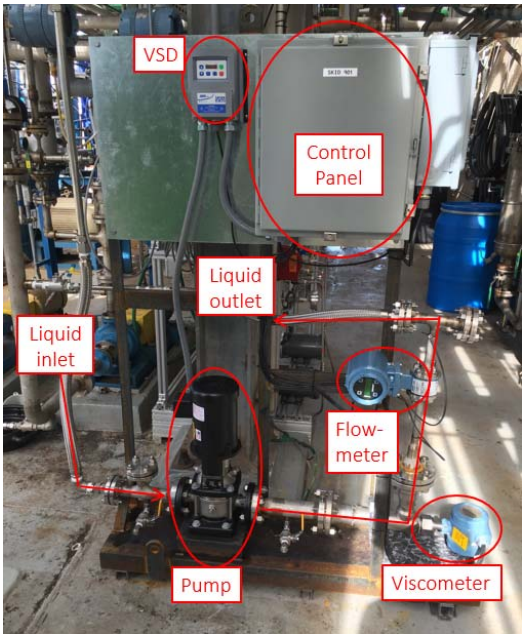

Figure 3.20: Viscometer skid

(a) Viscometer skid

(b) Bypass inlet line

(c) Bypass outlet line

Figure 3.21: Viscometer skid connected to AWC

Toluene concentrations of the liquid samples for k_L experiments were measured by FID gas chromatography (Hewlett Packard 6890). The analytical method was similar to that used by the Separations Research Program for water. Heptane was used to extract toluene from liquid samples with 1-bromo-4-fluorobenzene (B4FB) used as the internal standard. Larger heptane extraction ratio (8:1 compared to 4:1) was used for glycerol solutions than for water to obtain greater measurement resolution. The sampling procedure is shown in Figure 3.22. Details of data analysis of GC samples are shown in Appendix D.

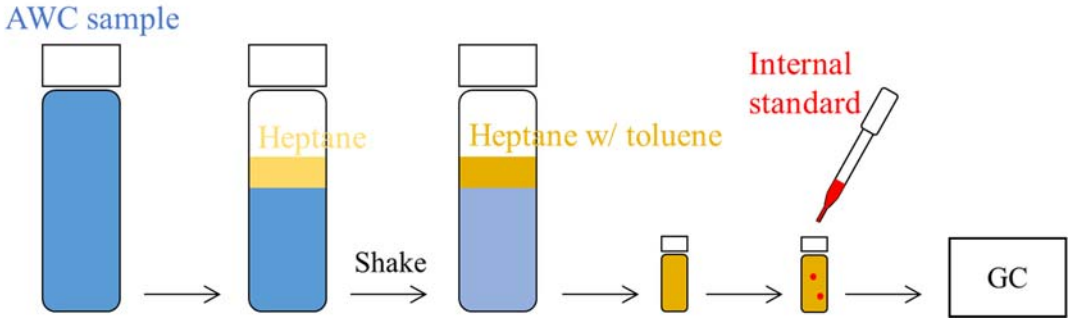

Figure 3.22: Sampling procedure for GC analysis

The solubility of glycerol in n-heptane is lower than 0.7 mmol/L over the temperature range 20–100 °C (Staveley & Milward, 1957). This agrees with the qualitative analysis that solubility of NaOH and glycerol in n-heptane should be very low because of the high hydrophilicity. Standard samples prepared gravimetrically were measured with GC to check whether the method works for aqueous glycerol. Per Table 3.12, the method works well for glycerol samples of 40 and 82 wt %, which covers the range of glycerol concentration in the AWC experiments.

Table 3.12: Test of GC method with aqueous glycerol

GC standard	Glycerol (wt%)	Actual toluene (ppmw)	Measured toluene (ppmw)	Ratio measured/actual
1	0	177	166	0.94
2	40	158	149	0.94
3	40	53	46	0.87
4	82	217	201	0.93
5	82	54	54	1.00

3.5 CHEMICALS AND MATERIALS

Distilled and deionized (DDI) water, 1N sodium hydroxide solution (Fisher), 1N sodium carbonate solution (Fisher), and glycerol (Fisher, 0.995-0.998 purity) were used in solution preparation of WWC experiments. Pure N_2 and 5000 ppm_v CO_2 in N_2 were from Praxair.

In the pilot column experiments, NaOH pellets (Fisher) were used to prepare the caustic batch. The 0.1 N HCl and phenolphthalein used in titration were purchased from Sigma Aldrich. Concentrated (36-38%) hydrochloric acid (J. T. Baker) was used to neutralize the caustic batch before disposal. The ultra-pure nitrogen and 450 ppm_V CO_2 cylinders used for CO_2 analyzer calibration were purchased from Praxair. The USP grade glycerol (99.7%) used to prepare the batch was purchased from Acme-Hardesty. The n-heptane and 1-bromo-4-fluorobenzene used in liquid sample extraction was purchased from Fisher and Aldrich Chemistry, respectively. The 90 ppm_V SO_2 cylinder used for SO_2 analyzer calibration was from Praxair. The 2 volume % SO_2 injected to the air in the k_G experiments was from Praxair.

Chapter 4: Wetted-Wall Column Results[3]

Chapter 4 includes the experimental and modeling results of the wetted-wall column (WWC) experiments. k_g' for CO_2/NaOH/H_2O measured in this work is slightly (~15%) greater compared to literature data (Pohorecki & Moniuk, 1988),. k_g' for aqueous glycerol initially increases because of the catalytic effect of glycerol, and then rapidly decreases because of the increased μ_L and subsequently decreased D when glycerol is further increased. The kinetic model for CO_2/NaOH/H_2O/glycerol developed based on WWC data is used in the air-water column (AWC) experiments and provides reasonable results.

4.1 Kinetic Model for Water and Aqueous Glycerol

Figure 4.1 shows the measured and calculated k_g' obtained from the WWC. When glycerol is added to the liquid, k_g' initially increases because of its catalytic effect (k_{gly}- > k_{OH}-), and then k_g' rapidly decreases because of the increased μ_L and decreased D. This non-monotonic trend applies for all temperatures (20, 30, and 40 °C) and caustic concentrations (0.1 and 0.3 mol/L) investigated. At the highest glycerol (80–89 wt %), k_g' is only 25% of the pure aqueous caustic solution. The addition of 0.025 mol/L (0.05 N) Na_2CO_3 in the 0.1 mol/L NaOH batch (equivalent to 50% bulk carbonate accumulation) does not significantly affect k_g'. In addition, turning off the gas pre-saturator and varying the liquid flow rate do not affect k_g'. The provided k_g' values shown in Figure 4.1 include a correction for depletion of surface alkalinity, which is a small correction that will be discussed in section 4.2.

[3] D. Song, G.T. Rochelle. "Reaction kinetics of carbon dioxide and hydroxide in aqueous glycerol." Chem Eng Sci. (2017) 161:151-8

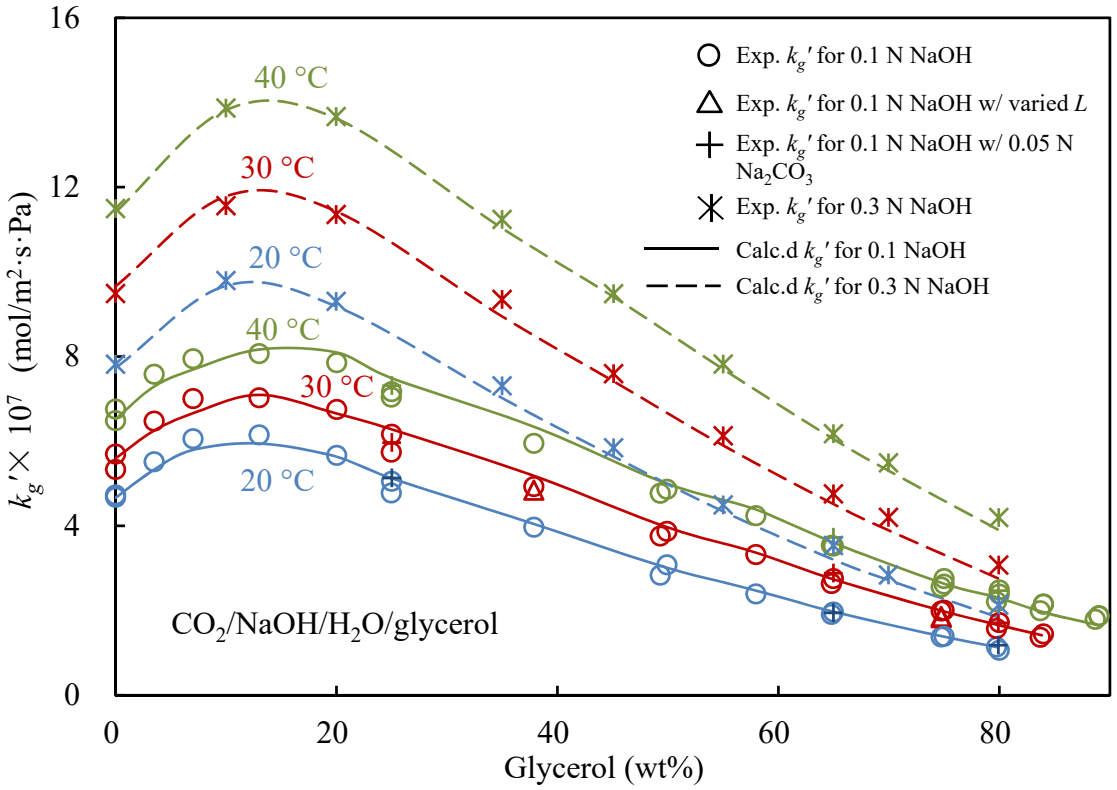

Figure 4.1: Measured and calculated k_g' for CO_2/NaOH/H_2O/glycerol

A fit of the overall reaction rate constant (k_{Alk}) determined from experimental k_g' (Equation 3.41), with the theoretical value (Equations 3.33–40) gives parameters in Equations 3.35, 3.36, and 3.38 (Table 4.1). The fitting was performed with Matlab® using least-square rule. As is shown in Figure 4.1, the k_g' calculated from the kinetic models (shown here) and physical property models (shown in section 3.1.2) fits the experimental k_g' well.

$$\ln\left(\frac{k_{OH^-}}{k_{OH^-,298.15K}}\right) = \frac{-E_{OH}}{R}\left(\frac{1}{T} - \frac{1}{298.15}\right) \tag{3.35}$$

$$\ln\left(\frac{k_{Glycerol^-}}{k_{Glycerol^-,298.15K}}\right) = \frac{-E_G}{R}\left(\frac{1}{T} - \frac{1}{298.15}\right) \tag{3.36}$$

$$\ln\left(\frac{K_{b,Glycerol}}{K_{b,Glycerol,298.15K}}\right) = \frac{-H_{KG}}{R}\left(\frac{1}{T} - \frac{1}{298.15}\right) \quad (3.38)$$

Table 4.1: Parameters in the reaction rate model for CO_2/NaOH/H_2O/glycerol

Equation	Fitted parameters	
3.35	$k_{OH\text{-},298.15K}$ (m^3/mol·s)	E_{OH} (kJ/mol)
	12.68 ± 3.49	49.03 ± 2.09
3.36	$k_{Glycerol\text{-},298.15K}$ (m^3/mol·s)	E_G (kJ/mol)
	80.68 ± 10.2	45.32 ± 2.28
3.38	$K_{b,Glycerol,298.15K}$ (m^3/mol·s)	H_{KG} (kJ/mol)
	3.79 ± 0.69	6.1 ± 0.53

k_g' for water is compared internally (to other researchers using the same equipment) and externally (to other researchers measuring the same system using different equipment) to check the reproducibility of the WWC measurement. Per Figure 4.2, the calculated k_{OH}- from Equation 3.35 is about 40% greater than that from Equations 3.61 and 3.62 by Pohorecki & Moniuk (1988). This difference resulted from a 17% greater k_g' measured in this work compared to that measured by Pohorecki and Moniuk with a laminar jet. The k_g' measured by Tsai (2010) is also 10–15% greater than the literature data (Figure 4.3). Therefore, the WWC shows good internal reproducibility, but gives k_g' slightly higher than obtained by Pohorecki & Moniuk (1988).

In order to keep conformity with previous SRP data, the Pohorecki & Moniuk model (Equation 3.61 and 3.62) is used to interpret AWC data for pure aqueous caustic solutions without glycerol. However, for glycerol solutions, the model based on the

WWC measurement (Equation 3.35) is used to calculate the overall rate constant, k_{Alk}, for better agreement with the WWC data.

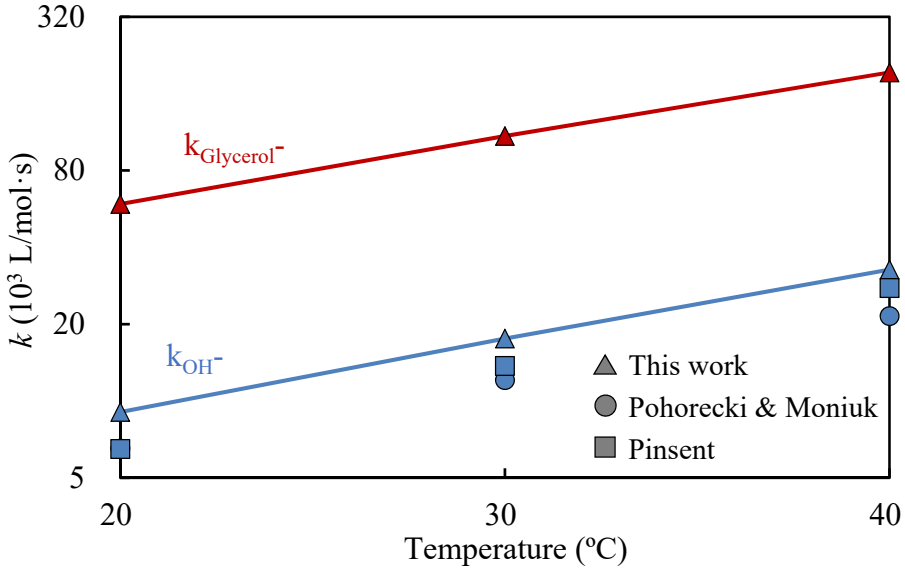

Figure 4.2: Calculated k_{OH}- and $k_{Glycerol}$-

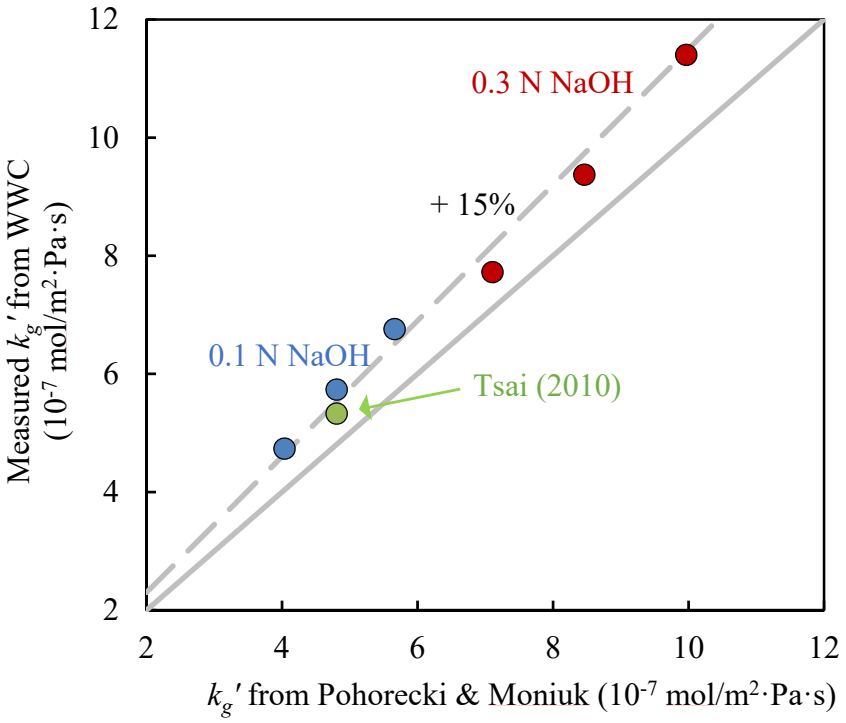

Figure 4.3: k_g' measured by WWC compared to Pohorecki & Moniuk (1988) for CO_2/NaOH/H_2O

In Figure 4.2, the CO_2-glyceroxide reaction ($k_{Glycerol}$-) is 6–7 times faster than the CO_2-hydroxide reaction. Other measurements of alkoxide kinetics show the CO_2 insertion into metal alkoxide is significantly faster than the reaction between CO_2 and hydroxide in an aqueous environment (Faurholt, 1927b; Heston et al., 1943).

Figure 4.4 shows the experimental k_{Alk} based on WWC k_g' (Equation 3.41) and the calculated values from Equations 3.33–40. The overall rate constant k_{Alk} initially increases rapidly with glycerol, and then becomes asymptotic. This is a result of the greater value of $k_{Glycerol}$- than k_{OH}- and the increasing ratio of glyceroxide in the total alkalinity when glycerol concentration increases.

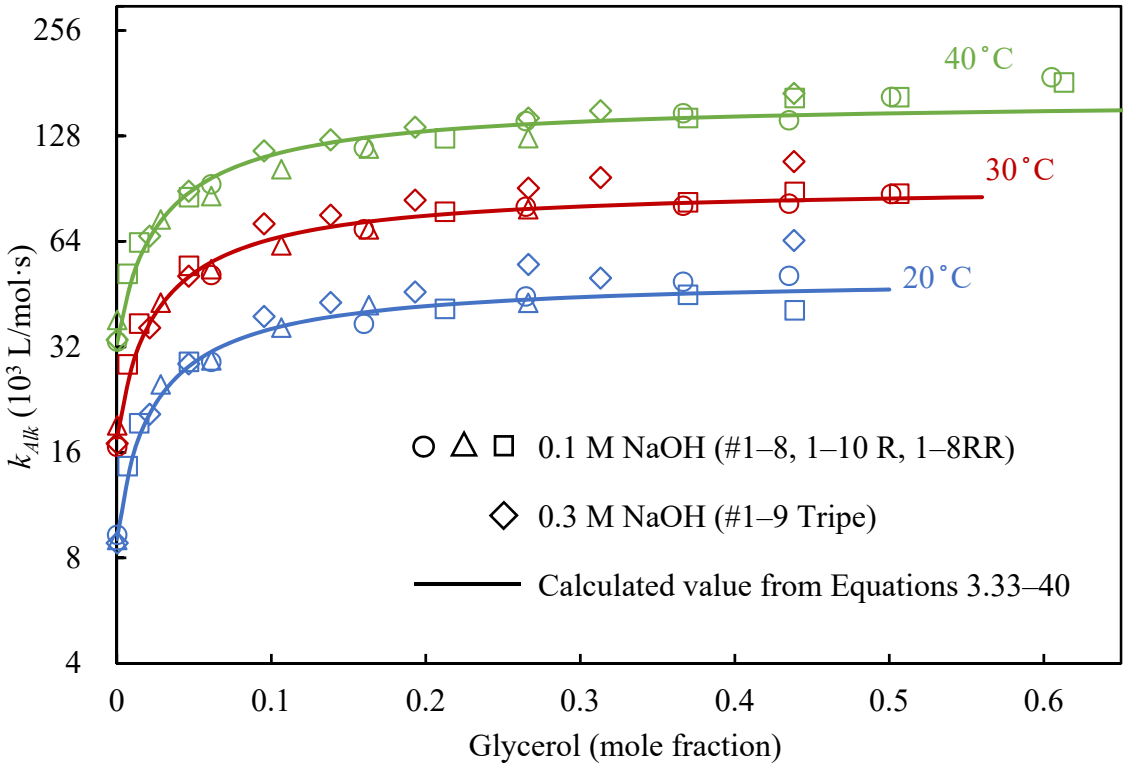

Figure 4.4: Experimental and calculated k_{Alk} for CO_2/NaOH/H_2O/glycerol

Figure 4.5 compares the calculated alkoxide/alkalinity ratio in this work with literature data obtained by precipitation method for aqueous methanol solution at 0 °C with 0.2 N NaOH (Faurholt, 1927b; Heston et al., 1943). The higher alkoxide ratio in the literature results from the significantly larger pKa of methanol than glycerol (Ballinger & Long, 1960).

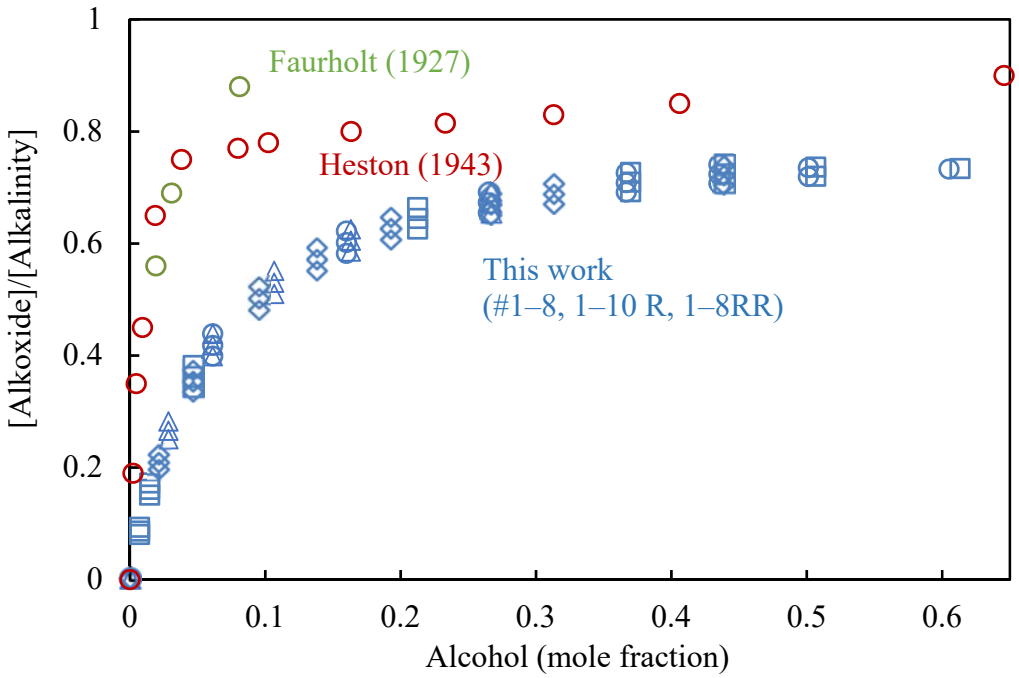

Figure 4.5: Alkoxide to alkalinity ratio from literature and this work

Figure 4.6 shows that the pKa of aqueous glycerol estimated from pH measurement is lower than the literature data (Ballinger & Long, 1960; White et al., 1977), while the calculated value from Equation 3.38 is greater than the literature data. No conclusion can be drawn from this comparison, and the difference may result from the inaccuracy of pH measurement for dilute solutions and the relative simplicity of the kinetic model.

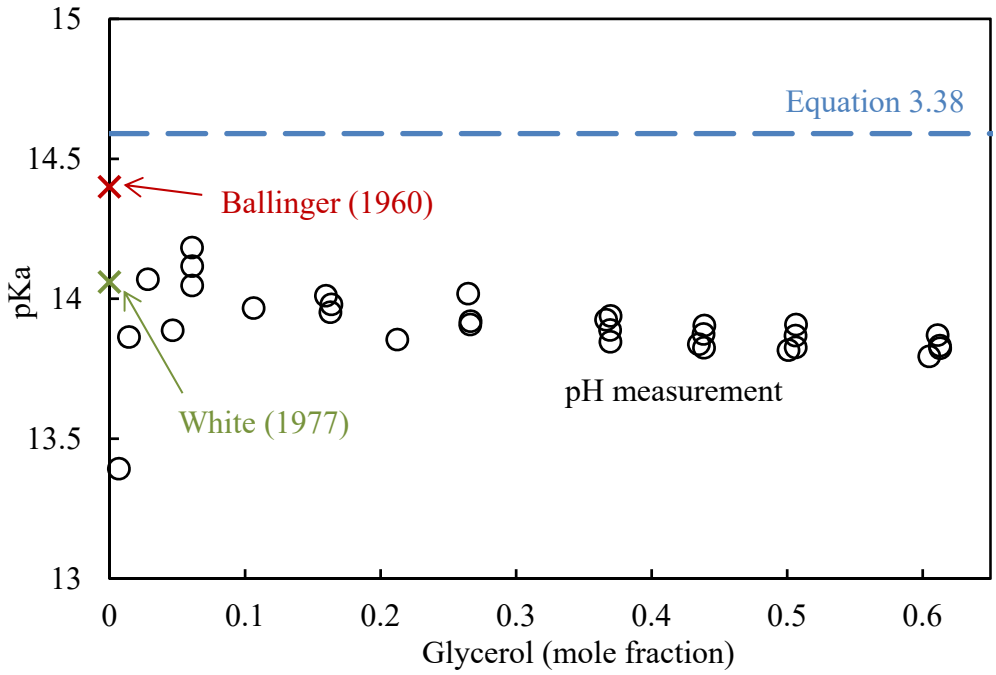

Figure 4.6: pKa of aqueous glycerol at 25 ºC

Sharma and Danckwerts (1963) investigated a number of anions that have a catalytic effect on the CO_2-H_2O reaction:

$$CO_2 + H_2O \longrightarrow HCO_3^- + H^+ \qquad (4.1)$$

They divided the anions into several groups and found that group A (anions with a negatively-charged oxygen atom and at least one hydroxyl group attached to the same central atom) obeys the Brönsted relationship. Group B (including trifluoroethanol and trichloroethanol) and group C (sugars including glucose, fructose, sucrose, and lactose) showed significantly less catalytic effect and do not obey the Brönsted relationship. They explained that the lower catalytic power of group C was a result of the formation of mono-alkyl carbonates (CO_2 insertion):

$$RO^- + CO_2 \longrightarrow RCO_3^- \qquad (4.2)$$

Faurholt and co-workers (1927a, 1927b, 1927c) were cited by Sharma and Dankwerts to support the CO_2 insertion mechanism, however, in their work CO_2 insertion was found to be faster instead of slower than the CO_2-hydroxide reaction.

Glycerol is structurally close to sugars in group C with multiple hydroxyl groups each attached to different carbons, however, it is close to the curve of group A in the Brönsted plot (Figure 4.7). This observation needs further investigation before any firm conclusion can be drawn.

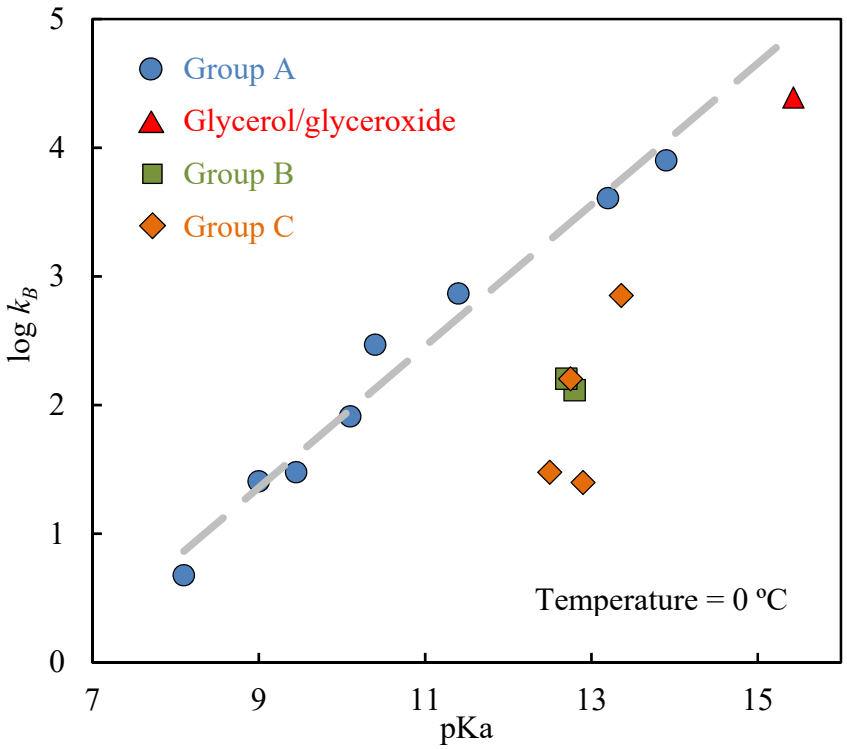

Figure 4.7: Brönsted plot for glycerol and other anion catalysts for CO_2-H_2O reaction (Information of groups A, B, and C from Sharma and Danckwerts (1963))

4.2 Correction for Alkalinity Depletion

As is discussed in section 3.2.4.3, two approaches can be used to determine k_g' from the experimental WWC data: "point-by-point" or "overall slope". Ideally the two approaches should give the same k_g', and that is true for caustic solutions without glycerol (Figure 4.8 and Table 4.2). However, for caustic solutions with glycerol, the flux-partial pressure curve no longer goes through zero, which makes the two approaches give significantly different k_g' (Figure 4.9 and Table 4.3).

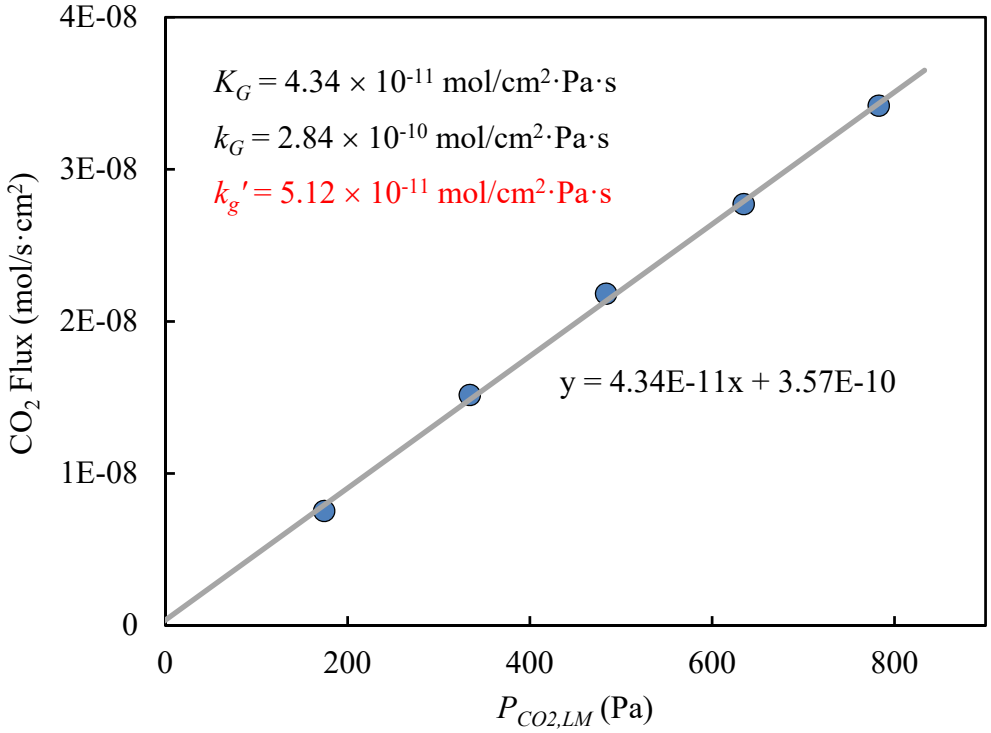

Figure 4.8: Determine k_g' using overall slope approach for caustic solution without glycerol (WWC Solution #1: 0.1 M NaOH, 30 °C)

Table 4.2: Determine *kg′* using point by point approach for caustic solution without glycerol (WWC Solution #1: 0.1 M NaOH, 30 °C)

$P_{CO2,LM}$ (Pa)	$K_G \times 10^{11}$ (mol/cm^2·Pa·s)	$k_G \times 10^{11}$ (mol/cm^2·Pa·s)	$k_g' \times 10^{11}$ (mol/cm^2·Pa·s)
174	4.32	28.4	5.09
334	4.54	28.4	5.40
483	4.51	28.4	5.36
634	4.36	28.4	5.16
782	4.36	28.4	5.16
Avg.	4.42	28.4	**5.23**

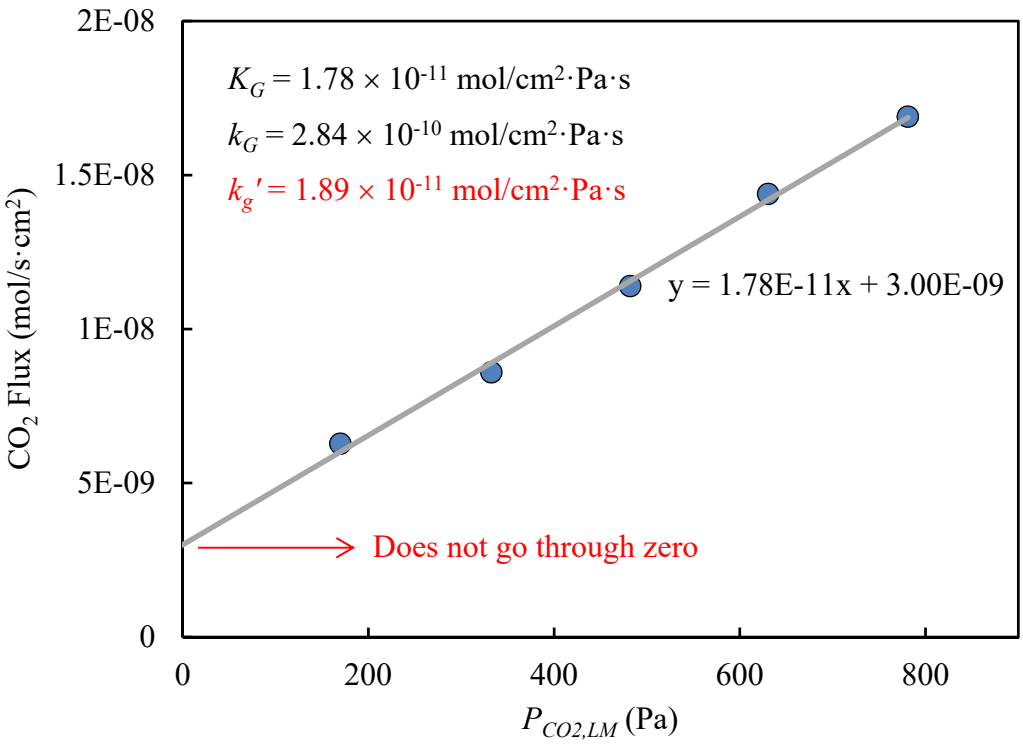

Figure 4.9: Determine k_g' using overall slope approach for caustic solution with glycerol (WWC Solution #4: 0.1 M NaOH, 65 wt % glycerol, 30 °C)

Table 4.3: Determine of k_g' using point by point approach for caustic solution with glycerol (WWC Solution #4: 0.1 M NaOH, 65 wt % glycerol, 30 °C)

$P_{CO2,LM}$ (Pa)	$K_G \times 10^{11}$ (mol/cm^2·Pa·s)	$k_G \times 10^{11}$ (mol/cm^2·Pa·s)	$k_g' \times 10^{11}$ (mol/cm^2·Pa·s)
170	3.69	28.4	**4.25**
332	2.58	28.4	**2.84**
482	2.36	28.4	**2.58**
631	2.28	28.4	**2.48**
781	2.16	28.4	**2.34**
Average	2.62	28.4	**2.90**

Typically for amine solutions, the non-zero intercept of the flux-partial pressure curve implies a CO_2 loading of the solution. However, introducing pure N_2 stream after each experiment shows no visible CO_2 peak in the analyzer, which implies negligible CO_2 loading and that the CO_2-glyceroxide reaction is effectively non-reversible. After analyzing the intercept of WWC runs (Figure 4.10), it is found that the intercept increases consistently with increasing glycerol, and decreases with increasing temperature and caustic concentration. These trends suggest that the non-zero intercept is caused by depletion of surface alkalinity, which is more pronounced when μ_L is increased with increasing glycerol and decreasing temperature. Within one set of k_g' measurements, the higher partial pressure of CO_2 results in more severe depletion, and this directly causes the non-zero-intercept seen in Figure 4.9.

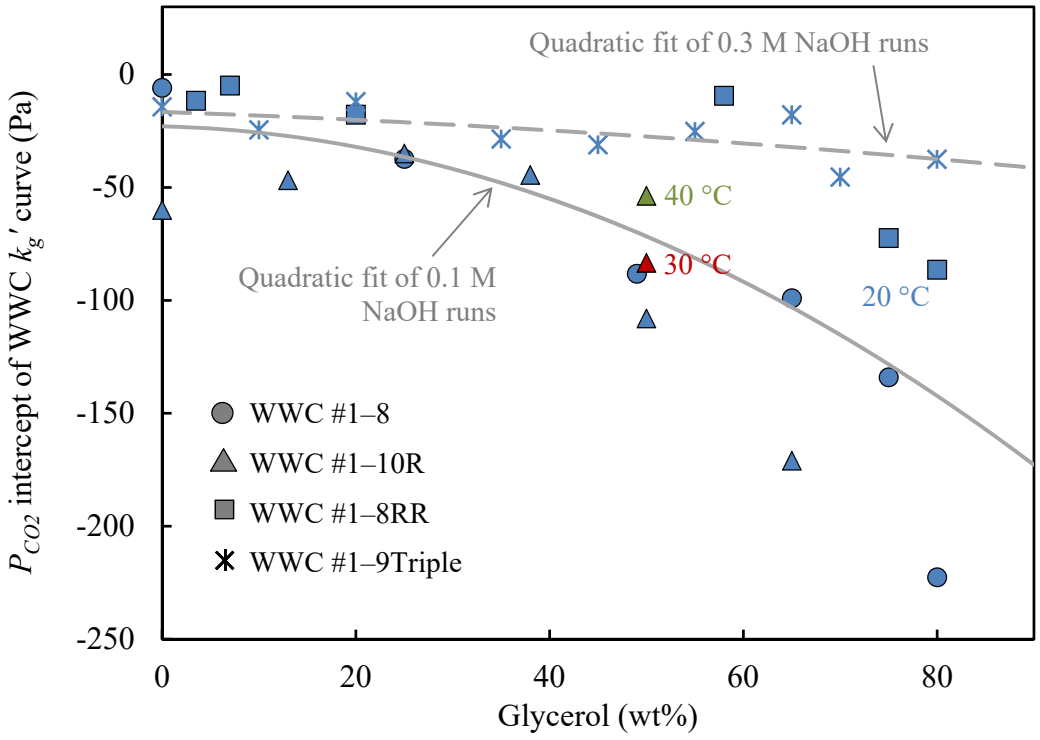

Figure 4.10: Non-zero intercept of WWC k_g' curve

Depletion of surface alkalinity is calculated using the method shown in section 3.2.4.2. The average depletion at 40 °C is shown in Figure 4.11. The depletion is a weak function of temperature because of the competing effects of increased flux and decreased μ_L when temperature is increased. The depletion increases to above 10% when glycerol was greater than 70 wt % with nominal 0.1 N NaOH. Depletion is below 5% for solutions with nominal 0.3 N NaOH. The effect of surface alkalinity depletion on k_g' is not as apparent as shown in Figure 4.11, considering the square root dependence on alkalinity concentration indicated by Equation 3.32.

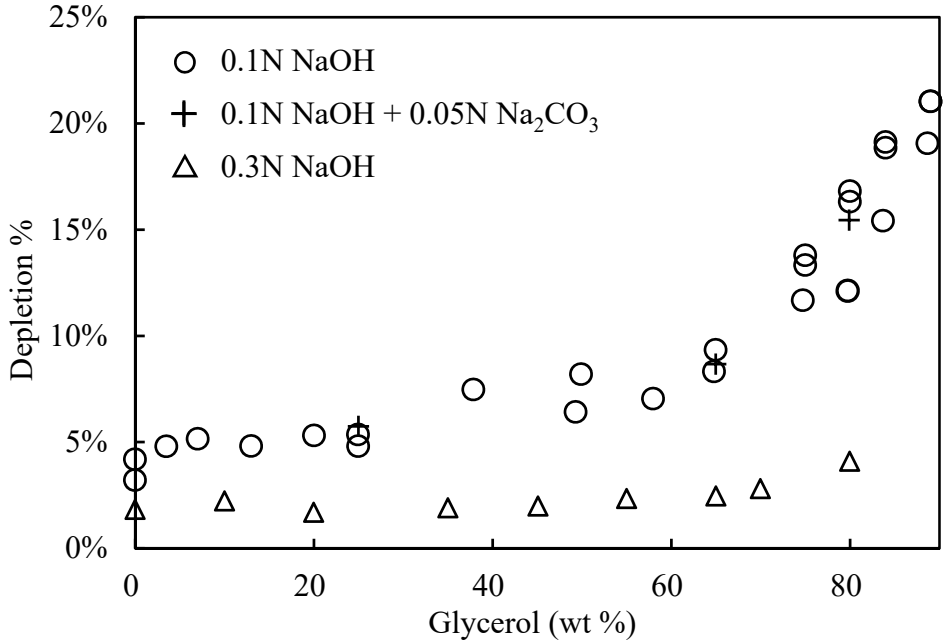

Figure 4.11: Depletion of surface alkalinity for WWC runs at 40 °C

After the depletion correction, the flux-partial pressure curves extrapolate to zero with increased slope and thus increased k_g' (Figure 4.12). Figures 4.13 and 4.14 show the k_g' before and after the correction. As previously discussed, the correction is not drastic, and the k_g' used for the kinetic model development is based on the corrected data (Figure 4.1). Applying the model to AWC experiments assumes that no significant depletion occurs during the a_e experiments, which is reasonable considering the relatively low partial pressure of CO_2 (ambient) in the pilot experiments compared to the WWC condition.

As is discussed in section 2.1.3, Equation 2.22 central to the kinetic model is based on the pseudo-first order assumption, which is only valid when: 1. $Ha^2 >> 1$; 2. $E_\infty/Ha > 5$. The first criterion is satisfied for all WWC runs with the lowest Ha being 12. The value of E_∞/Ha is well above 5 (23 being the lowest) for all 0.3 N runs, however, it goes slightly below 5 (4.7) for some most viscous cases with 0.1 N NaOH. The gas film mass transfer resistance is relatively small for all WWC runs (e.g. Table 4.2).

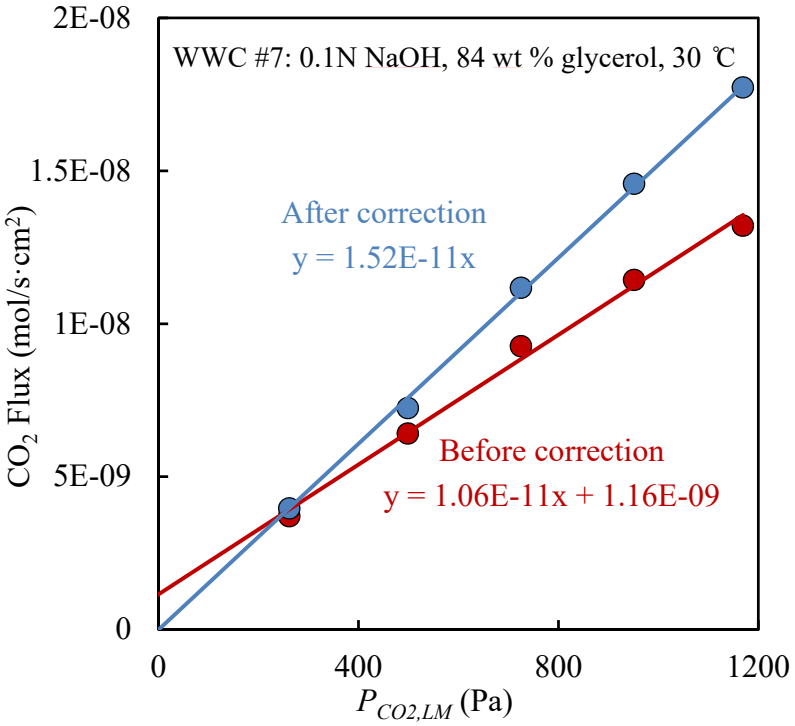

Figure 4.12: Example of alkalinity surface depletion correction

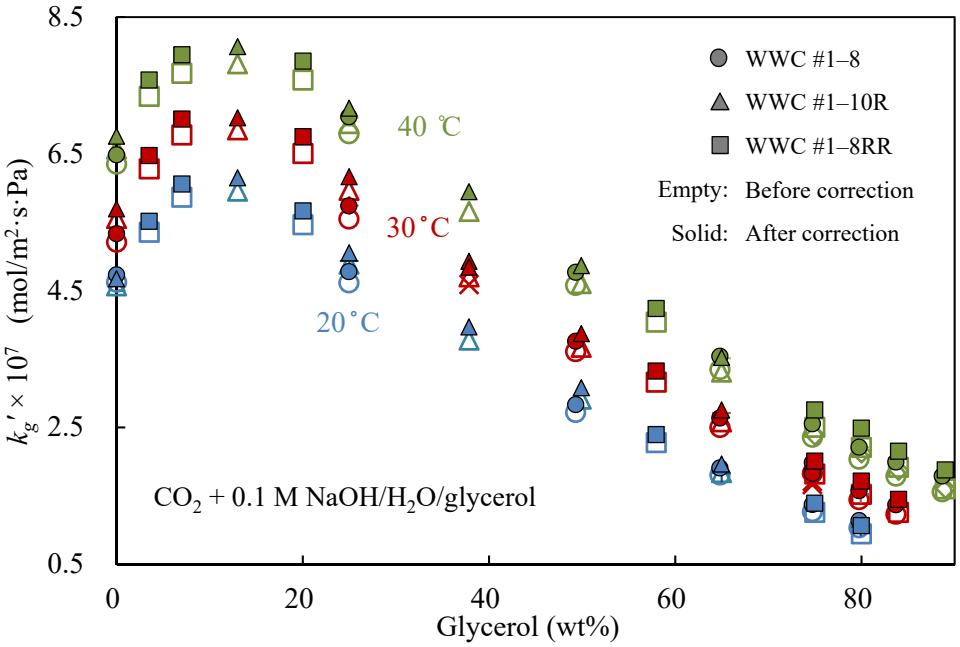

Figure 4.13: WWC k_g' before and after depletion correction (0.1 M NaOH)

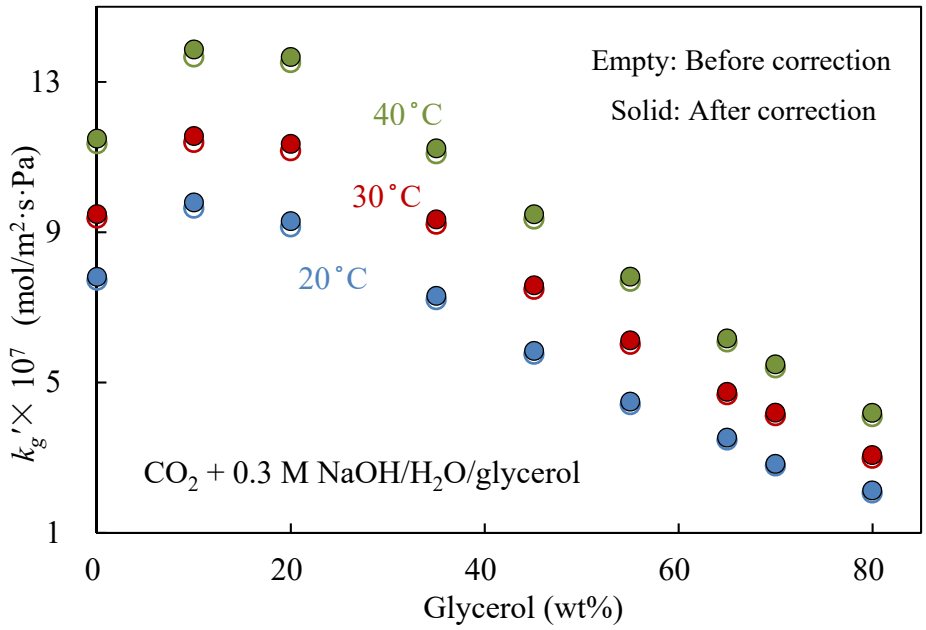

Figure 4.14: WWC k_g' before and after depletion correction (0.3 M NaOH)

The depletion of bulk alkalinity during WWC runs is not significant since new solution was prepared for each run that lasted no longer than three hours. Table 4.4 shows the depletion of bulk alkalinity for WWC runs # 1–8.

Table 4.4: Total inorganic carbon in WWC runs #1–8

WWC Run #	1	2	3	4	5	6	7	8
Total alkalinity (mol/L)	0.098	0.090	0.092	0.090	0.090	0.091	0.098	0.090
Total inorganic carbon (mol/L)	0.0050	0.0029	0.0028	0.0016	0.0035	0.0024	0.0054	0.0036
Ratio of bulk alkalinity depletion	0.10	0.063	0.058	0.036	0.079	0.052	0.12	0.079

Chapter 5: Packed Column Results[4]

In this work, a_e and k_L were measured in a 0.43-m ID packed column with a bed height of either 3 or 1.8 m of packing. Seven structured packings (M 125Y, M 250Y, M 250X, GTO 250Y, B1 250MN, GTP 350Y, GTP 500Y), one random packing (RSR 1.5), and one hybrid (RSP 250Y) were studied. Liquid viscosities were ranged from 0.8 to 70 mPa·s by adding glycerol to water. The effective wetted area, a_e, was determined by reactive absorption of ambient CO_2 into dilute NaOH, and the liquid film mass transfer coefficient, k_L, was determined by air stripping of toluene from the liquid. Liquid viscosity has an insignificant effect on a_e. The total dependence of k_L on μ_L is -0.75, of which -0.35 is from the indirect influence through diffusivity, and -0.4 is from the direct influence through liquid turbulence.

Models of a_e and k_L were developed based on the nine measured packings together with another 30 packings in the database of the Separations Research Program (SRP). The effects of packing type and material, loading condition, and secondary mechanisms (wall and end area) were included in the area model. The effect of packing height (liquid maldistribution) was corrected in the k_L model. The gas film mass transfer coefficient, k_G, in the SRP database was measured by absorption of trace SO_2 with dilute NaOH with 0.5 to 1.0 meters of packing. A model of k_G was developed based on five packings measured in this work and another 15 packings in the SRP database.

[4] D. Song, G.T. Rochelle, A.F. Seibert, "Mass transfer parameters for packings: effect of viscosity." (in press)

5.1 EFFECTIVE MASS TRANSFER AREA (A_E)

Experiments were performed to confirm the result of Tsai (2010) that a_e is not a function of μ_L. Tsai used polyethylene glycol (PEG) as the viscosity enhancer, which, as a polymer, may have different effect on a_e than glycerol, a small molecule. The range of μ_L by Tsai was 1–12 mPa·s, which is smaller than the μ_L range studied in this work (1–70 mPa·s). Therefore, a_e experiments with glycerol are necessary before any pilot-scale k_L experiments.

5.1.1 Effect of Liquid Viscosity

Several tests using glycerol were initially performed with GTO 250Y (Table 5.1). A packing characterization test with water (SRP1501) was first performed as a routine for new packings. k_La_e with glycerol (SRP1503) was then measured. To check the repeatability of a_e measured with glycerol, two parallel experiments were performed (SRP1601 & SRP1602). To maximize the use of the column and minimize the cost of glycerol, k_L was measured simultaneously with a_e in the two repeated runs, before which simultaneous measurement of k_L and a_e with water (SRP1504) was performed to validate the method.

The effective mass transfer area (a_e) obtained from individual and simultaneous measurement for GTO 250Y with water is compared in Figure 5.1. The two sets of data are in good agreement with an average absolute deviation (AAD) of only 4.6%. Therefore, the simultaneous measurement provides reliable a_e measurement. The kinetic model for data interpretation was shown in Chapter 4.

Table 5.1: Experiments performed with GTO 250Y

Test #	Property measured	Purpose	μ_L (mPa·s)
SRP1501	k_L, k_G, a_e, h, ΔP	Comprehensive packing characterization with water	~1
SRP1503	$k_L a_e$	Investigate the effect of μ_L on k_L	1–60
SRP1504	k_L & a_e	Check simultaneous measurement of k_L and a_e with water	~1
SRP1601	k_L & a_e	Investigate the effect of μ_L on k_L and a_e with simultaneous measurement	1–45
SRP1602	k_L & a_e	Repeat SRP1601	1–65

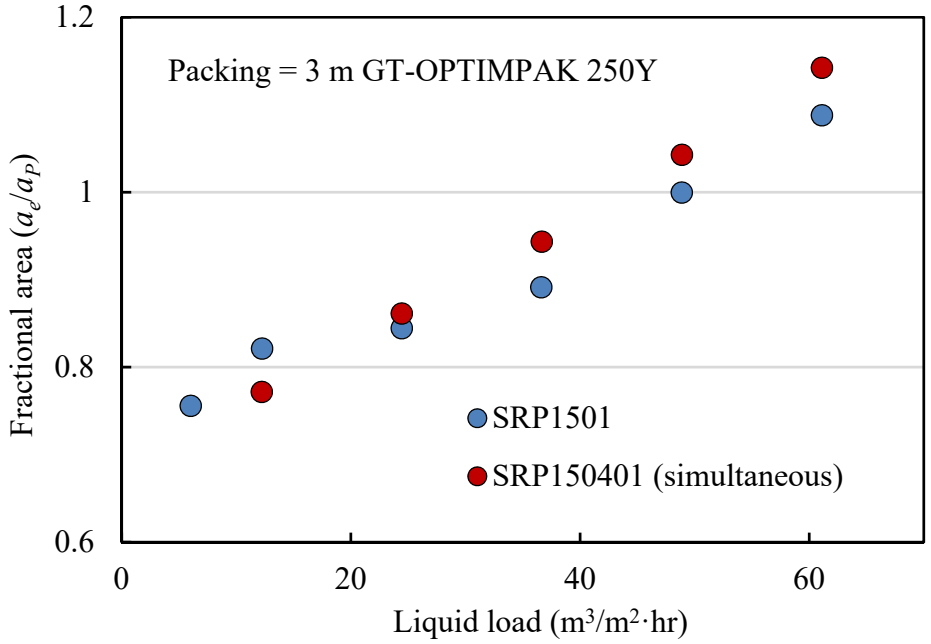

Figure 5.1: Individual and simultaneous measurement of a_e with water in GTO 250Y

Figure 5.2 shows the a_e of GTO 250Y measured with water and aqueous glycerol. As shown in the figure, a_e is not a function of μ_L, even with a four-fold change of k_g' and variation in ambient temperature and humidity. Typically, a fluctuation of 15% is acceptable for a_e measurement in the column.

The two parallel experiments with aqueous glycerol (SRP1601 & SRP1602) showed good reproducibility. The area with glycerol was not affected by μ_L at 3 to 60 mPa·s. Experiments were performed with relatively low gas rate (0.6 m/s) to avoid premature flooding and to slow down bulk alkalinity depletion, so that the batch could last longer without significant change in the bulk properties. Compared to the a_e measured with water at the same gas rate, the data were very close at high liquid load (> 30 $m^3/m^2 \cdot hr$). At relatively low liquid load (< 30 $m^3/m^2 \cdot hr$), a_e for glycerol solutions was about 15% lower than for water. This could result from the capillary effect of viscous liquids that only pass through packing perforations above a certain liquid velocity (Thongpakdi, 1991). This could also result from the liquid flow along the bottom of the distributor. Instead of going directly to the packing top via jets, those "bottom flows" go to the column wall that contributes less, if at all, to the reactive mass transfer. Surface tension should not affect a_e significantly for glycerol solutions compared to water, whose σ is no more than 15% higher than that of glycerol solution. However, a higher density and holdup may also cause reduced wetting at low liquid rates for glycerol solutions.

The modified Tsai model (Equation 5.1) overpredicts a_e for GTO 250Y by about 18% compared to the water data of SRP1501. This might be because the model was developed mostly on a_e measured at gas rate of 1 m/s instead of the low value of 0.6 m/s used for the glycerol tests. Theoretically, the gas rate should not affect a_e for the reactive system CO_2/NaOH/H_2O when the packing surface is fully wetted, since the gas film resistance at experiment operating conditions is negligible. However, at a low gas rate

such as 0.6 m/s, the gas-liquid friction is not high enough to enhance liquid spreading, which results in a smaller a_e. In the column used in this work, the effect of gas rate on a_e will disappear at any rate greater than 1 m/s, which is also the gas rate the a_e correlation of Tsai was built on. For the reasons already noted, the a_e measurement for glycerol solutions was performed at a low gas rate of 0.6 m/s and compared with the data for water at the same gas rate. The fact that a_e for glycerol solutions and water are the same at 0.6 m/s gas rate does not necessarily mean they will still be the same at higher gas rates. Here the assumption has been made that the effect of gas rate change from 0.6 m/s to higher values on a_e is the same for water as for glycerol solutions.

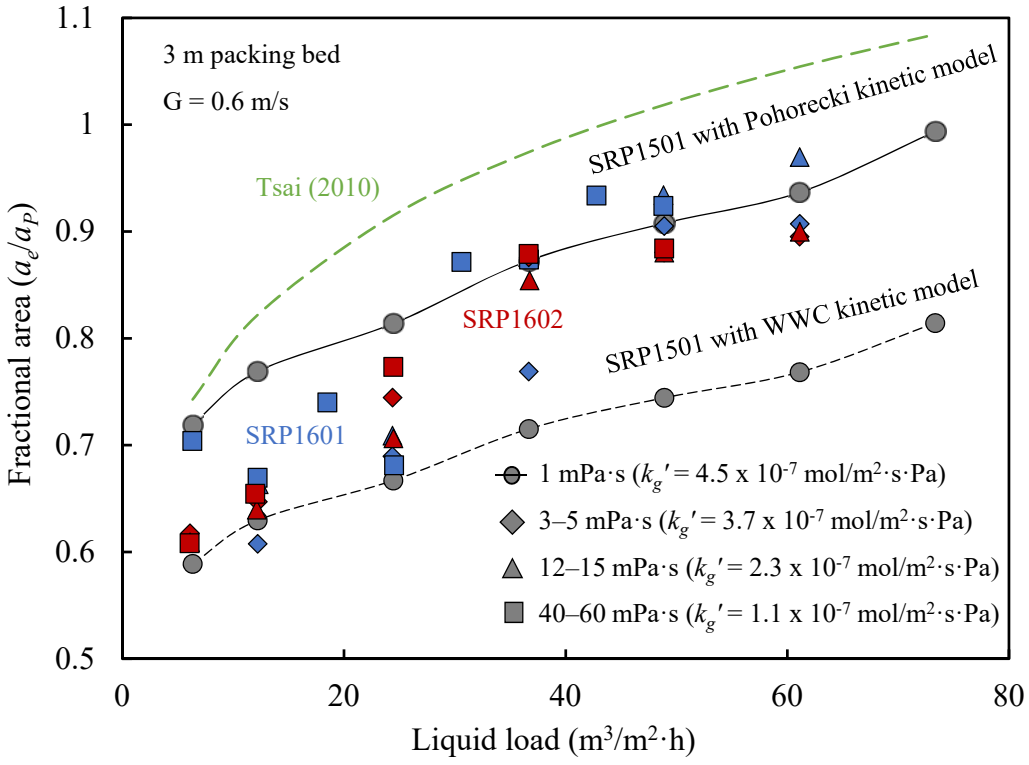

Figure 5.2: Measured a_e for GTO 250Y with water and aqueous glycerol

As is discussed in Chapter 4, There is inconsistency between the kinetic models used for water and aqueous glycerol. For water, the model of Pohorecki and Moniuk (1988) has been used for CO_2-NaOH reaction rate constant calculation. For aqueous glycerol, the model based on the WWC data was used (Song & Rochelle, 2017). Though the kinetic model for aqueous glycerol is consistent with itself and has a reasonable asymptotic curve of overall rate constant (k_{Alk}) against glycerol concentration, the absolute value of k_{Alk} at zero glycerol is about 40% higher than k_{OH}- in Pohorecki and Moniuk. This difference will translate to a k_g' 17% greater, which will lead to a smaller a_e compared to the model of Pohorecki and Moniuk (Figure 5.2). Since the Pohorecki model has been used for all the previous a_e tests with water in the SRP, it was used for water test SRP1501 for consistency to compare with glycerol data calculated based on the WWC kinetic model. The a_e for water test SRP1501 based on the WWC kinetic data (dashed black line in Figure 5.2) was also included for comparison purpose.

Despite the difference in a_e for water resulting from different kinetic models, the two sets of water data are not drastically different in Figure 5.2. The two sets of water data with 17% relative difference "include" the glycerol data within, matching them at either low or high liquid load. Typically, a fluctuation of 15% is acceptable for a_e measurement in the column in this work. Therefore, it was confirmed that a_e is not a function of μ_L, with a four-fold change of k_g', the relatively large scale of column which brings corresponding uncertainty, and variation in experiment conditions such as temperature and humidity. This result is believed to be applicable to other structured packings with similar geometry.

5.1.2 Secondary Mechanism of Effective Mass Transfer Area

As is discussed in section 3.3.4.1, $a_{secondary}$ is deducted from the experimental a_e to give $a_{e,corr}$ (Equation 3.64). With the 0.43 m ID column in this work, the secondary area is not significant for normal to fine packing (a_P > 200 m^2/m^3), but it starts to play an important role for coarse packing (Figure 5.3). Since the wall area is dominant in the secondary area for the whole range of packing a_P, the top and bottom areas are omitted in the future correction for secondary mechanism for simplification. As expected, the column diameter will greatly affect the $a_{secondary}$ (Figure 5.4). For columns with ID greater than 0.5 m with M 250Y as an internal, the secondary area is less than 7%. Therefore, this correction to area measured in a pilot-scale column will enable wider application of the model to columns of greater sizes where $a_{secondary}$ is negligible. The overall secondary area is a weak function of liquid load because the increase in top/bottom area and decrease in wall area offset each other as liquid load increases (Figure 5.5).

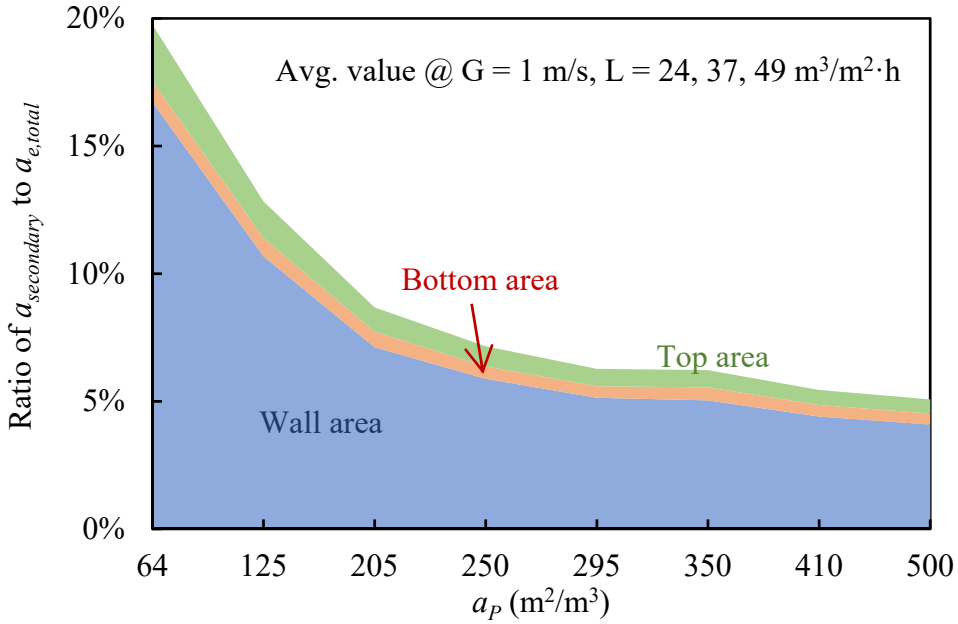

Figure 5.3: Effect of a_P on $a_{secondary}$ for structured packings

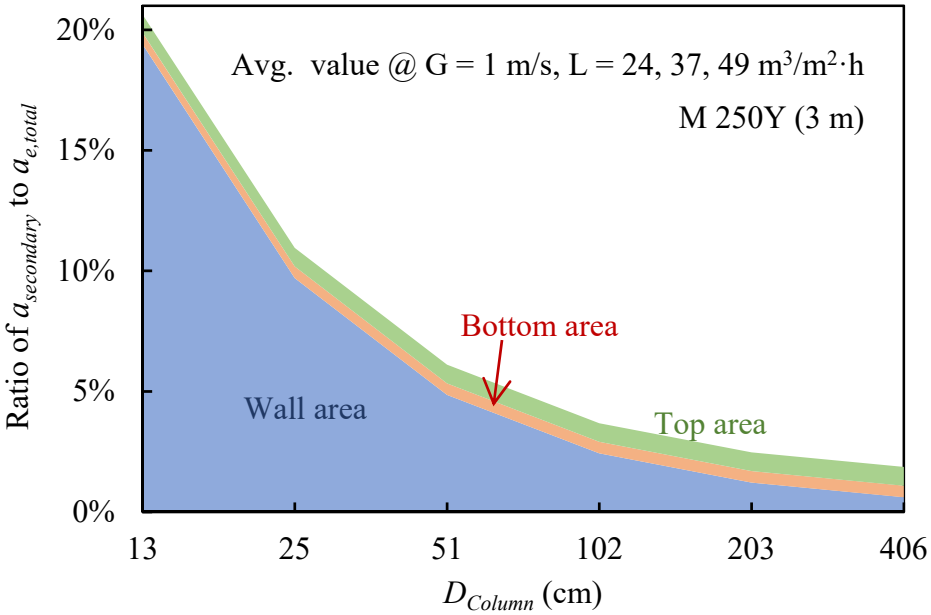

Figure 5.4: Effect of column size on $a_{secondary}$ for M 250Y

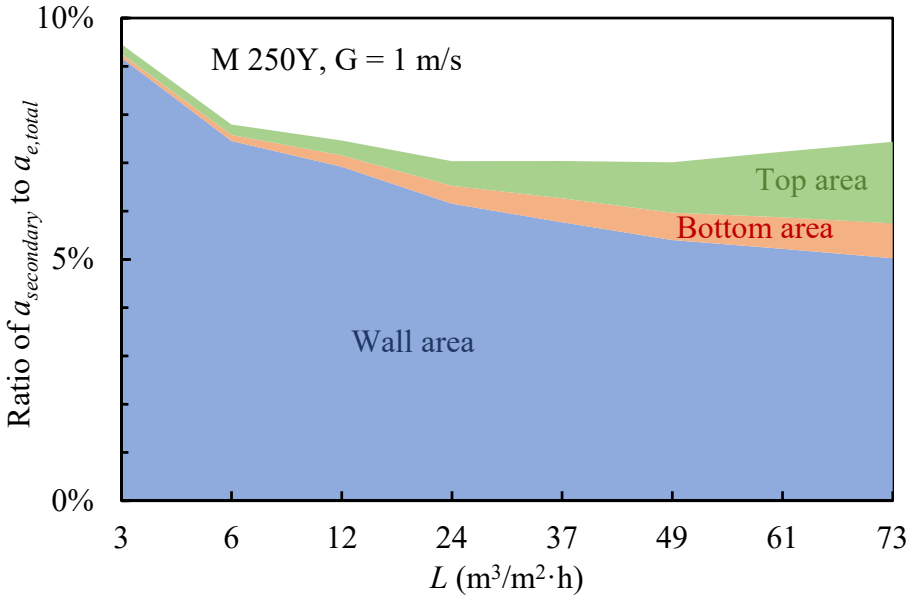

Figure 5.5: Effect of liquid load on $a_{secondary}$ for M 250Y

Different regimes of packing area are shown in Figure 5.6. The coarsest packing (MG 64Y) has been taken for illustration. The correction of secondary area effectively shifts the area down proportionally since secondary area is a weak function of liquid load. The wetted packing area below unity results from the liquid film on the surface of packing metal, and the part above unity is from the satellite droplets in the corrugation channel and the mass transfer happening at packing element junctions. The later part becomes less significant when the a_P increases.

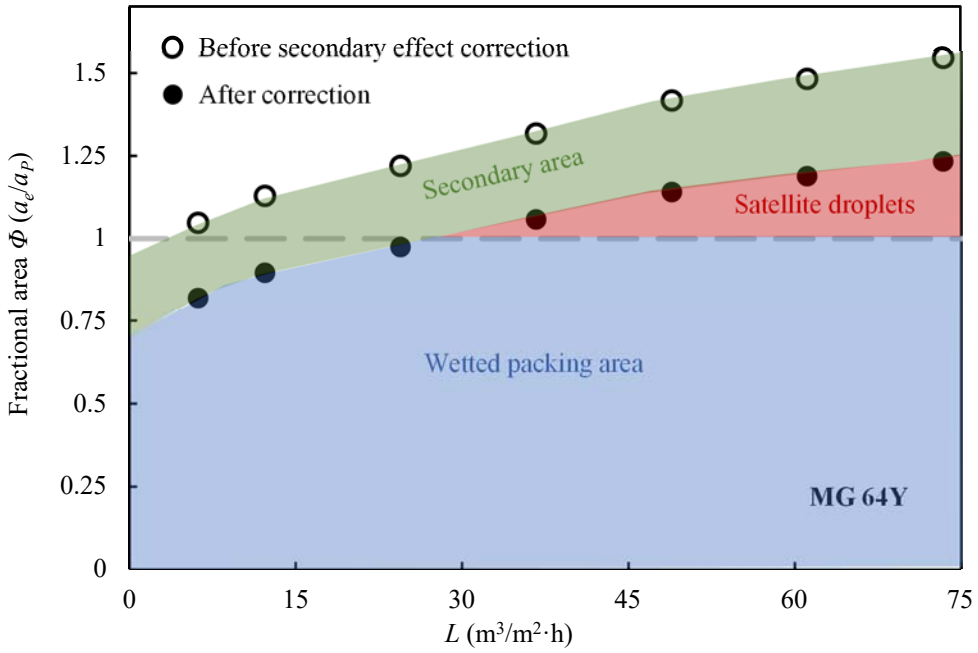

Figure 5.6: Packing area regimes of MG 64Y

5.1.3 Model of Effective Mass Transfer Area

A model representing a_e was developed (Equation 5.2) based on measurements with water and aqueous glycerol reported here and on data for water, surfactant liquid, and

solutions of polyethylene glycol (PEG) measured by previous researchers (Tsai, 2010; Wang, 2015; Wilson, 2004) using the same equipment. Thirty-nine structured, random, hybrid, and gauze packings are included (Table 3.10). Because of the partly shared database, the form of the model is similar to that of Tsai (Tsai et al., 2011) with the same dimensionless groups. However, this new model uses an expanded database and corrects for the secondary area, which makes it more widely applicable to variable packing sizes.

Figure 5.7 compares the measured and calculated area for water. Empirical correction factors are included in the model to account for deviation of random/hybrid packings, plastic packings, and data measured at the loading zone (Equation 5.3 and Table 5.2). The packing type correction is a linear function of a_P to optimize the overall fitting of the 16 random/hybrid packings in the database. The model works surprisingly well for the one gauze packing in the database without correction. The correction for plastic packing is obtained by comparing the data for two packings of which both the stainless steel and plastic versions were measured (PR 1.0 and CMR 2A). Besides the area measured at the pre-loading zone ($\Delta P < 400$ Pa/m) for all 39 packings, area at the loading zone ($\Delta P > 400$ Pa/m) was investigated for one structured packing (B1 250), three random packings (IMTP 25, PR 2.0 and 1.0,), and one gauze packing (A3 500X). A constant 15% increase of the area was seen for the five packings regardless of packing type or liquid load (Figure 5.8). For 39 packings with drastically different geometry, the model shows an average absolute deviation (AAD) of only 8.9 percent.

$$\frac{a_{e,packing}}{a_P} = 1.34 \cdot \left(We \cdot Fr^{-\frac{1}{3}}\right)^{0.116} = 1.34 \cdot \left[\left(\frac{\rho_L}{\sigma}\right) \cdot g^{1/3} \cdot \left(\frac{u_L}{a_P}\right)^{4/3}\right]^{0.116} \quad (5.1)$$

$$\frac{a_{e,packing}}{a_P} = 1.16 \cdot \eta \cdot \left(We \cdot Fr^{-\frac{1}{2}}\right)^{0.138} = 1.16 \cdot \eta \cdot \left[\left(\frac{\rho_L}{\sigma}\right) \cdot g^{1/2} \cdot u_L \cdot a_P^{-3/2}\right]^{0.138} \quad (5.2)$$

$$\eta = \eta_{type} \cdot \eta_{material} \cdot \eta_{loading} \quad (5.3)$$

Table 5.2: Packing correction factor in Equation 5.3

η_{type}	Structured	Random/Hybrid
	1.0	$1.34 - 0.26\left(\frac{a_P}{250}\right)$
$\eta_{material}$	Stainless Steel	Plastic
	1.0	0.62
$\eta_{loading}$	Pre-loading zone ($\Delta P < 400$ Pa/m)	Loading zone ($\Delta P \geq 400$ Pa/m)
	1.0	1.15

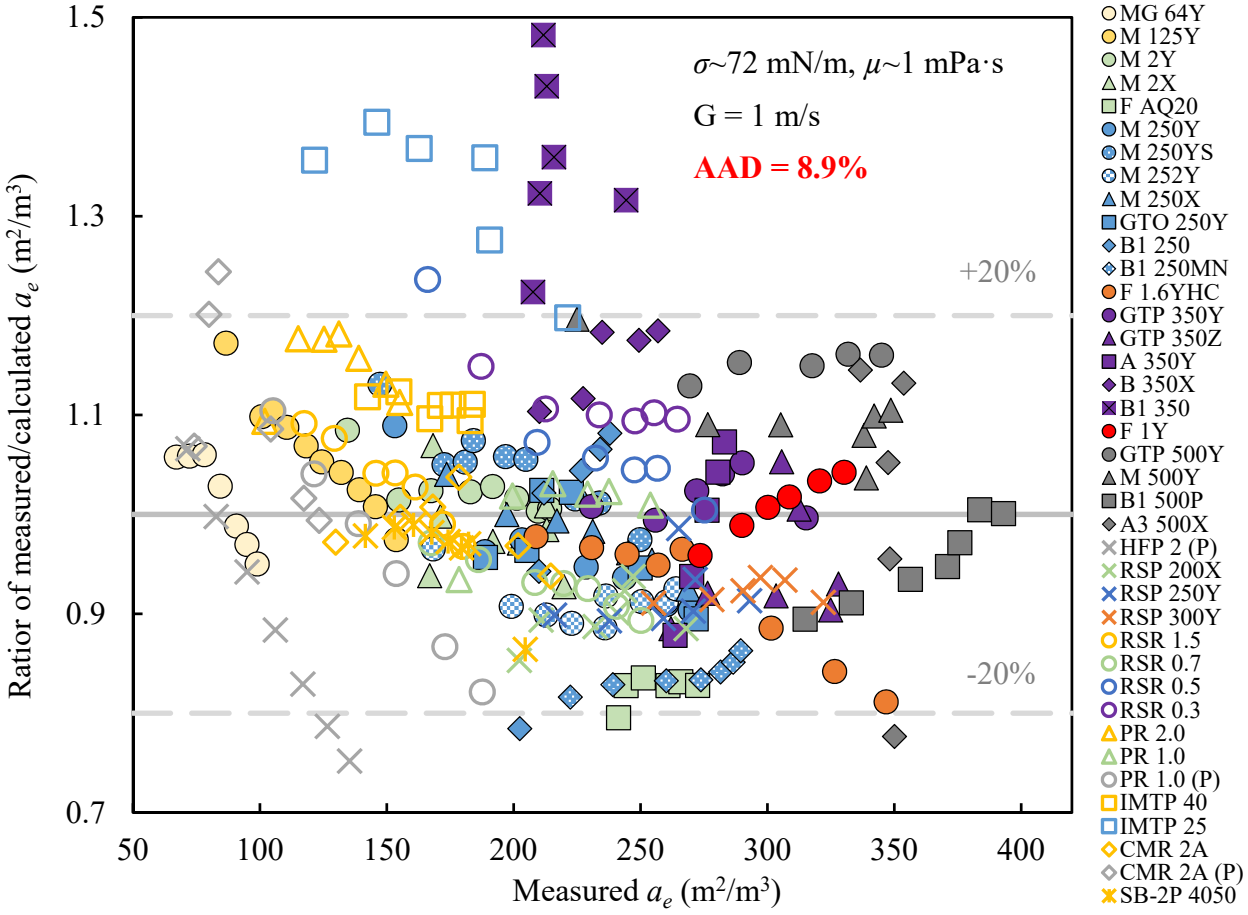

Figure 5.7: Measured a_e and a_e calculated from Equation 5.2 for water

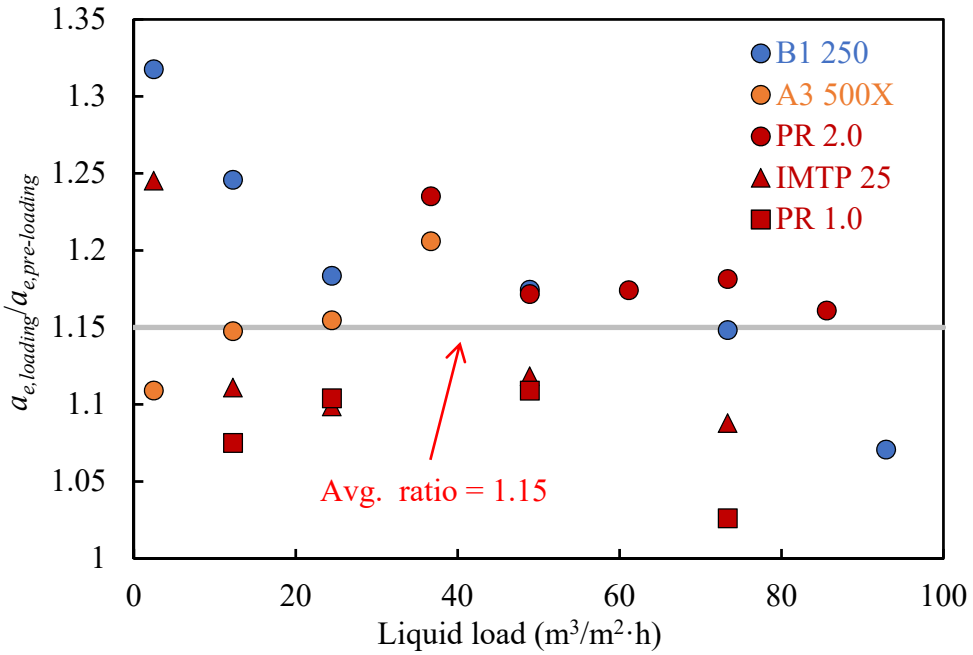

Figure 5.8: Comparison of area at loading and pre-loading zone

Figure 5.7 shows that there is no systematic relative error of the model as a function of packing geometry, a_P. Though a slight overprediction is observed for the finest packings (a_P = 350–500 m^2/m^3), the relative error is still close to 20%, which is acceptable. Per the model, surface tension affects $a_{e,packing}$ but viscosity does not. This is confirmed by Figures 5.9 and 5.10 where relative errors of Equation 5.2 as a function of liquid properties are plotted. Figure 5.9 shows the data measured by Tsai (2010), where the surface tension varied from 72 to 30 mN/m with the addition of a surfactant (TERGITOL™ NP-7). No systematic bias of the model was found as a function of surface tension. In fact, the model does a slightly better job for surfactant liquid than water. Figure 5.10 shows the relative error of the model as a function of liquid viscosity. Neither the PEG data (1–15 mPa·s) from Tsai, nor the glycerol data (1–50 mPa·s) reported here show that $a_{e,packing}$ is affected by μ_L in the range investigated. The relative error of the model is mostly within 10% for viscous liquids.

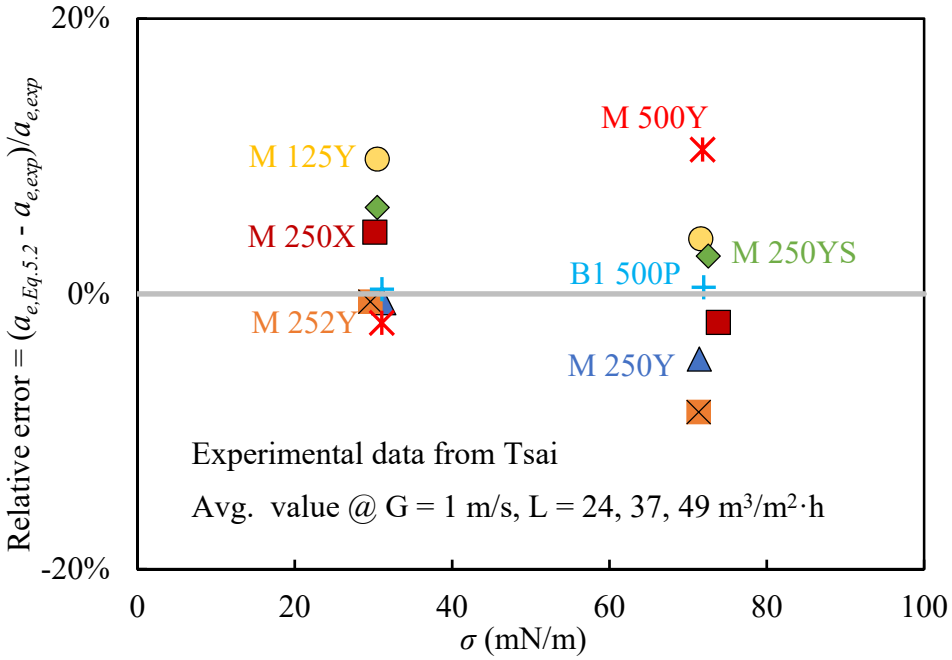

Figure 5.9: Relative error of Equation 5.2 with variable surface tension

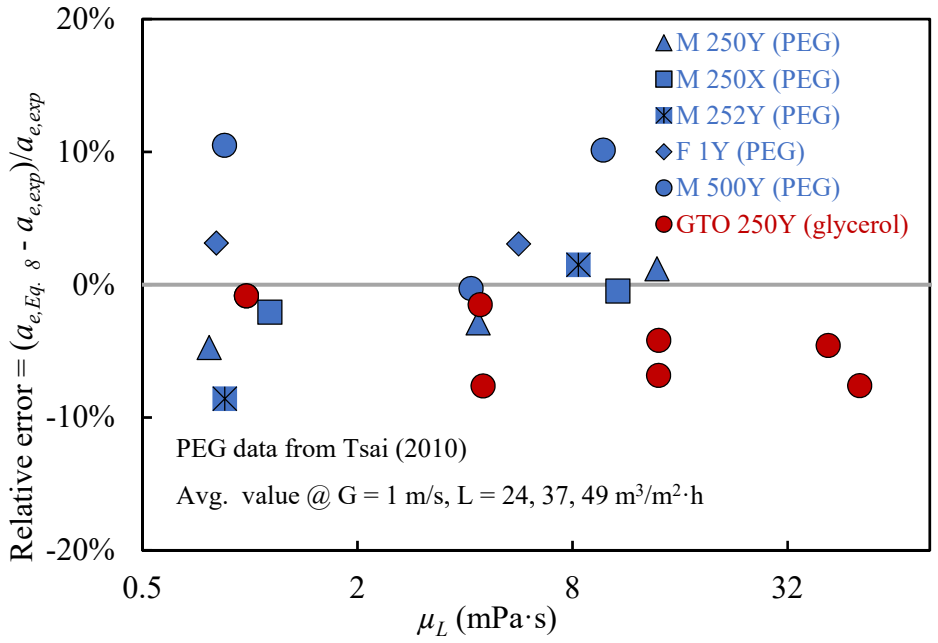

Figure 5.10: Relative error of Equation 5.2 with variable viscosity

5.1.4 Analysis of SRP Database

5.1.4.1 Effect of Liquid Flow Sequence on a_e

The effect of liquid flow sequence on a_e was examined with water in GTO 250Y. In the experiment, the a_e was first measured with increasing liquid flow rates (12 to 61 $m^3/m^2 \cdot h$). After the point has been taken at the highest liquid flow rate, the system was kept at close-to-flooding condition (400 Pa/m packing) for 5 minutes, a_e was then measured with decreasing liquid flow rates from 61 to 12 $m^3/m^2 \cdot h$. The data are shown in Figure 5.11.

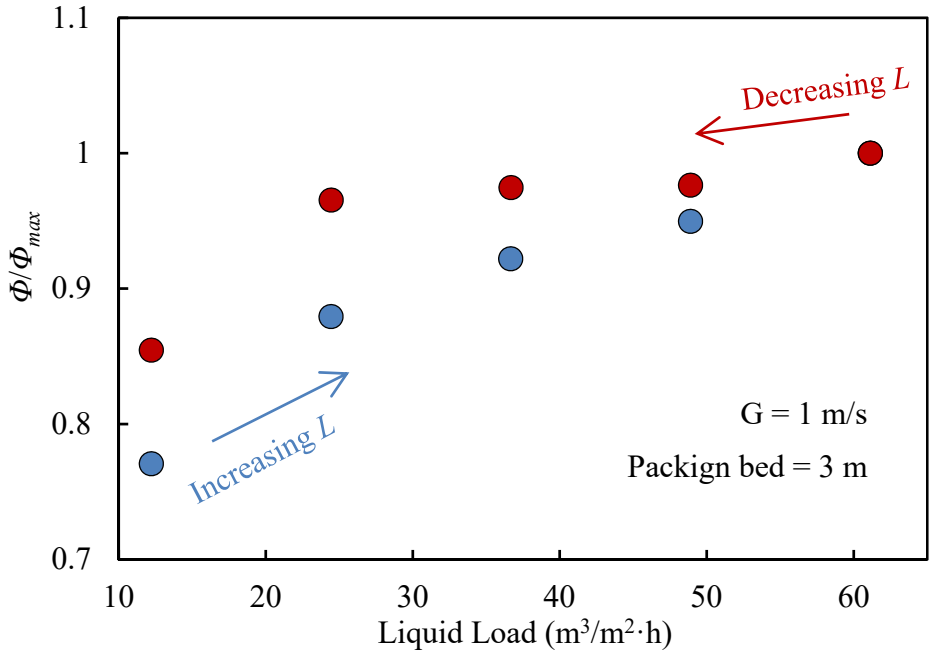

Figure 5.11: Effect of liquid flow sequence on a_e for GTO 250Y

a_e measured with increasing liquid flow rates is always lower than with decreasing liquid flow rates. The hysterisis is more pronounced at low liquid rates. This phenomenon was also observed by Thongpakdi (1991) in his experiments on metal sheet hydrodynamic tests. The argument is that the increase in liquid flow is important for the initial wetting of the packing surface especially for a high surface tension liquid such as

water. However, once the surface has been wetted, liquid flow rate plays a less important role. According to section 3.3.3.1, the experiment protocol for a_e measurement lies between the increasing and decreasing order of liquid rate: the liquid rate is first increased from a medium-high liquid load (37 or 49 $m^3/m^2 \cdot h$) till it reaches the pump limit, and then decreased. The typical sequence of liquid rate is: 49, 61, 73, 37, 24, 12, and 6 $m^3/m^2 \cdot h$. Although the difference is not drastic between the two experimental approaches (~ 10%), it is more rigorous to include the sequence of liquid flow when comparing a_e measured with different packings and by different researchers.

5.1.4.2 Effect of Packing Geometry on a_e

The effect of packing geometry (a_P, α, type, and material) on a_e for water at the preloading zone ($\Delta P < 400$ Pa/m packing) is shown in Figure 5.12. The average a_e increases linearly with a_P until 250 m^2/m^3, from which a_e starts to deviates from a_P as it is further increased. This agrees with experience that the utilization of the metal surface will be decreased when a_P increases. Compared to a_e for structured packing with the same a_P, a_e for random packing (RSR series) and gauze packing (A3 500X) is not drastically different, while a_e for hybrid packings (RSP series) is slightly greater. Corrugation angle, α, of structured packing does not have a significant effect on a_e. Packing without surface modification (M 250YS) and packing with modified corrugation sheet (M 252Y) have similar a_e to ordinary packings. Plastic packings showed smaller a_e compared with stainless steel ones. These effects of packing geometry are reflected in the correction factor of the area model (Equation 5.3).

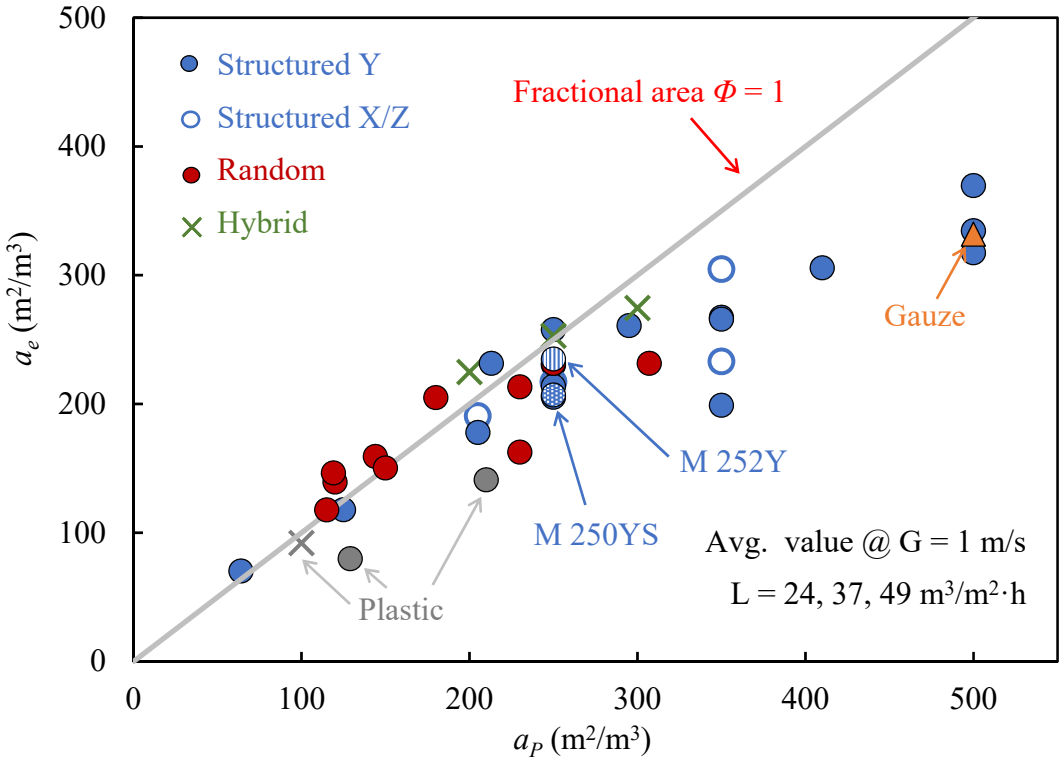

Figure 5.12: Effect of packing geometry on a_e for water at pre-loading zone ($\Delta P < 400$ Pa/m packing)

5.2 Liquid Film Mass Transfer Coefficient (k_L)

5.2.1 Experiment Reproducibility

The k_L for water measured in this work is compared with that measured previously by Wang and Perry (2015). Among the five packings (four structured and one hybrid) that have been measured by multiple investigators, four show good reproducibility with 10% relative error (Figure 5.13). The four packings (M 250Y, GTP 350Y, GTP 500Y, and RSP 250Y) have different geometry and specific areas. The average ratio of k_L measured with 8:1 and 4:1 (heptane : sample) is 0.98 for M 250Y (see section 3.4 for details). The effect of the GC sampling technique is insignificant.

For the only outlier in the figure, M 250X, the k_L measured by the author is twice that previously measured with both 1.8 and 3 m of packing. The fact that both the 1.8 m and 3 m packing data showed the same difference reduces the probability of operational error in the experiment in the current work. A detailed look at the experimental data for outlet toluene of all $a_P = 250$ m^2/m^3 packings tested is shown in Figure 5.14. The M 250X shows abnormally high outlet toluene (at lowest liquid load) with its lowest toluene higher than the highest toluene of other packings. This implies experimental error (such as collecting the outlet sample from wall flow instead of flows through the packing bed). In the data analysis and model development, the new data will be used for M 250X. Apart from this outlier, the repeatability of the k_L experiment is good, justifying combination of the data measured by different researchers for model development.

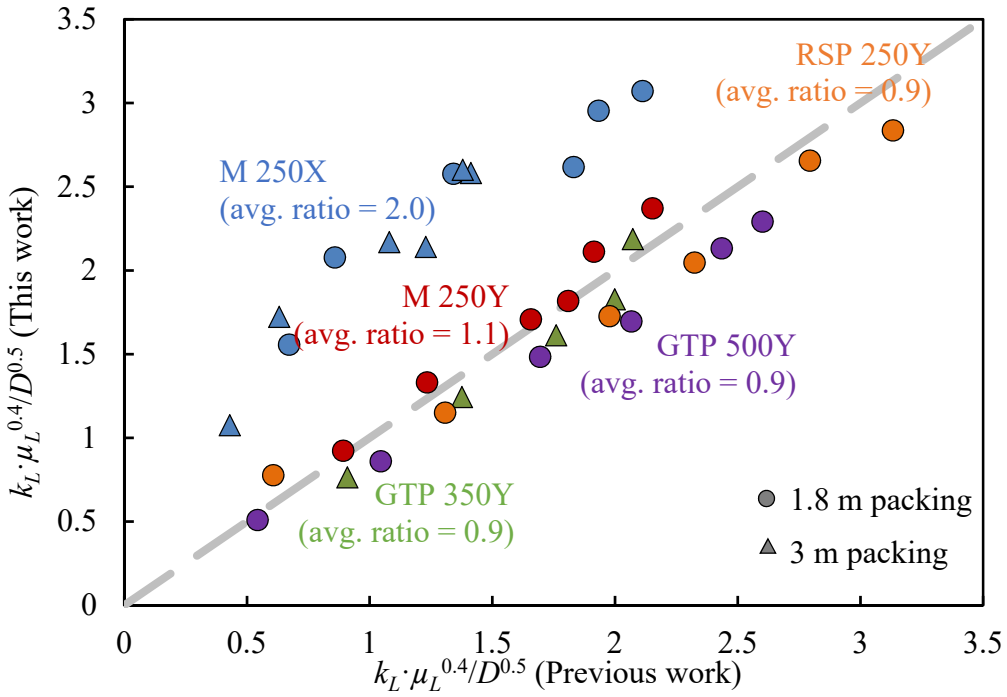

Figure 5.13: Comparison of k_L measured in this and previous work

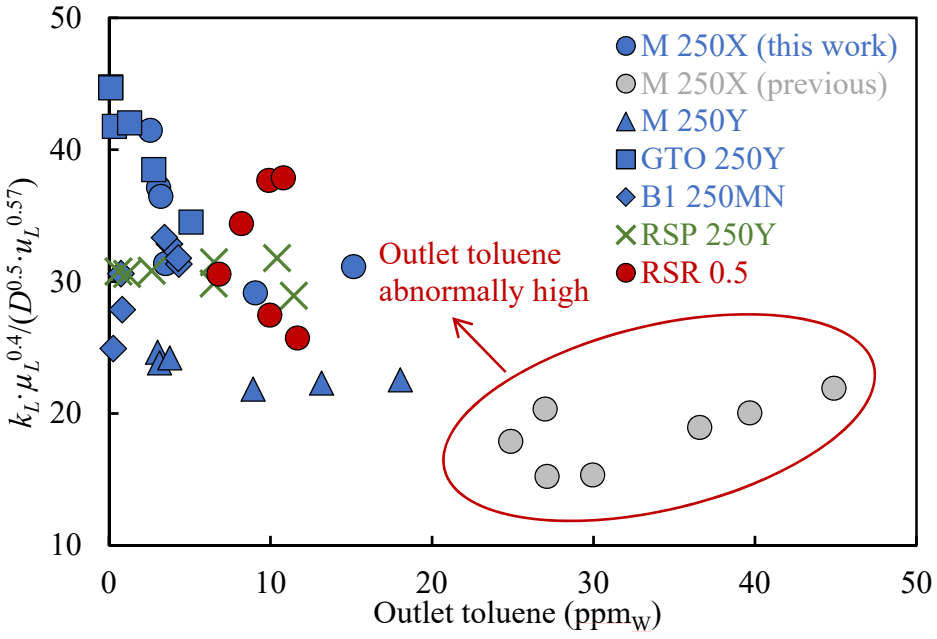

Figure 5.14: Comparison of measured outlet toluene for a_P = 250 m^2/m^3 packings

5.2.2 Effect of Packing bed height

Figure 5.15 compares the k_L obtained from individual and simultaneous measurement (see details in section 5.1.1) for water with GTO 250Y. Both methods give essentially the same k_L with 3 m packing (SRP150401 & SRP150402). The individual measurement with 1.8 m packing resulted in k_L 30% greater than with 3 m packing. According to Figures 5.1 and 5.15, the simultaneous measurement not only gives reliable a_e, but also reliable k_L. The difference in k_L is not caused by simultaneous measurement approach, but resulted from the difference in the height of the packing.

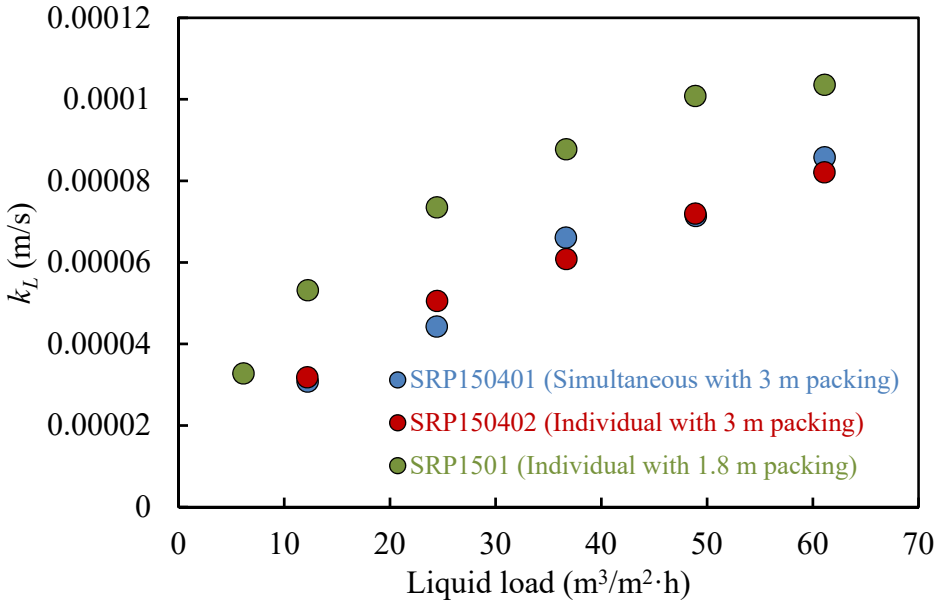

Figure 5.15: Comparison of individual and simultaneous measurement of k_L for water with GTO 250Y

The variance of k_L at different packing height is seen not only in GTO 250Y, but also in other packings in the database (Figure 5.16). The experimental protocol for k_L measurement at SRP has changed over time. A total of 3 m of packing was initially used. The height was then reduced to 1.8 m because the low outlet toluene is close to the detection limit of the gas chromatograph (GC). Theoretically, k_L should not be affected by packing height when there is no issue with liquid distribution and GC detection. However, greater k_L was observed with the 1.8 m bed than the 3 m bed, regardless of packing type and geometry. For data measured in this work, the ratio is greater at relatively low liquid load and low outlet toluene (Figures 5.17 and 5.18), which indicates that the difference of k_L may be caused by both the poorer liquid distribution and the gas chromatograph detection limit with greater toluene removal. The average 1.8-to-3-m ratio of k_L is 1.32, with random packings slightly greater than structured packings. The effect of packing height on the mass transfer efficiency was observed in many previous studies (Bravo & Fair, 1982;

Brunazzi & Paglianti, 1997; de Brito et al., 1994). Though the dependence varies from -0.06 to -0.4 in different work, shorter bed always gave greater efficiency. In this work, the effect of packing height is included in the k_L model (Equation 11) with a dependence of -0.54 ($= \frac{\ln(1.32/1)}{\ln(1.8/3.0)}$).

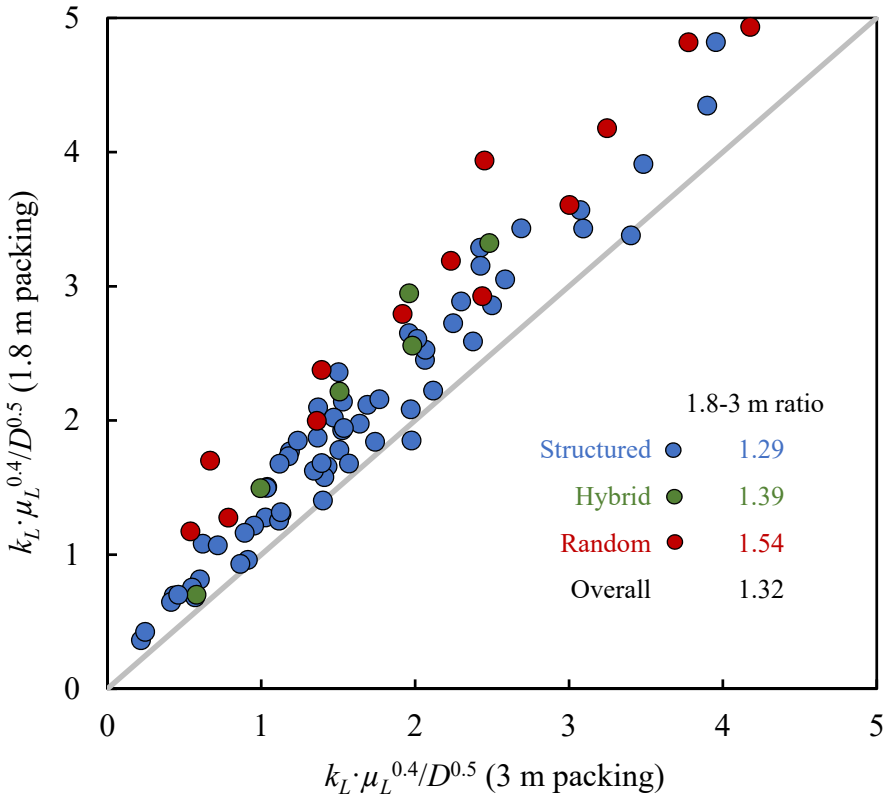

Figure 5.16: Comparison of k_L measured with 3 m and 1.8 m packing

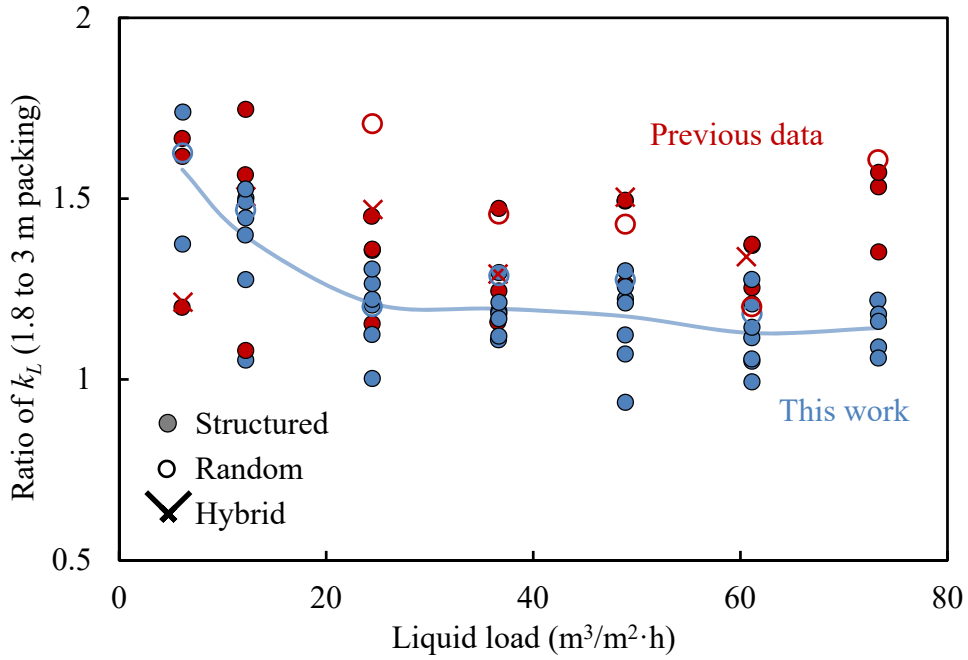

Figure 5.17: 1.8-to-3-m k_L ratio as a function of liquid load

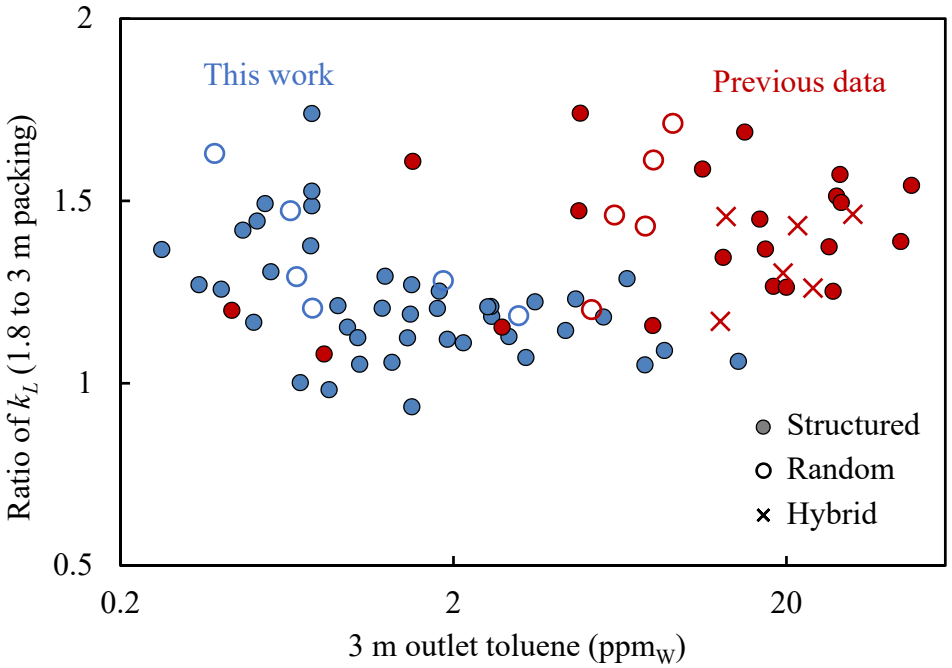

Figure 5.18: The 1.8-to-3-m k_L ratio as a function of outlet toluene

5.2.3 Model of Liquid Film Mass Transfer Coefficient

A model of k_L (Equation 5.4) was developed based on data from 20 structured, random, and hybrid packings. Glycerol tests were performed on nine of the 20 packings. The k_L used to develop the model is separated from experimental k_La by using measured instead of area calculated by the generalized are model. Figure 5.19 compares the model and experimental k_L. Greater uncertainty was observed for k_L than a_e. The k_L model shows an AAD of 24% for all 20 packings (compared to an AAD of 8.9% for the area model). Unlike the area model, the k_L model does not require a correction for packing type or material.

The model assumes square root dependence on diffusivity (and thus *Sc*) in accordance with the penetration theory (Higbie, 1935). Dimensionless groups (*Re*, *Ga*) were selected with combined considerations of results in the least square fitting and physical significance of the mass transfer process. Since surface tension was not significantly varied in the experiment and is not believed to be affecting k_L, dimensionless groups that contain surface tension (such as *We*, or *Ca*) were excluded in the regression. Per the model, the liquid film mass transfer is affected by packing geometry (a_P), liquid properties (μ_L, *D*, and ρ_L), liquid flow (u_L), and gravity (*g*).

$$Sh_L = 0.12 \cdot Sc_L^{0.5} \cdot Re_L^{0.565} \cdot Ga_L^{1/6} \cdot \left(\frac{Z}{1.8}\right)^{-0.54} \tag{5.4a}$$

$$k_L = 0.12 \cdot u_L^{0.565} \cdot \left(\frac{\mu_L}{\rho_L}\right)^{-0.4} \cdot D_L^{0.5} \cdot g^{1/6} \cdot a_P^{-0.065} \cdot \left(\frac{Z}{1.8}\right)^{-0.54} \tag{5.4b}$$

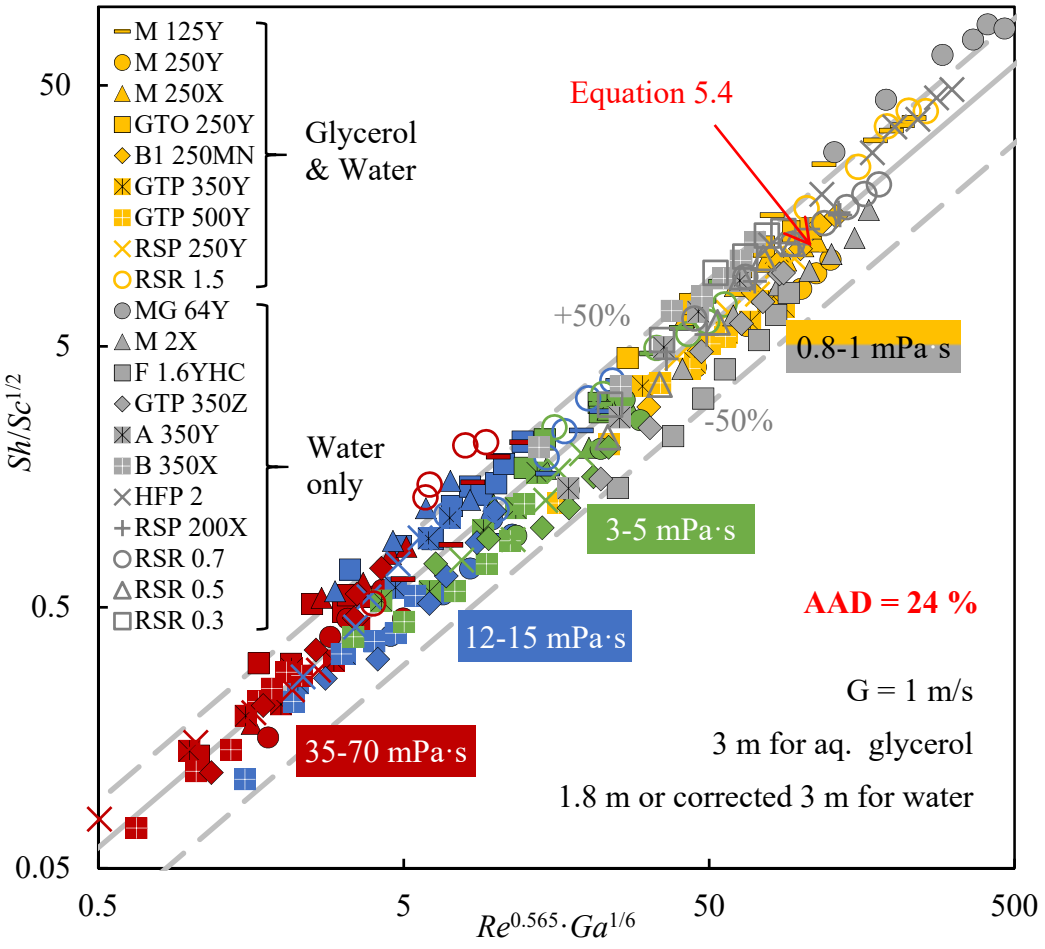

Figure 5.19: Comparison of measured k_L and k_L calculated from Equation 5.4

Figures 5.20 and 5.21 show the relative error of Equation 5.4 as a function of a_P and μ_L, respectively. The model underpredicts k_L for coarse packings in Figure 5.20. No systematic bias of the model as a function of μ_L is apparent in Figure 5.21.

The k_La of M 250Y measured by other researchers via oxygen desorption together with the data reported here are compared with various literature models in Figure 5.22. In the figure, the experimental data from different sources with different systems are close to each other after normalization with diffusivity. It is notable that the measured data with a shorter bed are consistently greater than those measured with a taller bed. This agrees

with the "maldistribution" effect of packing bed height on k_L seen in Figure 5.16. Both the model in this work and the Billet model (Billet & Schultes, 1999) predict the k_La for water reasonably well. The models of Delft (Olujic et al., 1999) and Valenz (Valenz et al., 2011) overpredict k_La, and the Rocha model (Rocha et al., 1996) underpredicts it.

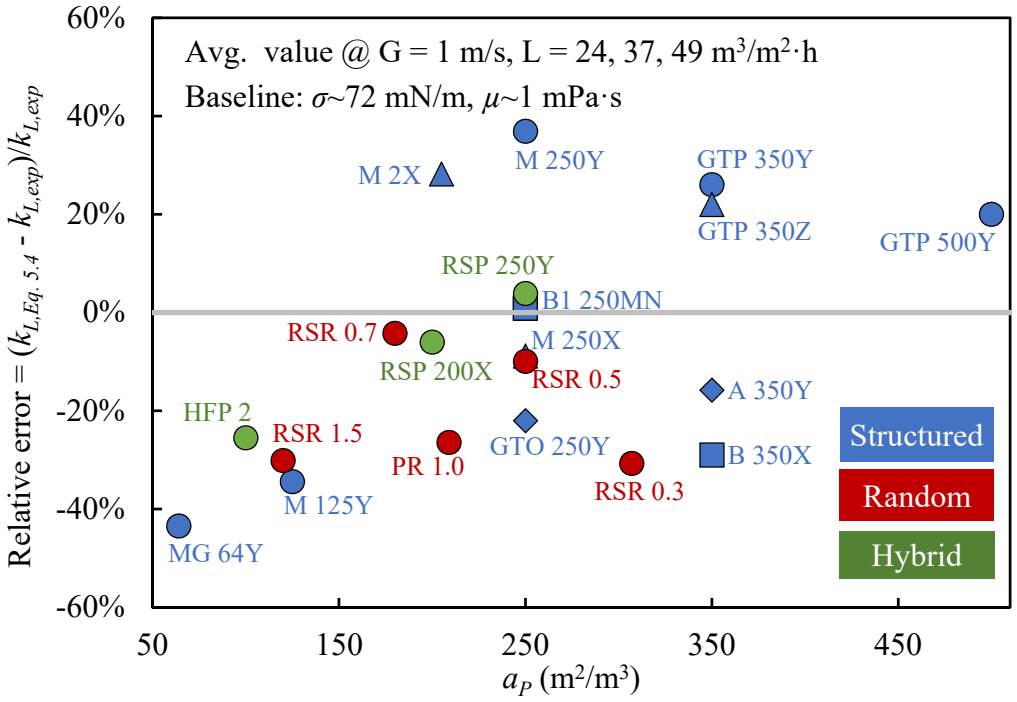

Figure 5.20: Relative error of Equation 5.4 with packing geometry

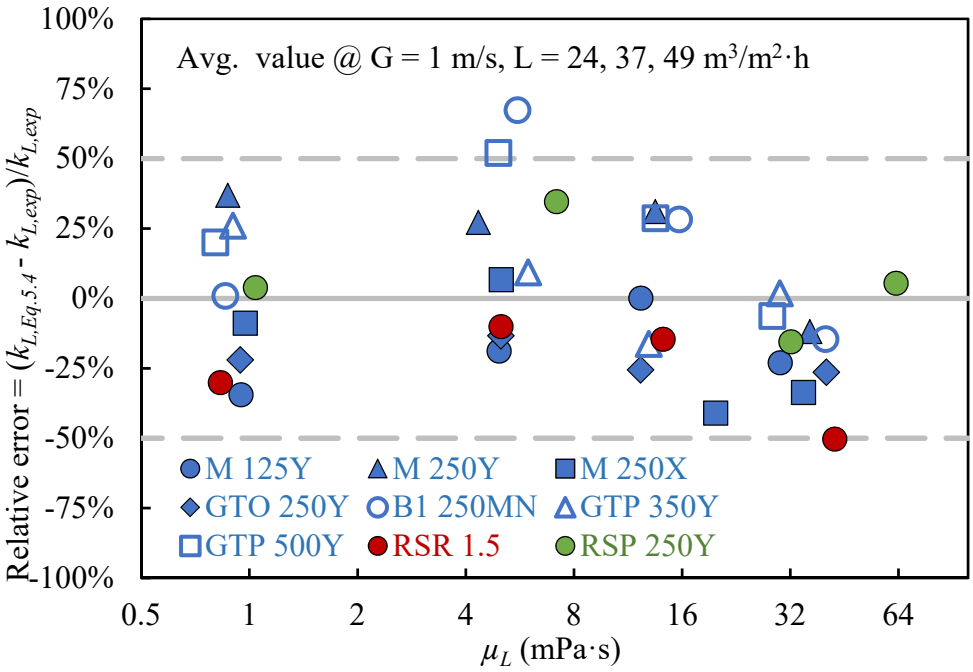

Figure 5.21: Relative error of Equation 5.4 with variable viscosity

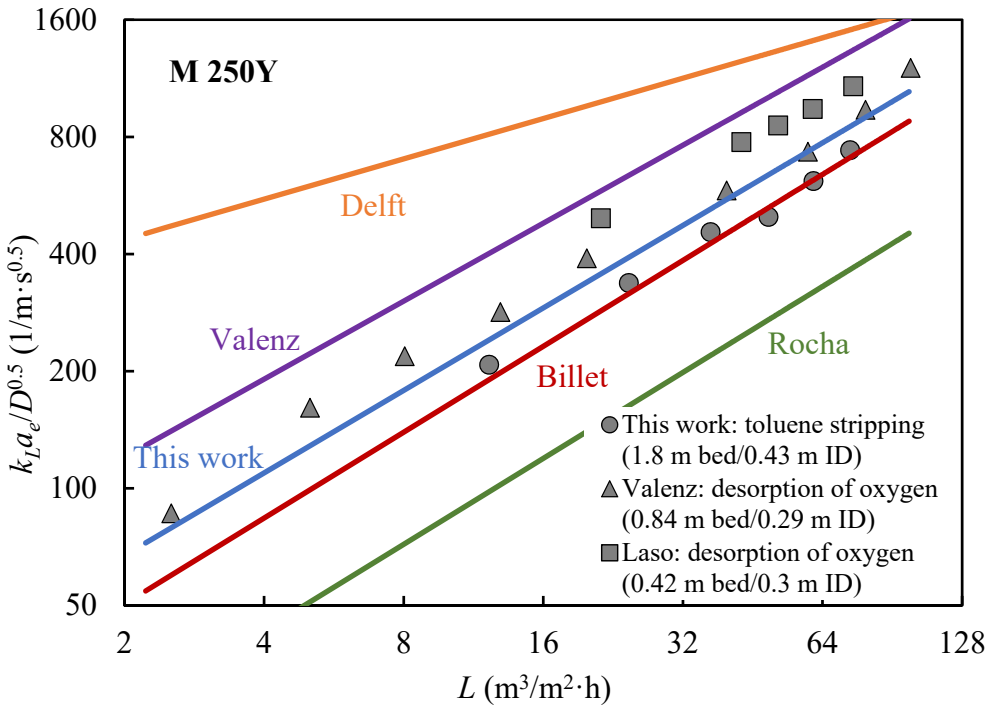

Figure 5.22: Comparison of k_La models in the literature with experimental data for water

Models of k_L/k_G and a_e from different sources should generally not be mixed, since k_L and k_G are usually determined from a k_La and k_Ga measurement. For many industrial applications, it is the volumetric mass transfer coefficient (k_La_e) instead of individual mass transfer property that matters. For these cases, the recommended combined form of $k_L \cdot a_e$ is:

$$k_L \cdot a_{e,packing} = 0.14 \cdot \eta \cdot a_P^{0.73} \cdot u_L^{0.7} \cdot g^{0.24} \cdot \mu_L^{-0.4} \cdot D_L^{0.5} \cdot \rho_L^{0.54} \cdot \sigma^{-0.14} \cdot \left(\frac{Z}{1.8}\right)^{-0.54} \quad (5.5)$$

Equation 5.4a shares the form of the theoretical prediction of k_L for a laminar falling film as in a wetted-wall column (Bird et al., 2002; Higbie, 1935):

$$Sh = 0.724 \cdot Sc^{1/2} \cdot Re^{1/3} \cdot Ga^{1/6} \quad (5.6a)$$

$$k_L^0 = 1.15 \left(\frac{q^{1/3}}{l^{1/2} W^{1/3}}\right) \left(\frac{g \sin\alpha \rho}{\mu}\right)^{1/6} D^{1/2} \quad (5.6b)$$

Derivation of Equation 5.6a can be found in Mshewa (1995). Equation 5.4a and Equation 5.6a have the same dependence on *Sc* and *Ga*, so they have identical predictions of the effect of gravity and diffusivity. However, because of the difference in *Re* dependence, Equation 5.4a shows a greater effect of liquid load (0.565 compared to 0.333) and viscosity (-0.4 compared to -0.167) on k_L than the analytical solution for the wetted wall column (Equation 5.4a). The difference results from the turbulent nature of liquid flows in packings compared to the laminar flow of falling films described in Equation 5.6a. For the latter, the liquid load and μ_L only affect mass transfer via the change of film thickness (and thus surface velocity and contact time), while for flow in packings, it is believed to be turbulence induced by either surface modification of packings (embossing, perforation, etc.), gas-liquid friction in packing channels, or liquid re-mixing at packing joints. Both liquid load and μ_L will affect not only the film thickness but also the degree

of liquid turbulence and thus the surface renewal and mass transfer rate in packing flows. This explains the greater dependence on *Re* in Equation 5.4a than Equation 5.6a.

The liquid flow in each triangular channel in the structured packings can be regarded as a tilted falling film, as described in Equation 5.6a. The k_L can thus be calculated by Equations 5.6–10:

$$q_{channel} = Q_{column}/n_{channel} \tag{5.7}$$

$$n_{channel} = \frac{A_{column}}{a_{channel}} = \frac{\frac{\pi}{4}\cdot D_{column}^2}{\left(\frac{b}{\sin\alpha}\cdot h\right)/2} \tag{5.8}$$

$$l_{total\ mixing} = \frac{b}{2\cdot\sin\alpha\cos\alpha} \tag{5.9a}$$

$$l_{no\ mixing} = H_{packing\ element}/\sin\alpha \tag{5.9b}$$

$$w = 2s \tag{5.10}$$

In the calculation, liquid is assumed to be evenly distributed to each fully-wetted channel, with no mixing at perforations, and no flow along the column wall. The length of the falling film, *l*, has a significant effect on k_L. If complete mixing happens between two adjacent corrugation channels, the length can be calculated by Equation 5.9a (sketched in Figure 5.23). If no mixing is assumed, *l* is 10–15 times longer and can be approximated by Equation 5.9b. This is limiting calculation for the longest possible *l*, since sometimes the channel length is restricted by the cross-section length instead of $H_{packing\ element}$. These are estimates of the two limiting values of the length of the falling film, and comparison of their predictions with the experimental k_L can reveal which situation is closer to the actual packing behavior.

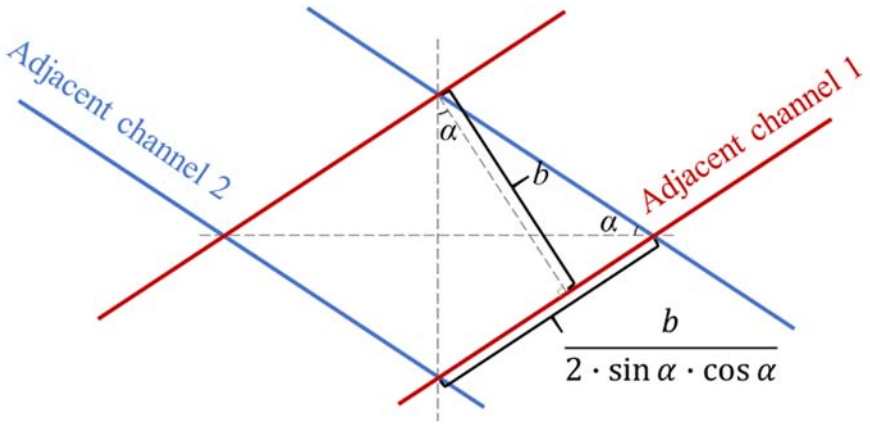

Figure 5.23: Length of falling film in packing channel if total mixing is assumed

Similar calculations can be done for the falling film along the column wall (Equations 5.6 and 5.11–13):

$$q_{wall} = Q_{column} \tag{5.11}$$

$$l_{wall} = H_{packing\ element} \tag{5.12}$$

$$w_{wall} = \pi \cdot d_{column} \tag{5.13}$$

In this calculation, it is assumed that all the liquid flows along the wall instead of through the packing. Another assumption is that complete liquid mixing happens once in each packing element. This is a simplified assumption since elements for some packings have more than one wiper band, and whether complete liquid mixing happens at wiper bands is also arguable.

Comparison of the falling film k_L from Equations 5.6–13 and experimental k_L for M 250Y is shown in Figure 5.24. If total mixing between adjacent corrugation channels is assumed, falling film k_L for both the wall and packing are significantly greater (more than two times) than the measured value. This is not reasonable because the k_L of

turbulent flows in the packings should be greater than the theoretical value for the laminar falling films. Two assumptions can be made to explain the abnormality: the "no-mixing" assumption, and the "big rivulet" assumption.

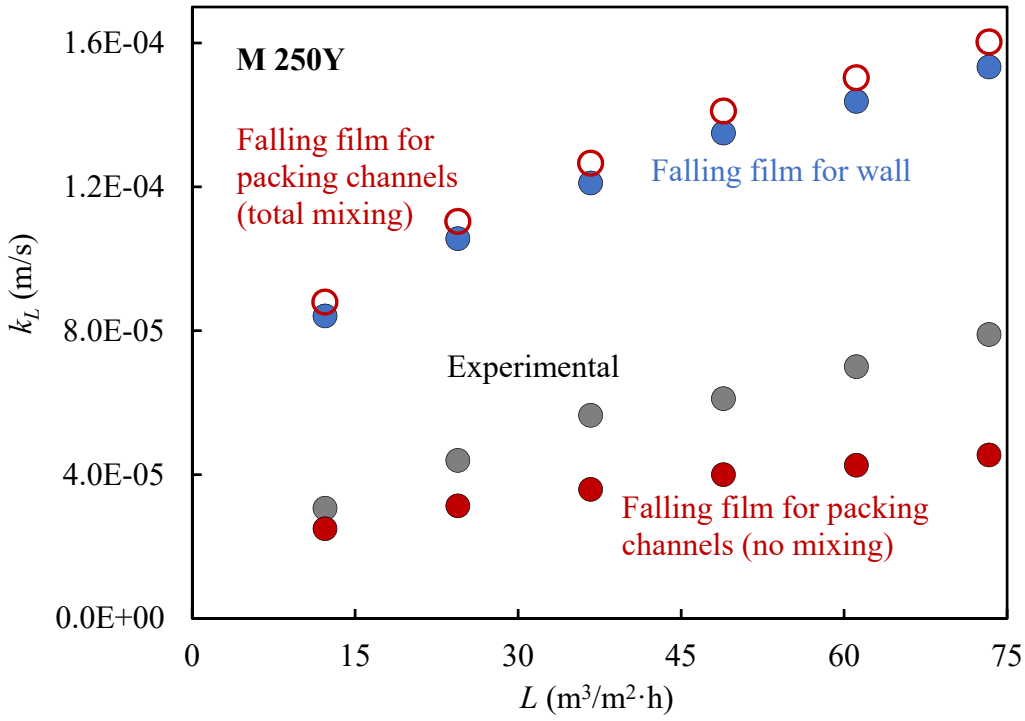

Figure 5.24: Comparison of the theoretical k_L from Equations 5.6–13 and experimental k_L for M 250Y

The first assumption is that no mixing (or only partial/insignificant mixing) occurs between adjacent corrugation channels. Based on this assumption, Equation 5.9b instead of 5.9a is used to calculate the length of the falling film, l. The significantly longer l makes the falling film k_L for packings channels lower than the experimental k_L, which itself lies below the falling film k_L for wall flows (Figure 5.24). The experimental k_L is closer

to the falling film k_L for packings than that for wall, which agrees with Figure 5.3 that shows secondary wall flow is relatively small for packings with a_P of 250 m^2/m^3.

Another explanation is the "big rivulet" assumption, in which it is believed that the area measured using caustic scrubbing of CO_2 is significantly greater than the a_e contributable to liquid film mass transfer in the toluene stripping experiment. Thus, a significantly smaller k_L is obtained when separating it from experimental k_La using a significantly greater a_e. A computational fluid dynamics (CFD) study also suggested a lower area compared to the experimental data (Basden, 2014). The difference in the area for the two experiments results from the two regimes of liquid flow on the packing surface: big rivulets that contain the majority of volumetric liquid flow but cover relatively small portion of the packing surface, and spread-out thin films that cover most of the packing surface with limited volume flow. Both regimes contribute to a_e in the CO_2 scrubbing experiment because of the relative abundance of NaOH, however, only the big rivulets contribute to a_e in the toluene stripping experiment because of the fast depletion and slow renewal of toluene in the thin films. Moreover, due to the difference in the toluene concentration and fluid velocity of the two flow regimes, effective back-mixing occur when the two regimes mix either at packing element joints or when big rivulets shift. The back-mixing detrimental to mass transfer efficiency will also lead to lower k_L.

Figure 5.25 shows the ratio of the experimental k_L to calculated k_L for falling film from Equations 5.6–10 with variable viscosity. The packing not only enhances mass transfer area, but also enhances k_L because the ratio is mostly greater than unity at different viscosities. The ratio decreases with increasing μ_L, however, because Equation 5.6 predicts a significantly less dependence on μ_L (-1/6) compared to Equation 5.4 (-0.4). This can be explained by the "big rivulet" assumption that when viscosity increases, depletion of toluene in the thin film becomes slower because of the decreased mass transfer

efficiency, thus decreasing the difference in the area in the experiments of caustic scrubbing of CO_2 and air stripping of toluene.

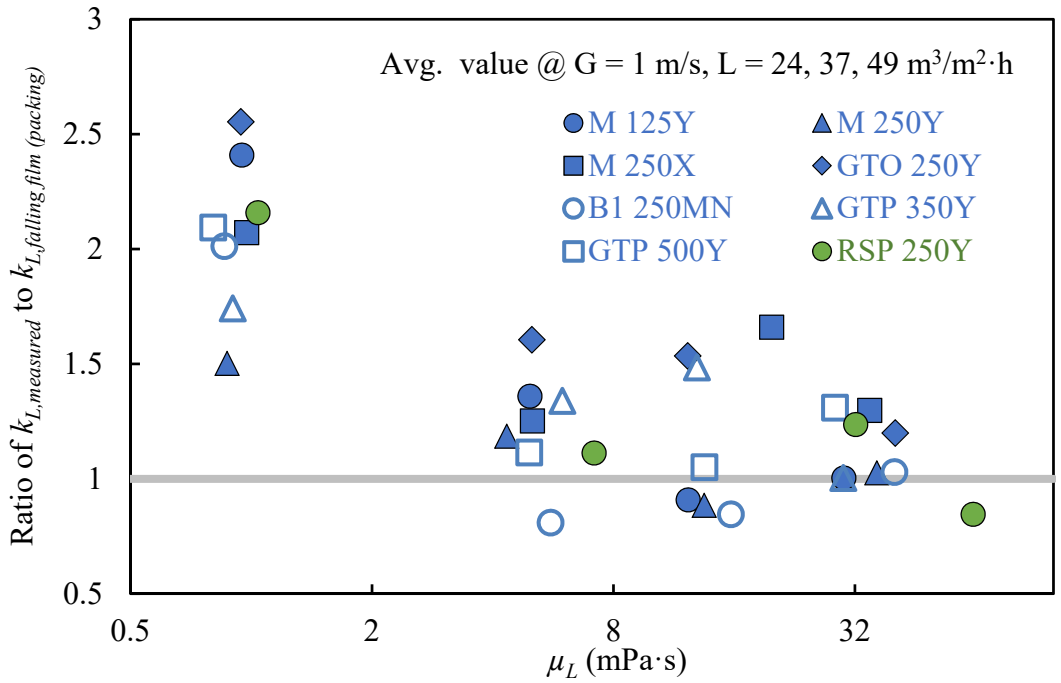

Figure 5.25: Ratio of experimental k_L to falling film k_L (no mixing) from Equations 6–10 with variable viscosity

The two assumptions to explain the difference between the experimental k_L and calculated k_L for falling films seen in Figure 5.24 are only qualitative ones. Either or both of them could be true. Rigorous quantitative study in this area is promising but is not in the scope of this work.

Though $a_{secondary}$ has been corrected in the area model, it is the measured total area, a_e, that has been used to separate k_L from the experimental $k_L \cdot a_e$. This assumes that the liquid in the secondary area has the same k_L as in the packing section, which is not true according to Figure 5.24. However, since secondary area is less than 10% for higher area packings (a_P > 200 m^2/m^3), this simplification is still valid for most of the packings.

Differentiating and quantifying k_L in different flow regimes would be a more rigorous way of modeling, but it is not within the scope of this work due to the limited data for coarse packings for which secondary flow is more significant.

The operating condition for a_e and k_L measurement in this work is well below the loading point (20–40% flooding for water), so the result may not be valid for operating conditions close to or above loading zone, especially for viscous liquids that have drastically different hydraulic behavior than water. Caution should also be exercised when the conclusions about the viscosity effect on mass transfer are extrapolated beyond the μ_L range of this work (0.8-70 mPa·s). Due to different degrees of maldistribution, a systematic difference in k_L with different packing height has been observed (Figure 5.16) and all k_L has been normalized to the shorter bed (1.8 m). Therefore, error will arise when applying the models in this work to a column with different size and packing bed height (and thus different degrees of liquid maldistribution). Many other factors that affect mass transfer efficiency will also be different from column to column, such as how tight the packing fits the column, the condition and number of wiper bands of packing elements, degree of packing damage due to (re)install, etc. This is a universal and important problem for all models and requires systematic research in the future.

5.2.4 Effect of Liquid Viscosity

The overall dependence on μ_L of k_L predicted by Equation 5.4b is -0.75, of which -0.35 is from the indirect influence of μ_L through diffusivity ($D_{toluene} \propto \mu_L^{-0.7}$ in aqueous glycerol, see section 3.1.2), and -0.4 is from the direct influence of μ_L on k_L through liquid turbulence. The direct part is universally applicable to all Newtonian liquids. The indirect part is believed to be system dependent, and requires knowledge of the D-μ

relationship. If this analysis were repeated with a -0.8 dependence of diffusivity on viscosity, which is what has been used in CO_2/aqueous amine absorber modeling, both the direct and indirect influence would be -0.4. Figure 5.26 shows the dependence of k_L normalized by other factors (liquid load, density, gravity, and a_P) on μ_L. The μ_L dependence (-0.75) is the same for structured, random, and hybrid packings.

In Figure 5.27, only the model developed here works as well for aqueous glycerol as for water. The other models fail to correctly predict the k_La of the viscous liquid because they either do not include (Valenz et al., 2011) or underestimate the effect of μ_L on k_La. Another advantage of the model reported here is its simplicity: it does not require packing-specific constant or detailed packing geometry (b, s, h).

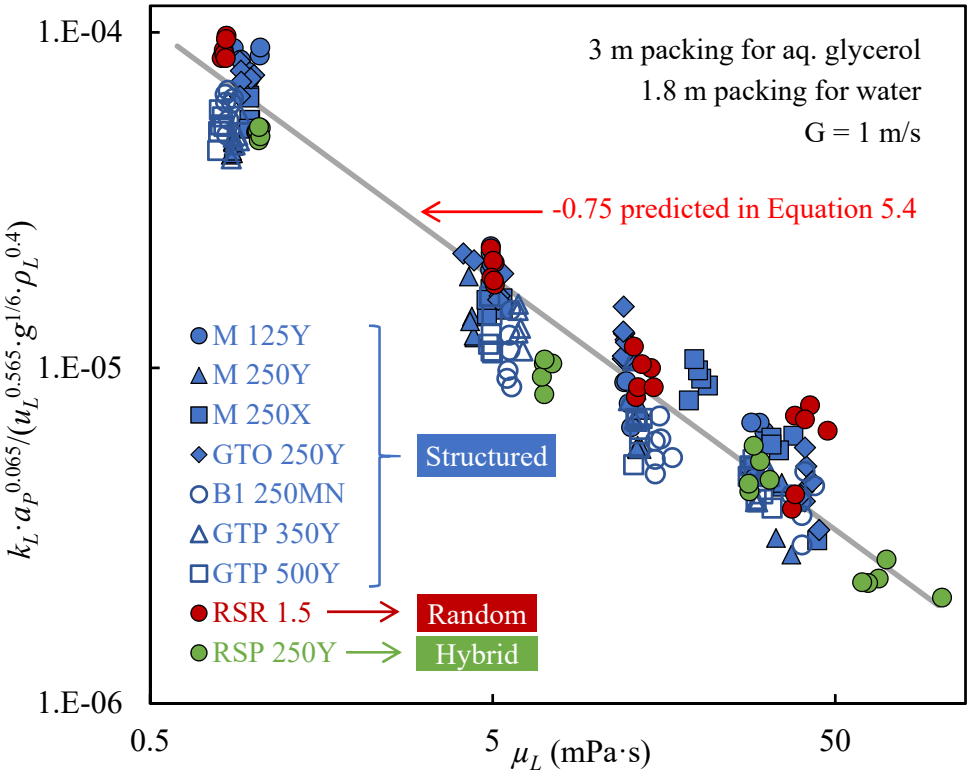

Figure 5.26: Total dependence on μ_L of k_L

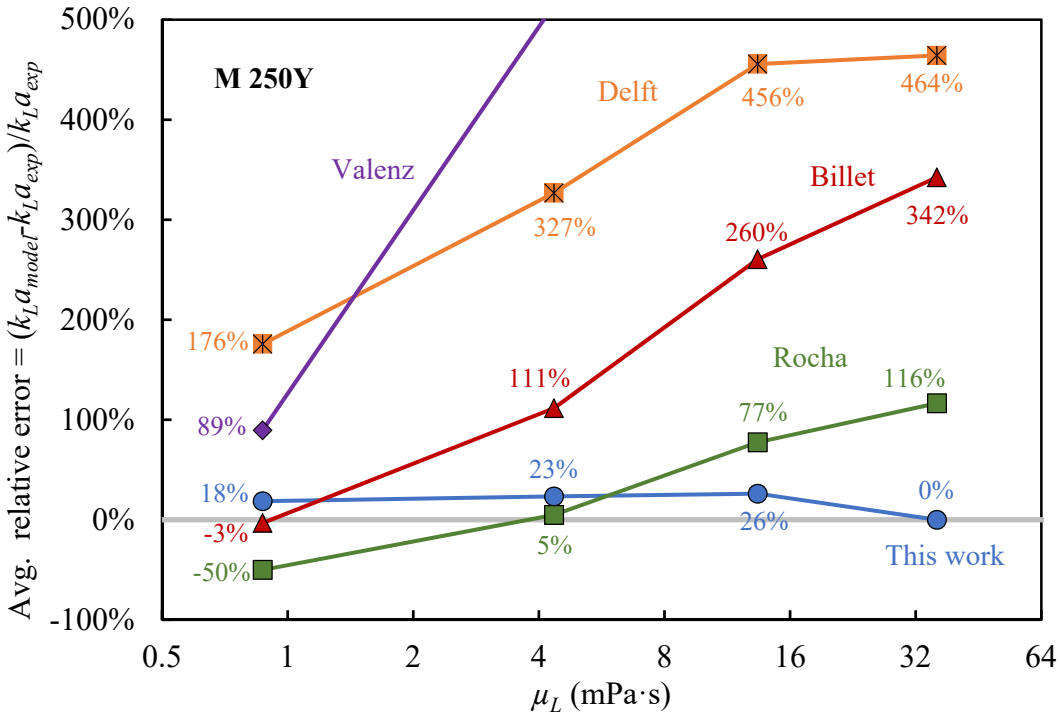

Figure 5.27: Comparison of k_La models in the literature with experimental data for aqueous glycerol

Figure 5.28 compares the result of this work and other k_L (k_La) correlations in the literature. Details of the correlations in the figure can be found in Table 2.1. The direct dependence on μ_L of k_L predicted in Equation 5.4 (-0.4) is similar to the other four experiments on random packings with relatively large viscosity variance (the four solid squares in the figure).

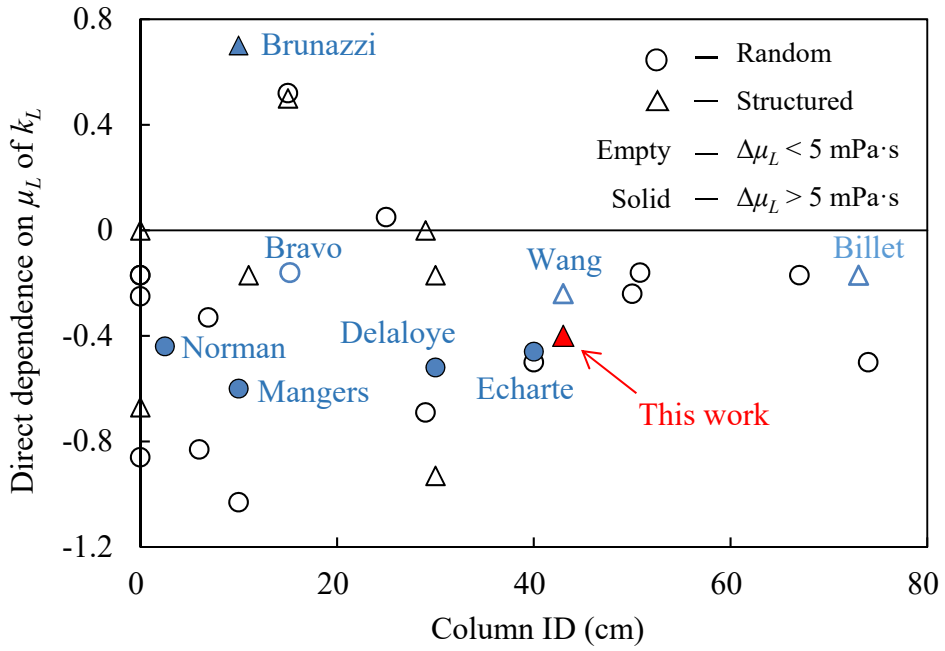

Figure 5.28: Result of this work compared to literature correlations

5.2.5 Analysis of SRP Database

The average k_L in the SRP database of structured, random, and hybrid packings at 1 m/s gas rate and 24, 37, and 49 $m^3/m^2 \cdot h$ liquid loads is plotted against a_P (Figure 5.29). Because of the more stable flow pattern, k_L measured at medium liquid loads (24–49 gpm/ft^2) has greater reproducibility than at low or high loads. Therefore, the average value at medium liquid loads for each packing is used for comparison. The lines in the figure are the average value for the same type of packing.

A previous theory of mixing points (Wang et al., 2016) suggests that k_L should increase with increasing packing a_P and decreasing α because there are more opportunities for mixing of the liquid film. However, Figure 5.29 shows an opposite trend for structured and hybrid packings. For these packings, the k_L decreases with increasing a_P.

If the average k_L is compared at the same flooding fraction instead of operating conditions, this trend will be more pronounced due to the greater capacity of coarse packings. The Y packing does not consistently out-perform X/Z packing in the same family, so the corrugation angle does not have a clear effect on k_L. For random packing, the trend is not monotonic. The average k_L first decreases, then increases with increasing a_P. No systematic trend is found for random packing, probably because of the limited data for this type.

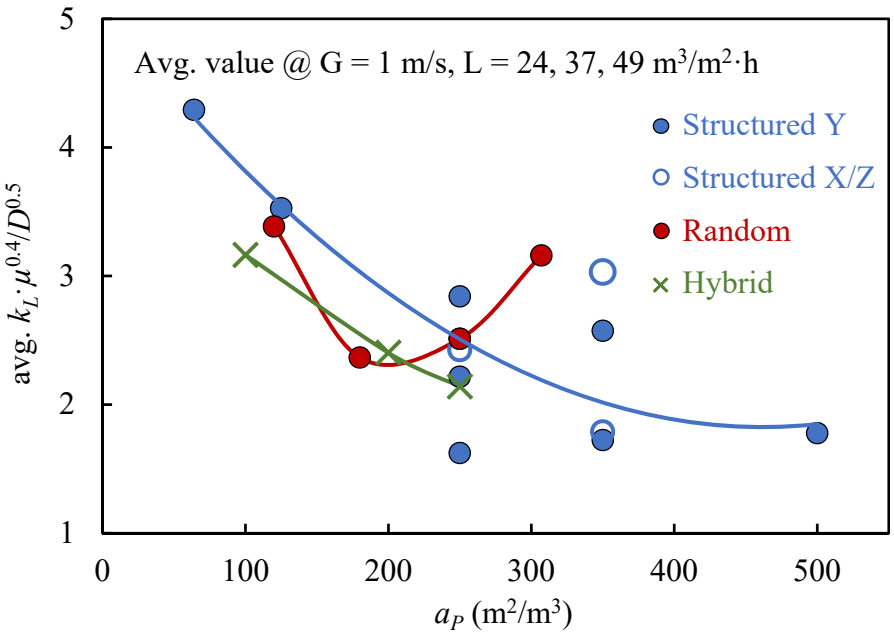

Figure 5.29: Average k_L as a function of a_P

This "counter-intuitive" trend of k_L for structured and hybrid packings can be explained by both the "big rivulet" and "no mixing" assumptions discussed in section 5.2.3. As the "big rivulet" assumes, the dominant liquid flow pattern in coarse packings is large and thick liquid streams, which are believed to contribute to greater mass transfer efficiency than the spread-out, thin liquid films that would be more common in fine

packings. The "no-mixing" assumption also explains the trend shown in Figure 5.29. Because of the insignificant mixing, the flow path length l, is only a weak function of a_P, but is dictated by $H_{packing\ element}$, which does not vary significantly between packings (usually 20–25 cm). As a result, the increase in the liquid flow per channel in coarse packings due to the decrease in the number of corrugation channels leads to greater k_L compared to finer packings at the same liquid load. This effect become less and less significant when packing area (and thus the number of corrugation channels) further increases, which explains the gradually flattened slope in Figure 5.29. Therefore, the theory of mixing point that is based on total mixing at joints of packing corrugation channels may not be valid for liquid film mass transfer (Wang et al., 2016).

5.2.6 Results of Viscometer Skid

A viscometer skid was connected to the AWC as an inlet liquid bypass stream (Figure 3.21). It can provide online measurement of liquid density and viscosity. Figures 5.30 and 5.31 compare the density and viscosity of aqueous glycerol in the experiments of GTO 250Y measured online by the viscometer skid and offline by densitometer and plate-and-cone viscometer (see Section 3.4 for details).

Due to the unreasonably high reading with the skid pump turned on, the skid bypass was closed for the 30–60 mPa·s solution. For batches with lower μ_L, the bypass was open with the pump turned off (liquid was driven solely by static pressure difference). As can be seen in the figures, even with the skid pump off, the viscometer skid still showed fluctuating viscosity readings which were on average 20% higher than the offline measurement. Overall, the lack of stability and accuracy of the viscometer skid in both density and viscosity readings makes it unreliable for serious data acquisition.

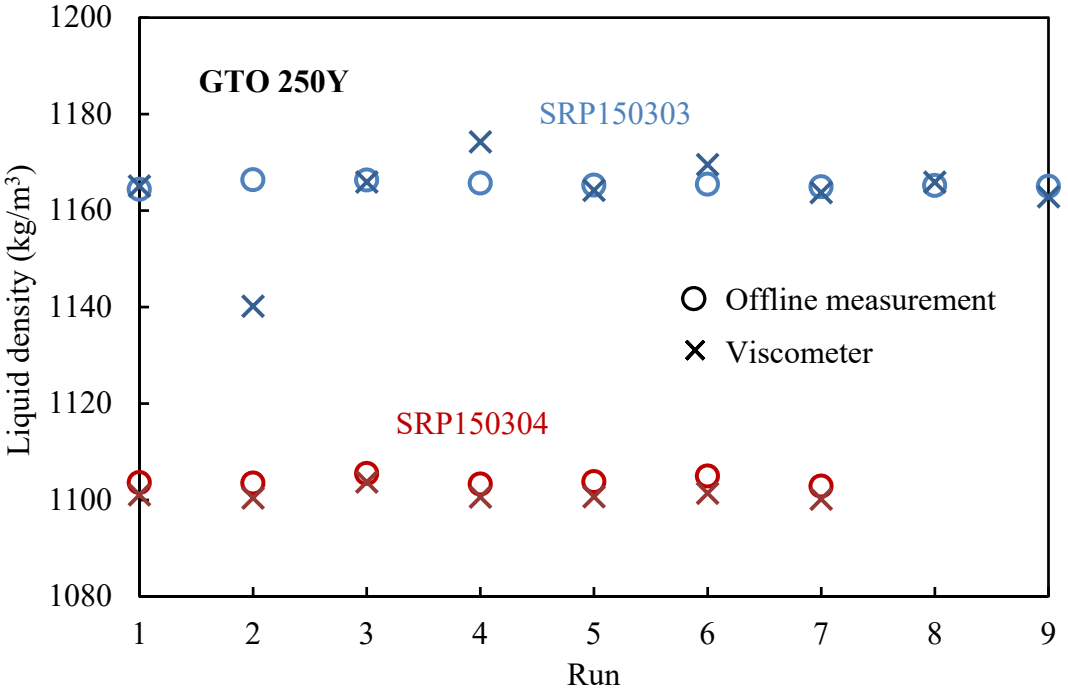

Figure 5.30: Liquid density measured online by viscometer and offline by densitometer

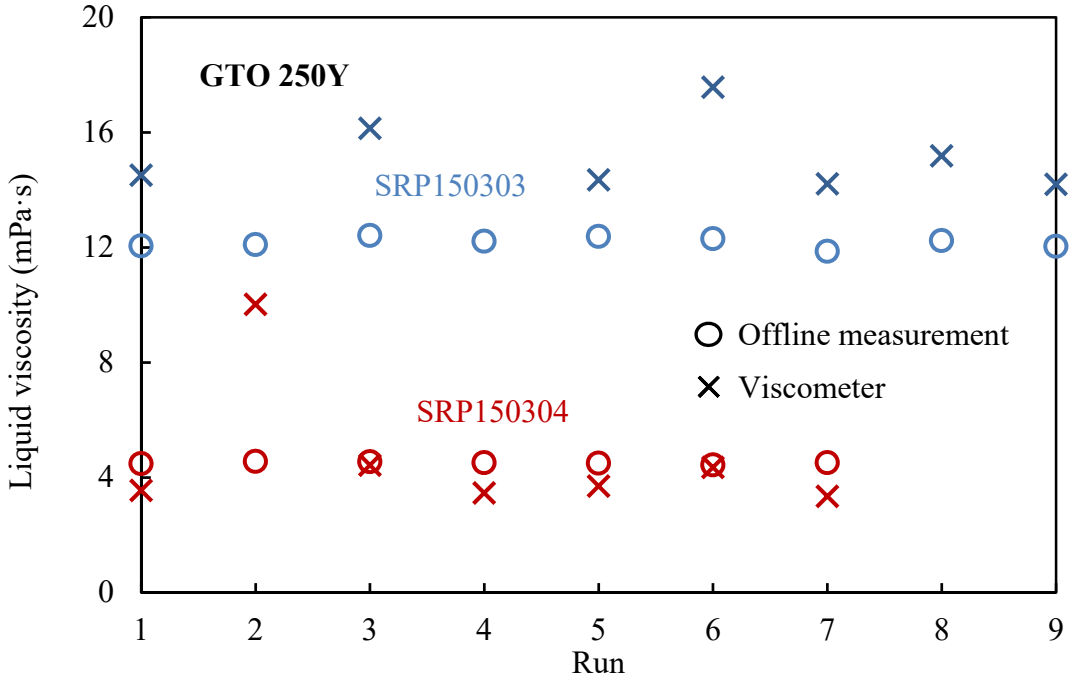

Figure 5.31: Liquid viscosity measured online and offline by viscometer

To trouble-shoot the viscometer skid, it was disconnected from the column and configured in a recycled liquid loop with different setups: original setup, skid with filter, skid with gear pump (instead of centrifugal pump), skid with longer flow path before viscometer. Figure 3.20 shows the original setup. A filter was then added to the loop to help diminish gas bubbles created by the pump that may significantly affect μ_L reading (Figure 5.32a). The centrifugal pump was then replaced by a gear pump which is expected to generate less liquid turbulence and gas bubbles (Figure 5.32b). A longer flow path before the viscometer flow chamber was used to see it can facilitate settlement of liquid turbulence at the viscometer (Figure 5.32c). None of the configurations provide either correct absolute value or calibratable values (Table 5.2), even when all the calibration constants were the same as the factory calibration certificate.

Table 5.2: Results of viscometer skid trouble-shooting with different setups

Setup	1	2	3	4
Glycerol	√	√	×	×
Filter	×	√	√	√
Gear pump	×	×	√	×
Longer flow path	×	×	×	√
Correct absolute value	×	×	×	×
Calibratable value	×	×	×	×

(a)

(b)

(c)

Figure 5.32: Configurations of viscometer skid loop: (a) skid with filter, (b) skid with gear pump, (c) skid with longer liquid flow path before viscometer

5.3 GAS FILM MASS TRANSFER COEFFICIENT (k_G)

Although k_G is not the primary focus of this work, a modified k_G model (Equation 5.14) was developed with an expanded database.

$$Sh_G = 0.28 \cdot {Sc_G}^{0.5} \cdot {Re_G}^{0.62} \cdot \left(\frac{\sin 2\alpha}{\sin(2\times 45°)}\right)^{0.65} \tag{5.14a}$$

$$k_G = 0.28 \cdot u_G^{0.62} \cdot \left(\frac{\mu_G}{\rho_G}\right)^{-0.12} \cdot D_G^{0.5} \cdot a_P^{0.38} \cdot (\sin 2\alpha)^{0.65} \tag{5.14b}$$

$$\alpha_{effective} = 45° \text{ (for random and hybrid packings)} \tag{5.14c}$$

Figure 5.33 compares the experimental k_G and k_G calculated from the model. The model shows an AAD of 21% for all 20 structured, random, and hybrid packings. It is notable that there was no significant change in the gas property (μ_G, ρ_G, or D_{SO2}) other than those caused by ambient temperature or operating condition change. Therefore, few dimensionless numbers are used in the model as possible because of the limited range of gas physical property variance. The effect of corrugation angle for structured packings is reflected in the term, $\sin(2\alpha)$, which is fundamentally identical to the form of the mixing point density, *Mi*, of the Wang correlations (Wang et al., 2016). For structured Y packings, the angle correction is essentially one. Effective corrugation angle of 45° was assigned to random (RSR) and hybrid (RSP) packings for optimum fitting (Equation 5.14c). The dependence on *Sc* was fixed to 0.5 to satisfy the penetration theory (Higbie, 1935).

Compared to the k_L model, the k_G model shows a positive dependence on a_P, similar dependence on the fluid superficial velocity (0.62 compared to 0.565), and lower dependence on the kinematic viscosity (-0.14 compared to -0.4). The relative error of Equation 5.14 is plotted against a_P in Figure 5.34. No systematic bias of the model as a function of packing geometry is observed.

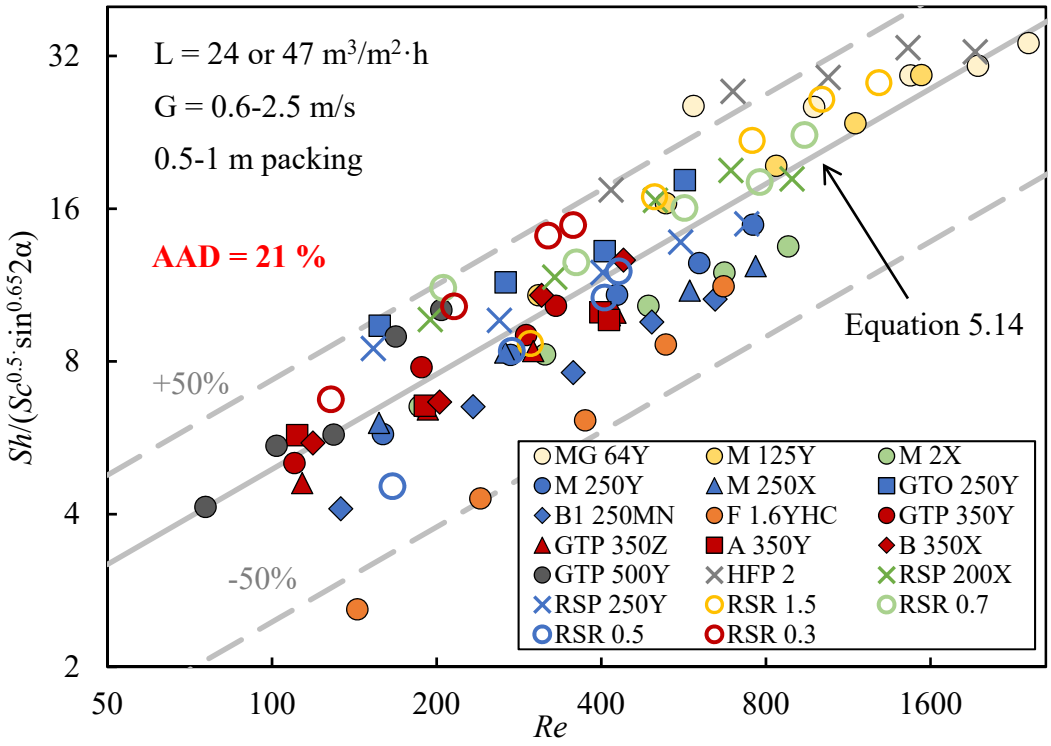

Figure 5.33: Comparison of measured k_G and k_G calculated from Equation 5.14

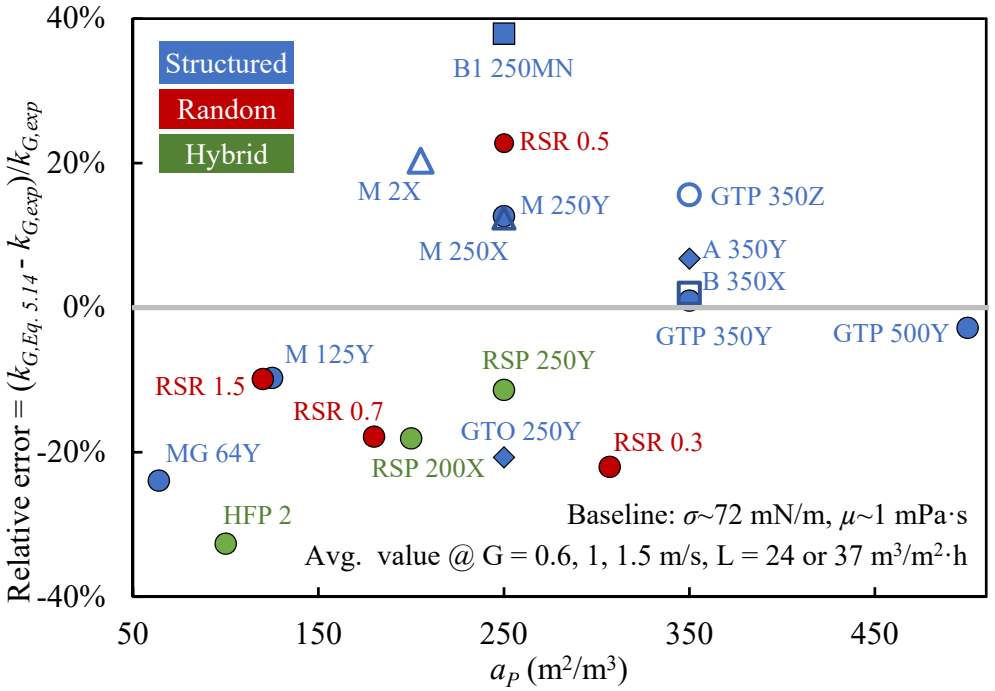

Figure 5.34: Relative error of Equation 5.14 with packing geometry

The recommended combined forms of $k_G \cdot a_e$ is:

$$k_G \cdot a_{e,packing} = 0.325 \cdot \eta \cdot u_L^{0.14} \cdot u_G^{0.62} \cdot a_P^{1.17} \cdot (\sin 2\alpha)^{0.65} \cdot D_G^{0.5} \cdot \left[\frac{\rho_L}{\sigma} \cdot g^{\frac{1}{2}}\right]^{0.14} \cdot \left(\frac{\mu_G}{\rho_G}\right)^{-0.12} \quad (5.15)$$

The average k_G for different packings at liquid load of 24 or 37 $m^3/m^2 \cdot h$ and gas rates at 0.6, 1, and 1.5 m/s is plotted against a_P in Figure 5.35. The k_G for structured packings increases with packing a_P. Y packings perform better at gas film mass transfer than X/Z packings. The trend in a_P is not monotonic for random packings, while the k_G for hybrid packings remains unchanged as a_P varies. The non-systematic behavior of k_G for random and hybrid packings probably results from the open geometry of these packings.

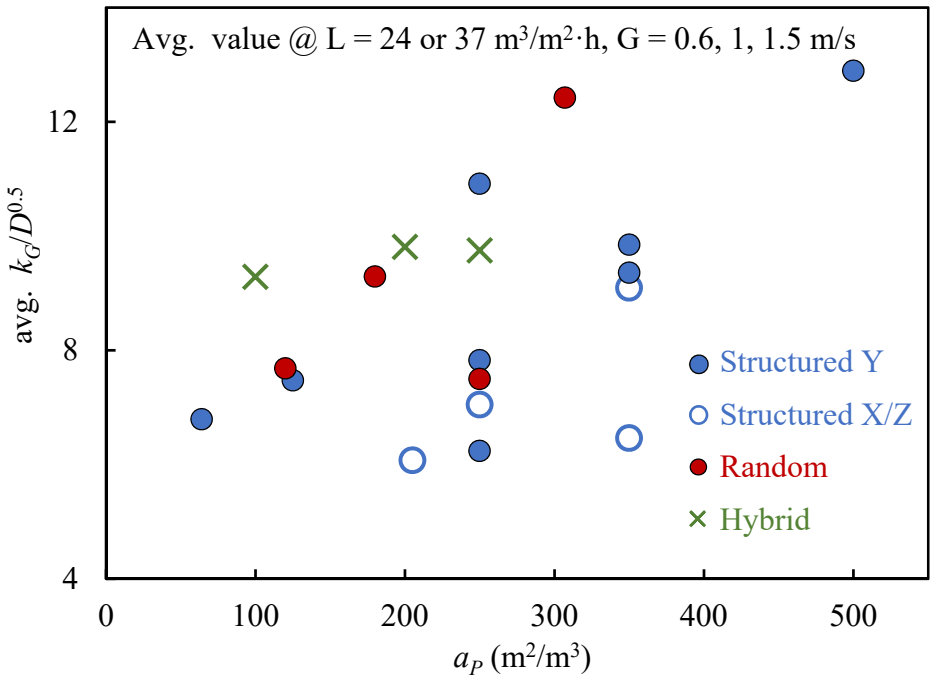

Figure 5.35: Average k_G as a function of a_P

Chapter 6: Conclusions and Recommendations

This chapter summarizes the experimental and modeling work completed in this research. Conclusions are stated and recommendations for future work provided.

6.1 Summary of Work Completed

Figure 6.1 summarizes the main work completed in this current research.

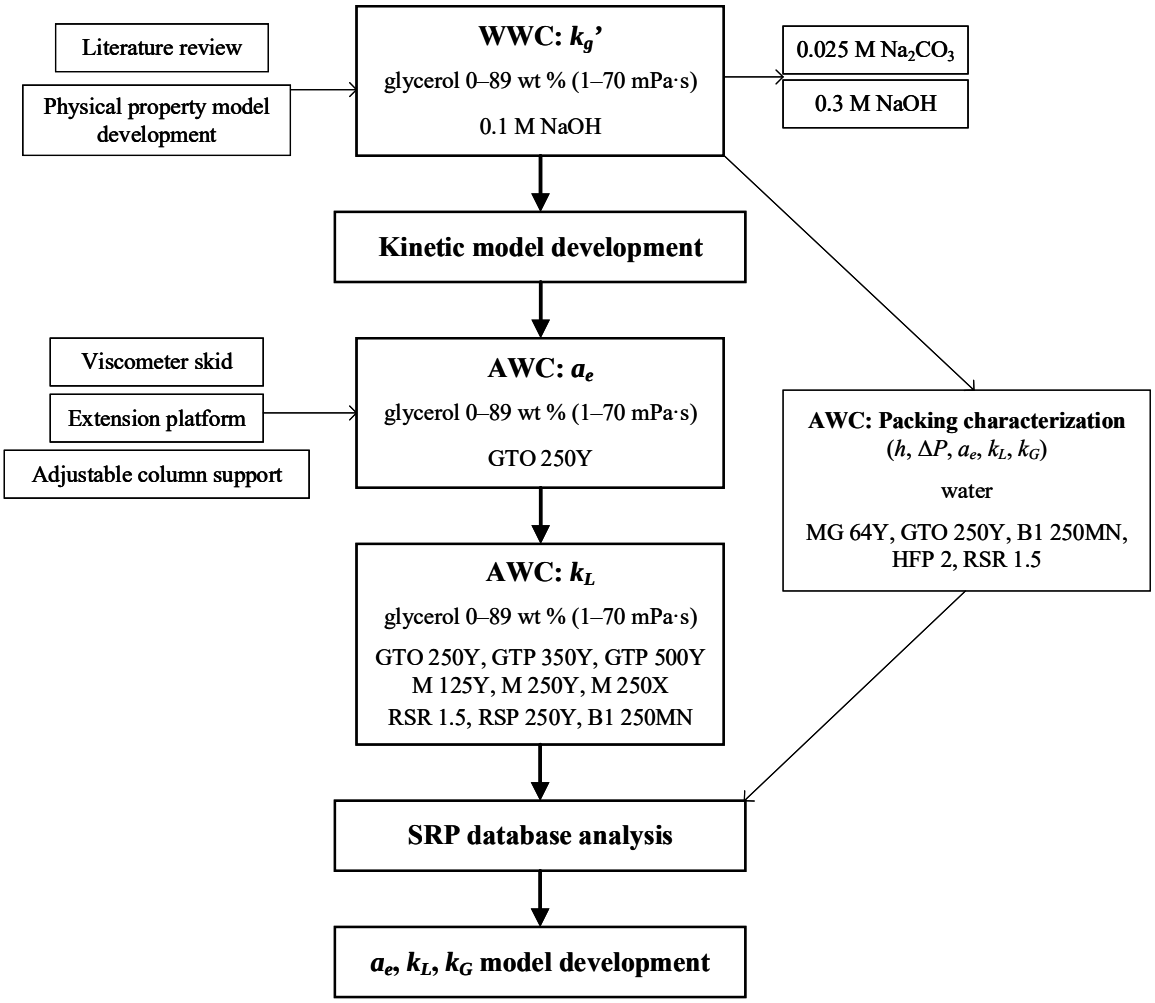

Figure 6.1: Work completed in this research

Glycerol was chosen as liquid viscosity enhancer mainly for its complete and easy dissolution in water, and Newtonian behavior of its aqueous solution. Physical property (ρ_L, μ_L, diffusivity, Henry constant of CO_2, σ, and activity coefficient) models of aqueous glycerol were developed based on various literature data. Sterilization experiments were performed indoor and outdoor to check the bacteria growth in aqueous glycerol. Reaction kinetics (k_g') of CO_2/NaOH/H_2O/glycerol was measured using the bench-scale WWC at 20, 30, and 40 °C. μ_L was varied 1–70 mPa·s by adding 0–89 wt % glycerol. Baseline experiments (0.1 M NaOH), experiments with elevated caustic (0.3 M NaOH), and with carbonate (0.025 M Na_2CO_3) were performed to provide raw data of kinetic model development and to check the effect of accumulated carbonate.

Based on the kinetic model, two parallel a_e experiments in the AWC with GTO 250Y were performed to confirm the result of Tsai (2010) that μ_L does not affect a_e. k_L for water and aqueous glycerol (1–70 mPa·s with 0–89 wt % glycerol) was then measured by air stripping of toluene in seven structured packings (GTO 250Y, GTP 350Y, GTP 500Y, M 125Y, M 250Y, M 250X, B1 250MN), one random packing (RSR 1.5), and one hybrid packing (RSP 250Y). Packing characterization tests with water (including hydraulic properties h, ΔP, and mass transfer properties of a_e, k_L, and k_G) were performed with five packings (MG 64Y, GTO 250Y, B1 250MN, HFP 2, and RSR 1.5). Major and minor modifications were performed on the AWC during the research: connecting viscometer skid to liquid inlet bypass, installing extension platform on the AWC 3rd floor, installing adjustable column stand, rerouting entrained water line, welding washers onto the sampling bayonet.

Because of the decrease in k_L caused by increased μ_L, it is of interest to investigate other types of separators that can provide mechanical agitation on the liquid phase (such as rotating packed bed) with viscous liquid. These types of separators might be good

candidate to perform separations with viscous liquid considering their potential to increase the k_L.

By analyzing both the data measured in this research (11 packings) and those available in the SRP database (28 packings), universal models to predict a_e, k_L, and k_G of structured, random, and hybrid packings were developed.

6.2 CONCLUSIONS

6.2.1 Wetted-Wall Column

- Glyceroxide reacts with CO_2 6 times faster than hydroxide ($k_{Glycerol^-} = 6\ k_{OH^-}$).
- With increasing glycerol added to aqueous NaOH solution, the CO_2 absorption rate (k_g') initially increased by 30% because glyceroxide is more reactive than hydroxide, then decreased rapidly by 75% because of increasing viscosity and decreasing diffusion coefficients.
- The kinetic model for CO_2/NaOH/H_2O/glycerol is given by:

$$k_{Alk} = k_{OH^-}\left(\frac{[\mathrm{OH^-}]}{[\mathrm{Alk}]}\right) + k_{Glycerol^-}\left(\frac{[\mathrm{Glycerol^-}]}{[\mathrm{Alk}]}\right) \tag{3.33}$$

$$[\mathrm{Alk}] = [\mathrm{OH^-}] + [\mathrm{Glycerol^-}] \tag{3.34}$$

$$\ln\left(\frac{k_{OH^-}}{k_{OH^-,298.15K}}\right) = \frac{-E_{OH}}{R}\left(\frac{1}{T} - \frac{1}{298.15}\right) \tag{3.35}$$

$$\ln\left(\frac{k_{Glycerol^-}}{k_{Glycerol^-,298.15K}}\right) = \frac{-E_G}{R}\left(\frac{1}{T} - \frac{1}{298.15}\right) \tag{3.36}$$

$$K_{b,Glycerol} = \frac{K_W}{K_{a,Glycerol}} = \frac{[OH^-][Glycerol]}{[Glycerol^-]} \tag{3.37}$$

$$\ln\left(\frac{K_{b,Glycerol}}{K_{b,Glycerol,298.15K}}\right) = \frac{-H_{KG}}{R}\left(\frac{1}{T} - \frac{1}{298.15}\right) \tag{3.38}$$

$$[Glycerol]_T = [Glycerol^-] + [Glycerol] \quad (3.39)$$

$$[Gly^-]^2 - \{[Gly]_T + K_{b,Glycerol} + [Alk]\}[Gly^-] + [Alk][Gly]_T = 0 \quad (3.40)$$

Parameters in Equations 3.35, 3.36, and 3.38 are summarized in Table 4.1.

- Average depletion of alkalinity at the gas/liquid interface in 0.1 N NaOH is 4% in water and 20% in 89 wt % glycerol.
- The addition of 0.025 M sodium carbonate to 0.1 M NaOH has an insignificant effect on k_g'.

6.2.2 Air-Water Column

- Consistent models of a_e, k_L, and k_G are given by Equations 5.2–4 and 5.14.based on the SRP air-water column database with 39 packings of various type, a_P, and materials. With a relatively large equipment size and packing database, this work has the greatly expanded the data of mass transfer in viscous liquids available in the open literature.

$$\frac{a_{e,packing}}{a_P} = 1.16 \cdot \eta \cdot \left(We \cdot Fr^{-\frac{1}{2}}\right)^{0.138} = 1.16 \cdot \eta \cdot \left[\left(\frac{\rho_L}{\sigma}\right) \cdot g^{1/2} \cdot u_L \cdot a_P^{-3/2}\right]^{0.138} \quad (5.2)$$

$$\eta = \eta_{type} \cdot \eta_{material} \cdot \eta_{loading} \quad (5.3)$$

$$Sh_L = 0.12 \cdot Sc_L^{0.5} \cdot Re_L^{0.565} \cdot Ga_L^{1/6} \cdot \left(\frac{Z}{1.8}\right)^{-0.54} \quad (5.4a)$$

$$k_L = 0.12 \cdot u_L^{0.565} \cdot \left(\frac{\mu_L}{\rho_L}\right)^{-0.4} \cdot D_L^{0.5} \cdot g^{1/6} \cdot a_P^{-0.065} \cdot \left(\frac{Z}{1.8}\right)^{-0.54} \quad (5.4b)$$

$$Sh_G = 0.28 \cdot {Sc_G}^{0.5} \cdot {Re_G}^{0.62} \cdot \left(\frac{\sin 2\alpha}{\sin(2\times 45°)}\right)^{0.65} \quad (5.14a)$$

$$k_G = 0.28 \cdot u_G^{0.62} \cdot \left(\frac{\mu_G}{\rho_G}\right)^{-0.12} \cdot D_G^{0.5} \cdot a_P^{0.38} \cdot (\sin 2\alpha)^{0.65} \quad (5.14b)$$

$$\alpha_{effective} = 45°\ \text{(for random and hybrid packings)} \qquad (5.14c)$$

- Liquid viscosity, μ_L, has a strong effect on the liquid film mass transfer coefficient, k_L, with a total dependence of -0.75, of which -0.35 is from the indirect influence through diffusivity, and -0.4 is from the direct influence through liquid turbulence.
- k_L decreases with increasing a_P for structured packings.
- k_L is consistently smaller with a reduced packing height. The experimental k_L is significantly smaller than predicted by the analytical solution for a falling film as in a wetted wall column.
- Liquid viscosity has no effect of the wetted area of the packing, a_e, at the conditions of these measurements, all well below the loading point.
- The wall effect is the most significant secondary effect on a_e, and is corrected for in the a_e model.

6.3 Recommendations for Future Work

The conclusion that μ_L does not affect a_e is based on the research of Tsai with PEG and experiments performed in this work with aqueous glycerol for one structured packing – GTO 250Y. Assumption was made that the effect of μ_L on a_e for the one measured structured packing is the same with other structured packings, and that the effect is the same with other types of packings. This assumption is somewhat overly-applied, and it is recommended that a_e with viscous liquid be measured with more packings with different geometry.

Due to the limited time, diffusivity in aqueous glycerol is calculated instead of directly measured. Moreover, the dependence on the diffusivity of k_L was assumed directly to be 0.5 based on the penetration theory. Ideally, the value and dependence of

diffusivity should be determined experimentally, especially for viscous liquid for which the reliability of models is not as good as for water or organic solution with low viscosity. A good knowledge in diffusivity enables a more accurate separation of the direct and indirect influence of μ_L on k_L.

The conclusions of this work should be verified with other systems apart from toluene/air/H_2O/glycerol. Liquid viscosity can be varied using other viscosity enhancer (such as sugar), and diffusivity can be varied using other volatile substance (such as oxygen). The models developed in this work should be validated with data of different applications using packings.

The effect of secondary area and liquid maldistribution should be measured by systematically varying the height of packed bed, distributor, and (if possible) column diameter. By including a factor of column geometry into the correlation, the model will work with column of different sizes with more confidence. This will solve the problem shared by most correlations where only one column (and thus one degree of liquid maldistribution) is investigated in the research.

The packing in the k_G experiments was short (0.5–1 m), which resulted in a relatively significant end effect. Despite the short bed, the outlet SO_2 (1000–5000 ppbv) was still close to the lower detection limit of the analyzer. The mass transfer caused by condensed water in the sampling lines also adds uncertainty to the measured k_G. Data with better accuracy can be obtained by redesign the experiments.

Appendix A: Pictures of the Air-Water Column and Packings

A.1 Pictures of the Air-Water Column

Pictures of the air-water column are shown in this appendix. Process flow diagram is shown in Figure A.1 with liquid valves (Table A.1 and Figures A.2–7). Gas valves are summarized in Table A.2 and shown in Figures A.8–10. Tubing of pressure transmitters are shown in Figures A.11–12.

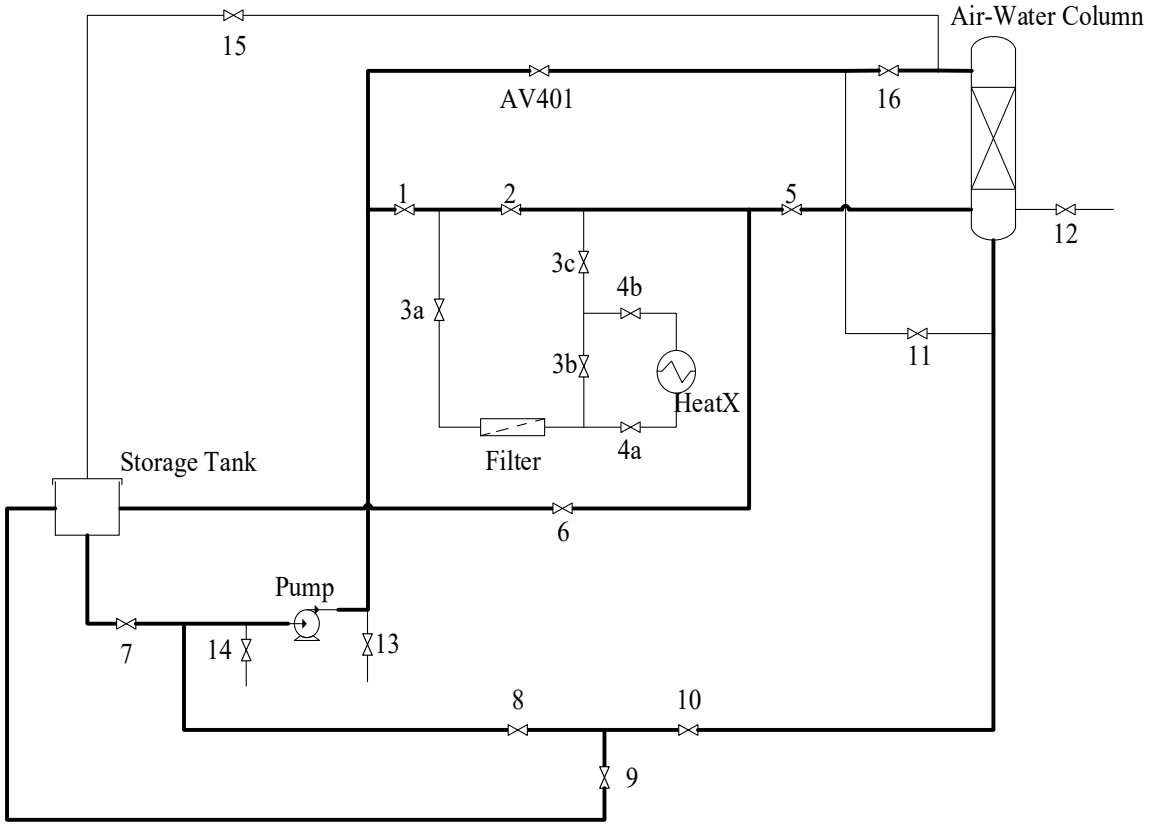

Figure A.1: AWC process flow diagram with valves

Table A.1: Liquid valves in the AWC

Valve	Description	Notes
1	Pump outlet (sump)	
2	Filter bypass	
3	Filter valves	
4	Heat exchanger valves	Only open at extreme temperatures
5	Sump return	
6	Post-filter tank return	
7	Pump suction (tank)	
8	Pump suction (sump)	
9	Tank return	
10	Sump outlet	
11	Dead-leg	Only open during drainage
12	Sump drainage	Only open during drainage
13	Pump discharge	Used for waste discharge into drums
14	Pump drainage	Only open during filling/drainage
15	Column-top tank return	Only open during drainage
16	Pump discharge throttle valve	Adjusted based on liquid flow rate
AV401	Pump outlet (column top)	Pneumatic valve

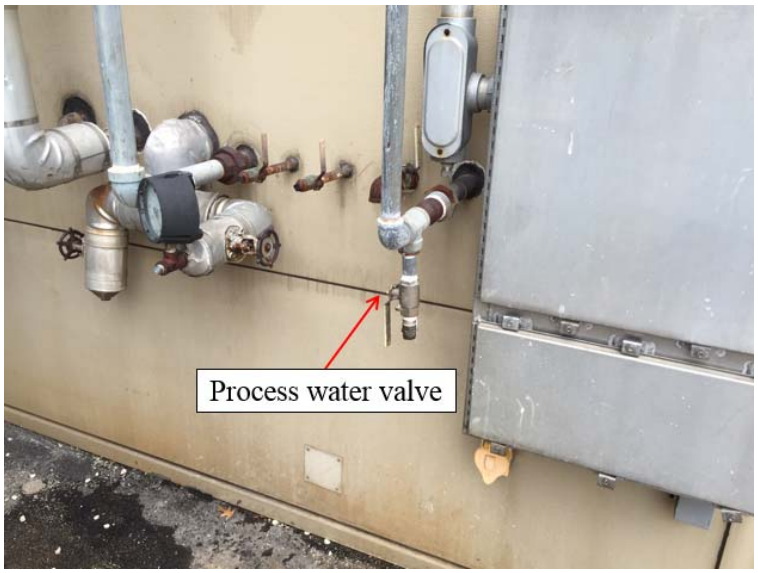

Figure A.2: Process water source

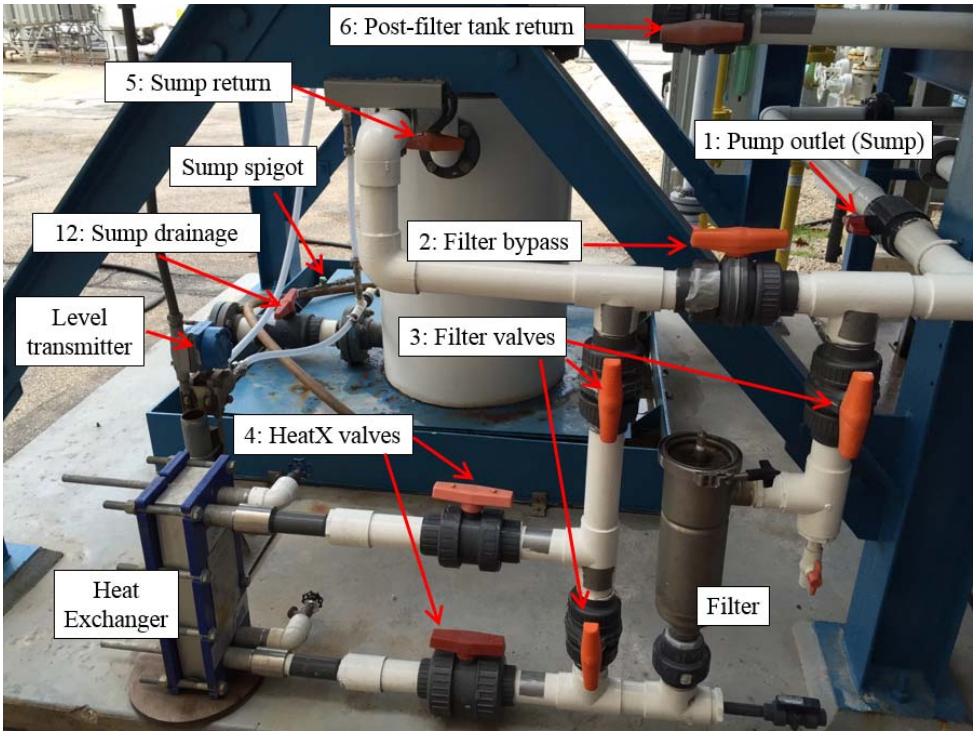

Figure A.3: Liquid line valves (north)

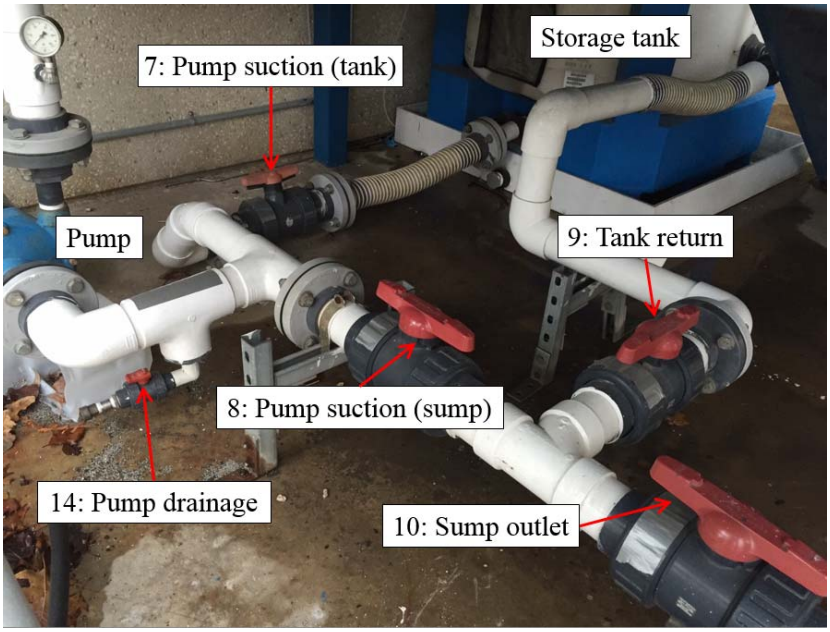

Figure A.4: Pump and associated valves (south)

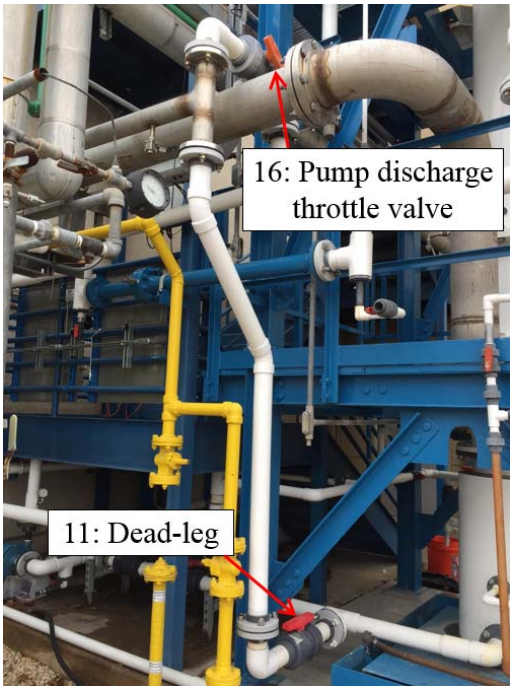

Figure A.5: Valves at columns side

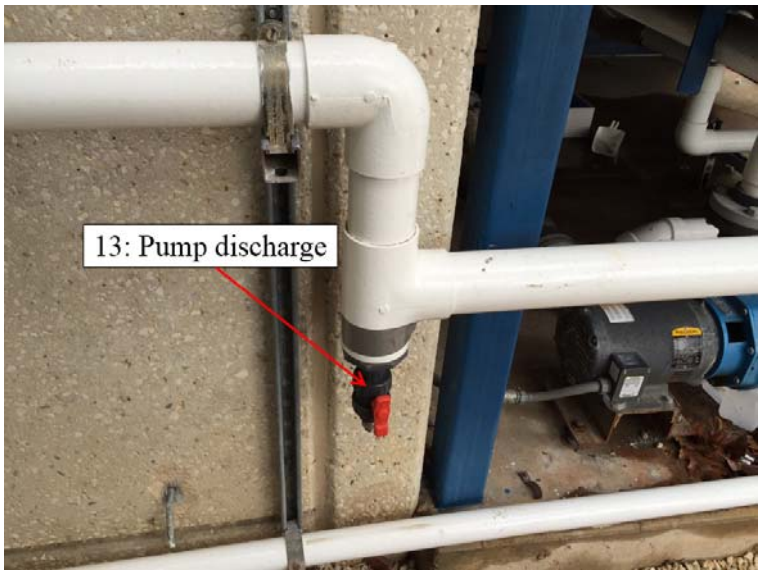

Figure A.6: Pump discharge valve

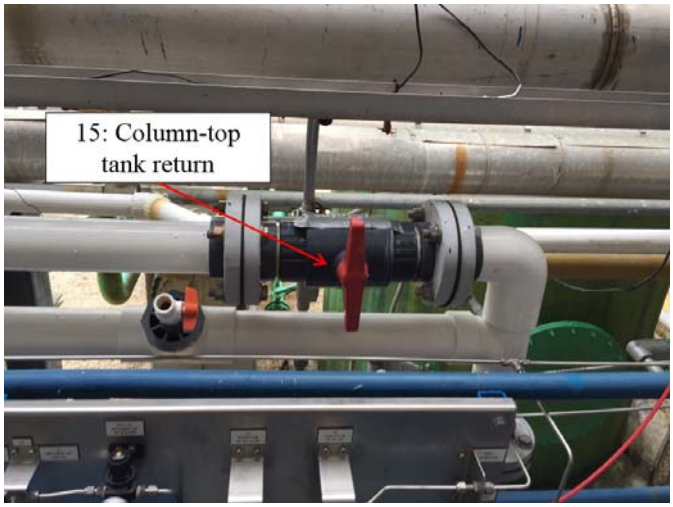

Figure A.7: Valve at the first platform

Table A.2: Gas valves in the AWC

Valve	Description	Comments
17	Zero inlet valve	Only open during leak check
18	Span inlet valve	
19	Sample inlet valve	
20	Sample/zero/span switch valve	

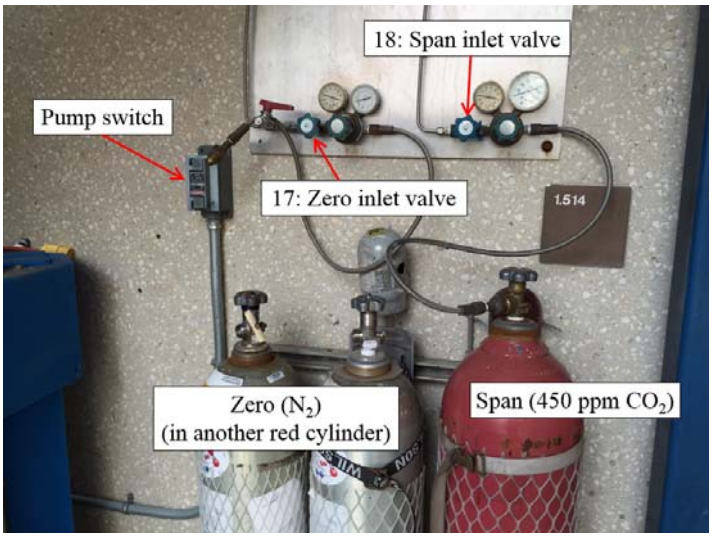

Figure A.8: Gas cylinders

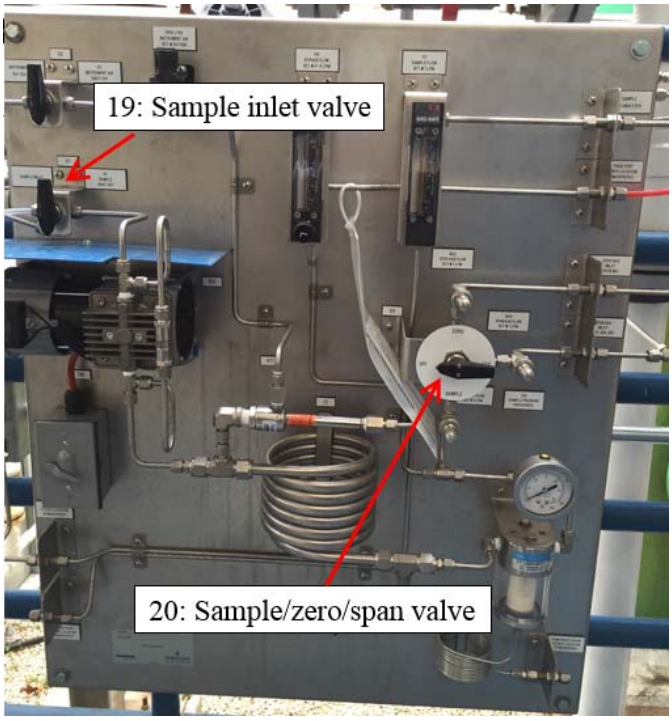

Figure A.9: Sampling panel at the first platform

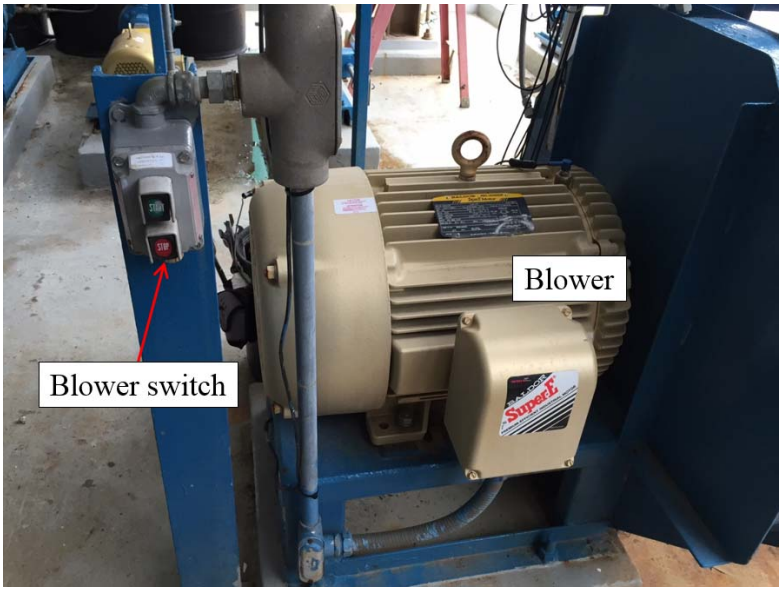

Figure A.10: Blower

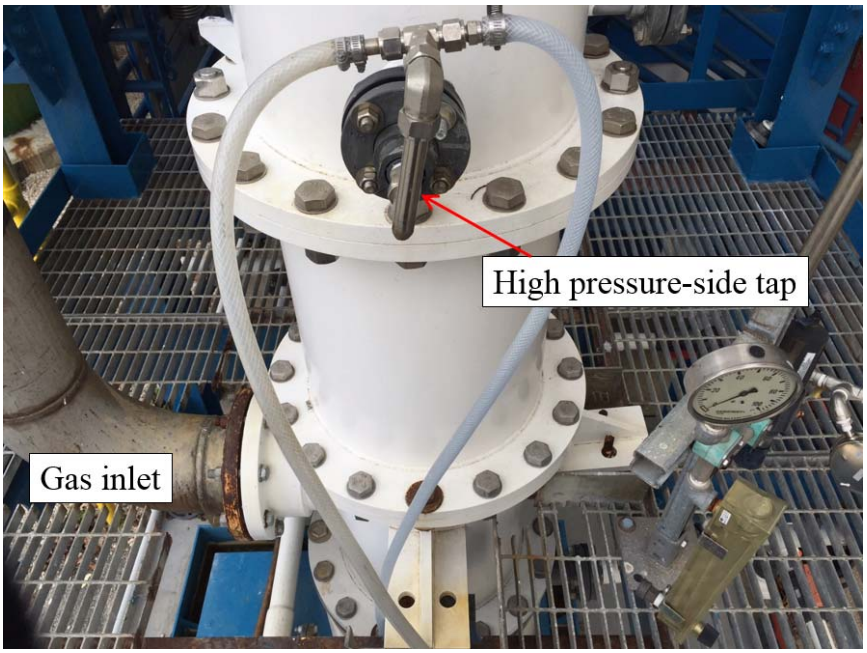

Figure A.11: Column mid-section

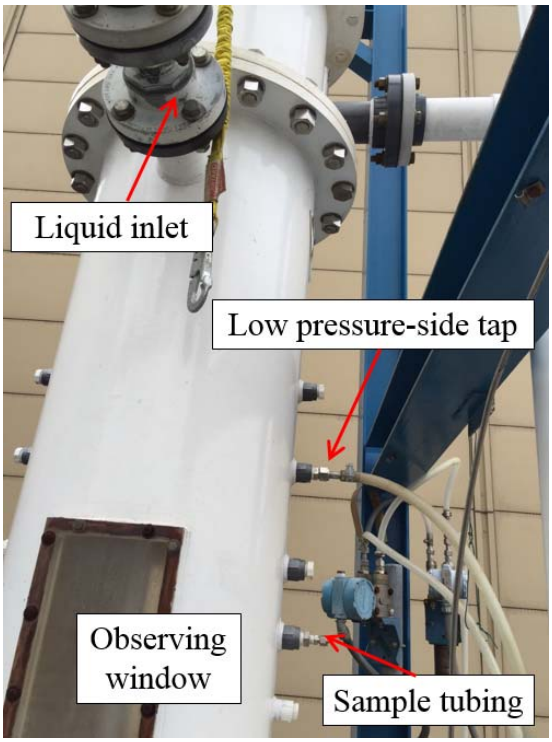

Figure A.12: Column top

A.2 PICTURES OF PACKINGS

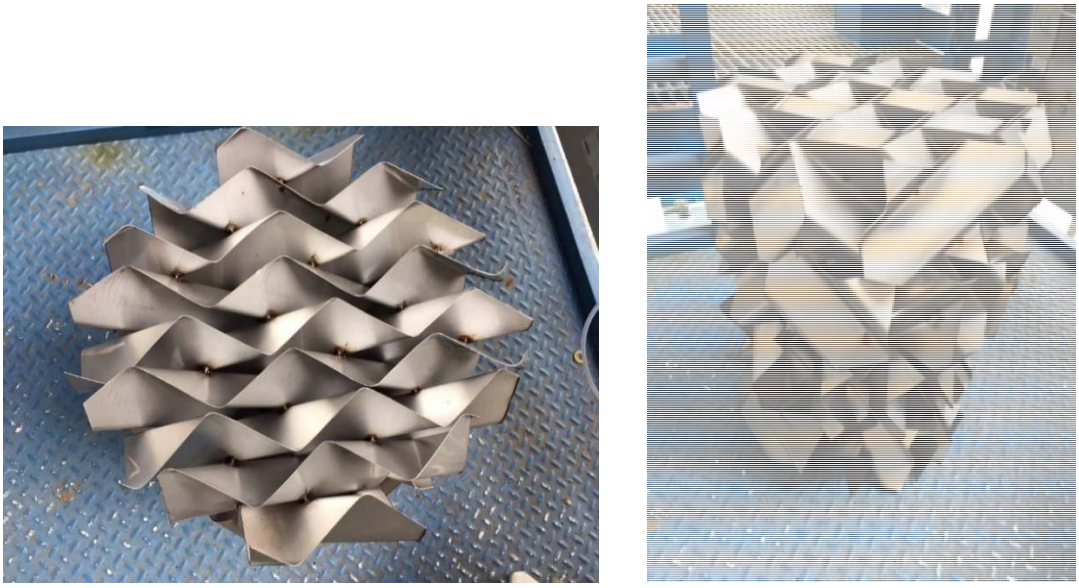

Figure A.13: Top and side views of MG 64Y

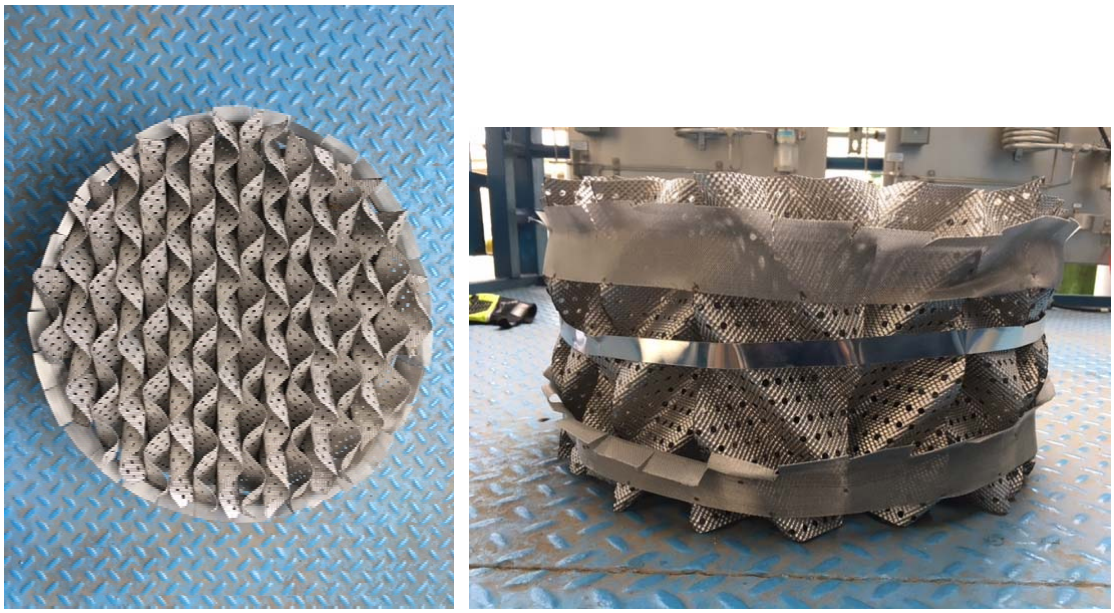

Figure A.14: Top and side views of M 125Y

Figure A.15: Top and side views of M 2Y

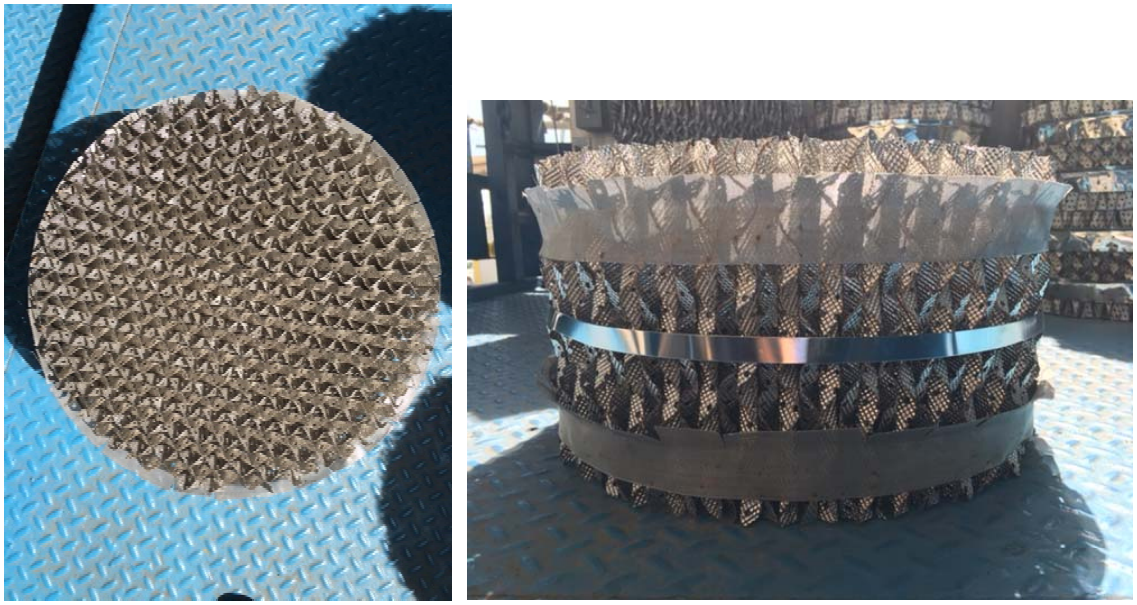

Figure A.16: Top and side views of M 250X

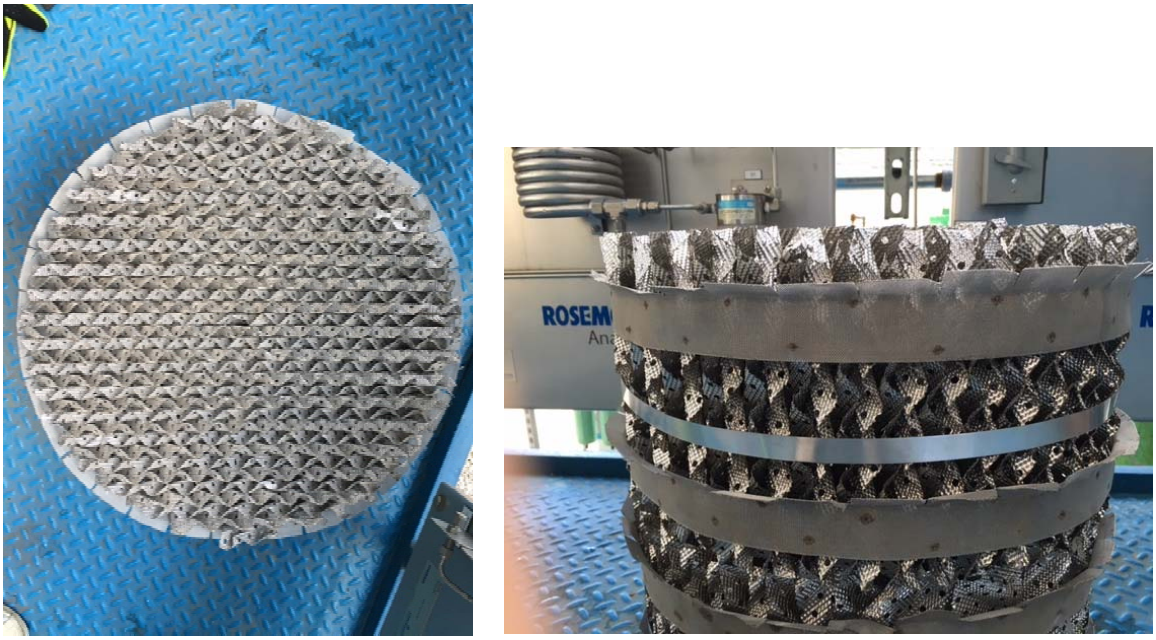

Figure A.17: Top and side views of M 250Y

Figure A.18: Top and side views of M 250YS

Figure A.19: Top and side views of GTO 250Y

Figure A.20: Top and side views of B1 250MN

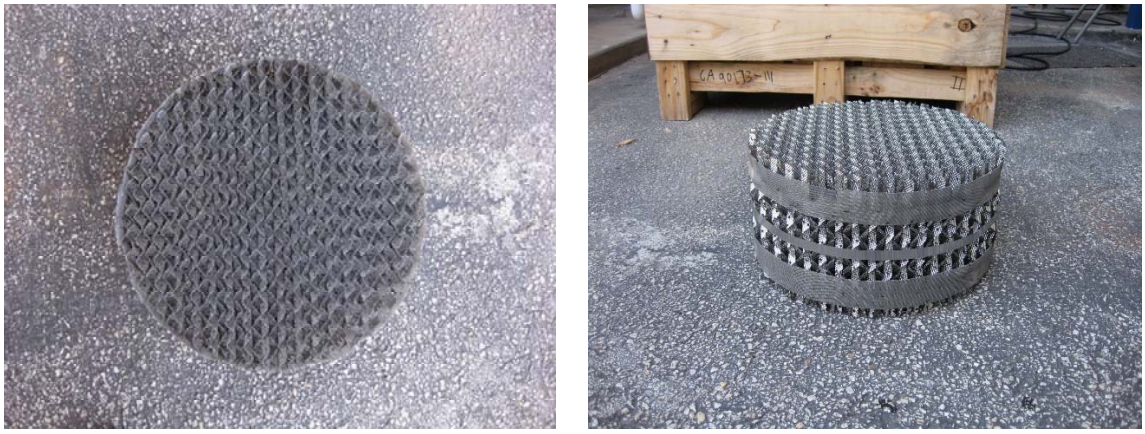

Figure A.21: Top and side views of M 252Y

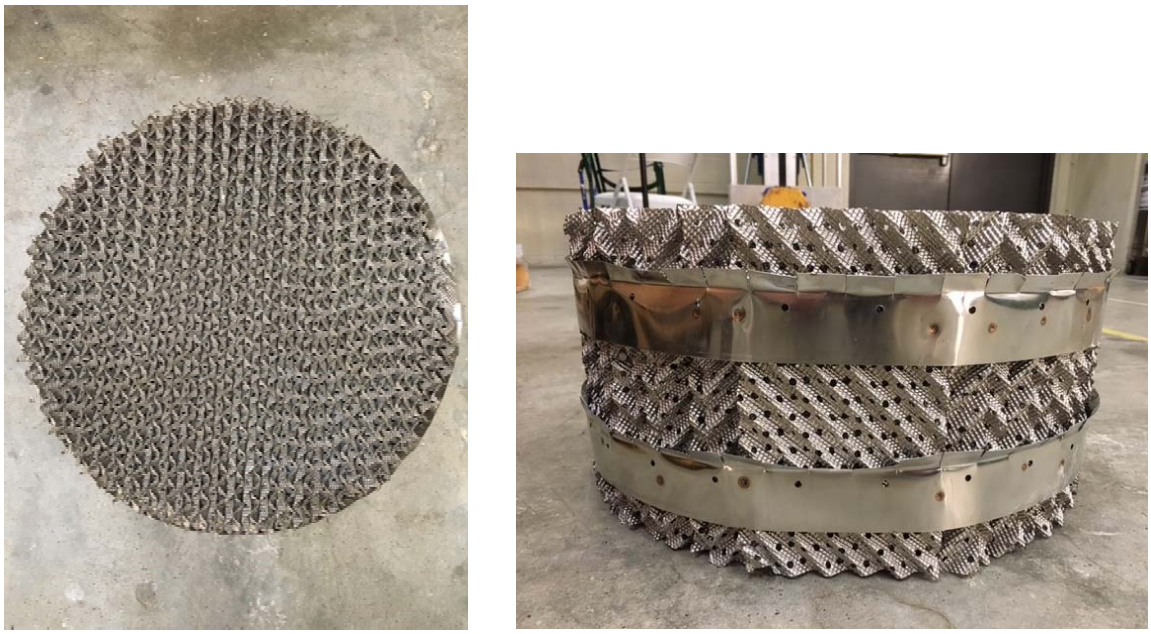

Figure A.22: Top and side views of GTP 350Y

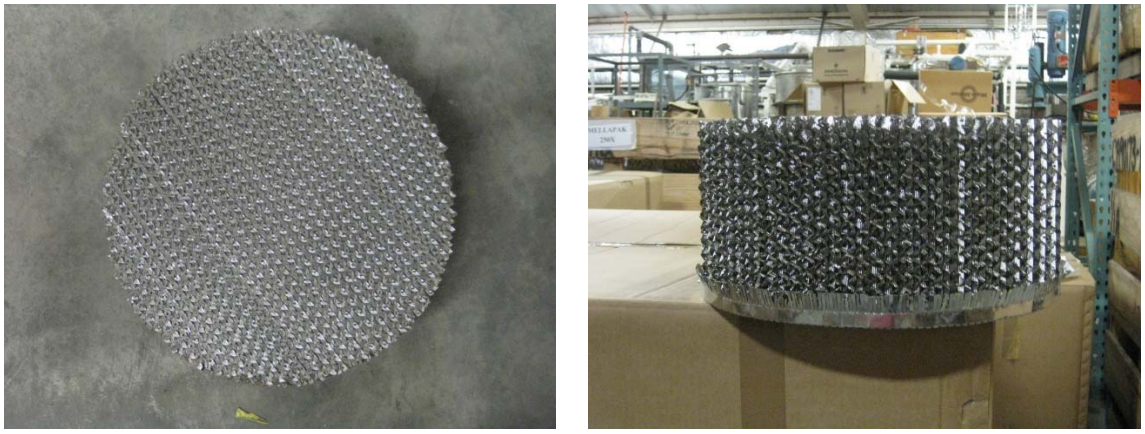

Figure A.23: Top and side views of B1 500P

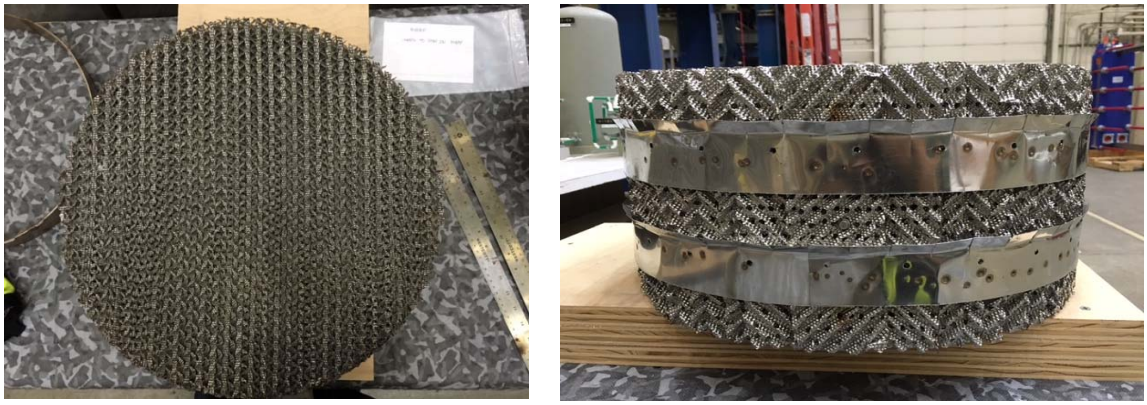

Figure A.24: Top and side views of GTP 500Y

Figure A.25: Top and side views of element of RSR 1.5

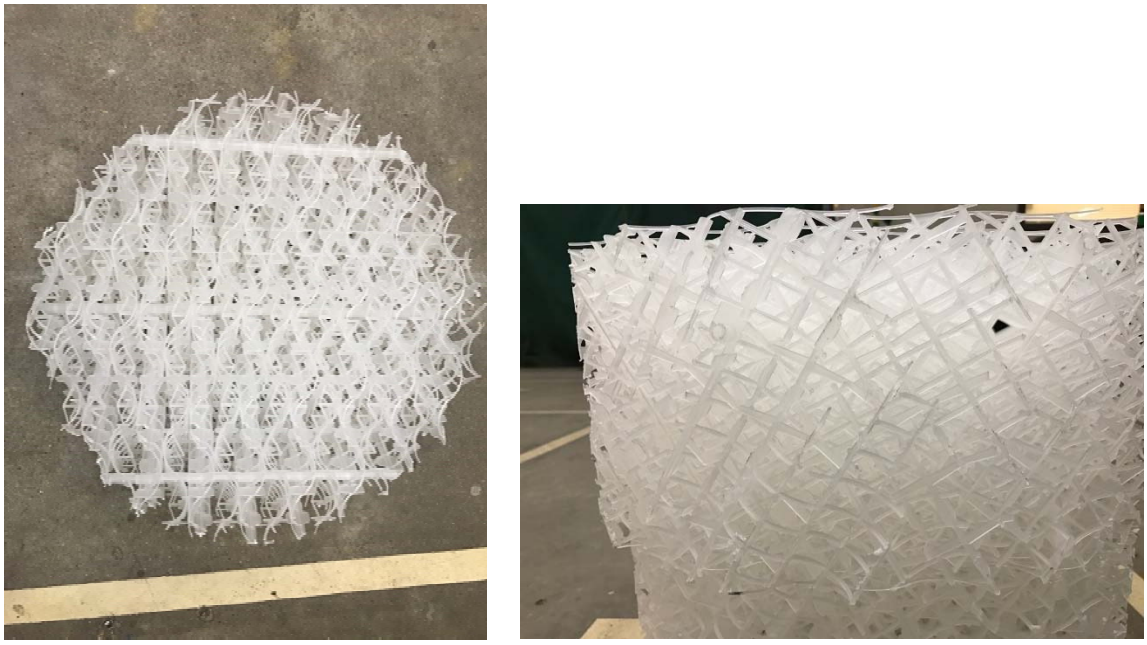

Figure A.26: Top and side views of HFP 2

Figure A.27: Top and side views of RSP 250Y

Appendix B: Standardized Operating Procedure (SOP) of Air-Water Column Experiments

B.1 SOP FOR HYDRAULIC EXPERIMENTS

Leakage Check

1. Fill storage tank with water (connection point: valve 14).
    a. Open valves: 1, 3, 6, 7, 9, 10, AV401.
    b. Closed valves: 2, 5, 8.
    c. Add tap water to the column for 7.5 min.
2. Circulated liquid and gas through the column.
    a. Start the pump at "MAN" 40%.
    b. Start the blower at "MAN" 10%.
    c. Change the pump and blower to "AUTO" and set the flowrates to the highest value in the upcoming experiment.
3. Check liquid leakage in the column.
    a. If there is leakage, change the pump and blower back to "MAN" 40% and "MAN" 10%, respectively, and turn them off in DeltaV.
    b. Stop the leakage by tightening up screws/bolts, changing new Teflon tapes, or new flange gasket.
    c. Go back to step 2 until there is no leakage in the system.
    d. If there's no leakage, change the pump and blower back to "MAN" 40% and "MAN" 10%, respectively, and turn them off in DeltaV.
4. Drain the system to the sanitary sewer by attaching hoses to valves 12 and 14 and stringing the hoses to the sewer. Open all valves and allow system to drain.

Start-up

1. Record the background pressure (pressure reading when there is not liquid and gas), and input in the spreadsheet for offset.
2. Input and update the temperature and relative humidity of the ambient temperature throughout the experiments to correct for the bulk water vaporization.
3. Charge water to column sump.
    a. Arrange valves so that all water flows to sump bypassing tank.
        i. Open valves: 8, 10, AV401.
        ii. Closed valves: all others.
    b. Add tap water until sump level reaches 30 inches.
    c. Turn on feed pump at "MAN" 40%.
    d. Continue adding water with pump running until sump level reaches 0.5–0.6 m.
    e. Turn off tap water.
4. Determine baseline level.
    a. Keep the pump running at "MAN" 40% with the liquid circulation loop go through packing with tank bypassed.
    b. Close valves 8, 10, and AV401 simultaneously using a second person. Keep the pump running to prime the liquid lines.
    c. Wait for 3–5 minutes for the sump level to stabilize to 0.5–0.6 inches.
        i. If the sump level < 0.5 m, briefly turn on tap water to add more water.
        ii. If the sump level > 0.6 m, briefly open valves 1, 2, and 6 to pump some water back to storage tank and then purge level transmitter tubing.
    d. Record the established sump level under and input it into DeltaV.
5. Open valves 8, 10, and AV401 to begin hydraulic tests.

Steady-state Operation

1. Collect pressure drop and hold-up data with varied liquid rates at fixed low gas rate to avoid data curve overlap
    a. Turn on the blower at "MAN" 10%.
    b. Change the blower to target low gas rate with "AUTO" mode (such as 0.6, 1.0, and 1.5 m/s)
    c. Change liquid rate in full range in an increasing order with "AUTO" mode (typically 6–74 $m^3/m^2 \cdot h$) at the fixed gas rate.
    d. Collect pressure drop and holdup data (calculated automatically with baseline and experimental sump levels) quickly when the values have remained constant for 1 min.
    e. Re-establish sump level under baseline conditions.
    f. Change gas rate to a higher value and repeat steps b–e until data curves become more spread out.
2. Collect pressure drop and hold-up data with varied gas rates at fixed liquid rate.
    a. Change liquid rate back to the lowest value (usually 6 $m^3/m^2 \cdot h$).
    b. Change gas rate in an increasing order at fixed liquid rate until flooding (about 1600 Pa/m packing).
    c. Collect pressure drop and holdup data quickly when the values have remained constant for 1 min.
    d. Re-establish sump level under baseline conditions.
    e. While waiting for the level to stabilize, check the impulse tubing of the pressure drop and level transmitters for entrained liquid. The line should remain clear at all times.

f. Change liquid rate to a higher value and repeat steps a–e until satisfactory number of data has been taken.

Shut-down

1. Change pump back to "MAN" 40%.
2. Change the blower to "MAN" 10%.
3. Turn of the blower and the pump in DeltaV.
4. Open all valves and allow water to settle. Drain the system to the sanitary sewer by attaching hoses to valves 12 and 14 and stringing the hoses to the sewer.
5. Drain water in the dead-leg from valve 13 using buckets.

B.2 SOP FOR MASS TRANSFER AREA EXPERIMENTS

Leakage Check with Water

Same with the leakage check process in B.1.

Start-up

1. Prepare solution (If new batch needs to be prepared).
   a. Calculate the mass of water, glycerol, and sodium hydroxide pellets needed to prepare a 0.75 m^3 batch at target glycerol and caustic.
   b. Arrange valves so that all water flows once-through Micromotion flowmeter.
      i. Open valves: 1, 6, 9, 10, AV401.
      ii. Closed valves: 2, 3, 5, 7, 8.
   c. Collect tap water into column tank.
   d. Arrange valves so that water circulates between column sump and storage tank.

i. Open valves: 1, 2, 6, 7.

ii. Closed valves: 3, 5, 8, 9, 10, AV401.

e. Start pump at “MAN” 40% and then change to “MAN” 60%.

f. Dissolve target weight of NaOH pellets to tap water to form concentrated (about 2 wt %) caustic solution in 19 L (5 gallon) carboys.

g. Add the concentrated caustic solution to the tank for circulation.

h. Move pure glycerol drums to the dike area.

i. Hoist the drum onto the weight and take notes of the initial weight.

j. Connect air pump to the glycerol drum and column tank. Secure the two ends of the hose firm to a stable end and have one person watch over at both ends.

k. Pump glycerol (or reused solution) from its container to storage tank to target total weight using air-driven diaphragm pump. Take notes of the final weight of drum. The total weight of pumped glycerol is calculated from the difference of the initial and final weight.

l. Pump some water from plastic tank to storage tank using the air-driven pump to clean the hose.

m. Put away pumps and hoses. Check and stop any leakage in the system.

n. Allow liquid to circulate between column sump and storage tank for another 60 min.

1. Prepare solution (If there was caustic batch in the system from previous experiment).

i. Check the free caustic of the btach by acid titration and TIC analysis.

ii. Check composition by offline density measurement.

iii. Calculate the mass of water and sodium hydroxide pellets needed to target glycerol and caustic.

iv. Arrange valves so that all water flows once-through Micromotion flowmeter.

i. Open valves: 1, 6, 9, 10, AV401.

ii. Closed valves: 2, 3, 5, 7, 8.

v. Collect tap water into column tank.

vi. Arrange valves so that water circulates between column sump and storage tank.

i. Open valves: 1, 2, 6, 7.

ii. Closed valves: 3, 5, 8, 9, 10, AV401.

vii. Start pump at "MAN" 40% and then change to "MAN" 60%.

viii. Dissolve target weight of NaOH pellets to tap water to form concentrated (about 2 wt %) caustic solution in 19 L (5 gallon) carboys.

o. Add the concentrated caustic solution to the tank and allow liquid to circulate between column sump and storage tank for at least 60 min.

2. Calibrate CO_2 analyzer using 450 ppm$_V$ CO_2 in N_2 and ultra-pure N_2 while circulating the batch.

3. Leak-check sample line tubing.

a. Arrange valves so that analyzer draws from N_2 cylinder.

b. Turn sample pump on and adjust regulator so that gas is sampled under minimal pressure (<0.07 atm). Analyzer reading should approach zero.

c. Shut down sample pump afterward. Close valve and orient valve to draw from air outlet.

4. Take liquid samples from column sump before experiment starts.

a. Verify active alkalinity by acid titration and TIC analysis. The mixing is complete when three consecutive titration gives the same results.

b. Input the active alkalinity to DeltaV for online estimation of bulk caustic depletion.

5. Pre-wet the packing.
    a. Open valve 9, 10, and AV401 to allow liquid to circulate through packing.
    b. Change pump to "AUTO" at 49 $m^3/m^2 \cdot h$ for 15 min.

Steady-state Operation

1. Start the blower at "MAN" 10% and then change to "AUTO" 1 m/s.
2. Start measurement by varying the liquid load in the sequence: 49, 61, 73, 37, 24, 12, and 6 $m^3/m^2 \cdot h$. Change the liquid load when CO_2 readings are steady for 3 min.
3. After satisfactory number of data have been taken at 1 m/s gas rate. Take another three points at a medium liquid load (24 or 37 $m^3/m^2 \cdot h$) with higher gas rates (1.5, 2, 2.5 m/s) to verify that gas rate does not affect the result and to provide area data for k_G experiments.

Shut-down

(If there is no further experiment with the existing batch)

1. Change pump to "MAN" 40% and blower to "MAN" 10%. Turn off the pump and the blower.
2. Take liquid samples from column sump to 25 mL vials for offline physical property measurement.
3. Transfer batch to drums.
    a. Open all valves except for valves 12, 13, and 14.
    b. Using air-driven diaphragm pump to pump the batch to 208-L (55-gallon) drums using suction hose connected to valve 14.
4. Dispose the drums properly to Environmental and Health Service (EHS).

(If there is upcoming experiment with the existing batch)

1. Turn off the blower
2. Pump solution back to storage tank.
    a. Rearrange valves so that liquid flows back to tank:
        i. Open valves: 8, 11, 15.
        ii. Close valves: 7, 9, AV401.
    b. Leave the pump operating for 5 min.
    c. Ensure the pump is at "MAN" 40% and turn off the pump
3. Close valves: 6, and 15.
4. Close the lid of storage tank.

Notes for Experiments with Aqueous Glycerol

1. Extreme care should be taken to prevent spill or leakage of aqueous glycerol. Any leakage or spill will cause at least "2–3 months or permanent exile from the pilot plant."
2. For any experiment with low liquid rate, valve 16 should be closed down partly to allow better control of the flow rate.
3. Before turning on/off the pump and the blower, always ensure the setting on the DeltaV operator screen is in "MAN" mode, and at 40% and 10% setpoints, respectively.
4. Automatic calculation of water evaporation in DeltaV can be modified by inputting data of partial pressure of water in the water/glycerol mixture.

B.3 SOP FOR LIQUID FILM MASS TRANSFER COEFFICIENT EXPERIMENTS

Leakage Check with Water

Same with the leakage check process in B.1.

Start-up

1. Prepare solution (If new batch needs to be prepared).
   a. Calculate the mass of water and glycerol needed to prepare a 0.75 m^3 batch at target glycerol and temperature.
   b. Arrange valves so that all water flows once-through Micromotion flowmeter.
      i. Open valves: 1, 6, 9, 10, AV401.
      ii. Closed valves: 2, 3, 5, 7, 8.
   c. Collect tap water into column tank.
   d. Move pure glycerol drums to the dike area.
   e. Hoist the drum onto the weight and take notes of the initial weight.
   f. Connect air pump to the glycerol drum and column tank. Secure the two ends of the hose firm to a stable end and have one person watch over at both ends.
   g. Pump glycerol to storage tank to target total weight using air-driven diaphragm pump. Take notes of the final weight of drum. The total weight of pumped glycerol is calculated from the difference of the initial and final weight.
   h. Pump some water from plastic tank to storage tank using the air-driven pump to clean the hose.
   i. Put away pumps and hoses. Check and stop any leakage in the system.
   j. Arrange valves so that water circulates between column sump and storage tank.
      iii. Open valves: 1, 2, 6, 7.
      iv. Closed valves: 3, 5, 8, 9, 10, AV401.

k. Start pump at “MAN” 40% and then change to “MAN” 60%.

l. Allow liquid to circulate between column sump and storage tank for at least 60 min.

1. Prepare solution (If there is reused batch)

a. Check the free caustic of the reused batch by acid titration and TIC analysis.

b. Check composition by offline density measurement.

c. Calculate the mass of water or glycerol needed back to target glycerol.

(If more water is needed)

d. Arrange valves so that all water flows once-through Micromotion flowmeter.

i. Open valves: 1, 6, 9, 10, AV401.

ii. Closed valves: 2, 3, 5, 7, 8.

e. Collect target weight of tap water into column tank, then proceed to step h.

(If more water is needed)

d. Move pure glycerol drums to the dike area.

e. Hoist the drum onto the weight and take notes of the initial weight.

f. Connect air pump to the glycerol drum and column tank. Secure the two ends of the hose firm to a stable end and have one person watch over at both ends.

g. Pump target weight of glycerol to storage tank using air-driven diaphragm pump. Take notes of the final weight of drum. The total weight of pumped glycerol is calculated from the difference of the initial and final weight.

h. Move drums of the reused batch to the dike area.

i. Connect air pump to the glycerol drum and column tank. Secure the two ends of the hose firm to a stable end and have one person watch over at both ends.

j. Pump the reused batch to storage tank using air-driven diaphragm pump.

k. Pump some water from plastic tank to storage tank using the air-driven pump to clean the hose.

l. Put away pumps and hoses. Check and stop any leakage in the system.

m. Arrange valves so that water circulates between column sump and storage tank.

   i. Open valves: 1, 2, 6, 7.

   ii. Closed valves: 3, 5, 8, 9, 10, AV401.

n. Start pump at "MAN" 40% and then change to "MAN" 60%.

o. allow liquid to circulate between column sump and storage tank for at least 60 min.

2. While mixing, turn on the gas chromatograph, and shoot blank samples of pure heptane to check the functionality of the instrument.

3. Take liquid samples from column sump for offline physical property before experiment starts.

4. Pre-wet the packing.

   c. Open valve 9, 10, and AV401 to allow liquid to circulate through packing.

   d. Change pump to "AUTO" at 49 $m^3/m^2 \cdot h$ for 15 min.

Steady-state Operation

1. Start the blower at "MAN" 10% and then change to "AUTO" 1 m/s.

2. Add 1–1.5 L toluene to the feed tank, and start toluene metering pump at proper metering speed according to the liquid load.

3. Wait for at least 30 min to allow the system to reach steady-state with toluene.

4. Start measurement by varying the liquid load in the sequence: 49, 61, 73, 37, 24, 12, and 6 $m^3/m^2 \cdot h$. For each operating condition, take inlet and outlet liquid samples after 30–45 min.
5. After satisfactory number of data have been taken at 1 m/s gas rate. Take another two or three points at a medium liquid load (24 or 37 $m^3/m^2 \cdot h$) with different gas rates (0.6, 1.5, or 2 m/s) to verify that gas rate does not affect the result.

Shut-down

1. Turn off the toluene metering pump.
2. Change pump to "MAN" 40% and blower to "MAN" 10%. Turn off the pump and the blower.
3. Take liquid samples from column sump to 25 mL vials for offline physical property.
4. Transfer reused batch back to drums.
    c. Open all valves except for valves 12, 13, and 14.
    d. Using air-driven diaphragm pump to pump the batch to 208-L (55-gallon) drums using suction hose connected to valve 14.

B.4 SOP FOR GAS FILM MASS TRANSFER COEFFICIENT EXPERIMENTS

Leakage Check with Water

Same with the leakage check process in B.1.

Start-up

1. Prepare solution.
    a. Fill storage tank with water (connection point: valve 14).

i. Open valves: 1, 3, 6, 7, 9, 10, AV401.

ii. Closed valves: 2, 5, 8.

d. Add tap water to the column for 7.5 min.

e. Arrange valves so that water circulates between column sump and storage tank.

i. Open valves: 1, 2, 6, 7.

ii. Closed valves: 3, 5, 8, 9, 10, AV401.

f. Start pump at "MAN" 40% and then change to "MAN" 60%.

g. Dissolve 3.6 kg NaOH pellets to storage tank to make dilute caustic (~ 0.1 mol/L) solution.

a. Allow liquid to circulate between column sump and storage tank for at least 60 min.

2. Calibrate SO_2 analyzer using 90 ppm$_v$ SO_2 in N_2 and zero air instrument while circulating the batch.

3. Move and connect 2% SO_2 cylinder to the outlet duct of the blower.

4. Pre-saturate the inlet and outlet gas sample lines.

a. Turn on the blower at "MAN" 10%.

b. Turn on the regulator of the SO_2 cylinder to make ~90 ppm$_v$ SO_2 gas.

c. Wait until SO_2 analyzer gives steady inlet SO_2 reading that is close to 90 ppm$_v$.

d. Arrange sample line so that SO_2 analyzer draws sample from outlet gas.

e. Wait for the outlet sampling line to saturate with SO_2, which is indicated by identical outlet and inlet SO_2 readings (90 ppm$_v$).

6. Pre-wet the packing.

a. Open valve 9, 10, and AV401 to allow liquid to circulate through packing.

b. Turn on the pump at "MAN" 40% and change to "AUTO" at 49 $m^3/m^2 \cdot h$ for 15 min.

Steady-state Operation

1. Keep the liquid load constant at 24 or 37 $m^3/m^2 \cdot h$.
2. Start measurement by varying the gas rate in increasing order: 0.6, 1, 1.5, 2, 2.5 m/s. Change the gas rate when SO_2 readings are steady for 1 min.
3. During experiments, keep an eye on the pressure of the SO_2 cylinder. Change new cylinder when the old one is depleted.
4. After satisfactory number of data have been taken at the fixed liquid load. Take another two or three points at higher liquid load (37 or 49 $m^3/m^2 \cdot h$) with medium gas rate (1.5 m/s) to verify that liquid load does not affect the result.

Shut-down

1. Turn off the SO_2 cylinder.
2. Change pump to "MAN" 40% and blower to "MAN" 10%. Turn off the blower.
3. Arrange valves so that water circulates between column sump and storage tank.
    a. Open valves: 1, 2, 6, 7.
    b. Closed valves: 3, 5, 8, 9, 10, AV401.
    c. Change pump to "MAN" 60%.
4. Neutralize the batch to pH 6–9 using 30 wt % hydrochloric acid.
5. Turn off the blower.
6. Open all valves and allow water to settle. Drain the system to the sanitary sewer by attaching hoses to valves 12 and 14 and stringing the hoses to the sewer. Drain water in the dead-leg from valve 13 using buckets.

Appendix C: Tabulated Data

C.1 WETTED-WALL COLUMN (WWC) DATA

The raw data of WWC experiments is summarized in Table 7.1.

Table C.1: WWC experimental data

T (°C)	P_{sys} (kPa)	glycerol (wt %)	$P_{CO2,LM}$ (Pa)	L (cm^3/s)	u_G (m/s)	$k_g' \times 10^7$ before correction ($mol/m^2 \cdot Pa \cdot s$)	K_G/k_G (%)	CO_2 removal (%)	Depletion (%)
#1				01/06/2014					
20	377	0	174	5.00	0.19	4.21	13	12.5	1.1
20	377	0	333	5.00	0.19	5.13	15	15.0	2.6
20	377	0	488	5.00	0.19	4.49	14	13.7	3.4
20	377	0	641	5.00	0.19	4.71	14	14.3	4.6
20	377	0	789	5.00	0.19	4.55	14	13.9	5.5
30	377	0	174	5.46	0.20	5.09	15	14.5	1.2
30	377	0	334	5.46	0.20	5.40	16	15.6	2.5
30	377	0	484	5.46	0.20	5.36	16	15.7	3.6
30	377	0	635	5.46	0.20	5.16	15	15.3	4.5
30	377	0	783	5.46	0.20	5.16	15	15.3	5.6
40	377	0	172	5.85	0.20	6.38	19	17.1	1.4
40	377	0	331	5.85	0.20	6.24	18	17.3	2.6
40	377	0	479	5.85	0.20	6.34	18	17.7	3.8
40	377	0	627	5.85	0.20	6.38	18	17.8	5.0
40	377	0	763	5.85	0.20	6.79	19	18.7	5.7
#2				01/08/2014					
20	377	25	171	3.41	0.19	5.30	16	15.1	2.1
20	377	25	327	3.41	0.19	4.96	15	14.7	3.8
20	377	25	479	3.41	0.19	4.59	14	14.0	5.2
20	377	25	623	3.41	0.19	4.66	14	14.2	6.8
20	377	25	767	3.41	0.19	4.50	14	13.8	8.1
30	377	25	169	3.93	0.19	6.62	19	17.8	2.1
30	377	25	325	3.93	0.19	5.79	17	16.5	3.7
30	377	25	470	3.93	0.19	5.91	17	16.9	5.4

30	377	25	612	3.93	0.19	5.65	17	16.4	6.8
30	377	25	760	3.93	0.19	5.25	16	15.6	8.1
40	377	25	167	4.37	0.20	7.54	21	19.5	2.1
40	377	25	324	4.37	0.20	6.83	19	18.6	3.7
40	377	25	467	4.37	0.20	6.70	19	18.5	5.3
40	377	25	607	4.37	0.20	7.00	20	19.1	7.2
40	377	25	747	4.37	0.20	6.65	19	18.5	8.5
#3				01/09/2014					
20	377	49.3	172	1.67	0.19	3.80	12	11.6	3.0
20	377	49.3	336	1.67	0.19	3.02	10	9.8	4.7
20	377	49.3	489	1.67	0.19	2.68	9	8.9	6.1
20	377	49.3	637	1.67	0.19	2.68	9	9.0	8.0
20	377	49.3	786	1.67	0.19	2.64	8	8.9	9.7
30	377	49.3	171	2.13	0.19	5.59	16	15.7	3.3
30	377	49.3	330	2.13	0.19	4.08	12	12.6	4.8
30	377	49.3	481	2.13	0.19	3.56	11	11.3	6.2
30	377	49.3	628	2.13	0.19	3.56	11	11.4	8.1
30	377	49.3	777	2.13	0.19	3.47	11	11.1	9.8
40	377	49.3	169	2.58	0.20	6.44	18	17.4	3.0
40	377	49.3	327	2.58	0.20	4.70	14	14.0	4.5
40	377	49.3	475	2.58	0.20	4.60	14	13.8	6.5
40	377	49.3	617	2.58	0.20	4.57	14	13.8	8.3
40	377	49.3	733	2.58	0.20	4.45	13	13.6	9.7
#4				01/10/2014					
20	377	64.8	177	0.78	0.19	2.29	7	7.5	3.7
20	377	64.8	338	0.78	0.19	2.08	7	7.1	6.5
20	377	64.8	492	0.78	0.19	1.86	6	6.4	8.5
20	377	64.8	791	0.78	0.19	1.71	6	5.8	12.7
20	377	64.8	641	0.78	0.19	1.66	5	6.0	13.9
30	377	64.8	170	1.09	0.19	4.25	13	12.6	4.6
30	377	64.8	332	1.09	0.19	2.84	9	9.3	6.3
30	377	64.8	482	1.09	0.19	2.58	8	8.6	8.4
30	377	64.8	631	1.09	0.19	2.48	8	8.3	10.6
30	377	64.8	781	1.09	0.19	2.34	8	7.9	12.4
40	377	64.8	170	1.42	0.20	4.40	13	12.9	3.8
40	377	64.8	330	1.42	0.20	3.41	11	10.7	5.8
40	377	64.8	479	1.42	0.20	3.23	10	10.3	8.1
40	377	64.8	618	1.42	0.20	3.31	10	10.6	10.6
40	377	64.8	765	1.42	0.20	3.36	10	10.7	13.3

#5				01/07/2014					
20	377	74.7	183	0.37	0.19	1.62	5	5.5	5.2
20	377	74.7	354	0.37	0.19	1.49	5	5.2	9.3
20	377	74.7	514	0.37	0.19	1.38	5	4.9	12.5
20	377	74.7	671	0.37	0.19	1.31	4	4.7	15.6
20	377	74.7	825	0.37	0.19	1.14	4	4.1	16.8
30	377	74.7	182	0.57	0.19	2.36	8	7.7	5.3
30	377	74.7	349	0.57	0.19	2.05	7	6.9	8.9
30	377	74.7	506	0.57	0.19	1.78	6	6.2	11.3
30	377	74.7	664	0.57	0.19	1.79	6	6.2	14.9
30	377	74.7	823	0.57	0.19	1.81	6	6.3	18.7
30	377	74.7	184	0.44	0.19	2.52	8	8.1	6.2
30	377	74.7	351	0.44	0.19	1.94	6	6.6	9.2
30	377	74.7	509	0.44	0.19	1.69	6	5.9	11.7
30	377	74.7	664	0.44	0.19	1.73	6	6.0	15.7
30	377	74.7	821	0.44	0.19	1.63	5	5.7	18.3
30	377	74.7	185	0.31	0.19	1.96	6	6.5	5.5
30	377	74.7	350	0.31	0.19	1.76	6	6.0	9.4
30	377	74.7	509	0.31	0.19	1.60	5	5.6	12.6
30	377	74.7	663	0.31	0.19	1.65	5	5.8	16.8
30	377	74.7	822	0.31	0.19	1.67	6	5.8	21.1
40	377	74.7	181	0.81	0.20	3.00	9	9.4	5.2
40	377	74.7	347	0.81	0.20	2.54	8	8.3	8.6
40	377	74.7	504	0.81	0.20	2.32	7	7.7	11.4
40	377	74.7	653	0.81	0.20	2.35	8	7.9	15.0
40	377	74.7	808	0.81	0.20	2.31	7	7.8	18.2
#6				01/13/2014					
20	377	79.7	401	0.23	0.19	1.18	4	4.2	12.2
20	377	79.7	504	0.23	0.19	1.14	4	4.1	14.9
20	377	79.7	609	0.23	0.19	1.04	4	3.7	16.4
20	377	79.7	711	0.23	0.19	1.01	3	3.7	18.8
20	377	79.7	813	0.23	0.19	0.97	3	3.5	20.6
30	377	79.7	399	0.38	0.19	1.53	5	5.3	10.4
30	377	79.7	497	0.38	0.19	1.56	5	5.4	13.2
30	377	79.7	603	0.38	0.19	1.45	5	5.1	14.9
30	377	79.7	698	0.38	0.19	1.47	5	5.2	17.5
30	377	79.7	803	0.38	0.19	1.36	5	5.8	18.7
40	377	79.7	177	0.56	0.20	2.43	8	7.8	5.1
40	377	79.7	341	0.56	0.20	2.20	7	7.3	9.0
40	377	79.7	495	0.56	0.20	2.05	7	6.9	12.3

40	377	79.7	646	0.56	0.20	1.95	6	6.6	15.3
40	377	79.7	764	0.56	0.20	2.04	7	7.0	18.9
#7				01/14/2014					
30	377	83.7	182	0.26	0.19	1.45	5	4.9	6.2
30	377	83.7	348	0.26	0.19	1.33	4	4.7	11.0
30	377	83.7	507	0.26	0.19	1.23	4	4.4	14.9
30	377	83.7	660	0.26	0.19	1.24	4	4.4	19.4
30	377	83.7	815	0.26	0.19	1.20	4	4.3	23.3
40	377	83.7	179	0.41	0.20	1.90	6	6.3	5.8
40	377	83.7	344	0.41	0.20	2.01	7	6.8	11.8
40	377	83.7	498	0.41	0.20	1.90	6	6.5	16.2
40	377	83.7	651	0.41	0.20	1.75	6	6.0	19.5
40	377	83.7	800	0.41	0.20	1.73	6	6.0	23.8
#8				01/15/2014					
40	377	88.7	180	0.26	0.20	1.82	6	6.0	7.8
40	377	88.7	347	0.26	0.20	1.74	6	5.9	12.5
40	377	88.7	502	0.26	0.20	1.60	5	5.5	16.4
40	377	88.7	657	0.26	0.20	1.51	5	5.3	21.0
40	377	88.7	807	0.26	0.20	1.52	5	5.3	24.7
#1R				04/07/2014					
20	377	0	170	4.38	0.15	6.16	21	21.0	1.5
20	377	0	335	4.38	0.15	4.87	17	17.7	2.5
20	377	0	490	4.38	0.15	4.59	16	16.9	3.4
20	377	0	640	4.38	0.15	4.56	16	16.9	4.5
20	377	0	790	4.38	0.15	4.45	16	16.6	5.4
30	377	0	172	4.62	0.16	6.64	22	22.0	1.5
30	377	0	331	4.62	0.16	5.82	20	20.1	2.7
30	377	0	481	4.62	0.16	5.66	19	19.7	3.8
30	377	0	630	4.62	0.16	5.52	19	19.4	4.8
30	377	0	775	4.62	0.16	5.44	19	19.2	5.9
40	377	0	168	4.57	0.16	7.23	23	23.2	1.6
40	377	0	323	4.57	0.16	6.78	22	22.3	2.9
40	377	0	478	4.57	0.16	6.72	22	22.1	4.3
40	377	0	621	4.57	0.16	6.55	22	21.8	5.5
40	377	0	765	4.57	0.16	6.46	21	21.6	6.6
#2R				03/13/2014					
20	377	13	171	4.30	0.15	7.51	24	23.9	2.0
20	377	13	336	4.30	0.15	6.47	22	21.7	3.5
20	377	13	491	4.30	0.15	5.96	20	20.5	4.7

20	377	13	644	4.30	0.15	5.74	20	20.0	6.0
20	377	13	787	4.30	0.15	5.94	20	20.5	7.6
30	377	13	172	4.77	0.16	7.68	25	24.2	1.8
30	377	13	331	4.77	0.16	7.40	24	23.7	3.3
30	377	13	482	4.77	0.16	6.99	23	22.8	4.7
30	377	13	632	4.77	0.16	6.57	22	21.9	5.8
30	377	13	775	4.77	0.16	6.47	22	21.7	7.1
40	377	13	167	4.78	0.16	10.29	30	28.8	2.0
40	377	13	325	4.78	0.16	8.22	26	25.2	3.4
40	377	13	472	4.78	0.16	8.56	26	25.9	5.1
40	377	13	625	4.78	0.16	7.49	24	23.8	6.1
40	377	13	766	4.78	0.16	7.58	24	24.0	7.5
#3R				04/09/2014					
20	377	25	176	3.47	0.15	5.76	20	20.1	2.0
20	377	25	339	3.47	0.15	5.05	18	18.2	3.5
20	377	25	494	3.47	0.15	4.97	18	18.0	5.0
20	377	25	641	3.47	0.15	4.88	17	17.8	6.4
20	377	25	791	3.47	0.15	4.79	17	17.5	7.8
30	377	25	172	3.97	0.16	7.16	23	23.3	2.0
30	377	25	330	3.97	0.16	6.32	21	21.4	3.5
30	377	25	482	3.97	0.16	6.03	20	20.7	4.9
30	377	25	631	3.97	0.16	5.96	20	20.5	6.3
30	377	25	777	3.97	0.16	5.83	20	20.2	7.7
40	377	25	169	4.42	0.16	8.02	25	25.0	1.9
40	377	25	324	4.42	0.16	7.33	24	23.5	3.4
40	377	25	476	4.42	0.16	6.99	23	22.8	4.8
40	377	25	623	4.42	0.16	6.90	22	22.6	6.2
40	377	25	766	4.42	0.16	6.83	22	22.4	7.6
#4R				03/16/2014					
20	377	37.9	233	2.50	0.15	4.14	15	15.6	2.8
20	377	37.9	447	2.50	0.15	3.96	15	15.1	5.2
20	377	37.9	650	2.50	0.15	3.86	14	14.8	7.4
20	377	37.9	843	2.50	0.15	3.89	14	14.9	9.6
20	377	37.9	1050	2.50	0.15	3.62	13	14.1	11.2
30	377	37.9	228	3.07	0.16	5.42	19	19.1	2.8
30	377	37.9	440	3.07	0.16	5.02	18	18.1	5.1
30	377	37.9	638	3.07	0.16	4.76	17	17.4	7.0
30	377	37.9	837	3.07	0.16	4.63	16	17.0	9.0
30	377	37.9	1027	3.07	0.16	4.64	16	17.0	11.1
30	377	37.9	231	2.00	0.16	5.39	19	19.0	3.3

30	377	37.9	440	2.00	0.16	4.90	17	17.7	5.7
30	377	37.9	639	2.00	0.16	4.71	17	17.2	8.1
30	377	37.9	839	2.00	0.16	4.56	16	16.8	10.3
30	377	37.9	1027	2.00	0.16	4.46	16	16.6	12.4
40	377	37.9	225	2.92	0.16	6.39	21	21.4	2.9
40	377	37.9	432	2.92	0.16	5.95	20	20.3	5.3
40	377	37.9	628	2.92	0.16	6.01	20	20.5	7.8
40	377	37.9	821	2.92	0.16	5.69	19	19.7	9.7
40	377	37.9	1012	2.92	0.16	5.42	19	19.0	11.5
#5R				04/10/2014					
20	377	49.9	236	1.70	0.15	3.67	14	14.3	3.6
20	377	49.9	450	1.70	0.15	3.33	13	13.2	6.3
20	377	49.9	659	1.70	0.15	2.97	11	12.0	8.4
20	377	49.9	860	1.70	0.15	2.91	11	11.8	10.8
20	377	49.9	1057	1.70	0.15	2.78	11	11.4	12.7
30	377	49.9	232	2.19	0.16	4.39	16	16.3	3.3
30	377	49.9	443	2.19	0.16	4.07	15	15.4	5.9
30	377	49.9	645	2.19	0.16	3.81	14	14.6	8.1
30	377	49.9	844	2.19	0.16	3.69	14	14.3	10.3
30	377	49.9	1038	2.19	0.16	3.50	13	13.7	12.1
40	377	49.9	227	2.46	0.16	5.33	18	18.8	3.3
40	377	49.9	438	2.46	0.16	4.87	17	17.6	5.9
40	377	49.9	636	2.46	0.16	4.70	17	17.1	8.3
40	377	49.9	835	2.46	0.16	4.69	16	17.1	10.8
40	377	49.9	1028	2.46	0.16	4.43	16	16.4	12.7
#6R				04/11/2014					
20	377	65	240	1.00	0.15	2.78	11	11.3	5.0
20	377	65	462	1.00	0.15	2.03	8	8.7	7.2
20	377	65	677	1.00	0.15	1.91	8	8.2	10.0
20	377	65	879	1.00	0.15	1.80	7	7.8	12.3
20	377	65	1086	1.00	0.15	1.76	7	7.6	14.9
30	377	65	237	1.41	0.16	3.30	12	13.0	4.2
30	377	65	458	1.41	0.16	2.79	11	11.4	7.0
30	377	65	662	1.41	0.16	2.66	10	10.9	9.7
30	377	65	869	1.41	0.16	2.57	10	10.6	12.4
30	377	65	1067	1.41	0.16	2.48	10	10.3	14.7
40	377	65	235	1.85	0.16	4.08	15	15.3	4.0
40	377	65	448	1.85	0.16	3.55	13	13.7	6.7
40	377	65	654	1.85	0.16	3.48	13	13.5	9.7
40	377	65	853	1.85	0.16	3.26	12	12.8	11.9

40	377	65	1045	1.85	0.16	3.19	12	12.6	14.3
8RR				08/07/2014					
20	377	4	182	4.05	0.15	5.71	20	18.8	1.7
20	377	4	346	4.05	0.15	5.39	19	18.5	3.0
20	377	4	506	4.05	0.15	5.37	19	18.7	4.4
20	377	4	658	4.05	0.15	5.35	19	18.7	5.7
20	377	4	809	4.05	0.15	5.32	19	18.7	7.0
30	377	4	179	4.21	0.16	6.71	22	20.9	1.7
30	377	4	341	4.21	0.16	6.47	22	21.0	3.2
30	377	4	494	4.21	0.16	6.35	21	20.9	4.6
30	377	4	646	4.21	0.16	6.31	21	20.9	6.0
30	377	4	794	4.21	0.16	6.18	21	20.7	7.2
40	377	4	174	4.22	0.16	8.11	25	23.4	1.9
40	377	4	333	4.22	0.16	7.59	24	23.2	3.4
40	377	4	486	4.22	0.16	7.40	24	23.1	4.8
40	377	4	635	4.22	0.16	7.61	24	23.6	6.5
40	377	4	778	4.22	0.16	7.06	23	22.6	7.5
1RR				07/20/2014					
20	377	7	187	4.02	0.15	5.82	20	19.2	1.7
20	377	7	358	4.02	0.15	6.12	21	20.4	3.4
20	377	7	513	4.02	0.15	5.86	20	19.9	4.8
20	377	7	674	4.02	0.15	5.75	20	19.7	6.1
20	377	7	826	4.02	0.15	5.90	20	20.2	7.7
30	377	7	184	4.34	0.16	7.01	23	21.6	1.9
30	377	7	348	4.34	0.16	6.41	21	20.9	3.3
30	377	7	501	4.34	0.16	7.16	23	22.8	5.2
30	377	7	657	4.34	0.16	6.80	22	22.1	6.5
30	377	7	809	4.34	0.16	6.67	22	21.9	7.9
40	377	7	178	4.41	0.16	8.18	26	23.6	1.9
40	377	7	338	4.41	0.16	7.80	25	23.6	3.6
40	377	7	500	4.41	0.16	7.70	24	23.7	5.2
40	377	7	650	4.41	0.16	7.84	25	24.1	6.9
40	377	7	799	4.41	0.16	7.52	24	23.6	8.2
2RR				07/22/2014					
20	377	20	188	3.38	0.15	5.69	20	18.8	2.0
20	377	20	356	3.38	0.15	5.76	20	19.5	3.9
20	377	20	517	3.38	0.15	5.57	19	19.2	5.5
20	377	20	674	3.38	0.15	5.32	19	18.6	6.9
20	377	20	827	3.38	0.15	5.45	19	19.0	8.6
30	377	20	183	3.72	0.16	6.93	23	21.5	2.1

30	377	20	347	3.72	0.16	6.61	22	21.4	3.8
30	377	20	504	3.72	0.16	6.92	23	22.3	5.8
30	377	20	662	3.72	0.16	6.43	21	21.3	7.1
30	377	20	812	3.72	0.16	6.35	21	21.2	8.7
40	377	20	179	3.99	0.16	8.22	26	23.9	2.0
40	377	20	343	3.99	0.16	7.62	24	23.4	3.7
40	377	20	497	3.99	0.16	7.37	24	23.1	5.2
40	377	20	649	3.99	0.16	7.72	25	23.9	7.1
40	377	20	798	3.99	0.16	7.53	24	23.6	8.5
3RR				07/24/2017					
20	377	58	198	1.25	0.15	2.31	9	9.2	2.7
20	377	58	375	1.25	0.15	2.33	9	9.5	5.1
20	377	58	546	1.25	0.15	2.25	9	9.3	7.2
20	377	58	712	1.25	0.15	2.34	9	9.6	9.8
20	377	58	874	1.25	0.15	2.24	9	9.3	11.5
30	377	58	195	1.68	0.16	3.15	12	11.8	2.6
30	377	58	367	1.68	0.16	3.26	12	12.5	5.1
30	377	58	534	1.68	0.16	3.22	12	12.5	7.4
30	377	58	696	1.68	0.16	3.14	12	12.3	9.5
30	377	58	855	1.68	0.16	3.13	12	12.3	11.6
40	377	58	189	2.13	0.16	3.96	14	14.1	2.5
40	377	58	361	2.13	0.16	4.17	15	15.1	5.0
40	377	58	524	2.13	0.16	4.01	14	14.8	7.1
40	377	58	683	2.13	0.16	4.08	15	15.1	9.3
40	377	58	841	2.13	0.16	4.00	14	14.9	11.3
4RR				07/27/2014					
20	377	75	265	0.42	0.15	1.42	6	6.0	5.8
20	377	75	501	0.42	0.15	1.30	5	5.7	10.0
20	377	75	731	0.42	0.15	1.32	5	5.8	14.8
20	377	75	952	0.42	0.15	1.30	5	5.7	19.1
20	377	75	1177	0.42	0.15	1.19	5	5.3	21.6
30	377	75	260	0.65	0.16	2.14	8	8.7	5.8
30	377	75	496	0.65	0.16	2.01	8	8.4	10.4
30	377	75	718	0.65	0.16	1.87	7	7.9	14.1
30	377	75	941	0.65	0.16	1.77	7	7.6	17.6
30	377	75	1159	0.65	0.16	1.78	7	7.6	21.7
40	377	75	256	0.93	0.16	2.79	11	10.8	5.5
40	377	75	484	0.93	0.16	2.61	10	10.4	9.7
40	377	75	702	0.93	0.16	2.63	10	10.5	14.3
40	377	75	922	0.93	0.16	2.55	10	10.3	18.2

40	377	75	1139	0.93	0.16	2.39	9	9.8	21.2
40	377	75	258	0.93	0.16	2.71	10	10.7	5.4
40	377	75	492	0.93	0.16	2.43	9	9.9	9.3
40	377	75	714	0.93	0.16	2.41	9	10.0	13.4
40	377	75	936	0.93	0.16	2.46	10	10.2	17.9
40	377	75	1150	0.93	0.16	2.30	9	9.6	20.7
5RR				07/29/2014					
20	377	80	268	0.26	0.15	1.12	5	4.8	6.9
20	377	80	506	0.26	0.15	1.02	4	4.5	11.9
20	377	80	736	0.26	0.15	0.97	4	4.4	16.6
20	377	80	962	0.26	0.15	0.94	4	4.2	20.8
20	377	80	1189	0.26	0.15	0.92	4	4.2	25.3
30	377	80	260	0.42	0.16	1.76	7	7.3	6.8
30	377	80	496	0.42	0.16	1.67	7	7.1	12.4
30	377	80	723	0.42	0.16	1.62	6	6.9	17.6
30	377	80	944	0.42	0.16	1.53	6	6.6	21.8
30	377	80	1165	0.42	0.16	1.43	6	6.3	25.3
40	377	80	258	0.63	0.16	2.41	9	9.5	6.5
40	377	80	489	0.63	0.16	2.33	9	9.4	12.0
40	377	80	712	0.63	0.16	2.41	9	9.8	18.1
40	377	80	936	0.63	0.16	2.24	9	9.2	22.2
40	377	80	1142	0.63	0.16	2.07	8	8.6	25.2
40	377	80	258	0.63	0.16	2.48	10	9.8	6.7
40	377	80	491	0.63	0.16	2.20	9	9.1	11.5
40	377	80	712	0.63	0.16	2.30	9	9.5	17.3
40	377	80	930	0.63	0.16	2.17	8	9.0	21.4
40	377	80	1153	0.63	0.16	2.01	8	8.5	24.7
6RR				07/31/2014					
30	377	84	262	0.29	0.15	1.51	6	6.3	8.1
30	377	84	499	0.29	0.15	1.36	5	5.9	14.0
30	377	84	725	0.29	0.15	1.35	5	5.9	20.2
30	377	84	951	0.29	0.15	1.27	5	5.6	25.0
30	377	84	1169	0.29	0.15	1.19	5	5.2	28.8
40	377	84	258	0.45	0.16	2.12	8	8.5	7.7
40	377	84	490	0.45	0.16	1.87	7	7.8	13.0
40	377	84	713	0.45	0.16	2.02	8	8.4	20.3
40	377	84	934	0.45	0.16	1.85	7	7.8	24.5
40	377	84	257	0.45	0.16	2.20	9	8.9	7.9
40	377	84	490	0.45	0.16	2.02	8	8.4	13.9
40	377	84	714	0.45	0.16	1.97	8	8.3	19.8

40	377	84	937	0.45	0.16	1.85	7	7.9	24.5
40	377	84	1151	0.45	0.16	1.81	7	7.7	29.5
7RR				08/02/2014					
40	377	89	234	0.29	0.15	1.92	7	7.8	8.9
40	377	89	441	0.29	0.15	1.75	7	7.3	15.4
40	377	89	645	0.29	0.15	1.68	7	7.1	21.7
40	377	89	839	0.29	0.15	1.63	6	7.0	27.5
40	377	89	1030	0.29	0.15	1.52	6	6.6	31.6
40	377	89	233	0.29	0.16	1.90	8	7.8	8.8
40	377	89	444	0.29	0.16	1.76	7	7.5	15.6
40	377	89	649	0.29	0.16	1.64	7	7.1	21.4
40	377	89	844	0.29	0.16	1.62	7	7.0	27.3
40	377	89	1043	0.29	0.16	1.53	6	6.7	32.1
$1Na_2CO_3$				08/10/2014					
20	377	25	183	3.00	0.15	5.40	19	18.0	2.2
20	377	25	352	3.00	0.15	4.97	18	17.4	4.0
20	377	25	513	3.00	0.15	4.90	17	17.4	5.7
20	377	25	671	3.00	0.15	4.87	17	17.4	7.5
20	377	25	819	3.00	0.15	4.96	18	17.7	9.2
30	377	25	182	3.42	0.16	6.17	21	19.7	2.1
30	377	25	347	3.42	0.16	5.84	20	19.5	3.9
30	377	25	502	3.42	0.16	5.70	20	19.4	5.5
30	377	25	657	3.42	0.16	5.78	20	19.7	7.3
30	377	25	806	3.42	0.16	5.70	20	19.6	8.9
40	377	25	176	3.60	0.16	7.68	24	22.6	2.2
40	377	25	336	3.60	0.16	7.14	23	22.3	4.0
40	377	25	492	3.60	0.16	6.98	23	22.2	5.7
40	377	25	644	3.60	0.16	6.98	23	22.3	7.5
40	377	25	789	3.60	0.16	7.04	23	22.5	9.3
$2Na_2CO_3$				08/12/2014					
20	377	65	194	0.77	0.15	2.09	8	8.3	3.5
20	377	65	374	0.77	0.15	1.95	8	8.1	6.4
20	377	65	541	0.77	0.15	1.88	7	7.9	9.0
20	377	65	706	0.77	0.15	1.88	7	7.9	11.7
20	377	65	873	0.77	0.15	1.75	7	7.5	13.6
30	377	65	190	1.08	0.16	2.82	11	10.7	3.4
30	377	65	362	1.08	0.16	2.87	11	11.2	6.5
30	377	65	527	1.08	0.16	2.97	11	11.7	9.7
30	377	65	690	1.08	0.16	2.69	10	10.8	11.7
30	377	65	847	1.08	0.16	2.59	10	10.5	13.8

40	377	65	186	1.43	0.16	3.81	14	13.6	3.3
40	377	65	356	1.43	0.16	3.59	13	13.4	6.1
40	377	65	519	1.43	0.16	3.62	13	13.6	8.9
40	377	65	677	1.43	0.16	3.52	13	13.4	11.4
40	377	65	833	1.43	0.16	3.44	13	13.2	13.7
$3Na_2CO_3$				08/13/2014					
20	377	80	235	0.24	0.15	1.21	5	5.1	6.9
20	377	80	448	0.24	0.15	1.14	5	5.0	12.4
20	377	80	652	0.24	0.15	1.06	4	4.7	16.9
20	377	80	853	0.24	0.15	1.04	4	4.6	21.6
20	377	80	1045	0.24	0.15	1.02	4	4.6	25.9
30	377	80	232	0.38	0.16	1.75	7	7.1	6.4
30	377	80	443	0.38	0.16	1.64	7	6.9	11.5
30	377	80	645	0.38	0.16	1.61	6	6.9	16.4
30	377	80	840	0.38	0.16	1.54	6	6.6	20.5
30	377	80	1040	0.38	0.16	1.46	6	6.3	24.1
40	377	80	229	0.57	0.16	2.46	9	9.6	6.1
40	377	80	434	0.57	0.16	2.28	9	9.2	10.9
40	377	80	634	0.57	0.16	2.21	9	9.0	15.4
40	377	80	827	0.57	0.16	2.26	9	9.3	20.5
40	377	80	1022	0.57	0.16	2.15	8	8.9	24.3
1Triple				10/22/2014					
20	377	0	179	3.72	0.19	7.51	21	19.3	0.6
20	377	0	338	3.72	0.19	7.84	22	20.5	1.3
20	377	0	486	3.72	0.19	8.51	23	21.9	1.9
20	377	0	638	3.72	0.19	7.53	21	20.2	2.3
20	377	0	788	3.72	0.19	7.55	21	20.3	2.9
30	377	0	171	4.13	0.19	9.19	24	21.7	0.6
30	377	0	327	4.13	0.19	9.53	25	23.1	1.2
30	377	0	471	4.13	0.19	9.82	26	23.8	1.8
30	377	0	621	4.13	0.19	9.23	25	23.1	2.3
30	377	0	770	4.13	0.19	9.29	25	23.3	2.8
40	377	0	165	4.33	0.20	12.31	30	25.7	0.7
40	377	0	321	4.33	0.20	11.93	29	26.3	1.3
40	377	0	463	4.33	0.20	11.45	29	26.0	1.8
40	377	0	608	4.33	0.20	11.25	28	26.0	2.4
40	377	0	750	4.33	0.20	11.24	28	26.1	2.9
2Triple				10/23/2014					
20	377	10	172	3.67	0.19	10.66	27	24.1	0.9
20	377	10	330	3.67	0.19	10.15	26	24.2	1.7

20	377	10	478	3.67	0.19	9.83	26	24.0	2.4
20	377	10	627	3.67	0.19	9.55	25	23.7	3.0
20	377	10	772	3.67	0.19	9.49	25	23.7	3.7
30	377	10	168	3.98	0.19	11.75	29	25.6	0.8
30	377	10	323	3.98	0.19	11.55	29	26.2	1.6
30	377	10	466	3.98	0.19	11.86	29	26.9	2.3
30	377	10	613	3.98	0.19	11.29	28	26.3	2.9
30	377	10	758	3.98	0.19	11.23	28	26.3	3.6
40	377	10	163	4.28	0.20	14.67	34	28.8	0.8
40	377	10	315	4.28	0.20	14.21	33	29.3	1.6
40	377	10	457	4.28	0.20	13.82	32	29.2	2.2
40	377	10	598	4.28	0.20	13.60	32	29.2	2.9
40	377	10	739	4.28	0.20	13.50	32	29.1	3.6
3Triple				10/24/2014					
20	377	20	175	3.30	0.19	9.45	25	22.5	1.0
20	377	20	334	3.30	0.19	9.45	25	23.2	1.8
20	377	20	482	3.30	0.19	9.22	25	23.1	2.6
20	377	20	631	3.30	0.19	9.16	25	23.1	3.4
20	377	20	778	3.30	0.19	9.02	24	22.9	4.1
30	377	20	169	3.70	0.19	11.95	30	25.7	0.9
30	377	20	325	3.70	0.19	11.40	29	25.9	1.7
30	377	20	468	3.70	0.19	11.95	30	27.0	2.5
30	377	20	616	3.70	0.19	10.93	28	25.7	3.1
30	377	20	760	3.70	0.19	10.96	28	25.9	3.9
40	377	20	112	3.75	0.20	14.26	33	27.6	0.6
40	377	20	215	3.75	0.20	14.48	34	29.2	1.2
40	377	20	318	3.75	0.20	13.54	32	28.6	1.7
40	377	20	415	3.75	0.20	13.38	32	28.7	2.2
40	377	20	508	3.75	0.20	13.39	32	28.8	2.7
4Triple				10/26/2014					
20	377	35	90	2.69	0.19	8.68	23	19.9	0.6
20	377	35	174	2.69	0.19	7.92	22	19.9	1.1
20	377	35	282	2.69	0.19	7.85	21	20.3	1.8
20	377	35	388	2.69	0.19	7.30	20	19.5	2.4
20	377	35	492	2.69	0.19	7.01	20	19.1	2.9
20	377	35	590	2.69	0.19	6.97	20	19.1	3.5
30	377	35	88	3.05	0.20	10.27	27	22.0	0.6
30	377	35	171	3.05	0.20	9.83	26	22.8	1.1
30	377	35	275	3.05	0.20	10.55	27	24.6	1.8
30	377	35	377	3.05	0.20	9.87	26	23.8	2.4

30	377	35	477	3.05	0.20	8.91	24	22.4	2.8
30	377	35	577	3.05	0.20	8.79	24	22.3	3.4
40	377	35	84	3.51	0.20	13.69	32	26.0	0.6
40	377	35	164	3.51	0.20	11.77	29	25.4	1.0
40	377	35	270	3.51	0.20	11.27	28	25.5	1.6
40	377	35	365	3.51	0.20	11.48	29	26.1	2.2
40	377	35	464	3.51	0.20	10.80	27	25.3	2.7
40	377	35	559	3.51	0.20	10.96	28	25.6	3.3
5Triple				10/27/2014					
20	377	45	92	2.05	0.19	7.07	20	17.3	0.7
20	377	45	178	2.05	0.19	5.91	17	16.1	1.2
20	377	45	281	2.05	0.19	6.79	19	18.3	2.1
20	377	45	393	2.05	0.19	5.60	17	16.0	2.5
20	377	45	494	2.05	0.19	5.83	17	16.7	3.2
20	377	45	595	2.05	0.19	5.51	16	16.0	3.7
30	377	45	88	2.59	0.20	8.33	23	19.2	0.6
30	377	45	171	2.59	0.20	8.15	22	20.1	1.2
30	377	45	280	2.59	0.20	7.45	21	19.5	1.8
30	377	45	379	2.59	0.20	8.08	22	20.8	2.5
30	377	45	479	2.59	0.20	7.53	21	20.0	3.0
30	377	45	581	2.59	0.20	7.13	20	19.3	3.5
40	377	45	85	3.11	0.20	10.79	27	22.5	0.6
40	377	45	167	3.11	0.20	9.84	26	22.7	1.1
40	377	45	270	3.11	0.20	9.85	26	23.4	1.7
40	377	45	368	3.11	0.20	9.54	25	23.2	2.3
40	377	45	464	3.11	0.20	9.30	24	22.9	2.9
40	377	45	562	3.11	0.20	9.12	24	22.8	3.4
6Triple				10/28/2014					
20	377	55	93	1.36	0.19	5.13	15	13.5	0.8
20	377	55	182	1.36	0.19	4.70	14	13.5	1.4
20	377	55	292	1.36	0.19	4.60	14	13.6	2.3
20	377	55	401	1.36	0.19	4.64	14	13.9	3.1
20	377	55	507	1.36	0.19	4.34	13	13.2	3.7
20	377	55	610	1.36	0.19	4.25	13	13.1	4.4
30	377	55	90	1.82	0.20	7.64	21	18.1	0.8
30	377	55	177	1.82	0.20	6.68	19	17.6	1.4
30	377	55	287	1.82	0.20	5.94	17	16.5	2.1
30	377	55	391	1.82	0.20	6.04	18	16.9	2.9
30	377	55	493	1.82	0.20	6.06	18	17.1	3.6
30	377	55	595	1.82	0.20	5.90	17	16.8	4.3

40	377	55	88	2.30	0.20	8.60	23	19.5	0.7
40	377	55	171	2.30	0.20	8.08	22	19.9	1.3
40	377	55	277	2.30	0.20	8.15	22	20.6	2.0
40	377	55	379	2.30	0.20	7.85	21	20.3	2.7
40	377	55	477	2.30	0.20	7.60	21	20.0	3.3
40	377	55	577	2.30	0.20	7.54	21	20.0	4.0
7Triple				10/29/2014					
20	377	65	124	0.77	0.19	3.88	12	11.2	1.3
20	377	65	213	0.77	0.19	3.45	11	10.6	2.1
20	377	65	297	0.77	0.19	3.50	11	10.9	2.9
20	377	65	380	0.77	0.19	3.54	11	11.1	3.8
20	377	65	461	0.77	0.19	3.37	10	10.7	4.4
30	377	65	122	1.11	0.20	4.70	14	13.0	1.1
30	377	65	208	1.11	0.20	4.70	14	13.6	1.9
30	377	65	293	1.11	0.20	4.91	15	14.3	2.8
30	377	65	373	1.11	0.20	4.77	14	14.1	3.4
30	377	65	455	1.11	0.20	4.49	14	13.5	4.0
40	377	65	120	1.49	0.20	6.48	18	16.5	1.1
40	377	65	205	1.49	0.20	6.32	18	16.9	1.8
40	377	65	286	1.49	0.20	6.30	18	17.2	2.5
40	377	65	367	1.49	0.20	5.94	17	16.6	3.1
40	377	65	443	1.49	0.20	6.01	17	16.8	3.8
8Triple				10/30/2014					
20	377	70	126	0.55	0.19	3.34	11	9.8	1.6
20	377	70	216	0.55	0.19	2.97	10	9.3	2.4
20	377	70	301	0.55	0.19	2.90	9	9.3	3.3
20	377	70	387	0.55	0.19	2.80	9	9.1	4.1
20	377	70	467	0.55	0.19	2.64	9	8.7	4.7
30	377	70	121	0.81	0.20	4.12	13	11.6	1.3
30	377	70	209	0.81	0.20	4.24	13	12.5	2.2
30	377	70	294	0.81	0.20	4.13	13	12.4	3.1
30	377	70	375	0.81	0.20	4.26	13	12.9	4.0
30	377	70	455	0.81	0.20	3.99	12	12.3	4.6
40	377	70	120	1.13	0.20	5.81	17	15.2	1.2
40	377	70	205	1.13	0.20	5.57	16	15.3	2.1
40	377	70	289	1.13	0.20	5.44	16	15.3	2.8
40	377	70	369	1.13	0.20	5.38	16	15.4	3.6
40	377	70	446	1.13	0.20	5.31	16	15.3	4.3
9Triple				11/01/2014					
20	377	80	129	0.23	0.19	2.44	8	7.5	2.5

20	377	80	222	0.23	0.19	2.15	7	7.0	3.8
20	377	80	311	0.23	0.19	2.00	7	6.7	5.0
20	377	80	395	0.23	0.19	2.25	7	7.5	7.1
20	377	80	479	0.23	0.19	1.91	6	6.5	7.4
30	377	80	126	0.37	0.20	3.53	11	10.3	2.2
30	377	80	217	0.37	0.20	3.11	10	9.6	3.4
30	377	80	306	0.37	0.20	3.03	10	9.6	4.6
30	377	80	390	0.37	0.20	2.95	9	9.5	5.8
30	377	80	473	0.37	0.20	2.92	9	9.5	6.9
40	377	80	125	0.57	0.20	4.65	14	12.8	1.9
40	377	80	215	0.57	0.20	4.23	13	12.4	3.0
40	377	80	301	0.57	0.20	4.15	13	12.4	4.1
40	377	80	383	0.57	0.20	4.12	13	12.5	5.2
40	377	80	465	0.57	0.20	3.97	12	12.2	6.2

C.2 AIR-WATER COLUMN (AWC) DATA

The raw data of AWC experiments performed in this work (not including other data in the SRP database) is summarized in this section.

C.2.1 Hydraulic Data

Table C.2: Experimental AWC data (hydraulic)

L ($m^3/m^2 \cdot h$)	G (m/s)	T_{liquid} (°C)	T_{gas} (°C)	ΔP (Pa/m packing)	h (m^3/m^3)
GTO 250Y	Z = 3.0 m	04/02&03/2015			
0.0	0.3	20.8	21.4	5	-
0.0	0.7	20.8	21.5	19	-
0.0	1.0	20.8	21.6	40	-
0.0	1.3	20.8	22.0	67	-
0.0	1.6	20.8	22.6	101	-
0.0	2.0	20.8	23.2	140	-
0.0	2.3	20.9	24.2	185	-
0.0	2.6	20.9	25.4	238	-
0.0	3.0	20.9	26.6	296	-

0.0	3.3	20.9	28.9	358	-
0.0	3.6	21.0	30.5	428	-
0.0	4.0	21.0	33.0	502	-
0.0	4.6	21.0	36.2	671	-
12.2	0.3	20.7	23.8	7	0.04
12.2	0.7	21.5	23.1	24	-
12.2	1.0	21.8	24.0	50	0.04
12.2	1.3	21.8	24.3	83	-
12.2	1.7	21.8	24.8	125	0.04
12.2	2.0	21.8	25.5	173	-
12.2	2.3	21.8	26.1	238	0.04
12.2	2.6	21.9	26.9	307	-
12.2	3.0	22.0	27.9	399	0.05
12.2	3.3	22.2	29.2	509	-
12.3	3.6	22.5	30.7	645	0.06
12.2	3.8	22.9	31.8	725	-
12.2	3.9	23.2	32.9	766	-
12.3	4.0	23.6	33.5	812	0.06
12.2	4.0	24.0	34.1	868	-
12.2	4.1	24.3	34.6	928	0.07
12.2	4.2	24.6	35.2	991	-
12.2	4.3	24.9	35.7	1075	0.08
12.2	4.4	25.3	36.8	1157	-
12.2	4.5	25.5	37.5	1277	0.09
12.2	4.5	25.8	37.8	1440	-
24.4	0.3	20.8	23.3	8	0.06
24.4	0.7	21.4	23.1	27	-
24.5	1.0	26.0	30.6	54	0.07
24.5	1.3	25.9	29.4	89	-
24.4	1.6	25.6	29.1	136	0.07
24.5	2.0	25.3	29.1	192	-
24.5	2.3	24.9	29.9	270	0.07
24.4	2.6	24.8	30.7	362	-
24.4	3.0	24.6	31.4	497	0.07
24.5	3.3	24.5	32.6	721	0.08
24.5	3.5	25.1	34.2	868	0.09
24.4	3.6	24.7	35.3	1238	0.12
24.5	3.8	25.1	35.6	1666	-

36.7	0.3	20.8	23.1	9	0.08
36.7	0.7	21.4	23.0	31	-
36.7	1.0	25.2	30.6	59	0.08
36.7	1.3	25.1	29.7	98	-
36.7	1.7	25.0	29.2	151	0.08
36.7	2.0	24.8	29.4	215	-
36.7	2.3	24.6	30.0	328	0.08
36.7	2.5	21.7	25.5	490	-
36.7	2.6	21.9	25.8	632	0.09
36.7	2.7	21.6	26.2	704	-
36.7	2.8	21.6	26.7	810	0.10
36.7	2.9	21.7	27.4	1098	-
36.7	3.0	21.9	29.1	1639	0.14
48.9	0.3	20.9	23.0	10	0.09
48.9	0.7	21.4	23.0	36	0.09
48.9	1.0	22.0	24.5	73	0.09
48.9	1.3	21.9	23.8	122	0.10
48.9	1.6	21.8	23.8	190	0.10
48.9	1.8	21.6	25.1	255	-
48.9	2.0	21.5	24.8	431	0.10
48.9	2.1	-17.8	2.0	0	0.11
48.9	2.3	21.5	25.7	811	0.12
48.9	2.5	21.5	27.5	1663	0.16
61.1	0.3	21.1	22.9	14	0.10
61.1	0.7	21.4	22.9	51	0.10
61.1	1.0	21.6	23.7	133	0.10
61.1	1.3	21.5	23.4	214	0.11
61.1	1.6	21.5	24.2	464	0.11
61.1	1.8	21.4	24.9	623	0.12
61.1	2.0	21.6	26.1	1037	0.14
61.1	2.1	21.6	26.7	1574	0.19
73.3	0.3	21.2	22.8	22	0.11
73.3	0.7	21.3	22.9	88	0.11
73.4	1.0	21.9	24.7	238	0.12
73.4	1.2	22.0	24.7	332	0.12
73.3	1.3	22.1	25.0	450	0.12
73.3	1.5	22.1	25.4	621	0.13

73.3	1.6	22.8	28.4	943	0.15
73.3	1.8	23.1	29.7	1688	0.20
MG 64Y	Z = 2.9 m	05/19-22/2015			
0.0	0.7	23.6	23.9	5	-
0.0	1.3	23.6	24.3	20	-
0.0	2.0	23.6	25.2	44	-
0.0	2.6	23.6	26.7	76	-
0.0	3.3	23.7	29.0	117	-
0.0	4.0	23.7	31.8	165	-
0.0	4.6	23.7	35.8	219	-
12.7	0.5	24.6	26.0	3	0.01
12.0	0.7	25.1	27.1	6	-
12.3	1.0	25.0	27.2	13	0.01
12.2	1.3	25.6	30.2	22	-
12.0	2.0	25.6	30.7	48	0.01
12.6	2.6	25.5	31.4	83	0.01
12.3	3.3	25.4	33.1	134	0.01
12.7	4.0	25.5	35.4	196	0.01
12.2	4.6	25.5	37.4	293	0.01
24.5	0.5	24.6	25.8	4	0.02
24.4	0.7	25.1	27.0	7	-
24.5	1.0	24.8	27.4	15	0.02
24.4	1.3	25.7	29.8	25	-
24.4	2.0	26.8	32.5	51	0.02
24.4	2.6	26.3	33.3	88	0.02
24.4	3.3	26.2	34.3	143	0.02
24.4	4.0	26.1	36.2	215	0.02
24.5	4.6	26.2	38.5	348	0.03
36.7	0.5	24.5	25.6	6	0.02
36.7	0.7	25.1	26.9	9	-
36.6	1.0	24.7	27.1	17	0.02
36.7	1.3	25.7	29.4	28	-
36.7	1.6	20.5	20.2	42	0.02
36.7	2.0	20.2	21.5	59	0.02
36.7	2.6	20.1	22.6	102	0.02
36.7	3.3	20.1	24.3	165	0.03

36.7	3.6	20.3	25.8	205	-
36.7	4.0	20.6	27.2	262	0.03
36.7	4.3	21.1	28.8	334	-
36.7	4.6	21.3	29.6	457	0.04
48.9	0.5	24.5	25.5	7	0.03
48.9	0.7	25.1	26.9	11	-
48.9	1.0	24.7	26.7	20	0.03
48.9	1.3	25.7	29.1	32	-
48.9	1.7	26.8	30.4	45	0.03
48.9	2.0	21.6	23.7	64	0.03
48.9	2.6	21.4	24.1	112	0.03
48.9	3.0	21.4	24.7	144	-
48.9	3.3	21.3	25.7	182	0.04
48.9	3.6	21.4	26.7	235	-
48.8	4.0	21.5	27.9	303	0.04
48.9	4.3	21.6	29.2	406	0.05
48.9	4.6	22.5	32.2	824	0.07
61.1	0.5	24.5	25.5	10	0.03
61.1	0.7	25.1	26.9	14	-
61.1	1.0	24.7	26.5	23	-
61.1	1.3	25.7	29.0	36	0.03
61.1	2.0	23.0	25.3	72	0.03
61.1	2.6	22.8	25.4	125	0.04
61.1	3.3	22.7	26.5	206	0.04
61.1	3.6	22.6	27.6	270	-
61.1	4.0	22.6	28.7	359	0.05
61.1	4.3	22.8	30.5	568	0.06
61.1	4.6	23.3	33.3	1195	0.10
73.3	0.5	24.7	25.8	13	0.04
73.3	0.7	25.0	26.7	17	-
73.3	1.0	25.0	26.9	27	-
73.3	1.3	25.7	28.9	41	0.04
73.3	2.0	23.6	26.4	80	0.04
73.4	2.6	23.5	26.2	139	0.04
73.3	3.3	23.3	27.1	237	0.04
73.3	3.6	23.2	28.1	310	-
73.3	4.0	23.2	29.5	432	0.05

73.3	4.3	23.4	31.8	892	0.08
73.3	4.5	23.6	33.1	1444	0.12
RSR 1.5	Z = 3.0 m	08/02/2016			
0.0	0.5	26.3	27.5	7	-
0.0	0.7	26.3	27.5	12	-
0.0	1.3	26.4	27.8	45	-
0.0	2.0	26.5	28.7	99	-
0.0	2.6	26.5	30.6	170	-
0.0	3.3	26.6	33.1	261	-
0.0	4.0	26.7	35.9	367	-
0.0	4.6	26.7	40.0	488	-
12.2	0.5	27.7	31.5	8	0.01
12.2	0.7	27.8	31.1	14	-
12.2	1.0	27.7	31.6	29	0.01
12.3	1.3	27.8	31.8	51	-
12.2	2.0	27.5	32.4	109	0.02
12.1	2.6	27.5	33.3	189	0.02
12.2	3.3	27.3	34.6	315	0.02
12.3	4.0	27.1	36.3	473	0.02
12.2	4.6	27.2	38.8	732	0.04
24.4	0.5	27.6	31.3	9	0.03
24.4	0.7	27.6	31.2	16	-
24.4	1.0	27.9	34.1	33	0.03
24.4	1.3	28.0	33.7	54	-
24.5	2.0	27.9	34.1	117	0.03
24.4	2.6	27.8	35.2	210	0.03
24.4	3.3	27.7	36.4	351	0.04
24.4	4.0	27.6	38.7	570	0.05
24.4	4.6	27.7	38.8	1146	0.09
36.7	0.5	27.6	31.2	12	0.04
36.7	0.7	27.6	31.2	18	-
36.6	1.0	27.7	35.1	36	0.04
36.7	1.3	27.7	34.8	58	-
36.7	2.0	27.8	34.9	127	0.04
36.7	2.6	27.7	35.5	237	0.04
36.7	3.3	27.7	36.9	412	0.05
36.7	4.0	27.6	39.2	781	0.08

36.7	4.3	27.6	40.5	1302	0.11
48.9	0.5	27.6	31.1	13	0.05
48.9	0.7	27.6	31.2	20	-
48.9	1.0	27.7	36.5	41	0.05
48.9	1.3	27.8	35.4	63	-
48.9	2.0	27.8	35.0	140	0.05
48.9	2.6	27.8	35.6	270	0.06
48.9	3.0	27.7	36.4	365	0.06
48.9	3.3	27.7	37.5	501	0.07
48.9	3.6	27.7	39.0	708	0.08
48.9	3.8	27.7	40.4	888	0.10
48.9	3.9	27.8	41.0	1417	0.13
61.1	0.5	27.6	31.1	15	0.05
61.1	0.7	27.6	31.3	22	-
61.1	1.0	28.0	36.3	44	0.06
61.1	1.3	28.1	35.4	70	-
61.1	2.0	28.0	35.2	155	0.06
61.1	2.6	28.0	36.0	309	0.06
61.1	3.0	27.8	36.8	433	0.07
61.1	3.3	27.8	38.0	623	0.08
61.1	3.5	27.7	39.0	776	0.09
61.1	3.6	27.7	40.1	1088	0.13
61.1	3.7	27.7	40.7	1751	-
73.3	0.5	27.7	31.2	17	0.06
73.3	0.7	27.7	31.3	26	-
73.3	1.0	27.9	35.7	49	0.06
73.3	1.3	28.0	35.2	77	-
73.3	2.0	28.0	35.4	174	0.07
73.3	2.6	27.9	35.9	365	0.07
73.4	3.0	27.8	36.9	532	0.08
73.3	3.1	27.7	38.1	653	0.09
73.3	3.3	27.7	38.6	848	0.10
73.3	3.4	27.7	39.7	1631	0.15
B1 250MN	Z = 3.0 m	09/27-28/2016			
0.0	0.5	21.4	23.2	13	-
0.0	0.7	21.5	22.8	21	-
0.0	1.3	21.5	22.6	74	-

0.0	2.0	21.6	23.1	151	-
0.0	2.6	21.6	24.4	257	-
0.0	3.3	21.6	26.6	386	-
0.0	3.6	21.7	29.4	455	-
0.0	4.0	21.7	31.2	534	-
0.0	4.3	21.8	34.3	614	-
0.0	4.6	21.8	37.5	704	-
12.2	0.5	24.4	27.8	16	0.04
12.2	0.7	24.4	26.2	27	-
12.2	1.0	23.9	26.2	57	0.04
12.2	1.3	23.8	26.4	95	-
12.2	2.0	23.5	27.2	200	0.04
12.2	2.6	23.2	28.7	347	0.04
12.2	3.3	22.8	30.3	549	0.05
12.2	3.6	22.7	31.7	702	0.05
12.2	3.8	22.5	32.8	790	0.06
12.2	4.0	22.6	34.2	891	0.06
12.2	4.1	22.7	35.0	1016	0.07
12.2	4.3	26.8	35.7	1180	0.07
24.4	0.5	24.4	27.5	18	0.06
24.4	0.7	24.2	26.2	30	-
24.5	1.0	23.6	27.4	66	0.07
24.4	1.3	23.5	27.5	110	0.07
24.5	2.0	23.3	27.8	219	0.07
24.4	2.6	23.1	28.8	399	0.07
24.4	3.0	22.7	30.2	604	0.08
24.5	3.1	22.5	30.9	737	0.08
24.4	3.3	22.4	31.6	918	0.09
24.4	3.4	22.4	32.3	1139	0.10
24.4	3.6	24.2	36.1	1522	0.12
36.6	0.5	24.3	27.1	22	0.07
36.7	0.7	24.0	26.0	35	-
36.7	1.0	22.5	27.7	69	0.07
36.7	1.3	22.5	27.0	113	0.07
36.7	2.0	22.4	27.0	252	0.08
36.6	2.3	22.3	27.5	470	0.08
36.7	2.5	22.1	27.9	608	0.08
36.7	2.6	22.0	28.6	828	0.09

36.7	2.8	21.9	29.5	1133	0.10
36.7	3.0	23.5	33.3	1614	0.14
48.9	0.5	25.3	32.2	41	0.08
48.9	0.7	25.5	31.9	62	-
48.9	1.0	25.6	31.3	104	0.08
48.9	1.3	25.4	31.3	157	0.08
48.9	1.7	25.2	31.7	229	0.08
48.9	1.8	24.6	32.1	343	0.08
48.9	2.0	24.7	32.3	484	0.09
48.9	2.1	24.4	32.6	673	0.10
48.9	2.3	24.2	33.6	977	0.11
48.9	2.5	23.0	32.2	1533	0.15
61.1	0.5	24.6	31.8	88	0.09
61.1	0.7	25.0	31.5	122	0.09
61.1	1.0	25.2	31.2	198	0.09
61.1	1.3	25.3	31.2	330	0.09
61.1	1.6	25.2	31.6	576	0.10
61.1	1.8	25.1	32.2	807	0.11
61.1	2.0	25.0	33.2	1256	0.13
61.1	2.1	22.8	31.6	1821	0.17
73.3	0.5	24.7	32.4	152	0.11
73.3	0.7	25.0	32.1	211	0.11
73.3	0.8	25.1	31.8	265	0.11
73.3	1.0	25.2	31.6	353	0.11
73.3	1.2	25.2	31.6	472	0.12
73.3	1.3	25.2	31.7	605	0.12
73.3	1.5	25.1	32.1	829	0.13
73.3	1.6	25.0	32.8	1431	0.15
73.3	1.7	22.8	31.2	1821	0.20
HFP 2	Z = 3.0 m	02/17/2017			
0.0	0.5	11.8	10.4	4	-
0.0	0.7	11.8	10.4	7	-
0.0	0.8	11.8	10.5	11	-
0.0	1.0	11.8	10.9	15	-
0.0	1.2	11.8	11.1	20	-
0.0	1.3	11.8	11.2	24	-
0.0	1.5	11.8	11.6	30	-

0.0	1.7	11.8	11.9	36	-
0.0	2.0	11.8	12.5	52	-
0.0	2.3	11.8	13.4	68	-
0.0	2.6	11.8	14.5	87	-
0.0	3.0	11.8	16.1	109	-
0.0	3.3	11.8	17.7	132	-
0.0	3.6	11.9	19.8	157	-
0.0	4.0	11.9	21.8	184	-
0.0	4.3	12.0	24.2	213	-
12.2	0.5	14.6	17.9	5	0.02
12.2	1.0	15.5	17.4	18	0.02
12.2	1.5	16.4	19.4	37	0.02
12.2	2.0	17.6	22.4	63	0.02
12.2	2.6	17.8	23.1	112	0.02
12.2	3.3	17.9	24.9	180	0.02
12.2	3.6	18.0	26.2	221	0.03
12.2	4.0	18.1	27.7	274	0.03
12.2	4.3	18.3	28.9	331	0.03
24.4	0.5	14.7	17.1	6	0.03
24.4	1.0	15.5	17.6	19	0.03
24.4	1.5	16.4	19.5	40	0.03
24.4	2.0	18.9	24.0	67	0.03
24.4	2.6	18.9	24.6	119	0.03
24.5	3.3	18.9	26.3	194	0.03
24.5	3.6	18.9	26.8	242	0.03
24.5	4.0	18.9	28.4	299	0.03
24.4	4.3	19.1	29.6	388	0.04
36.7	0.5	14.8	17.0	7	0.03
36.7	1.0	15.7	17.9	21	0.03
36.7	1.5	16.5	19.6	43	0.03
36.7	2.0	19.4	24.8	73	0.03
36.7	2.6	19.4	25.3	128	0.03
36.7	3.3	19.3	26.6	212	0.03
36.7	3.6	19.3	27.8	269	0.03
36.7	4.0	19.8	29.5	354	0.04
36.7	4.3	19.5	30.7	592	0.05
48.9	0.5	14.9	16.9	8	0.04
48.9	1.0	15.8	18.1	22	0.04

48.9	1.5	16.6	19.8	47	0.04
48.9	2.0	19.9	24.8	79	0.04
48.9	2.6	19.8	25.2	142	0.04
48.9	3.3	19.5	26.9	242	0.04
48.9	3.6	19.5	28.0	313	0.05
48.9	4.0	19.6	30.0	533	0.06
48.9	4.1	19.8	30.7	750	0.07
48.9	4.3	20.0	32.3	1048	0.10
61.1	0.5	15.1	16.9	9	0.04
61.1	1.0	16.0	18.3	26	0.04
61.1	1.5	16.7	19.8	52	0.04
61.1	2.0	20.3	26.7	88	0.05
61.1	2.6	20.3	26.2	162	0.05
61.1	3.3	20.2	27.1	277	0.05
61.1	3.6	20.1	28.1	384	0.06
61.1	3.9	20.1	29.8	880	0.10
61.1	4.1	20.1	30.7	1434	-
73.3	0.5	15.4	17.1	11	0.05
73.3	1.0	16.2	18.6	29	0.05
73.3	1.5	16.9	20.0	57	0.05
73.3	2.0	20.3	26.8	98	0.05
73.3	2.6	20.3	26.5	184	0.05
73.3	3.3	20.2	27.2	324	0.06
73.3	3.6	20.2	29.2	706	0.08
73.3	3.9	20.2	30.1	1575	0.14

C.2.2 a_e Data

Table C.3: Experimental AWC data (a_e)

L	G	T_{sys}	glycerol	[Alk]	$CO_{2,in}$	$CO_{2,out}$	μ_L	$D_{CO2}\times10^{9}$	$H_{CO2}\times10^{-3}$	$K_{OG}a$	kg'×10^{7}	a_e	Φ
$m^3/m^2\cdot h$	m/s	C	wt %	gmol/L	ppm_V	ppm_V	mPa·s	m^2/s	$m^3\cdot Pa/mol$	1/s	$gmol/m^2\cdot Pa\cdot s$	m^2/m^3	
GTO 250Y		Z = 3.0 m		SRP1501		04/14&15/2015							
6.3	0.60	25.4	0.0%	0.108	381.7	139.3	0.9	2.09	3.10	0.199	4.53	176.5	0.71
12.2	0.60	25.4	0.0%	0.107	382.4	132.1	0.9	2.09	3.09	0.211	4.50	188.6	0.75
24.4	0.59	25.0	0.0%	0.106	380.8	123.2	0.9	2.07	3.06	0.221	4.45	199.5	0.80
36.7	0.59	25.1	0.0%	0.105	381.9	113.2	0.9	2.07	3.07	0.236	4.43	214.1	0.86
48.9	0.60	24.9	0.0%	0.103	381.0	110.7	0.9	2.06	3.05	0.243	4.39	222.5	0.89
61.1	0.60	24.8	0.0%	0.102	381.1	107.5	0.9	2.06	3.04	0.249	4.36	229.6	0.92
73.3	0.58	25.3	0.0%	0.099	380.0	95.1	0.9	2.09	3.08	0.264	4.34	244.0	0.98
6.0	0.99	21.2	0.0%	0.094	382.2	218.6	1.0	1.88	2.74	0.183	3.96	188.9	0.76
12.3	0.99	21.1	0.0%	0.095	381.9	207.8	1.0	1.87	2.73	0.199	3.97	205.3	0.82
24.4	0.99	21.1	0.0%	0.094	382.6	204.6	1.0	1.87	2.73	0.204	3.96	211.1	0.84
36.6	0.98	21.1	0.0%	0.094	382.1	197.3	1.0	1.88	2.73	0.215	3.95	222.8	0.89
48.9	0.99	20.7	0.0%	0.096	383.3	182.7	1.0	1.85	2.70	0.242	3.97	249.9	1.00
61.1	0.99	20.9	0.0%	0.094	383.8	172.2	1.0	1.86	2.71	0.262	3.95	272.0	1.09
6.2	1.49	25.5	0.0%	0.109	368.9	250.3	0.9	2.10	3.09	0.190	4.14	185.2	0.74
12.2	1.49	26.1	0.0%	0.111	369.1	235.3	0.9	2.14	3.14	0.221	4.23	210.4	0.84
24.5	1.49	25.9	0.0%	0.110	367.8	232.9	0.9	2.13	3.12	0.224	4.19	215.4	0.86
36.7	1.48	25.6	0.0%	0.108	369.0	227.5	0.9	2.11	3.10	0.237	4.14	230.9	0.92

48.9	1.48	26.3	0.0%	0.110	368.8	209.4	0.9	2.15	3.15	0.277	4.22	263.8	1.06
24.4	1.98	25.5	0.0%	0.104	367.2	262.6	0.9	2.11	3.08	0.219	4.03	219.9	0.88
36.7	1.98	25.3	0.0%	0.102	366.7	257.6	0.9	2.10	3.06	0.231	3.98	235.0	0.94
24.5	2.47	25.8	0.0%	0.105	367.2	279.5	0.9	2.12	3.11	0.223	4.06	221.8	0.89
GTO 250Y		Z = 3.0 m		SRP150401		11/19/2015							
12.2	0.99	25.2	0.0%	0.100	386.4	203.6	0.9	2.08	3.07	0.209	4.34	192.9	0.77
24.4	0.99	24.4	0.0%	0.096	388.5	194.7	0.9	2.04	3.00	0.225	4.21	215.3	0.86
36.7	0.99	24.1	0.0%	0.091	388.2	186.8	0.9	2.03	2.97	0.239	4.09	235.8	0.94
48.9	0.99	24.0	0.0%	0.086	390.4	178.2	0.9	2.02	2.95	0.257	3.97	260.6	1.04
61.1	1.00	24.0	0.0%	0.082	387.8	168.5	0.9	2.03	2.95	0.274	3.87	285.6	1.14
GTO 250Y		Z = 3.0 m		SRP160101		01/13/2016							
12.2	0.59	21.2	77.0%	0.050	401.2	325.7	41.2	0.12	5.72	0.041	1.07	161.3	0.65
24.5	0.60	21.4	77.0%	0.048	396.7	321.3	40.8	0.12	5.75	0.041	1.06	164.1	0.66
36.7	0.59	21.6	77.0%	0.046	399.4	304.5	40.4	0.12	5.77	0.053	1.04	210.5	0.84
48.8	0.60	21.9	77.0%	0.044	395.2	296.8	39.8	0.12	5.80	0.056	1.03	222.6	0.89
18.5	0.59	21.6	77.0%	0.044	395.4	315.6	40.8	0.12	5.78	0.044	1.14	178.4	0.71
30.6	0.60	21.2	77.0%	0.042	396.3	307.7	41.9	0.12	5.74	0.050	0.97	210.1	0.84
42.8	0.59	20.8	77.0%	0.040	398.7	305.7	42.8	0.11	5.71	0.052	0.93	225.2	0.90
6.3	0.60	20.1	77.0%	0.041	400.9	331.7	44.9	0.11	5.65	0.037	1.01	170.0	0.68
GTO 250Y		Z = 3.0 m		SRP160102		01/14/2016							
12.3	0.60	22.1	64.6%	0.103	393.7	252.2	13.8	0.26	5.39	0.087	2.21	160.4	0.64
24.4	0.60	22.4	64.6%	0.098	392.7	243.3	13.6	0.26	5.41	0.094	2.22	171.4	0.69
36.7	0.60	22.0	64.6%	0.096	392.8	220.4	13.9	0.25	5.38	0.113	2.17	211.8	0.85
48.8	0.59	21.6	64.6%	0.093	396.5	215.8	14.1	0.25	5.34	0.118	2.13	226.0	0.90
61.1	0.60	21.6	64.6%	0.090	393.9	212.3	14.3	0.25	5.34	0.121	2.10	234.6	0.94

GTO 250Y		Z = 3.0 m		SRP160103		01/15/2016							
12.2	0.59	24.2	45.2%	0.093	385.3	181.0	4.1	0.63	4.72	0.146	3.97	152.0	0.61
24.4	0.60	23.2	45.2%	0.089	384.0	170.4	4.1	0.61	4.61	0.159	3.83	173.1	0.69
36.7	0.59	22.5	45.2%	0.086	386.2	158.4	4.3	0.58	4.57	0.171	3.70	196.9	0.79
48.9	0.60	21.7	45.2%	0.081	395.7	146.7	4.5	0.56	4.50	0.194	3.57	236.6	0.95
61.1	0.57	20.8	45.2%	0.078	403.2	146.8	4.6	0.54	4.42	0.188	3.46	239.6	0.96
24.5	0.60	19.8	45.2%	0.077	399.0	185.7	4.7	0.52	4.32	0.150	3.37	199.7	0.80
GTO 250Y		Z = 3.0 m		SRP160201		02/01/2016							
6.1	0.60	21.3	79.9%	0.088	384.8	310.7	57.0	0.09	5.83	0.042	1.18	146.4	0.59
12.0	0.59	22.5	79.9%	0.087	383.9	300.3	52.7	0.10	5.94	0.048	1.24	157.4	0.63
24.5	0.60	23.4	79.9%	0.085	382.0	284.0	49.9	0.11	6.02	0.059	1.28	186.0	0.74
36.7	0.60	24.0	79.9%	0.083	379.3	267.8	48.2	0.11	6.07	0.068	1.30	211.4	0.85
48.9	0.59	24.5	79.9%	0.080	376.3	263.1	46.9	0.11	6.12	0.070	1.32	212.7	0.85
GTO 250Y		Z = 3.0 m		SRP160202		02/02/2016							
6.1	0.60	20.5	63.7%	0.096	384.9	261.1	14.0	0.25	5.20	0.077	2.12	147.5	0.59
12.1	0.60	20.6	63.7%	0.093	384.6	255.9	14.1	0.25	5.21	0.080	2.11	154.9	0.62
24.5	0.60	20.5	63.7%	0.090	384.5	246.5	14.1	0.25	5.21	0.088	2.09	171.1	0.68
36.7	0.59	20.7	63.7%	0.086	382.8	222.7	14.2	0.24	5.23	0.105	2.07	206.9	0.83
48.9	0.59	21.2	63.7%	0.083	383.3	217.7	13.8	0.25	5.28	0.110	2.10	213.1	0.85
61.1	0.60	21.7	63.7%	0.080	381.5	212.8	13.5	0.26	5.32	0.114	2.13	217.6	0.87
GTO 250Y		Z = 3.0 m		SRP160203		02/03/2016							
6.1	0.59	15.8	40.2%	0.103	396.1	206.1	4.6	0.48	3.73	0.126	3.41	153.1	0.61
12.2	0.60	15.7	40.2%	0.100	394.7	202.8	4.6	0.48	3.72	0.130	3.37	160.5	0.64
24.4	0.60	16.0	40.2%	0.095	394.0	183.2	4.5	0.49	3.75	0.150	3.38	184.5	0.74
36.7	0.59	16.1	40.2%	0.090	392.5	158.7	4.5	0.49	3.76	0.176	3.37	216.9	0.87

48.9	0.59	16.4	40.2%	0.086	392.2	157.1	4.4	0.50	3.79	0.178	3.37	217.7	0.87
61.1	0.60	16.7	40.2%	0.082	391.2	155.3	4.4	0.50	3.81	0.181	3.37	221.2	0.88
MG 64Y		Z = 2.9 m		SRP1502		05/27&28/2015							
6.0	0.59	27.0	0.0%	0.099	361.1	255.1	0.8	2.18	3.23	0.071	4.46	63.5	0.99
12.2	0.59	27.1	0.0%	0.099	362.5	246.6	0.8	2.19	3.23	0.078	4.46	70.5	1.10
24.5	0.59	24.8	0.0%	0.097	372.6	248.1	0.9	2.06	3.03	0.081	4.26	77.3	1.21
36.7	0.59	24.8	0.0%	0.097	372.8	241.7	0.9	2.06	3.04	0.088	4.27	83.1	1.30
48.9	0.60	24.9	0.0%	0.097	373.9	237.5	0.9	2.06	3.04	0.093	4.27	88.4	1.38
61.1	0.60	24.8	0.0%	0.096	373.0	230.9	0.9	2.06	3.03	0.098	4.24	93.6	1.46
73.3	0.59	24.7	0.0%	0.096	373.0	223.8	0.9	2.06	3.03	0.103	4.22	98.3	1.54
6.2	0.99	26.4	0.0%	0.101	369.3	296.4	0.8	2.15	3.18	0.074	4.46	67.1	1.05
12.2	0.99	26.6	0.0%	0.101	370.0	291.7	0.8	2.16	3.19	0.081	4.47	72.3	1.13
24.5	0.99	26.6	0.0%	0.101	369.9	286.2	0.8	2.16	3.19	0.087	4.47	78.1	1.22
36.7	0.99	26.6	0.0%	0.100	368.7	279.7	0.8	2.16	3.19	0.094	4.46	84.3	1.32
48.9	0.99	26.6	0.0%	0.100	367.2	272.9	0.8	2.16	3.19	0.101	4.45	90.7	1.42
61.1	0.99	26.6	0.0%	0.100	365.8	268.3	0.8	2.16	3.19	0.105	4.44	94.9	1.48
73.4	0.99	26.7	0.0%	0.099	364.3	263.7	0.8	2.16	3.20	0.109	4.43	98.9	1.55
6.2	1.48	25.6	0.0%	0.098	386.9	334.8	0.9	2.10	3.10	0.074	4.33	68.6	1.07
12.2	1.48	25.6	0.0%	0.098	391.5	334.4	0.9	2.10	3.10	0.080	4.33	74.6	1.17
24.4	1.49	25.6	0.0%	0.099	392.8	331.7	0.9	2.10	3.10	0.086	4.35	79.8	1.25
36.7	1.49	25.6	0.0%	0.098	391.8	327.1	0.9	2.10	3.10	0.092	4.34	85.2	1.33
48.9	1.49	25.6	0.0%	0.099	394.2	325.0	0.9	2.10	3.11	0.098	4.35	90.9	1.42
61.1	1.48	25.6	0.0%	0.098	391.9	320.4	0.9	2.10	3.10	0.102	4.33	95.3	1.49
73.3	1.48	25.6	0.0%	0.097	391.4	317.9	0.9	2.10	3.10	0.106	4.32	98.7	1.54
36.7	1.98	25.8	0.0%	0.096	385.5	335.4	0.9	2.12	3.12	0.094	4.31	88.3	1.38

36.6	2.47	26.3	0.0%	0.095	384.4	342.7	0.9	2.14	3.16	0.097	4.33	90.8	1.42
RSR 1.5		Z = 3.0 m		SRP1614		08/04/2016							
6.2	0.60	32.7	0.0%	0.101	376.7	180.0	0.7	2.55	3.74	0.148	4.99	116.6	0.97
12.2	0.60	32.7	0.0%	0.102	377.0	169.1	0.7	2.54	3.74	0.162	4.99	127.3	1.06
24.4	0.60	32.6	0.0%	0.102	377.4	154.4	0.7	2.54	3.73	0.181	5.00	142.0	1.18
36.6	0.59	32.6	0.0%	0.104	373.5	139.3	0.7	2.54	3.73	0.194	5.04	150.2	1.25
48.9	0.60	32.6	0.0%	0.103	374.7	134.0	0.7	2.54	3.73	0.206	5.02	160.7	1.34
61.1	0.60	32.6	0.0%	0.103	375.7	128.0	0.7	2.54	3.73	0.215	5.02	167.8	1.40
73.3	0.60	32.6	0.0%	0.102	377.0	120.9	0.7	2.54	3.73	0.227	5.00	178.0	1.48
6.2	0.99	34.0	0.0%	0.094	367.6	235.4	0.7	2.64	3.85	0.148	4.92	117.4	0.98
12.2	0.99	34.0	0.0%	0.094	367.6	224.9	0.7	2.64	3.85	0.163	4.92	129.3	1.08
24.5	0.99	34.2	0.0%	0.095	367.7	210.4	0.7	2.65	3.87	0.185	4.95	145.7	1.21
36.7	0.99	35.3	0.0%	0.096	362.8	197.3	0.7	2.73	3.98	0.201	5.09	153.3	1.28
48.9	0.99	34.8	0.0%	0.096	365.9	195.1	0.7	2.70	3.93	0.209	5.04	161.2	1.34
61.1	0.99	34.6	0.0%	0.095	366.5	188.2	0.7	2.68	3.91	0.221	5.01	172.0	1.43
73.3	0.99	34.5	0.0%	0.095	367.1	183.1	0.7	2.67	3.90	0.230	4.99	180.1	1.50
6.1	1.49	31.1	0.0%	0.094	373.0	280.0	0.8	2.43	3.58	0.143	4.66	121.1	1.01
12.2	1.48	31.1	0.0%	0.094	373.2	273.6	0.8	2.44	3.59	0.154	4.66	130.7	1.09
24.4	1.48	31.2	0.0%	0.094	374.0	264.4	0.8	2.44	3.59	0.172	4.67	145.7	1.21
36.7	1.48	31.3	0.0%	0.094	373.2	256.1	0.8	2.45	3.60	0.187	4.69	157.7	1.31
48.9	1.49	31.5	0.0%	0.097	371.7	248.0	0.8	2.46	3.62	0.201	4.76	166.6	1.39
61.1	1.48	31.3	0.0%	0.096	372.3	242.2	0.8	2.45	3.60	0.214	4.72	178.6	1.49
73.3	1.48	31.3	0.0%	0.095	372.5	235.7	0.8	2.45	3.60	0.228	4.70	191.2	1.59
36.7	1.98	33.8	0.0%	0.092	367.3	272.2	0.7	2.62	3.83	0.198	4.85	159.9	1.33
36.7	2.47	34.1	0.0%	0.090	367.3	287.8	0.7	2.63	3.85	0.202	4.82	164.0	1.37

B1 250MN		Z = 3.0 m		SRP1616		10/04/2016							
6.1	0.60	28.9	0.0%	0.091	384.6	110.1	0.8	2.30	3.38	0.248	4.41	223.2	0.89
12.2	0.60	28.8	0.0%	0.091	384.7	100.9	0.8	2.29	3.38	0.265	4.42	237.6	0.95
24.5	0.59	28.8	0.0%	0.092	384.7	88.9	0.8	2.30	3.38	0.286	4.43	255.7	1.02
36.7	0.60	29.0	0.0%	0.092	384.3	83.4	0.8	2.30	3.39	0.301	4.45	268.1	1.07
48.9	0.60	29.0	0.0%	0.093	383.9	77.8	0.8	2.30	3.39	0.314	4.47	278.5	1.11
61.1	0.59	29.0	0.0%	0.094	384.8	76.9	0.8	2.31	3.40	0.314	4.49	277.1	1.11
73.3	0.59	29.1	0.0%	0.094	384.7	76.6	0.8	2.31	3.40	0.316	4.51	277.7	1.11
6.1	0.99	28.6	0.0%	0.095	381.1	177.0	0.8	2.28	3.36	0.251	4.49	222.3	0.89
12.2	0.99	28.8	0.0%	0.096	381.0	166.1	0.8	2.29	3.38	0.271	4.52	239.1	0.96
24.5	0.99	28.7	0.0%	0.096	383.3	155.1	0.8	2.29	3.37	0.296	4.53	260.2	1.04
36.7	0.99	28.7	0.0%	0.097	381.6	147.2	0.8	2.28	3.37	0.312	4.54	273.8	1.10
48.9	0.99	28.7	0.0%	0.098	382.0	143.1	0.8	2.28	3.37	0.322	4.55	281.5	1.13
61.1	0.99	28.4	0.0%	0.099	380.6	139.4	0.8	2.26	3.34	0.328	4.57	286.5	1.15
73.4	0.99	28.6	0.0%	0.098	381.4	137.6	0.8	2.28	3.37	0.332	4.57	289.5	1.16
6.1	1.48	31.2	0.0%	0.090	370.2	218.5	0.8	2.44	3.58	0.258	4.58	223.2	0.89
12.2	1.48	31.3	0.0%	0.091	371.2	207.9	0.8	2.45	3.60	0.284	4.61	243.7	0.97
24.5	1.49	31.4	0.0%	0.092	372.9	199.6	0.8	2.46	3.61	0.306	4.64	261.1	1.04
36.7	1.49	31.5	0.0%	0.092	370.5	193.5	0.8	2.46	3.62	0.319	4.66	270.7	1.08
48.9	1.48	31.8	0.0%	0.093	368.8	190.2	0.8	2.48	3.64	0.324	4.71	271.9	1.09
61.1	1.46	31.7	0.0%	0.093	369.9	182.2	0.8	2.48	3.64	0.341	4.70	286.2	1.14
24.5	1.98	28.8	0.0%	0.090	381.2	246.6	0.8	2.29	3.37	0.284	4.39	258.2	1.03
24.4	2.47	29.2	0.0%	0.089	382.0	267.3	0.8	2.31	3.40	0.291	4.39	264.9	1.06
HFP 2		Z = 3.0 m		SRP1703		02/21/2017							
6.1	0.60	22.6	0.0%	0.100	385.2	264.1	0.9	1.94	2.86	0.076	4.17	73.8	0.74

12.2	0.58	22.5	0.0%	0.100	385.4	248.4	0.9	1.94	2.85	0.085	4.16	82.9	0.83
24.4	0.60	22.5	0.0%	0.100	386.4	239.0	0.9	1.94	2.85	0.097	4.16	94.1	0.94
36.7	0.58	22.4	0.0%	0.100	385.6	221.5	0.9	1.93	2.85	0.108	4.16	105.1	1.05
48.9	0.60	22.4	0.0%	0.101	387.5	211.6	0.9	1.93	2.84	0.121	4.16	117.8	1.18
61.1	0.60	21.9	0.0%	0.101	387.1	203.0	0.9	1.91	2.81	0.128	4.15	125.9	1.26
73.3	0.60	22.3	0.0%	0.101	387.4	195.9	0.9	1.92	2.83	0.137	4.16	133.9	1.34
6.1	0.99	25.7	0.0%	0.099	371.2	293.0	0.9	2.11	3.11	0.078	4.37	71.6	0.72
12.2	0.99	25.8	0.0%	0.099	371.0	282.1	0.9	2.11	3.12	0.090	4.37	82.7	0.83
24.4	0.99	25.9	0.0%	0.099	371.6	271.2	0.9	2.12	3.13	0.104	4.38	94.9	0.95
36.7	0.99	26.0	0.0%	0.099	371.6	261.0	0.9	2.13	3.14	0.117	4.39	106.1	1.06
48.9	0.99	26.2	0.0%	0.100	371.1	250.7	0.9	2.14	3.16	0.129	4.42	117.0	1.17
61.1	0.99	26.7	0.0%	0.101	371.0	241.1	0.9	2.16	3.20	0.142	4.47	126.6	1.27
73.3	0.99	26.4	0.0%	0.100	371.1	235.5	0.9	2.15	3.17	0.150	4.43	135.3	1.35
6.1	1.48	23.7	0.0%	0.096	389.5	338.9	0.9	2.01	2.95	0.069	4.17	67.0	0.67
12.2	1.48	23.6	0.0%	0.096	386.6	329.5	0.9	2.00	2.94	0.079	4.16	77.0	0.77
24.4	1.48	23.6	0.0%	0.096	387.1	319.8	0.9	2.00	2.94	0.095	4.16	91.9	0.92
36.7	1.48	23.6	0.0%	0.096	386.4	311.6	0.9	2.00	2.94	0.107	4.16	103.5	1.04
48.9	1.49	23.7	0.0%	0.097	381.3	299.5	0.9	2.00	2.94	0.120	4.17	115.9	1.16
61.1	1.48	23.8	0.0%	0.098	385.8	296.2	0.9	2.01	2.96	0.131	4.21	125.0	1.25
73.4	1.49	23.8	0.0%	0.097	386.1	289.4	0.9	2.01	2.95	0.143	4.18	138.0	1.38
36.7	1.98	22.8	0.0%	0.097	384.0	325.1	0.9	1.96	2.87	0.110	4.13	108.0	1.08
36.7	2.47	22.9	0.0%	0.098	384.3	336.1	0.9	1.96	2.88	0.110	4.15	107.9	1.08

C.2.3 k_L Data

Table C.4: Experimental AWC data (k_L)

L	G	T_{sys}	Glycerol	Offline μ_L	Offline ρ_L	$D_{Toluene}$	Toluene In	Toluene Out	k_La	measured a_e	k_L (before packing height correction)
$m^3/m^2 \cdot h$	m/s	°C	wt frac	mPa·s	kg/m^3	m^2/s	ppm	ppm	s^{-1}	m2/m3	m/s
MG 64Y		Z = 2.1 m		SRP1502		06/10-12/2015					
6.1	1.0	25.4	0.00	0.9	996.8	9.73E-10	228.8	2.8	0.0035	67.1	5.21E-05
12.2	1.0	25.3	0.00	0.9	996.8	9.70E-10	151.7	3.5	0.0060	72.3	8.28E-05
24.5	1.0	27.0	0.00	0.9	996.3	1.02E-09	35.2	1.7	0.0096	78.1	1.23E-04
36.7	1.0	27.0	0.00	0.9	996.3	1.02E-09	62.0	5.1	0.0119	84.3	1.41E-04
48.9	1.0	24.4	0.00	0.9	997.0	9.49E-10	193.7	19.4	0.0146	90.7	1.61E-04
61.1	1.0	24.5	0.00	0.9	997.0	9.51E-10	339.4	53.1	0.0147	94.9	1.55E-04
73.3	1.0	24.6	0.00	0.9	997.0	9.53E-10	185.7	30.2	0.0173	98.9	1.75E-04
M 125Y		Z = 2.9 m		SRP1610		05/26/2016					
12.2	1.0	29.4	0.00	0.8	995.7	1.08E-09	107.9	0.5	0.0062	118.0	5.28E-05
24.4	1.0	29.2	0.00	0.8	995.7	1.07E-09	88.7	0.7	0.0109	128.5	8.50E-05
36.7	1.0	26.6	0.00	0.9	996.4	1.00E-09	128.7	2.1	0.0140	135.6	1.04E-04
48.9	1.0	27.1	0.00	0.9	996.3	1.02E-09	114.0	2.9	0.0167	142.0	1.18E-04
61.1	1.0	27.8	0.00	0.8	996.1	1.04E-09	45.5	1.5	0.0197	149.1	1.32E-04
73.3	1.0	28.5	0.00	0.8	995.9	1.06E-09	97.0	4.7	0.0208	157.3	1.32E-04

M 125Y		Z = 2.9 m		SRP161101		06/01/2016					
12.4	1.0	32.1	0.78	28.1	1204.6	9.26E-11	159.3	116.6	0.0004	118.0	3.05E-06
24.4	1.0	32.2	0.78	29.0	1204.6	9.08E-11	147.4	116.7	0.0005	128.5	4.15E-06
36.7	1.0	29.5	0.78	31.0	1204.1	8.43E-11	99.6	75.0	0.0010	135.6	7.19E-06
48.9	1.0	30.4	0.78	30.1	1204.1	8.69E-11	121.3	91.7	0.0013	142.0	9.00E-06
61.0	1.0	31.4	0.78	28.4	1204.1	9.13E-11	86.9	66.6	0.0015	149.1	1.02E-05
M 125Y		Z = 2.9 m		SRP161102		06/03/2016					
12.4	1.0	29.1	0.64	12.7	1168.9	1.57E-10	47.1	31.4	0.0005	118.0	3.96E-06
24.4	1.0	29.2	0.64	12.5	1168.9	1.59E-10	107.0	72.7	0.0009	128.5	6.86E-06
36.6	1.0	28.5	0.64	12.1	1167.2	1.61E-10	210.9	142.1	0.0014	135.6	9.96E-06
49.0	1.0	28.7	0.64	12.3	1167.7	1.60E-10	101.8	70.6	0.0017	142.0	1.18E-05
60.9	1.0	29.0	0.64	12.3	1168.2	1.60E-10	64.9	43.3	0.0023	149.1	1.55E-05
M 125Y		Z = 2.9 m		SRP161103		06/07/2016					
12.2	1.0	29.9	0.43	4.9	1111.4	3.07E-10	70.6	21.8	0.0013	118.0	1.14E-05
24.5	1.0	29.0	0.43	5.0	1111.4	3.02E-10	322.7	120.1	0.0023	128.5	1.76E-05
36.7	1.0	27.4	0.42	5.0	1109.3	2.97E-10	40.5	17.0	0.0030	135.6	2.20E-05
48.9	1.0	28.3	0.42	4.9	1109.9	3.02E-10	46.6	19.5	0.0040	142.0	2.80E-05
61.1	1.0	28.6	0.42	4.9	1110.5	3.02E-10	94.5	39.7	0.0049	149.1	3.32E-05
M 250X		Z = 1.8 m		SRP160401		03/28/2016					
12.2	1.0	21.9	0.00	1.0	997.6	8.86E-10	357.3	2.6	0.0093	197.3	4.71E-05
24.4	1.0	21.4	0.00	1.0	997.7	8.73E-10	110.7	3.1	0.0135	217.0	6.20E-05
36.7	1.0	21.3	0.00	1.0	997.7	8.73E-10	75.2	3.2	0.0178	231.1	7.70E-05

48.9	1.0	21.1	0.00	1.0	997.8	8.67E-10	44.3	3.5	0.0190	245.3	7.77E-05
61.1	1.0	21.3	0.00	1.0	997.7	8.71E-10	164.5	15.1	0.0224	254.5	8.81E-05
73.3	1.0	21.4	0.00	1.0	997.7	8.75E-10	81.0	9.1	0.0247	268.7	9.19E-05
M 250X		Z = 2.9 m		SRP160402		03/30/2016					
12.2	1.0	20.9	0.00	1.0	997.8	8.61E-10	116.4	0.5	0.0063	197.3	3.17E-05
24.5	1.0	21.1	0.00	1.0	997.8	8.68E-10	149.1	1.2	0.0111	217.0	5.12E-05
36.7	1.0	22.0	0.00	1.0	997.6	8.90E-10	119.4	1.5	0.0152	231.1	6.58E-05
48.9	1.0	21.3	0.00	1.0	997.7	8.72E-10	104.5	3.5	0.0157	245.3	6.39E-05
61.1	1.0	21.5	0.00	1.0	997.7	8.78E-10	131.7	4.3	0.0197	254.5	7.74E-05
73.4	1.0	21.9	0.00	1.0	997.6	8.86E-10	119.1	5.6	0.0211	268.7	7.87E-05
M 250X		Z = 2.9 m		SRP160501		04/11/2016					
12.4	1.0	26.5	0.79	44.3	1207.3	6.37E-11	165.8	123.0	0.0003	197.3	1.77E-06
24.5	1.0	29.0	0.78	37.7	1205.6	7.31E-11	76.6	46.5	0.0012	217.0	5.32E-06
36.7	1.0	30.7	0.78	34.3	1204.2	7.96E-11	39.1	26.2	0.0014	231.1	6.05E-06
48.9	1.0	31.3	0.77	32.6	1203.7	8.30E-11	54.3	36.0	0.0019	245.3	7.76E-06
60.3	0.6	32.5	0.77	32.6	1203.2	8.39E-11	49.7	35.4	0.0019	231.1	8.32E-06
M 250X		Z = 2.9 m		SRP160502		04/13/2016					
12.1	1.0	20.9	0.69	21.2	1181.8	1.00E-10	231.2	97.7	0.0010	197.3	5.01E-06
24.5	1.0	21.8	0.69	20.3	1181.3	1.05E-10	111.9	53.8	0.0017	217.0	7.80E-06
36.7	1.0	22.1	0.69	19.9	1180.9	1.07E-10	113.5	56.8	0.0024	231.1	1.04E-05
48.9	1.0	22.4	0.69	19.4	1181.1	1.09E-10	92.1	45.7	0.0032	245.3	1.32E-05
60.1	1.0	23.7	0.69	18.7	1180.6	1.13E-10	55.7	33.8	0.0028	254.5	1.12E-05

M 250X		Z = 2.9 m		SRP160503		04/15/2016					
12.2	1.0	20.4	0.47	5.3	1122.1	2.62E-10	236.3	51.0	0.0018	197.3	8.95E-06
24.5	1.0	20.8	0.47	5.3	1122.3	2.63E-10	55.8	17.7	0.0027	217.0	1.23E-05
36.8	1.0	25.4	0.47	4.8	1122.3	2.98E-10	147.6	54.6	0.0035	231.1	1.50E-05
48.9	1.0	24.4	0.47	4.9	1122.2	2.90E-10	66.5	21.9	0.0051	245.3	2.09E-05
61.1	1.0	24.8	0.47	4.8	1122.2	2.97E-10	77.5	29.4	0.0056	254.5	2.20E-05
M 250Y		Z = 1.9 m		SRP160601		04/22/2016					
12.2	1.0	26.1	0.00	0.9	996.6	9.91E-10	119.6	3.0	0.0065	213.7	3.06E-05
24.4	1.0	25.8	0.00	0.9	996.6	9.85E-10	61.5	3.1	0.0106	240.9	4.39E-05
36.7	1.0	25.9	0.00	0.9	996.6	9.88E-10	55.3	3.8	0.0143	253.6	5.65E-05
48.9	1.0	26.7	0.00	0.9	996.4	1.01E-09	82.7	8.9	0.0158	258.9	6.11E-05
61.1	1.0	26.0	0.00	0.9	996.6	9.90E-10	116.8	13.2	0.0194	277.2	7.00E-05
73.3	1.0	26.2	0.00	0.9	996.5	9.96E-10	161.0	18.0	0.0234	295.8	7.90E-05
M 250Y		Z = 2.9 m		SRP160602		04/26/2016					
12.2	1.0	24.9	0.00	0.9	996.9	9.61E-10	211.1	1.0	0.0061	213.7	2.83E-05
24.4	1.0	24.9	0.00	0.9	996.9	9.62E-10	64.6	0.7	0.0103	240.9	4.30E-05
36.7	1.0	26.7	0.00	0.9	996.4	1.01E-09	95.7	2.6	0.0123	253.6	4.87E-05
48.9	1.0	25.3	0.00	0.9	996.8	9.73E-10	54.5	1.5	0.0164	258.9	6.34E-05
61.1	1.0	25.7	0.00	0.9	996.7	9.82E-10	186.4	7.5	0.0183	277.2	6.61E-05
73.3	1.0	26.1	0.00	0.9	996.6	9.93E-10	194.6	8.6	0.0214	295.8	7.22E-05
M 250Y		Z = 2.9 m		SRP160701		04/27/2016					
11.8	1.0	29.7	0.77	37.2	1203.1	7.43E-11	60.6	44.8	0.0003	213.7	1.56E-06

24.4	1.0	29.1	0.76	34.9	1201.1	7.73E-11	92.2	62.1	0.0009	240.9	3.73E-06
36.7	1.0	29.1	0.78	39.1	1204.4	7.14E-11	148.1	106.5	0.0011	253.6	4.45E-06
49.0	0.6	30.1	0.77	34.9	1202.1	7.80E-11	74.3	55.2	0.0014	238.6	5.68E-06
60.8	0.6	30.7	0.77	33.6	1201.9	8.07E-11	53.9	44.5	0.0011	248.5	4.41E-06
M 250Y		Z = 2.9 m		SRP160702		04/28/2016					
12.2	1.0	30.1	0.66	13.3	1172.5	1.54E-10	63.5	34.1	0.0007	213.7	3.32E-06
24.4	1.0	30.5	0.66	13.2	1173.1	1.55E-10	73.8	44.5	0.0012	240.9	4.79E-06
36.7	1.0	30.4	0.66	13.6	1173.7	1.51E-10	154.5	98.8	0.0015	253.6	6.04E-06
49.0	0.6	30.1	0.66	13.6	1173.8	1.51E-10	94.7	58.3	0.0022	238.6	9.29E-06
61.1	0.6	30.3	0.66	13.2	1173.8	1.55E-10	100.2	70.4	0.0020	248.5	8.10E-06
M 250Y		Z = 2.9 m		SRP160703		04/29/2016					
12.2	1.0	26.8	0.46	4.4	1120.3	3.20E-10	129.9	36.1	0.0015	213.7	6.85E-06
24.4	1.0	26.9	0.46	4.4	1120.4	3.22E-10	89.5	30.4	0.0025	240.9	1.02E-05
36.7	1.0	27.0	0.46	4.3	1120.4	3.25E-10	86.8	29.2	0.0037	253.6	1.47E-05
48.9	0.6	28.2	0.46	4.3	1120.1	3.34E-10	80.4	24.5	0.0054	238.6	2.28E-05
61.1	0.6	27.9	0.46	4.3	1120.1	3.31E-10	46.7	20.4	0.0047	248.5	1.90E-05
GTO 250Y		Z = 1.9 m		SRP1501		04/22/2016					
6.2	1.0	20.0	0.00	1.0	998.0	8.40E-10	137.0	0.1	0.0062	188.9	3.28E-05
12.2	1.0	24.0	0.00	0.9	997.1	9.38E-10	61.3	0.1	0.0109	205.3	5.31E-05
24.5	1.0	23.7	0.00	0.9	997.2	9.30E-10	30.7	0.3	0.0155	211.1	7.35E-05
36.7	1.0	20.9	0.00	1.0	997.8	8.61E-10	56.1	1.3	0.0195	222.8	8.77E-05
48.9	1.0	23.6	0.00	0.9	997.2	9.28E-10	107.5	2.8	0.0252	249.9	1.01E-04

61.1	1.0	23.9	0.00	0.9	997.1	9.37E-10	133.6	5.1	0.0282	272.0	1.04E-04
GTO 250Y		Z = 3.0 m		SRP150401		11/19/2015					
12.2	1.0	25.2	0.00	0.9	996.8	9.68E-10	202.9	1.0	0.0059	192.9	3.08E-05
24.4	1.0	24.4	0.00	0.9	997.0	9.48E-10	195.5	2.7	0.0095	215.3	4.42E-05
36.7	1.0	23.9	0.00	0.9	997.1	9.37E-10	181.3	1.3	0.0165	235.8	7.00E-05
48.9	1.0	23.3	0.00	0.9	997.3	9.21E-10	54.2	1.4	0.0163	260.6	6.25E-05
61.1	1.0	24.0	0.00	0.9	997.1	9.38E-10	62.7	0.5	0.0273	285.6	9.56E-05
GTO 250Y		Z = 3.0 m		SRP150402		11/23/2015					
12.2	1.0	16.8	0.00	1.1	998.6	7.67E-10	191.0	0.8	0.0061	192.9	3.18E-05
24.5	1.0	17.1	0.00	1.1	998.6	7.74E-10	349.8	2.6	0.0109	215.3	5.05E-05
36.7	1.0	16.1	0.00	1.1	998.8	7.50E-10	133.4	1.8	0.0143	235.8	6.08E-05
48.9	1.0	15.9	0.00	1.1	998.8	7.45E-10	251.1	6.6	0.0161	260.6	6.18E-05
61.1	1.0	15.9	0.00	1.1	998.8	7.47E-10	58.2	0.8	0.0234	285.6	8.21E-05
GTO 250Y		Z = 3.0 m		SRP150302		08/13-18/2015					
6.2	0.6	31.4	0.84	51.4	1222.6	6.04E-11	83.4	42.4	0.0004	188.9	2.00E-06
12.2	0.6	31.4	0.84	53.6	1222.6	5.85E-11	89.0	49.3	0.0006	205.3	3.16E-06
18.4	0.6	29.1	0.84	55.2	1222.4	5.61E-11	166.4	94.5	0.0009	208.2	4.50E-06
24.5	0.6	40.9	0.85	40.0	1223.0	7.86E-11	251.1	160.7	0.0010	211.1	4.67E-06
30.6	0.6	30.0	0.84	51.4	1222.2	5.95E-11	93.2	61.7	0.0011	216.9	5.25E-06
36.7	0.6	30.3	0.85	58.9	1223.2	5.42E-11	259.2	180.3	0.0012	222.8	5.39E-06
42.8	0.6	31.3	0.84	48.1	1221.6	6.31E-11	103.4	69.9	0.0015	236.3	6.38E-06

48.8	0.6	33.9	0.84	46.9	1222.4	6.59E-11	274.1	184.8	0.0017	249.9	6.95E-06
24.5	1.0	36.0	0.85	44.8	1223.6	6.95E-11	49.4	32.2	0.0009	211.1	4.47E-06
GTO 250Y		Z = 3.0 m		SRP150303		08/20/2015					
6.1	0.6	28.5	0.64	12.1	1168.6	1.62E-10	85.9	11.7	0.0011	188.9	5.83E-06
12.2	0.6	27.1	0.64	12.1	1168.2	1.59E-10	34.6	9.1	0.0015	205.3	7.12E-06
18.3	0.6	26.8	0.64	12.0	1168.7	1.59E-10	24.3	9.4	0.0016	208.2	7.55E-06
24.4	0.6	26.9	0.64	12.2	1168.3	1.58E-10	41.6	15.7	0.0021	211.1	1.01E-05
30.6	0.6	27.5	0.64	12.1	1168.8	1.60E-10	33.5	13.0	0.0026	216.9	1.21E-05
36.7	0.6	27.2	0.64	12.3	1168.4	1.57E-10	137.4	64.4	0.0025	222.8	1.13E-05
42.8	0.6	28.2	0.64	12.0	1168.8	1.62E-10	52.6	24.5	0.0029	236.3	1.24E-05
49.0	0.6	27.5	0.64	12.2	1168.5	1.58E-10	252.7	109.8	0.0037	249.9	1.48E-05
61.3	0.6	28.3	0.64	12.0	1168.6	1.62E-10	107.2	44.2	0.0049	272.0	1.80E-05
GTO 250Y		Z = 3.0 m		SRP150304		08/25/2015					
6.1	0.6	34.5	0.43	4.5	1111.2	3.43E-10	218.9	5.4	0.0020	188.9	1.08E-05
12.2	0.6	31.3	0.42	4.6	1109.6	3.28E-10	63.9	5.7	0.0027	205.3	1.30E-05
24.4	0.6	31.7	0.42	4.6	1109.9	3.30E-10	49.9	10.2	0.0035	211.1	1.65E-05
36.7	0.6	32.4	0.42	4.5	1110.2	3.34E-10	96.7	20.2	0.0052	222.8	2.32E-05
48.8	0.6	33.2	0.42	4.5	1110.5	3.37E-10	20.8	5.1	0.0062	249.9	2.48E-05
61.1	0.6	34.0	0.42	4.4	1110.8	3.43E-10	56.0	10.8	0.0091	272.0	3.34E-05
36.7	1.0	34.0	0.43	4.5	1111.7	3.39E-10	37.5	7.5	0.0053	222.8	2.40E-05
GTO 250Y		Z = 3.0 m		SRP160101		01/13/2016					
6.3	0.6	20.1	0.77	44.9	1203.2	5.88E-11	54.7	37.2	0.0002	170.0	1.29E-06

12.2	0.6	21.2	0.77	41.2	1201.8	6.34E-11	432.1	282.1	0.0005	161.3	2.91E-06
18.5	0.6	21.6	0.77	40.8	1202.7	6.41E-11	109.0	80.0	0.0005	178.4	2.89E-06
24.5	0.6	21.4	0.77	40.8	1202.2	6.39E-11	308.0	214.0	0.0008	164.1	4.91E-06
36.7	0.6	21.6	0.77	40.4	1202.4	6.44E-11	190.0	142.0	0.0010	210.5	4.58E-06
42.8	0.6	20.8	0.77	42.8	1203.0	6.13E-11	60.0	44.0	0.0012	225.2	5.31E-06
48.8	0.6	21.9	0.77	39.8	1202.6	6.54E-11	157.5	121.0	0.0012	222.6	5.22E-06
GTO 250Y		Z = 3.0 m		SRP160102		01/14/2016					
12.1	0.6	19.5	0.65	15.6	1170.3	1.23E-10	215.0	49.0	0.0016	159.7	1.01E-05
24.5	0.6	19.9	0.65	15.3	1170.2	1.25E-10	280.5	108.5	0.0021	170.5	1.23E-05
36.7	0.6	20.6	0.64	14.8	1169.5	1.28E-10	134.4	47.0	0.0035	210.6	1.65E-05
48.9	0.6	19.3	0.65	15.8	1170.5	1.21E-10	149.5	69.8	0.0034	229.8	1.46E-05
61.1	0.6	19.2	0.65	16.0	1170.7	1.20E-10	132.3	75.6	0.0031	240.2	1.28E-05
GTO 250Y		Z = 3.0 m		SRP160103		01/19/2016					
12.2	0.6	24.2	0.45	4.1	1118.4	3.29E-10	206.3	40.3	0.0018	147.9	1.22E-05
24.4	0.6	17.7	0.46	5.4	1120.5	2.53E-10	193.0	59.0	0.0026	166.2	1.57E-05
36.7	0.6	22.5	0.45	4.4	1118.4	3.07E-10	198.1	58.2	0.0041	187.5	2.16E-05
48.9	0.6	18.4	0.46	5.2	1120.6	2.60E-10	130.2	48.6	0.0043	218.1	1.99E-05
61.1	0.6	19.1	0.46	5.2	1120.8	2.64E-10	165.3	69.0	0.0048	218.7	2.20E-05
GTO 250Y		Z = 3.0 m		SRP160201		02/01/2016					
6.1	0.6	21.3	0.80	57.0	1210.5	5.05E-11	337.7	175.9	0.0004	146.4	2.44E-06
12.0	0.6	22.5	0.80	52.7	1210.5	5.40E-11	167.4	98.2	0.0006	157.4	3.67E-06
24.5	0.6	23.4	0.80	49.9	1210.5	5.67E-11	86.5	51.0	0.0012	186.0	6.27E-06

36.7	0.6	24.0	0.80	48.2	1210.5	5.85E-11	46.0	30.0	0.0014	211.4	6.69E-06
48.9	0.6	24.5	0.80	46.9	1210.4	6.00E-11	84.6	49.6	0.0024	212.7	1.11E-05
GTO 250Y		Z = 3.0 m		SRP160202		02/02/2016					
6.1	0.6	22.2	0.64	13.4	1168.3	1.41E-10	147.3	27.4	0.0009	144.2	6.43E-06
12.1	0.6	20.6	0.64	14.1	1167.0	1.33E-10	329.8	133.2	0.0010	152.3	6.52E-06
24.5	0.6	20.5	0.64	14.1	1167.3	1.33E-10	229.8	103.0	0.0018	169.6	1.04E-05
36.7	0.6	20.7	0.64	14.2	1167.6	1.33E-10	82.8	35.2	0.0028	209.1	1.36E-05
48.9	0.6	21.2	0.64	13.8	1167.9	1.36E-10	15.4	7.9	0.0030	217.0	1.36E-05
61.1	0.6	21.7	0.64	13.5	1168.1	1.39E-10	122.7	69.7	0.0031	225.4	1.38E-05
GTO 250Y		Z = 3.0 m		SRP160203		02/03/2016					
6.1	0.6	17.0	0.41	4.4	1106.4	2.89E-10	315.4	31.3	0.0013	153.1	8.30E-06
12.2	0.6	15.7	0.41	4.6	1106.2	2.78E-10	128.1	35.7	0.0014	160.5	8.79E-06
24.4	0.6	16.0	0.41	4.5	1106.3	2.82E-10	59.4	26.7	0.0018	184.5	9.55E-06
36.7	0.6	16.1	0.41	4.5	1106.3	2.83E-10	36.3	14.3	0.0031	216.9	1.41E-05
48.9	0.6	16.4	0.41	4.4	1106.4	2.85E-10	75.5	28.4	0.0043	217.7	1.98E-05
61.1	0.6	16.7	0.41	4.4	1106.4	2.87E-10	163.0	57.2	0.0058	221.2	2.61E-05
B1 250MN		Z = 1.8 m		SRP161601		10/07/2016					
6.1	1.0	27.9	0.00	0.8	996.1	1.04E-09	49.4	0.3	0.0048	222.3	2.16E-05
12.2	1.0	27.3	0.00	0.8	996.3	1.02E-09	82.4	0.8	0.0085	239.1	3.55E-05
24.5	1.0	28.2	0.00	0.8	996.0	1.05E-09	48.4	0.7	0.0154	260.2	5.93E-05
36.7	1.0	25.9	0.00	0.9	996.6	9.86E-10	164.7	3.7	0.0210	273.8	7.66E-05
48.9	1.0	26.4	0.00	0.9	996.5	9.99E-10	119.7	4.3	0.0245	281.5	8.71E-05

61.1	1.0	27.5	0.00	0.8	996.2	1.03E-09	98.1	3.4	0.0309	286.5	1.08E-04
73.3	1.0	28.3	0.00	0.8	996.0	1.05E-09	89.7	4.3	0.0337	289.5	1.16E-04
B1 250MN		Z = 3.0 m		SRP161602		10/25/2016					
6.1	1.0	23.6	0.00	0.9	997.2	9.30E-10	82.1	0.3	0.0032	222.3	1.43E-05
12.2	1.0	23.6	0.00	0.9	997.2	9.29E-10	87.9	0.3	0.0061	239.1	2.57E-05
24.4	1.0	23.7	0.00	0.9	997.2	9.31E-10	58.6	0.4	0.0110	260.2	4.25E-05
36.7	1.0	24.6	0.00	0.9	997.0	9.53E-10	140.3	1.2	0.0157	273.8	5.74E-05
48.9	1.0	24.1	0.00	0.9	997.1	9.42E-10	119.6	1.8	0.0186	281.5	6.60E-05
61.1	1.0	23.7	0.00	0.9	997.2	9.32E-10	83.5	1.5	0.0223	286.5	7.78E-05
73.3	1.0	23.7	0.00	0.9	997.2	9.31E-10	49.2	1.0	0.0262	289.5	9.05E-05
B1 250MN		Z = 3.0 m		SRP161701		10/28/2016					
6.1	1.0	29.9	0.80	40.0	1211.0	7.08E-11	82.1	51.8	0.0003	222.3	1.15E-06
12.2	1.0	29.9	0.80	40.0	1211.1	7.08E-11	101.5	64.8	0.0005	239.1	2.08E-06
24.5	1.0	30.0	0.80	39.8	1211.1	7.11E-11	120.2	80.8	0.0009	260.2	3.39E-06
36.6	1.0	30.2	0.80	37.2	1210.9	7.48E-11	134.8	93.4	0.0012	273.8	4.46E-06
48.9	0.7	27.9	0.80	43.5	1211.1	6.54E-11	136.1	95.4	0.0016	281.5	5.59E-06
61.1	0.6	29.4	0.80	40.8	1211.1	6.95E-11	69.9	48.7	0.0020	286.5	6.99E-06
B1 250MN		Z = 3.0 m		SRP161702		11/01/2016					
6.1	1.0	30.4	0.68	14.9	1179.8	1.42E-10	60.4	23.8	0.0005	222.3	2.32E-06
12.3	1.0	30.2	0.68	14.9	1179.4	1.42E-10	87.4	48.4	0.0007	239.1	2.75E-06
24.4	1.0	29.8	0.68	14.9	1179.2	1.41E-10	115.5	68.2	0.0012	260.2	4.48E-06
36.7	1.0	26.4	0.68	16.7	1179.0	1.26E-10	157.8	98.7	0.0016	273.8	5.70E-06

48.9	1.0	28.4	0.68	15.5	1179.0	1.36E-10	151.4	93.3	0.0022	281.5	7.64E-06
61.1	0.8	29.1	0.68	15.3	1179.0	1.37E-10	87.0	51.6	0.0029	286.5	1.01E-05
B1 250MN		Z = 3.0 m		SRP161703		11/02/2016					
6.1	1.0	28.3	0.47	5.6	1123.5	2.74E-10	53.8	5.8	0.0012	222.3	5.58E-06
12.2	1.0	28.4	0.47	5.6	1123.2	2.77E-10	61.9	13.8	0.0017	239.1	6.97E-06
24.4	1.0	28.3	0.47	5.5	1122.8	2.79E-10	84.4	34.4	0.0020	260.2	7.65E-06
36.7	1.0	27.0	0.47	5.7	1122.2	2.69E-10	181.5	86.0	0.0025	273.8	9.08E-06
48.9	1.0	27.6	0.47	5.5	1122.2	2.76E-10	181.2	84.8	0.0034	281.5	1.20E-05
61.1	0.9	28.0	0.47	5.6	1122.3	2.75E-10	144.2	64.5	0.0045	286.5	1.56E-05
GTP 350Y		Z = 1.7 m		SRP160801		05/09/2016					
12.2	1.0	23.9	0.00	0.9	997.1	9.36E-10	236.8	2.1	0.0092	255.9	3.61E-05
24.4	1.0	24.1	0.00	0.9	997.1	9.41E-10	105.5	4.8	0.0121	272.1	4.44E-05
36.7	1.0	24.6	0.00	0.9	997.0	9.53E-10	73.0	4.5	0.0164	282.3	5.80E-05
48.9	1.0	25.4	0.00	0.9	996.8	9.73E-10	80.6	7.6	0.0185	290.0	6.39E-05
61.1	1.0	25.9	0.00	0.9	996.6	9.88E-10	106.9	9.2	0.0241	315.3	7.65E-05
73.3	0.6	26.5	0.00	0.9	996.5	1.00E-09	197.6	30.0	0.0222	303.6	7.31E-05
GTP 350Y		Z = 3.0 m		SRP160802		05/11/2016					
12.2	1.0	24.1	0.00	0.9	997.1	9.41E-10	131.9	0.5	0.0062	255.9	2.43E-05
24.4	1.0	24.4	0.00	0.9	997.0	9.48E-10	123.7	1.0	0.0108	272.1	3.98E-05
36.7	1.0	24.9	0.00	0.9	996.9	9.61E-10	147.4	1.9	0.0147	282.3	5.22E-05
48.9	1.0	25.5	0.00	0.9	996.7	9.76E-10	153.9	3.3	0.0174	290.0	5.99E-05
61.1	1.0	26.2	0.00	0.9	996.5	9.96E-10	76.0	1.3	0.0230	315.3	7.28E-05

73.4	0.6	26.8	0.00	0.9	996.4	1.01E-09	321.9	14.3	0.0211	303.6	6.95E-05
GTP 350Y		Z = 3.0 m		SRP160901		05/12&13/2016					
6.1	0.6	28.0	0.75	31.7	1198.2	8.17E-11	207.0	94.0	0.0004	236.1	1.88E-06
12.1	0.6	29.3	0.75	30.6	1198.0	8.48E-11	154.6	87.2	0.0006	251.0	2.56E-06
18.5	0.6	28.8	0.75	29.7	1197.8	8.63E-11	92.2	60.3	0.0007	258.1	2.82E-06
24.3	0.6	28.2	0.75	32.2	1197.8	8.09E-11	258.9	163.4	0.0010	265.2	3.90E-06
36.7	0.6	29.5	0.75	29.3	1196.8	8.78E-11	185.0	131.2	0.0012	281.4	4.15E-06
48.9	0.6	31.5	0.74	28.3	1195.9	9.17E-11	72.8	51.8	0.0015	278.5	5.55E-06
GTP 350Y		Z = 3.0 m		SRP160902		05/16/2016					
6.1	0.6	26.1	0.62	12.4	1162.9	1.54E-10	35.1	10.1	0.0007	236.1	2.98E-06
12.2	0.6	25.5	0.62	13.0	1163.2	1.49E-10	66.7	28.2	0.0010	251.0	3.87E-06
24.4	0.6	26.5	0.62	13.1	1163.0	1.49E-10	38.9	17.1	0.0019	265.2	7.00E-06
36.6	0.6	26.6	0.62	12.8	1162.7	1.52E-10	211.7	86.6	0.0030	281.4	1.08E-05
48.8	0.6	26.3	0.62	12.9	1162.8	1.51E-10	92.8	41.9	0.0036	278.5	1.29E-05
GTP 350Y		Z = 3.0 m		SRP160903		05/17/2016					
6.1	0.6	27.9	0.46	5.9	1119.0	2.63E-10	61.2	5.7	0.0013	236.1	5.69E-06
12.2	0.6	24.8	0.45	6.1	1118.7	2.50E-10	151.3	39.0	0.0015	251.0	6.10E-06
24.4	0.6	26.2	0.45	6.0	1118.4	2.56E-10	93.9	27.2	0.0028	265.2	1.05E-05
36.7	0.6	27.6	0.45	5.9	1118.0	2.63E-10	234.3	80.8	0.0036	281.4	1.28E-05
48.9	0.6	27.9	0.45	5.9	1117.6	2.64E-10	132.5	44.8	0.0049	278.5	1.76E-05
GTP 500Y		Z = 1.8 m		SRP161201		06/12/2016					

6.2	0.6	30.7	0.00	0.8	995.3	1.12E-09	209.1	0.7	0.0052	277.5	1.86E-05
12.2	0.6	30.4	0.00	0.8	995.4	1.11E-09	266.2	1.5	0.0094	301.3	3.12E-05
24.4	0.6	30.1	0.00	0.8	995.4	1.10E-09	211.2	1.8	0.0173	322.0	5.37E-05
36.7	0.6	29.8	0.00	0.8	995.5	1.09E-09	253.4	5.8	0.0207	339.6	6.09E-05
48.9	0.6	29.2	0.00	0.8	995.7	1.08E-09	68.0	1.8	0.0264	348.5	7.57E-05
61.1	0.6	28.7	0.00	0.8	995.8	1.06E-09	201.9	9.4	0.0280	347.4	8.05E-05
GTP 500Y		Z = 2.9 m		SRP161202		06/14/2016					
6.1	0.6	30.9	0.00	0.8	995.2	1.12E-09	121.9	0.8	0.0030	277.5	1.07E-05
12.2	0.6	30.6	0.00	0.8	995.3	1.11E-09	149.7	0.8	0.0062	301.3	2.06E-05
24.5	0.6	30.3	0.00	0.8	995.4	1.10E-09	164.6	0.6	0.0133	322.0	4.13E-05
36.7	0.6	28.8	0.00	0.8	995.8	1.06E-09	69.9	0.5	0.0173	339.6	5.11E-05
48.9	0.6	30.0	0.00	0.8	995.5	1.10E-09	101.0	0.9	0.0221	348.5	6.34E-05
61.1	0.6	29.4	0.00	0.8	995.7	1.08E-09	139.5	2.5	0.0235	347.4	6.75E-05
GTP 500Y		Z = 2.9 m		SRP161301		06/16/2016					
6.1	0.6	35.4	0.79	32.7	1207.6	8.60E-11	55.6	28.4	0.0004	277.5	1.41E-06
12.2	0.6	35.4	0.79	30.7	1207.4	8.99E-11	78.1	43.2	0.0007	301.3	2.30E-06
18.0	0.6	35.2	0.79	29.4	1207.3	9.26E-11	87.7	53.3	0.0009	311.6	2.76E-06
24.5	0.6	31.2	0.79	28.2	1206.9	9.16E-11	228.3	129.3	0.0013	322.0	4.14E-06
30.6	0.6	32.6	0.79	29.0	1207.0	9.11E-11	162.6	96.0	0.0015	330.8	4.67E-06
36.7	0.6	34.0	0.79	28.8	1207.0	9.28E-11	97.4	57.7	0.0018	339.6	5.43E-06
42.8	0.6	35.0	0.79	27.9	1207.1	9.58E-11	71.0	45.6	0.0018	344.0	5.27E-06
GTP 500Y		Z = 2.9 m		SRP161302		06/21/2016					

6.1	1.0	33.0	0.67	12.9	1176.7	1.61E-10	34.5	14.5	0.0005	269.5	1.89E-06
12.2	1.0	32.6	0.67	13.2	1176.1	1.58E-10	81.1	32.1	0.0011	288.9	3.75E-06
24.5	1.0	29.6	0.67	13.7	1175.0	1.50E-10	39.2	18.2	0.0018	317.6	5.66E-06
36.7	1.0	33.4	0.67	13.4	1177.2	1.57E-10	62.9	34.3	0.0021	331.8	6.41E-06
48.9	1.0	31.2	0.67	13.4	1175.5	1.54E-10	45.1	27.2	0.0024	345.0	6.84E-06
61.1	0.6	32.1	0.67	13.1	1175.8	1.58E-10	133.5	75.9	0.0033	347.4	9.51E-06
GTP 500Y		Z = 2.9 m		SRP161303		06/22/2016					
6.1	1.0	31.4	0.44	4.9	1114.4	3.12E-10	89.3	6.0	0.0016	269.5	5.85E-06
12.2	1.0	31.0	0.44	5.0	1114.4	3.09E-10	189.2	36.4	0.0019	288.9	6.68E-06
24.4	1.0	29.4	0.43	5.0	1113.4	3.02E-10	60.4	18.6	0.0028	317.6	8.68E-06
36.6	1.0	29.7	0.44	4.9	1113.8	3.05E-10	65.8	23.1	0.0037	331.8	1.10E-05
48.9	1.0	31.5	0.44	4.9	1114.6	3.15E-10	120.4	44.1	0.0047	345.0	1.36E-05
61.1	0.6	30.6	0.44	5.0	1114.1	3.07E-10	31.4	10.2	0.0066	347.4	1.89E-05
HFP 2		Z = 1.8 m		SRP1703		02/23/2017					
6.1	1.0	25.0	0.00	0.9	996.8	9.65E-10	110.9	6.9	0.0026	71.6	3.60E-05
12.2	1.0	24.8	0.00	0.9	996.9	9.58E-10	98.1	8.1	0.0046	82.7	5.61E-05
24.5	1.0	24.3	0.00	0.9	997.0	9.45E-10	87.6	11.1	0.0077	94.9	8.08E-05
36.7	1.0	21.4	0.00	1.0	997.7	8.74E-10	125.6	18.4	0.0107	106.1	1.01E-04
48.9	1.0	21.9	0.00	1.0	997.6	8.87E-10	180.0	32.9	0.0126	117.0	1.08E-04
61.1	1.0	22.6	0.00	0.9	997.4	9.05E-10	110.4	18.6	0.0166	126.6	1.31E-04
73.3	1.0	23.3	0.00	0.9	997.3	9.20E-10	104.9	19.0	0.0191	135.3	1.41E-04
RSP 250Y		Z = 1.9 m		SRP1701		01/20/2017					

6.1	1.0	19.4	0.00	1.0	998.1	8.27E-10	117.2	0.6	0.0048	216.1	2.22E-05
12.2	1.0	19.3	0.00	1.0	998.2	8.23E-10	83.0	1.1	0.0078	237.8	3.27E-05
24.4	1.0	19.0	0.00	1.0	998.2	8.18E-10	88.2	2.6	0.0127	259.0	4.88E-05
36.7	1.0	18.7	0.00	1.0	998.3	8.10E-10	202.2	11.5	0.0155	270.8	5.74E-05
48.9	1.0	18.2	0.00	1.1	998.4	7.98E-10	165.6	10.4	0.0200	271.6	7.36E-05
61.1	1.0	18.3	0.00	1.0	998.4	8.00E-10	76.2	6.5	0.0222	282.3	7.87E-05
73.3	1.0	18.7	0.00	1.0	998.3	8.09E-10	80.6	6.5	0.0273	293.0	9.30E-05
RSP 250Y		Z = 3.0 m		SRP170201		01/26/2017					
6.1	1.0	13.5	0.81	102.4	1212.7	3.07E-11	206.7	151.3	0.0002	216.1	8.03E-07
12.2	1.0	19.1	0.81	70.5	1212.4	4.24E-11	124.2	89.3	0.0004	237.8	1.54E-06
24.5	1.0	20.1	0.80	66.9	1212.1	4.45E-11	97.0	76.8	0.0005	259.0	2.00E-06
36.5	1.0	21.0	0.80	62.3	1211.7	4.73E-11	132.0	108.2	0.0007	270.8	2.43E-06
48.7	1.0	20.9	0.80	59.9	1210.7	4.86E-11	204.4	171.3	0.0008	271.6	2.88E-06
RSP 250Y		Z = 3.0 m		SRP170202		01/30/2017					
12.2	1.0	20.6	0.71	28.1	1187.8	8.23E-11	132.4	78.5	0.0006	237.8	2.44E-06
24.5	1.0	21.3	0.71	27.9	1188.1	8.32E-11	46.2	29.6	0.0010	259.0	3.81E-06
36.7	1.0	15.8	0.71	32.2	1185.7	7.08E-11	167.7	112.5	0.0013	270.8	4.91E-06
48.9	1.0	17.3	0.71	30.2	1186.2	7.54E-11	130.7	87.5	0.0018	271.6	6.56E-06
61.1	1.0	18.8	0.71	28.9	1186.7	7.90E-11	97.7	64.1	0.0023	282.3	8.28E-06
RSP 250Y		Z = 3.0 m		SRP170203		02/01/2017					
12.2	1.0	22.3	0.49	7.1	1128.9	2.20E-10	53.0	15.5	0.0014	237.8	5.75E-06
24.5	1.0	21.9	0.49	7.1	1128.6	2.19E-10	76.1	34.1	0.0018	259.0	6.88E-06

36.7	1.0	22.7	0.49	7.0	1129.2	2.24E-10	57.0	25.8	0.0026	270.8	9.77E-06
48.9	1.0	19.9	0.49	7.5	1128.3	2.07E-10	156.2	72.4	0.0034	271.6	1.26E-05
61.1	1.0	21.3	0.49	7.1	1128.5	2.17E-10	104.1	49.4	0.0041	282.3	1.47E-05
RSR 1.5		Z = 1.8 m		SRP161401		07/18/2016					
6.1	1.0	29.5	0.00	0.8	995.6	1.08E-09	142.3	1.0	0.0045	117.4	3.85E-05
12.2	1.0	28.8	0.00	0.8	995.8	1.06E-09	116.7	1.7	0.0078	129.3	6.00E-05
24.4	1.0	28.6	0.00	0.8	995.9	1.06E-09	81.7	2.6	0.0126	145.7	8.65E-05
36.7	1.0	28.0	0.00	0.8	996.0	1.04E-09	169.7	5.5	0.0189	153.3	1.23E-04
48.9	1.0	28.1	0.00	0.8	996.0	1.05E-09	154.9	6.9	0.0229	161.2	1.42E-04
61.1	1.0	28.2	0.00	0.8	996.0	1.05E-09	135.3	9.6	0.0243	172.0	1.41E-04
RSR 1.5		Z = 3.0 m		SRP161402		07/19/2016					
6.1	1.0	31.5	0.00	0.8	995.0	1.14E-09	67.3	0.4	0.0029	117.4	2.47E-05
12.2	1.0	31.4	0.00	0.8	995.1	1.13E-09	92.7	0.6	0.0056	129.3	4.31E-05
24.4	1.0	31.4	0.00	0.8	995.0	1.14E-09	106.8	0.8	0.0111	145.7	7.63E-05
36.7	1.0	31.3	0.00	0.8	995.1	1.13E-09	72.1	0.7	0.0157	153.3	1.03E-04
48.9	1.0	31.4	0.00	0.8	995.0	1.14E-09	133.4	1.9	0.0192	161.2	1.19E-04
61.1	1.0	31.1	0.00	0.8	995.1	1.13E-09	153.2	3.1	0.0218	172.0	1.27E-04
RSR 1.5		Z = 3.0 m		SRP161501		07/25/2016					
6.1	1.0	38.9	0.84	37.4	1220.5	8.09E-11	92.9	67.2	0.0002	117.4	1.55E-06
12.2	1.0	38.5	0.84	38.2	1220.4	7.94E-11	131.9	98.5	0.0003	129.3	2.53E-06
24.5	1.0	37.9	0.84	38.1	1220.4	7.91E-11	110.4	72.8	0.0009	145.7	6.44E-06
36.7	1.0	33.4	0.84	47.5	1220.6	6.50E-11	142.3	102.1	0.0011	153.3	7.29E-06

49.0	1.0	35.2	0.84	42.2	1220.4	7.19E-11	113.5	78.7	0.0016	161.2	1.02E-05
61.1	1.0	36.5	0.84	40.8	1220.2	7.45E-11	93.7	67.9	0.0018	172.0	1.05E-05
RSR 1.5		Z = 3.0 m		SRP161502		07/27/2016					
6.1	1.0	32.6	0.67	12.9	1177.0	1.61E-10	45.5	17.2	0.0005	117.4	4.66E-06
12.2	1.0	32.2	0.67	13.1	1177.0	1.58E-10	41.3	23.6	0.0006	129.3	4.87E-06
24.4	1.0	31.0	0.67	13.3	1177.0	1.55E-10	96.4	58.5	0.0011	145.7	7.70E-06
36.7	1.0	27.5	0.67	14.8	1177.5	1.39E-10	47.4	30.5	0.0015	153.3	9.69E-06
48.8	1.0	28.7	0.67	14.5	1177.3	1.42E-10	179.6	112.6	0.0021	161.2	1.30E-05
61.1	1.0	29.9	0.67	13.6	1177.0	1.51E-10	275.2	173.1	0.0026	172.0	1.51E-05
RSR 1.5		Z = 3.0 m		SRP161503		07/29/2016					
6.1	1.0	32.0	0.45	4.9	1117.6	3.13E-10	60.5	9.3	0.0011	117.4	8.94E-06
12.2	1.0	31.4	0.45	5.1	1117.6	3.05E-10	101.9	25.5	0.0016	129.3	1.20E-05
24.4	1.0	31.1	0.45	5.0	1117.6	3.07E-10	181.5	56.5	0.0026	145.7	1.80E-05
36.7	1.0	29.7	0.45	5.0	1116.8	3.05E-10	77.9	31.2	0.0031	153.3	2.01E-05
48.9	1.0	30.1	0.45	5.1	1117.2	3.01E-10	125.3	55.7	0.0036	161.2	2.26E-05
61.1	1.0	30.7	0.45	5.0	1117.5	3.04E-10	76.8	34.3	0.0045	172.0	2.63E-05

C.2.4 k_G Data

Table C.5: Experimental AWC data (k_G)

L	G	T_{sys}	D_{SO2}	ρ_{air}	μ_{air}	SO_2 In	SO_2 Out	$K_{OG}a$	measured a_e	kG
$m^3/m^2 \cdot h$	m/s	°C	m^2/s	kg/m^3	Pa·s	ppm_V	ppb_V	1/s	m^2/m^3	m/s
MG 64Y		Z = 0.67 m		SRP1502		07/07/2015				
37	0.6	27.3	1.27E-05	1.18	1.86E-05	91.8	4800	1.9	83	0.023
37	1.0	27.4	1.28E-05	1.18	1.86E-05	96.4	11700	1.9	84	0.023
37	1.5	27.5	1.28E-05	1.18	1.86E-05	79.3	12900	2.3	85	0.027
37	2.0	27.9	1.28E-05	1.17	1.86E-05	82.0	16100	2.5	88	0.028
37	2.5	29.7	1.29E-05	1.17	1.87E-05	80.2	16800	2.8	91	0.031
GTO 250Y		Z = 0.43 m		SRP1501		04/27/2015				
24	0.6	22.5	1.24E-05	1.21	1.83E-05	98.0	405	6.4	200	0.032
24	1.0	22.2	1.24E-05	1.24	1.83E-05	86.2	1059	8.2	211	0.039
37	1.5	26.6	1.27E-05	1.27	1.85E-05	94.0	2000	10.4	231	0.045
37	2.0	26.1	1.27E-05	1.33	1.85E-05	88.8	1747	14.2	235	0.060
B1 250MN		Z = 0.41 m		SRP1616		10/20/2016				
24	0.6	48.7	1.44E-05	1.12	1.96E-05	70.0	1109	4.2	256	0.016
24	1.0	47.9	1.43E-05	1.15	1.95E-05	60.5	1145	6.6	260	0.025
24	1.5	47.1	1.43E-05	1.18	1.95E-05	59.3	2049	7.6	261	0.029
24	2.0	46.4	1.42E-05	1.22	1.95E-05	64.7	2730	9.3	258	0.036
24	2.5	45.8	1.42E-05	1.27	1.94E-05	61.0	3179	10.3	265	0.039
HFP 2		Z = 0.60 m		SRP1703		03/03/2017				
37	0.6	14.7	1.18E-05	1.24	1.79E-05	72.1	1890	2.4	105	0.023
37	1.0	15.6	1.19E-05	1.26	1.80E-05	76.3	2230	3.8	106	0.035
37	1.5	21.0	1.23E-05	1.28	1.83E-05	47.6	2560	4.1	107	0.038
37	2.0	19.9	1.22E-05	1.34	1.82E-05	48.6	3390	4.6	108	0.043
37	2.5	19.4	1.22E-05	1.42	1.82E-05	48.8	4750	4.4	108	0.041
RSR 1.5		Z = 0.76 m		SRP1614		08/09/2016				
37	0.6	35.3	1.33E-05	1.15	1.89E-05	70.5	1221	2.3	150	0.015
37	1.0	34.7	1.33E-05	1.15	1.89E-05	61.4	622	4.6	153	0.030
37	1.5	33.9	1.32E-05	1.15	1.89E-05	50.4	780	6.1	158	0.039
37	2.0	32.9	1.32E-05	1.16	1.88E-05	58.3	1190	7.4	160	0.046
37	2.5	29.9	1.29E-05	1.17	1.87E-05	61.9	1830	8.0	164	0.049

Appendix D: Data Analysis of GC Samples

The liquid samples collected in the k_L experiments were analyzed by a FID gas chromatograph. Since water is incompatible with GC, toluene from the aqueous samples needs to be extracted to organic phase (n-heptane) for injection. Internal standard method is used for the analysis, with 1-bromo-4-fluorobenzene (B4FB) chosen as the internal standard. The response factor for toluene/B4FB was 0.473 ($R_{TOL}/R_{B4FB} = 0.473$) based on experiments with standard samples. The extraction process is illustrated in Figure 3.22.

Two auto-pipettes were used for the extraction, one set at 5 ml for heptane and the other set at 10 ml for aqueous samples. 5 ml of heptane was used to extract toluene from 40 ml of aqueous samples in a 60-ml vial. It is assumed that toluene was completed extracted to the organic phase after shaking the vial for 30 seconds. After phase separation is complete, 2 ml of heptane extract was then moved to small vial and weighted. Known amount of B4FB (~0.01 g) was added into the extract:

$$x_{B4FB}=m_{B4FB}/(m_{extract}+m_{B4FB}) \quad (D.1)$$

The sample was then injected into the GC. The peak areas for toluene and B4FB were recorded so that the toluene concentration in heptane can be calculated:

$$x_{tol,hep}=(R_{tol}\cdot A_{tol}\cdot x_{B4FB})/(R_{B4FB}\cdot A_{B4FB}) \quad (D.2)$$

The toluene in aqueous samples can thus be calculated:

$x_{tol,water}=(x_{tol,hep}\cdot\rho_{hep}\cdot V_{hep})/(\rho_{water}\cdot V_{water})$, where V_{hep} is 5 ml, and V_{water} is 40 ml.

Glossary

A – cross-sectional area of the column, m^2

a_e – effective area of mass transfer per volume of column, m^2/m^3

a_P – specific area of packing per volume of column, m^2/m^3

b – packing channel base, m

c – concentration, mol/m_3, ppm_V, or ppm_W

D – diffusivity, m^2/s

D_0 – infinite dilution diffusivity of ion in water, m^2/s

D_{ij}^0 – infinite dilution diffusivity for component i present in trace amount in component j, m^2/s

D_{column} – diameter of the column, m

d – characteristic length in dimensionless groups ($1/a_P$ in this work), m

d_h – hydraulic diameter defined in Equation 2.30, m

d_{WWC} – hydraulic diameter of WWC, 0.44 cm

E – reaction activation energy, kJ/mol

enhancement factor for mass transfer with chemical reactions

E^∞ – enhancement factor for instantaneous reactions

F – Faraday's constant, 96500 C/mol

F_{SE} – packing geometry parameter in Equation 2.27

g – gravitational acceleration, m/s^2

H – Henry's constant, $Pa \cdot m^3/mol$ (or $atm \cdot L/mol$ if noted)

$H_{element}$ – packing element height, m

h – packing crimp height, m

h_{WWC} – wetted-wall column height, 0.091 m

k – reaction rate constant, $m^3/mol \cdot s$

K – defined in Equations 3.53 and 3.54

$K_{b,Glycerol}$ – equilibrium constant of Equation 3.37, mol/L

k_g' – liquid film mass transfer coefficient with chemical reactions expressed in gas unit, $mol/m^2 \cdot Pa \cdot s$

k_L – liquid film mass transfer coefficient, m/s

k_G – gas film mass transfer coefficient expressed in liquid unit as driving force, m/s

K_{OG} – overall mass transfer coefficient expressed in gas unit as driving force, $mol/m^2 \cdot Pa \cdot s$

l – length of falling film in Equation 5.6b, m

N – molar flux, $mol/m^2 \cdot s$

n – number of packing corrugation channels in the cross-sectional area of the column

P – pressure, Pa

Q – volumetric liquid flow rate, m^3/s

q – pure-component Van der Waals surface area parameter

R – gas constant, 8.314 J/K·mol

r – chemical reaction rate, mol/L·s

pure-component Van der Waals volume parameter

s – packing channel side, m

T – temperature, °K (or °C if noted)

t – time, s

defined in Equation 3.52

u – superficial velocity, m/s

W – wetted wall column circumference, 3.96 cm

w – weight fraction

Z – packing height, m

coordination number in UNIQUAC model

z – ion charge number

Greek letters

α – corrugation angle of packing (degree)

non-randomness parameter in NRTL model

γ – activity coefficient

δ – thickness of the liquid film flowing down the wetted-wall column, m

ε – packing void fraction, m^3/m^3

η – correction factor in Equation 5.2 (detail in Equation 5.3 and Table 5.2)

θ – opening angle of packing corrugation channel (= 90°)

area fraction in UNIQUAC model

μ – dynamic viscosity, mPa·s

ν – kinematic viscosity, m^2/s

ρ – density, kg/m^3

σ – surface tension, N/m

τ – exposure time of liquid surface, s

Φ – fractional area of packing (= a_e/a_P)

segment fraction in UNIQUAC model

Ω – correction factor for packing void area in Equation 2.31

Dimensionless groups

Ca – Capillary number, $\mu \cdot u/\sigma$

Fr – Froude number, $u^2/g \cdot d$

Ga – Galilei number, $g \cdot d^3 \cdot \rho^2/\mu^2$

Ha – Hatta number, defined in Equation 2.20

Mi – Mixing point density, $\frac{3\sin(2\alpha)\left(\cos\left(\frac{\theta}{2}\right)\right)^2\sin\left(\frac{\theta}{2}\right)}{32}$

Re – Reynolds number, $d \cdot u \cdot \rho / \mu$

Sc – Schmidt number, $\mu / \rho \cdot D$

Sh – Sherwood number, $k_L \cdot d / D$

We – Webber number, $\rho \cdot u^2 \cdot d / \sigma$

Packing names

A3 - MONTZ-Pak Type A3™

B1 – MONTZ-Pak Type B1™

CMR – Cascade Mini-Rings®

F – Flexipac®

GTO – GT-OPTIMPAK™

GTP – GT-PAK™

HFP – Hiflow® Plus

IMTP – IMTP® random packing

M – MellaPak™

MG – MellaGrid™

PR – Pall Ring

RSP – Raschig Super-Pak®

RSR – Raschig Super-Ring®

SB-2P – SuperBlend 2-Pac®

References

Au-yeung PH, & Ponter AB. "Estimation of liquid film mass transfer coefficients for randomly packed absorption columns." *Can J Chem Eng*. 1983;61(4):481–493.

Ballinger P, & Long FA. "Acid ionization constants of alcohols. II. Acidities of some substituted methanols and related compounds." *J Am Chem Soc*. 1960;82:795-798.

Basden MA. *Characterization of structured packings via computational fluid dynamics.* University of Texas at Austin. Ph.D. Dissertation. 2014.

Billet R, & Schultes M. "Advantage in correlating packed column performance." *Inst Chem Eng Symp Ser*. 1992;128(Distillation and Absorption '92, Vol. 2):B129-B136.

Billet R, & Schultes M. "Predicting mass transfer in packed columns." *Chem Eng Technol*. 1993;16(1):1–9.

Billet R, & Schultes M. "Prediction of mass transfer columns with dumped and arranged packings - updated summary of the calculation method of Billet and Schultes." *Chem Eng Res Des*. 1999;77(6):498–504.

Bird RB, Stewart WE, & Lightfoot EN. *Transport Phenomena* (2 ed.). New York, John Wiley & Sons. 2002.

Bishnoi S, & Rochelle GT. "Absorption of carbon dioxide into aqueous piperazine-reaction kinetics, mass transfer and solubility." *Chem Eng Sci*. 2000;55(22):5531–5543.

Boden TA, Marland G, & Andres RJ. (2017). *Global, Reginal, and National Fossil-Fuel CO_2 Emissions*.

Bravo JL, & Fair JR. "Generalized correlation for mass transfer in packed distillation columns." *Ind Eng Chem Process Des Dev*. 1982;21(1):162-170.

Bravo JL, Rocha JA, & Fair JR. "A comprehensive model for the performance of columns containing structured packings." *Inst Chem Eng Symp Ser*. 1992;128(Distillation and Absorption '92, Vol. 1):A489-A507.

Bridgwater J, & Scott AM. "Statistical models of packing. Application to gas absorption and solids mixing." *Trans Inst Chem Eng*. 1974;52(4):317–324.

Brignole EA, & Echarte R. "Mass transfer in laminar liquid jets. Measurement of diffusion coefficients." *Chem Eng Sci*. 1981;36(4):695–703.

Brunazzi E, Nardini G, & Paglianti A. "An improved correlation for estimating liquid phase mass transfer coefficient in absorption columns equipped with structured packings." *Inst Chem Eng Symp Ser*. 1997;142(Distillation and Absorption '97, Vol. 1):477-482.

Brunazzi E, Nardini G, Paglianti A, & Petarca L. "Interfacial area of Mellapak packing: absorption of 1,1,1-trichloroethane by Genosorb 300." *Chem Eng Technol*. 1995;18(4):248–255.

Brunazzi E, & Paglianti A. "Liquid-film mass-transfer coefficient in a column equipped with structured packings." *Ind Eng Chem Res*. 1997;36(9):3792–3799.

Buzek J, & Jaroszynski M. "Determination of Henry's constant for the ternary system: carbon dioxide-glycerol-water." *Inzynieria Chemiczna*. 1973;3(3):449–460.

Calderbank PH. "Physical rate processes in industrial fermentation -- 2. Mass transfer coefficients in gas-liquid contacting with and without mechanical agitation." *Trans Inst Chem Eng*. 1959;37(3):173–185.

Carrillo-Nava E, Dohnal V, & Costas M. "Infinite dilution activity coefficients for toluene in aqueous solutions of the protein stabilizers glycerol, ethylene glycol, glucose, sucrose and trehalose." *J Chem Thermodyn*. 2002;34(4):443–456.

Chen X. *Carbon Dioxide Thermodynamics, Kinetics, and Mass Transfer in Aqueous Piperazine Derivatives and Other Amines.* The University of Texas at Austin. Ph.D. Dissertation. 2011.

Chen X, Closmann F, & Rochelle GT. "Accurate screening of amines by the Wetted Wall Column." *Energy Proc*. 2011;4(0):101–108.

Cheng N-S. "Formula for the Viscosity of a Glycerol−Water Mixture." *Ind Eng Chem Res*. 2008;47(9):3285–3288.

Cullinane JT. *Thermodynamics and Kinetics of Aqueous Piperazine with Potassium Carbonate for Carbon Dioxide Absorption.* The University of Texas at Austin. Ph.D. Dissertation. 2005.

D'Errico G, Ortona O, Capuano F, & Vitagliano V. "Diffusion Coefficients for the Binary System Glycerol + Water at 25 °C. A Velocity Correlation Study." *J Chem Eng Data*. 2004;49(6):1665–1670.

Danckwerts PV. "Significance of liquid-film coefficients in gas absorption." *Ind Eng Chem*. 1951;43(6):1460–1467.

Darensbourg DJ, Sanchez KM, & Rheingold AL. "Insertion of carbon dioxide into metal alkoxide bonds. Synthesis and structure of tungsten tetracarbonyl carbonate." *J Am Chem Soc*. 1987;109(1):290-292.

Davidson JF. "The hold-up and liquid film coefficient of packed towers Part 2: statistical models of the random packing." *Trans Inst Chem Eng*. 1959;37(1):131–136.

de Brito MH, von Stockar U, Bangerter AM, & Bomio P. "Effective mass-transfer area in a pilot plant column equipped with structured packings and with ceramic rings." *Ind Eng Chem Res*. 1994;33(3):647–456.

Deed DW, Schutz PW, & Drew TB. "Comparison of rectification and desorption in packed columns." *Ind Eng Chem*. 1947;39:766-774.

Delaloye MM, Stockar Uv, & Lu X-p. "The influence of viscosity on the liquid phase mass transfer resistance in packed columns." *Chem Eng J (Lausanne)*. 1991;47(1):51–61.

Dontula P, Macosko CW, & Scriven LE. "Does the Viscosity of Glycerin Fall at High Shear Rates?" *Ind Eng Chem Res*. 1999;38(4):1729-1735.

Dragan M, Dragan S, & Siminiceanu I. "Characterisation of Mellapak 750Y structured packing determining the effective mass transfer area." *Stud Univ Babes-Bolyai, Chem*. 2000;45(1-2):11-22.

Dugas RE. *Carbon Dioxide Absorption, Desorption, and Diffusion in Aqueous Piperazine and Monoethanolamine.* The University of Texas at Austin. Ph.D. Dissertation. 2009.

Echarte R, Campana H, & Brignole EA. "Effective area and liquid film mass transfer coefficient in packed columns." *Ind Eng Chem Process Des Dev*. 1984;23(2):349–354.

Eigen M. "Protonenübertragung, Säure-Base-Katalyse und enzymatische Hydrolyse. Teil I: Elementarvorgänge." *Angew Chem*. 1963;75(12):489-508.

EPA. (2017). *Inventory of U.S. Greenhouse Gas Emissions and Sinks: 1990-2015*.

Fairbourne A, Gibson GP, & Stephens DW. "The preparation, properties and uses of glycerol derivatives. I. Glycerol ethers." *Chem Ind (London, U K)*. 1930;49:1021-1023.

Fairbourne A, Gibson GP, & Stephens DW. "Partial esterification of polyhydric alcohols. XI. Five methyl ethers of glycerol and related compounds." *J. Chem. Soc.* 1931:445-458.

Faurholt C. "Studies on aqueous solutions of carbonic anhydride and carbonic acid." *J Chim Phys Phys-Chim Biol*. 1924;21:400-455.

Faurholt C. "Studies on monoalkyl carbonates. I. The formation of monoalkyl carbonates from sodium bicarbonate in aqueous solutions of alcohols. The equilibrium between alcohol, monoalkyl carbonate, carbonate and carbon dioxide in aqueous solution." *Z. physik. Chem.* 1927a;126:72-84.

Faurholt C. "Studies on monoalkyl carbonates. II. The formation of monoalkyl carbonic acids or their salts on dissolving carbon dioxide in aqueous solutions of alcohols of different degrees of acidity." *Z. physik. Chem.* 1927b;126:85-104.

Faurholt C. "Studies on monoalkyl carbonates. III. The kinetics of the decomposition of the monoalkyl carbonates and of the formation of the monoalkyl carbonates from bicarbonate in aqueous alkaline solutions." *Z. physik. Chem.* 1927c;126:211-226.

Fellinger LL. *Absorption of ammonia by water and acids in various standard packigns.* Massachusetts Institute of Technology. Ph.D. Dissertation. 1941.

Fuller EN, Schettler PD, & Giddings JC. "NEW METHOD FOR PREDICTION OF BINARY GAS-PHASE DIFFUSION COEFFICIENTS." *Industrial & Engineering Chemistry*. 1966;58(5):18-27.

Garner FH, & Marchant PJM. "Diffusivities of associated compounds in water." *Trans Inst Chem Eng*. 1961;39(1):397–408.

Ge M-L, Ma J-L, & Wu C-G. "Activity Coefficients at Infinite Dilution of Alkanes, Alkenes, and Alkyl Benzenes in Glycerol Using Gas−Liquid Chromatography." *J Chem Eng Data*. 2010;55(4):1714-1717.

Geankoplis CJ. *Transport Processes and Separation Process Principles: Includes Unit Operations* Prentice Hall Professional Technical Reference. 2003.

Glycerine Producers A. *Chemical properties and derivatives of glycerine*. New York, Glycerine Producers' Association. 1965.

Grossmann T, & Winkelmann J. "Ternary Diffusion Coefficients of Glycerol + Acetone + Water by Taylor Dispersion Measurements at 298.15 K." *J Chem Eng Data*. 2005;50(4):1396–1403.

Hansen J, Ruedy R, Sato M, & Lo K. "GLOBAL SURFACE TEMPERATURE CHANGE." *Reviews of Geophysics*. 2010;48(4):n/a-n/a.

Haubrock J, Hogendoorn JA, & Versteeg GF. "The applicability of activities in kinetic expressions: A more fundamental approach to represent the kinetics of the system CO2-OH- in terms of activities." *Int. J. Chem. React. Eng.* 2005;3:No pp. given.

Hayduk W, & Cheng SC. "Review of relation between diffusivity and solvent viscosity in dilute liquid solutions." *Chem Eng Sci*. 1971;26(5):635-646.

Henriques de Brito M, von Stockar U, & Bomio P. "Predicting the liquid phase mass transfer coefficient kL for the Sulzer structured packing Mellapak." *Inst Chem Eng Symp Ser*. 1992;128(Distillation and Absorption '92, Vol. 2):B137-B144.

Heston BO, Dermer OC, & Woodside JA. "Reaction of alkoxide ions with CO2." *Proc. Okla. Acad. Sci.* 1943;23:67-68.

Higbie R. "The rate of absorption of a pure gas into a still liquid during short periods of exposure." *Trans Am Inst Chem Eng*. 1935;31:365-389.

Hikita H, Asai S, & Takatsuka T. "Absorption of carbon dioxide into aqueous sodium hydroxide and sodium carbonate-bicarbonate solutions." *Chem Eng J (Lausanne)*. 1976;11(2):131-141.

Hoffmann A et al. "Standardization of mass transfer measurements a basis for the description of absorption processes." *Chem Eng Res Des*. 2007;85(A1):40–49.

Holtzhauer M. *Basic Methods for the Biochemical Lab*. Berlin, Springer Berlin Heidelberg. 2006.

Hoshino S, Yakura H, & Oike T. "Diffusion coefficient and microviscosity in viscous low-molecular-weight solutions." *Kagaku Kogaku*. 1972;36(4):433-438.

IPCC. (2014). *IPCC 5th Assessment Report*.

Jordan J, Ackerman E, & Berger RL. "Polarographic diffusion coefficients of oxygen, defined by activity gradients in viscous media." *J Am Chem Soc*. 1956;78:2979-2983.

Jordan J, & Bauer WE. "Correlations between Solvent Structure, Viscosity and Polarographic Diffusion Coefficients of Oxygen1." *J Am Chem Soc*. 1959;81(15):3915-3919.

Kanniche M et al. "Pre-combustion, post-combustion and oxy-combustion in thermal power plant for CO2 capture." *Appl Therm Eng*. 2010;30(1):53–62.

Kato M, & Ito T. "Facile carbon dioxide uptake by zinc(II)-tetraazacycloalkane complexes. 1. Syntheses, characterizations, and chemical properties of (monoalkyl carbonato)(tetraazacycloalkane)zinc(II) complexes." *Inorg Chem*. 1985;24(4):504-508.

Koch JHA, Stutzman LF, Blum HA, & Hutchings LE. "Gas absorption." *Chem Eng Prog*. 1949;45(11):677-682.

Kreulen H, Smolders CA, Versteeg GF, & van Swaaij WPM. "Microporous hollow fibre membrane modules as gas-liquid contactors Part 2. Mass transfer with chemical reaction." *J Membr Sci*. 1993;78(3):217–238.

Kucka L, Kenig EY, & Gorak A. "Kinetics of the Gas-Liquid Reaction between Carbon Dioxide and Hydroxide Ions." *Ind Eng Chem Res*. 2002;41(24):5952–5957.

Laddha SS, Diaz JM, & Danckwerts PV. "The nitrous oxide analogy: the solubilities of carbon dioxide and nitrous oxide in aqueous solutions of organic compounds." *Chem Eng Sci*. 1981;36(1):228–229.

Lane LB. "Freezing points of glycerol and its aqueous solutions." *Ind Eng Chem*. 1925;17:924.

Lewis WK, & Whitman WG. "Principles of gas absorption." *Ind Eng Chem*. 1924;16(12):1215-1220.

Li L. *Carbon Dioxide Solubility and Mass Transfer in Aqueous Amines for Carbon Capture.* The University of Texas at Austin. Ph.D. Dissertation. 2015.

Linek V, Moucha T, & Rejl FJ. "Hydraulic and Mass Transfer Characteristics of Packings for Absorption and Distillation Columns. Rauschert-Metall-Sattel-Rings." *Chem Eng Res Des*. 2001;79(7):725–732.

Linek V, Petricek P, Benes P, & Braun R. "Effective interfacial area and liquid side mass transfer coefficients in absorption columns packed with hydrophilized and untreated plastic packings." *Chem Eng Res Des*. 1984;62(1):13–21.

Lohse M, Alper E, Quicker G, & Deckwer WD. "Diffusivity and solubility of carbondioxide in diluted polymer solutions." *AIChE J*. 1981;27(4):626–631.

Mangers RJ, & Ponter AB. "Effect of Viscosity on Liquid Film Resistance to Mass Transfer in a packed column." *Ind Eng Chem Process Des Dev*. 1980;19(4):530–537.

McGlamery GG. *Liquid film transport characteristics of textured metal surfaces.* University of Texas at Austin. Ph.D. Dissertation. 1988.

Mehta VD, & Sharma MM. "Effect of diffusivity on gas-side mass-transfer coefficient." *Chem Eng Sci*. 1966;21(4):361-365.

Mohunta DM, Vaidyanathan AS, & Laddha GS. "Prediction of liquid-phase mass transfer coefficients in columns packed with Raschig rings." *Indian Chem Eng*. 1969;11(3):73–79.

Molstad MC, Abbey RG, Thompson AR, & McKinney JF. "Performance of drip-point grid tower packings. II. Liquid-film mass transfer data." *Trans Am Inst Chem Eng*. 1942;38(1):410–434.

Moucha T, Linek V, & Prokopova E. "Effect of packing geometrical details. Influence of free tips on volumetric mass transfer coefficients of Intalox saddles." *Chem Eng Res Des*. 2005;83(A1):88-92.

Mshewa MM. *Carbon dioxide desorption/absorption with aqueous mixtures of methyldiethanolamine and diethanolamine at 40 to 120 degrees C.* The University of Texas at Austin. Dissertation. 1995.

Nijsing RATO, Hendriksz RH, & Kramers H. "Absorption of carbon dioxide in jets and falling films of electrolyte solutions, with and without chemical reaction." *Chem Eng Sci*. 1959;10:88-104.

Nishijima Y, & Oster G. "Diffusion in Glycerol-Water Mixture." *Bull Chem Soc Jpn*. 1960;33(12):1649–1651.

Nogami H, & Kato Y. "Diffusion coefficient of oxygen in propylene glycol-water mixtures and glycerol-water mixtures." *Yakugaku Zasshi*. 1962;82:120-126.

Norman WS. *Absorption, distillation and cooling towers* (1 ed.). New York, John Wiley & Sons. 1961.

Norman WS, & Sammak FYY. "Gas absorption in a packed column Part 1: the effect of liquid viscosity on the mass transfer coefficient." *Trans Inst Chem Eng*. 1963a;41(3):109–116.

Norman WS, & Sammak FYY. "Gas absorption in a packed column part 2: the effect of mixing between packing elements on the liquid film mass transfer coefficient." *Trans Inst Chem Eng*. 1963b;41(4):117–119.

Offermans WK, Bizzarri C, Leitner W, & Mueller TE. "Surprisingly facile CO2 insertion into cobalt alkoxide bonds: a theoretical investigation." *Beilstein J Org Chem*. 2015;11:1340-1351.

Olujic Z. "Development of a complete simulation model for predicting the hydraulic and separation performance of distillation columns equipped with structured packings." *Chem Biochem Eng Q*. 1997;11(1):31-46.

Olujic Z, Kamerbeek AB, & de Graauw J. "A corrugation geometry based model for efficiency of structured distillation packing." *Chem Eng Process*. 1999;38(4-6):683-695.

Onda K. "Measurement of the diffusivity of carbon dioxide by liquid jets." *Mem. Fac. Eng., Nagoya Univ.* 1961;13:138-148.

Onda K, Okamoto T, & Yamaji Y. "Diffusion coefficient of carbon dioxide in packed columns." *Chem Eng (NY)*. 1960;24(12):918–925.

Onda K, Sada E, & Murase Y. "Liquid-side mass transfer coefficients in packed towers." *AIChE J*. 1959;5(1):235–239.

Onda K, Sada E, & Takeuchi H. "Gas absorption with chemical reaction in packed columns." *J Chem Eng Jpn*. 1968a;1(1):62–66.

Onda K, & Takeuchi H. "Effect of packing materials on the wetted surface area." *Kagaku Kogaku*. 1967;31(2):126-134.

Onda K, Takeuchi H, & Okumoto Y. "Mass transfer coefficients between gas and liquid phases in packed columns." *J Chem Eng Jpn*. 1968b;1(1):56–62.

Ostonen A, Sapei E, Uusi-Kyyny P, Klemela A, & Alopaeus V. "Measurements and modeling of CO2 solubility in 1,8-diazabicyclo-[5.4.0]-undec-7-ene-glycerol solutions." *Fluid Phase Equilib*. 2014;374:25-36.

Pacheco MA. *Mass transfer, kinetics and rate-based modeling of reactive absorption.* The University of Texas at Austin. Ph.D. Dissertation. 1998.

Pacheco MA, Kaganoi S, & Rochelle GT. "CO2 absorption into aqueous mixtures of diglycolamine and methyldiethanolamine." *Chem Eng Sci*. 2000;55(21):5125-5140.

Pigford RL. *Counter-diffusion in a wetted wall column.* The University of Illinois at Urbana Champaign. Ph.D. Dissertation. 1942.

Pinsent BRW, Pearson L, & Roughton FJW. "Kinetics of combination of carbon dioxide with hydroxide ions." *Trans Faraday Soc*. 1956;52:1512-1520.

Pohorecki R, & Moniuk W. "Kinetics of reaction between carbon dioxide and hydroxyl ions in aqueous electrolyte solutions." *Chem Eng Sci*. 1988;43(7):1677–1684.

Ponter AB, & Au-Yeung PH. "Estimation of liquid film mass transfer coefficients in columns packed randomly with partially wetted rings." *Can J Chem Eng*. 1982;60(1):94–99.

Rejl JF, Linek V, Moucha T, & Valenz L. "Methods standardization in the measurement of mass-transfer characteristics in packed absorption columns." *Chem Eng Res Des*. 2009;87(5):695–704.

Riede T, & Schlunder EU. "Diffusivities of the ternary liquid mixture 2-propanol-water-glycerol and three-component mass transfer in liquids." *Chem Eng Sci*. 1991;46(2):609–617.

Rischbieter E, Schumpe A, & Wunder V. "Gas Solubilities in Aqueous Solutions of Organic Substances." *J Chem Eng Data*. 1996;41(4):809–812.

Rixon FF. "The absorption of carbon dioxide in and desorption from water using packed towers." *Trans. Inst. Chem. Engrs.* 1948;26:119-129, discussion, 129-130.

Rocha JA, Bravo JL, & Fair JR. "Distillation Columns Containing Structured Packings: A Comprehensive Model for Their Performance. 2. Mass-Transfer Model." *Ind Eng Chem Res*. 1996;35(5):1660–1667.

Rochelle GT. "Amine scrubbing for CO2 capture." *Science*. 2009;325(5948):1652–1654.

Rochelle GT et al. "CO_2 Capture by Aqueous Absorption, Second Quarterly Progress Report 2014." Texas Carbon Management Program. The University of Texas at Austin. 2014.

Rochelle GT et al. "CO_2 Capture by Aqueous Absorption, First Quarterly Progress Report 2015." Texas Carbon Management Program. The University of Texas at Austin. 2015a.

Rochelle GT et al. "CO_2 Capture by Aqueous Absorption, Second Quarterly Progress Report 2015." Texas Carbon Management Program. The University of Texas at Austin. 2015b.

Rutten PWM. *Diffusion in liquids.* Technische Universiteit Delft (The Netherlands). C298751 Dissertation. 1992.

Sharma MM, & Danckwerts PV. "Catalysis by Broensted bases of the reaction between CO2 and water." *Trans Faraday Soc*. 1963;59:386-395.

Sharma MM, & Danckwerts PV. "Chemical methods of measuring interfacial area and mass transfer coefficients in two-fluid systems." *Br Chem Eng*. 1970;15(4):206–212.

Sherwood TK, & Holloway FAL. "Performance of packed towers - Liquid film data for several packings." *Trans Am Inst Chem Eng*. 1940;36(1-2):various pages.

Shi MG, & Mersmann A. "EFFECTIVE INTERFACIAL AREA IN PACKED COLUMNS." *Ger Chem Eng*. 1985;8(2):87–96.

Shulman HL, & DeGouff JJ, Jr. "Mass-transfer coefficients and interfacial areas for 1-inch Raschig rings." *Ind Eng Chem*. 1952;44:1915-1922.

Shulman HL, Ullrich CF, Proulx AZ, & Zimmerman JO. "Performance of packed columns. II. Wetted and effective-interfacial areas, gas - and liquid-phase mass transfer rates." *AIChE J*. 1955;1(2):253–258.

Song D, & Rochelle GT. "Reaction kinetics of carbon dioxide and hydroxide in aqueous glycerol." *Chem Eng Sci*. 2017;161:151-158.

Staveley LAK, & Milward GL. "Solutions of alcohols in nonpolar solvents. IV. Thermodynamic properties of glycol in benzene, heptane, and cyclohexane." *J. Chem. Soc.* 1957:4369-4375.

Stergiannakos T, Klontzas E, Tylianakis E, & Froudakis GE. "Enhancement of CO2 Adsorption in Magnesium Alkoxide IRMOF-10." *J Phys Chem C*. 2015;119(38):22001-22007.

Suess P, & Spiegel L. "Hold-up of mellapak structured packings." *Chem Eng Process*. 1992;31(2):119–124.

Takamura K, Fischer H, & Morrow NR. "Physical properties of aqueous glycerol solutions." *J Pet Sci Eng*. 2012;98–99(0):50–60.

Taylor R, & Krishna R. *Multicomponent Mass Transfer*. New York, Wiley. 1993.

Ternström G, Sjöstrand A, Aly G, & Jernqvist Å. "Mutual Diffusion Coefficients of Water + Ethylene Glycol and Water + Glycerol Mixtures." *J Chem Eng Data*. 1996;41(4):876–879.

Thomas WJ, & Adams MJ. "Measurement of the diffusion coefficients of carbon dioxide and nitrous oxide in water and aqueous solutions of glycerol." *Trans Faraday Soc*. 1965;61(0):668–673.

Thongpakdi D. *Transfer of gases to liquid films flowing over enhanced surfaces.* The University of Texas at Austin. M.S. Dissertation. 1991.

Tsai RE. *Mass Transfer Area of Structured Packing.* The University of Texas at Austin. Ph.D. Dissertation. 2010.

Tsai RE, Seibert AF, Eldridge RB, & Rochelle GT. "A dimensionless model for predicting the mass-transfer area of structured packing." *AIChE J*. 2011;57(5):1173–1184.

Tsuda T, & Saegusa T. "Reaction of cupric methoxide and carbon dioxide." *Inorg Chem*. 1972;11(10):2561-2563.

Valenz L, Rejl FJ, Sima J, & Linek V. "Absorption Mass-Transfer Characteristics of Mellapak Packings Series." *Ind Eng Chem Res*. 2011;50(21):12134–12142.

Van Krevelen DW, & Hoftijzer PJ. "Gas absorption. I. Liquid-film resistance to gas absorption in scrubbers." *Recueil des Travaux Chimiques des Pays-Bas et de la Belgique*. 1947;66(1):49–66.

Vazquez Una G, Chenlo Romero F, Pereira Goncalves G, & Peaguda Lorenzo J. "Solubility of CO_2 in Aqueous solutions of Saccharose, Glucose, Fructose, and Glycerin." *J Chem Eng Data*. 1994;39(4):639–642.

Versteeg GF, & Van Swaalj W. "Solubility and diffusivity of acid gases (carbon dioxide, nitrous oxide) in aqueous alkanolamine solutions." *J Chem Eng Data*. 1988;33(1):29–34.

Vivian JE, & King CJ. "The mechanism of liquid-phase resistance to gas absorption in a packed column." *AIChE J*. 1964;10(2):221-227.

Vivian JE, & Whitney RP. "Absorption of chlorine in water." *Chem Eng Prog*. 1947;43(No. 12, Trans. Am. Inst. Chem. Engrs.):691-702.

Wang C. *Mass Transfer Coefficients and Effective Area of Packing.* The University of Texas at Austin. Ph.D. Dissertation. 2015.

Wang C, Perry M, Rochelle GT, & Seibert AF. "Packing Characterization: Mass Transfer Properties." *Energy Proc*. 2012;23(0):23–32.

Wang C, Song D, Seibert FA, & Rochelle GT. "Dimensionless Models for Predicting the Effective Area, Liquid-Film, and Gas-Film Mass-Transfer Coefficients of Packing." *Ind Eng Chem Res*. 2016;55(18):5373-5384.

Wang GQ, Yuan XG, & Yu KT. "Review of Mass-Transfer Correlations for Packed Columns." *Ind Eng Chem Res*. 2005;44(23):8715–8729.

Weimer T, & Schaber K. "Absorption of CO2 from atmosphere as a method for estimation of effective interfacial areas in packed columns." *Inst Chem Eng Symp Ser*. 1997;142(Distillation and Absorption '97, Vol. 1):417-427.

White WN, Vogelmann T, Morse M, & White HS. "Acidity functions of hydrochloric acid, perchloric acid, and sulfuric acid and pKa values of some primary aromatic amines in 50% volume/volume aqueous ethanol." *J Org Chem*. 1977;42(1):162-165.

Whitney RP, & Vivian JE. "Absorption of sulfur dioxide in water." *Chem Eng Prog*. 1949;45:323-337.

Wilke CR, & Chang P. "Correlation of diffusion coefficient in dilute solutions." *AIChE J*. 1955;1(2):264–270.

Wilson I. *Gas-liquid contact area of random and structured packing.* University of Texas at Austin. M.S. Dissertation. 2004.

Yamamoto H et al. "Preliminary Ecological Risk Assessment of Butylparaben and Benzylparaben - 2. Fate and Partitioning in Aquatic Environments." *Environ Sci (Tokyo, Jpn)*. 2007;14(Suppl. 2007):97–105.

Yeh NK. *Liquid Phase Mass Transfer in Spray Contactors.* The University of Texas at Austin. Ph.D. Dissertation. 2002.

Zakeri A. *Characterization of packing materials for CO_2 absorption.* Norwegian University of Science and Technology. Doctoral Dissertation. 2011.

Zaoui-Djelloul-Daouadji M, Negadi A, Mokbel I, & Negadi L. "(Vapor-liquid) equilibria and excess Gibbs free energy functions of (ethanol+glycerol), or (water+glycerol) binary mixtures at several temperatures." *J Chem Thermodyn*. 2014;69(0):165–171.

Zirnsak MA, Boger DV, & Tirtaatmadja V. "Steady shear and dynamic rheological properties of xanthan gum solutions in viscous solvents." *J Rheol*. 1999;43(3):627-650.

Vita

Di Song was born in Luoyang, China in 1989 to Xiaowen Song and Jinjin Wang. After graduation from Nankai High School in Tianjin, China in 2007, he was enrolled in Zhejiang University where he received Bachelor of Science degree in Chemical Engineering and Bachelor of Arts degree in English in 2012. After that, he began his graduate study in Chemical Engineering in the University of Texas at Austin, where he was advised by Dr. Gary Rochelle and Dr. Frank Seibert.

Permanent email: songdi.zju@gmail.com

This dissertation was typed by the author.